INVESTIGATION OF THE RELATIONSHIP BETWEEN FRAGMENTATION AND BRITTLENESS OF ROCK, IN PARTICULAR CLASS II ROCK TYPE

Victor Abioye **AKINBINU**

A thesis submitted to the Faculty of Engineering and the Built Environment, University of the Witwatersrand, Johannesburg, in fulfilment of the requirements for the degree of Doctor of Philosophy in Engineering (Mining)

Johannesburg 2015

DECLARATION

I declare that this thesis is my own unaided work. It is being submitted for the Degree of Doctor of Philosophy in Engineering in the University of the Witwatersrand, Johannesburg. It has not been submitted before for any degree or examination at any other University.

(Signature of candidate)

.....day of..... (year).....2015.....

at.....

ABSTRACT

The aim of this research is to investigate the relationship between fragmentation and brittleness of rock by taking into account the influence of the Class II characteristic behaviour of the rocks have on this relationship. Fragmentation of rock under compressive failure depends on its self-sustaining failure and the energy available in the post-failure region to shatter the rock. The fragmentation produced under this condition depends to a large extent on the energy available to cause fragmentation and on the brittleness of the rock. From review of the literature, it appears that no research has attempted to link brittleness and fragmentation. Rock failure under dynamic loading conditions, such as in blasting, rockbursts, crushing, and milling, as well as during conventional unconfined compressive strength testing of rock specimens and the subsequent fragments size distribution is a little-understood phenomenon. This relationship will be helpful in the solution to many practical mining and civil engineering problems. This includes the prediction of optimal fragmentation and the design of stable structures as a result of dynamic processes particularly associated with fragmentation.

The research carried out involved the analysis of rock parameters determined from different rock Classes (Class I and Class II) under destructive tests using a soft testing machine and a closed loop servo-controlled testing machine (stiff machine). The tests were conducted according to ISRM suggested methods at the Genmin Laboratory, Wits University while the post-failure stress-strain curves estimation were done using a closed loop servo-controlled testing machine at the Rock Engineering Department at Aalto University Finland. In addition, non-destructive tests were conducted with the output being monitored using a dual-beam cathode ray oscilloscope. From the destructive tests, the static parameters were determined

while the dynamic parameters were estimated from the non-destructive tests. The fragments from the tests using the soft testing system were collected for size characterization/distribution.

Dynamic fracturing test entailed blasting a few rock blocks with explosive. The rock types used included Class I and Class II rocks. The rocks were prepared into blocks of dimensions 150 mm length x 100 mm width x 100 mm height. Holes were drilled into the blocks with 8 mm diameter drill bits to a depth of 80 mm. The holes were spaced at 44.7 mm with a burden of 28 mm in a rectangular blasting pattern. Each of the holes was charged with a 720 mg electric detonator to ensure consistent charge per hole and per rock block and shot instantaneously inside a cylindrical blasting chamber at AEL Mining Services. After each blast, the fragments were collected for size distribution/characterization.

The comparison of static mechanical and dynamic properties with fragments size as a measure of fragmentation from compression test show that the higher the property value the more the fragmentation produced for the Class II but the same cannot be said for the Class I rocks. The relationships between different measures of fragmentation with brittleness concepts based on static mechanical properties and moduli were analysed. Further assessment of the relationships between the different measures of fragmentation with brittleness concepts estimated from normalised stress-axial strain curve, and extension strain criterion show that, fragments size at X_{50} and X_{10} is a better measure of fragmentation than the "fragments volumes".

The brittleness concepts estimated from normalised stress-axial strain curve, designated as NSSC and the extension strain criterion (i.e. critical extension strain, e_c), show better correlation with fragmentation under compressive failure (for the segregated samples, Class

II and Class I) and the blasting test for the combined sample than shown with the brittleness concepts based on static mechanical properties and moduli. The relationship show that the higher the value of the brittleness concepts (i.e. NSSC and critical extension strain, e_c), the finer the fragmentation. Under compressive failure, NSSC is a better concept for quantifying the brittleness of rock for the segregated samples (Class II and Class I). On the other hand, the critical extension strain shows stronger correlation at both X_{50b} and X_{10b} than the NSSC for the blasting test. Therefore, critical extension strain is a better index for quantifying brittleness of rock under blasting test.

A modification was applied to the Kuz-Ram model to take into account the brittleness behaviour of rocks based on critical extension strain. Thus, understanding the relationship between fragmentation and brittleness can bring about optimal prediction of fragmentation, and consequently, result in an economic gain for the excavation industry.

DEDICATION

This work is dedicated to God the Father, the Son and the Holy Ghost.

ACKNOWLEDGEMENTS

I am earnestly thankful to my supervisor, Prof. JN. van der Merwe, for his encouragement and supervision from the initial framing up of the thesis topic to the final level which has facilitated my understanding of this research. I also want to thank him for approving Centennial Trust Fund funding for this research project for the past three years. It would have been difficult to write this thesis without his help and guidance. Thanks for giving me the privilege to learn under you.

I also want to express my appreciation to both academic and support staff members of the School of Mining Engineering. I am especially grateful to Professor Dick Stacey for his contribution in the framing up of the thesis topic and in the literature review. I'm appreciative to Mrs. Mona Shah and other support staff, Mr Andrew Carpede and his assistants at Genmin laboratory, Wits University. My thanks go to Sarah Glynn from the School of Geosciences Wits University, for petrographic examination of the rock samples. I'm also grateful to Howard Pooe, the Operation Manager at Afrisam Ferro Quarries for his assistance during sample collection. Thanks to Dr. E. J. Sellers, the group blasting manager at AEL (Ltd) Mining Services for his contribution and Mr. Robin Winslow and Mr. Mauritz Kotze of AEL (Ltd) Mining Services South Africa for carrying out the blasting tests.

I extended my gratitude to Prof. Mikael Rinne for inviting me to Aalto University, Finland to complete my tests on the post failure determination of rocks and also to Otto Hedstrom, the Laboratory Manager and Eloranta Pekka, the Laboratory Technical Engineer.

Without the support of these people it would have been difficult to complete this research work. Many thanks to others who had help me in one way but unfortunately their name would remain anonymous.

TABLE OF CONTENT

Content	Page
DECLARATION	i
ABSTRACT	ii
DEDICATION	v
ACKNOWLEDGEMENTS	vi
TABLE OF CONTENT	viii
FIGURES	xviii
TABLES	xxix

CHAPTER ONE

INTRODUCTION

1.1 Introduction…….1

1.2 Statement of Problem and Motivation for the Research…….3

1.3 Research Question……..5

1.4 Objective of Research…….5

1.5 Contribution to Knowledge……6

1.6 Laboratory Determination of Rock Parameters and Stiff Testing of Rock Specimen……7

1.7 Class I and Class II Rocks……..9

1.8 Elastic Strain Energy……11

1.9 Laboratory Determination of Fragmentation and Brittleness of Rocks……12

1.10 Thesis Layout…….....13

1.11 Chapter Summary……...14

CHAPTER TWO

LITERATURE REVIEW

2.1 Introduction ……..16

2.2 Micromechanics of Brittle Failure (Microscopic Failure)……16

2.2.1 Stages in the Deformation Process……20

2.3 Factors Affecting Laboratory Determination of Mechanical Properties of Rocks (Macroscopic Failure)……. 28

2.3.1 Effect of Shape and Size of Specimen on the UCS……...29

2.3.2 Height to Diameter Ratio Effect on the UCS……34

2.3.3 Non-homogeneity Effect on the UCS……39

2.3.4 Contact Condition between Specimen End Surface and Platen……41

2.3.5 Effect of Moisture, Temperature and Mineralogy on Strength Parameters……..45

2.3.6 Effect of Strain Rate on Strength Parameters……49

2.4 Rock Classification……...54

2.4.1 Post-Failure Characteristic Curves of Rock under Uniaxial Compression……54

2.4.2 Studies on Class II Behaviour of Rocks……56

2.4.3 Effect of Strain Rate on the Post-failure Behaviour of Rock in Uniaxial Compression……61

2.5 Rock Fragmentation……..64

2.5.1 Rock Fragmentation under Explosive or Dynamic Loading……65

2.5.2 Rock Fragmentation under a Compression Loading Condition……...77

2.5.3 Fragmentation and Effect of Strain Rate……...80

2.6 Concept of Rock Brittleness……82

2.6.1 Dimensionless Brittleness Indices……83

2.6.2 Dimensional Brittleness Indices……87

2.6.3 Factors Influencing Brittleness Determination……92

2.6.4 Assessment of the Various Brittleness Concepts……95

2.6.5 Brittleness and Fragmentation in Relation to the Research Study…….100

2.7 Chapter Summary……..110

CHAPTER THREE

TEST MATERIALS DESCRIPTION AND EXPERIMENTAL SET UP

3.1 Introduction…….113

3.2 Description of Rock Specimens……..114

3.2.1 Petrographic Examination of Rock Sample and Equipment Description……...115

3.2.1.1 *Procedure for Petrographic Examination of Rock Specimen*……..116

3.3 Sonic Velocities Determination and Equipment Description…….116

3.3.1 Procedure for Determination of Sonic Velocities of Rock Specimens……118

3.4 Brazilian Tensile Strength Determination and Equipment Description…….119

3.4.1 Procedure for Determination of Brazilian Tensile Strength of Rock Specimens……120

3.5 Description of Uniaxial Compressive Strength Determination and Equipment ……... 123

3.5.1 Procedure for Determination of Uniaxial Compressive Strength of Rock Specimen…….125

3.6 Deformation Parameters and Equipment Description……127

3.6.1 Procedure Used for Determination of the Deformation Parameters of the Rock Specimens……...127

3.7 Description of the Determination of Pre-failure and Post-failure Stress-Strain Curve in Uniaxial Compression and Equipment ……..129

3.8 Fragmentation by Blasting and Equipment Used for Analysis of Fragments……133

3.9 Procedure for Estimating Fragmentation by Sieve Analysis……..135

3.10 Chapter Summary…….136

CHAPTER FOUR

RESULTS OF THE LABORATORY WORK

4.1 Introduction…….139

4.2 Rock Specimen Description……139

4.2.1 Gabbro……140

4.2.2 Granite1……...141

4.2.3 Granite2……...143

4.2.4 Granite3……...144

4.2.5 Granite4……...145

4.2.6 Granite5……...146

4.2.7 Marble……..148

4.2.8 Mottled Anothosite……..148

4.2.9 Norite1……149

4.2.10 Norite2……...151

4.2.11 Norite3……...152

4.2.12 Quartz Arenite……153

4.2.13 Quartzite1……...154

4.2.14 Quartzite2……...155

4.2.15 Sandstone……...156

4.2.16 Spotted Anorthosite……...157

4.2.17 Troctolite1……..157

4.2.18 Troctolite2……..158

4.3 Sonic Velocities and Dynamic Parameters……160

4.4 Static Mechanical Properties of Rock……161

4.5 Pre-failure and Post-failure Curves……163

4.6 Stress-Axial, Radial and Total Volumetric Strain Curves……..167

4.7 Brittleness Based on Static Mechanical Properties of Rock……...179

4.8 Brittleness Based on Moduli……...180

4.9 Chapter Summary…..……182

CHAPTER FIVE

ANALYSIS OF FRAGMENT SIZE FROM THE COMPRESSION AND BLASTING TESTS

5.1 Introduction…….184

5.2 Fragments Size Produced During Uniaxial Compression Tests…….186

5.3 Comparison of Percentage Passing for steady Compression Tests for Rocks of Similar Strength ……..…191

5.4 Analysis of Fragment Size from Compression Using Probability Density Distribution Models……194

5.5 Analysis of Fragmentation from Blasting Using Probability Density Distribution Models……196

5.6 Assessment of the Relationship of Brittleness Concepts, Rock Parameters and Fragmentation Using Statistical Analysis……..199

5.6.1 Stepwise Statistical Analysis of Brittleness *k* with Fragmentation from Compression…….. 202

5.7 Fragmentation Produced During Uniaxial Compression Tests and Rock Properties ……209

5.7.1 Comparison of Fragmentation from Compression and Static Mechanical Properties…… 209

5.7.2 Fragmentation from Compression and Dynamic Properties……... 212

5.8 Fragmentation and Brittleness According to Selected Definitions…….213

5.8.1 Fragmentation and Brittleness Based on Static Mechanical Properties ……..213

5.8.2 Fragmentation and Brittleness Based on Moduli ……216

5.9 Interim Summary……..……..221

5.9.1 Comparison of Fragmentation with Static Mechanical Properties…..……... 222

5.9.2 Comparison of Fragmentation with Dynamic Properties……..……..223

5.9.3 Correlation of Fragmentation with Brittleness Based on Static Mechanical Properties……223

5.9.4 Correlation of Fragmentation with Brittleness Based on Moduli……...….224

5.10 Introducing a New Brittleness Concept Based on the Normalised Stress-Axial Strain Curve…….……224

5.11 Fragmentation from Compression and Brittleness Estimated from Extension Strain Criterion…..…….229

5.12 Interim Summary……..235

5.13 Comparison of Fragment Size from both Compression and Blasting Tests with Various Brittleness Concepts……..…….235

5.13.1 Comparison of Fragment Size from both Compression and Blasting Tests with Brittleness Based on Static Mechanical Properties…….…….235

5.13.2 Comparison of Fragment Size from both Compression and Blasting Tests with Brittleness Based on Moduli……..……...239

5.13.3 Comparison of Fragment Size for both Compression and Blasting Tests with Brittleness Estimated from Normalised Stress-Axial Strain Curve, NSSC……..……242

5.13.4 Comparison of Fragment Size for Compression and Blasting Tests with Brittleness Estimated from Extension Strain Criterion……..……..245

5.14 Chapter Summary…….248

5.14.1 Comparison of Fragment size from Compression with Static Mechanical Properties…..249

5.14.2 Comparison of Fragment size from Compression with Dynamic Properties……249

5.14.3 Correlation of Fragmentation with Brittleness Based on Static Mechanical Properties……..……..250

5.14.4 Correlation of Fragmentation with Brittleness Based on Moduli…….…….250

5.14.5 Correlation of Fragmentation with Brittleness Based on NSSC and e_c……251

CHAPTER SIX

ASSESSMENTS OF FRAGMENT VOLUMES FROM BOTH COMPRESSION AND BLASTING TESTS

6.1 Introduction…….253

6.2 Total Number of Fragments per Volume of Rock and Brittleness…….253

6.2.1 Total Number of Fragments per Volume of Rock and Brittleness Based on Static Mechanical Properties…….……...254

6.2.2 Total Number of Fragments per Volume of Rock and Brittleness Based on Moduli…….……...256

6.3 Volume of Fines per Volume of Rock and Brittleness……...257

6.3.1 Volume of Fines per Volume of Rock Produced and Brittleness Based on Static Mechanical Properties..……..258

6.3.2 Volume of Fines per Volume of Rock and Brittleness Based on Moduli……...260

6.3.3 Volume of Fines per Volume of Rock Produced and Brittleness Based on Extension Strain Criterion……..…….261

6.4 Energy and Fragment Volumes……..262

6.5 Chapter Summary……...264

CHAPTER SEVEN

RELATIONSHIP BETWEEN FRAGMENTATION AND BRITTLENESS

7.1 Introduction…….266

7.2 Fragmentation Based on the Percentage Passing Sieve Size……..266

7.2.1 Percentage Passing Sieve Size for the Compression Tests……..267

7.2.2 Percentage Passing Sieve Size for the Blasting Tests……..269

7.3 Fragmentation Based on Fragments Volumes……271

7.4 Selection of the Brittleness Concept for Different Measures of Fragmentation…….273

7.4.1 Brittleness Concepts and Fragment Size as a Measure of fragmentation from Compression Tests……..……...273

7.4.2 Brittleness Concepts and Fragment Size as a Measure of fragmentation for Blasting Tests……..……..274

7.4.3 Brittleness Concepts and Fragment Volumes as a Measure of fragmentation from Blasting Tests……..……..275

7.5 Modification to the Kuz-Ram Model……..276

CHAPTER EIGHT

CONCLUSIONS AND RECOMMENDATIONS

8.1 Conclusions ……281

8.1.1 Fragment Size from Compression Tests……..281

8.1.1.1 *Comparison of Fragment Size from Compression with Static Mechanical Properties*…..……..282

8.1.1.2 *Comparison of Fragment Size from Compression with Dynamic Properties*……..282

8.1.1.3 *Comparison of Fragment Size from Compression Tests with Brittleness Based on Static Mechanical Properties*…..……..282

8.1.1.4 *Comparison of Fragment Size from Compression Tests with Brittleness Based on Moduli*……..……...282

8.1.1.5 *Comparison of Fragment Size from Compression Tests with Brittleness Based on Normalised Stress-Axial Strain Curves and Extension Strain Criterion*……..……..283

8.1.2 Fragment Size from Blasting Tests……..284

8.1.2.1 *Fragment Size from Blasting Tests and Brittleness Concepts Based on Static Mechanical Properties*…..……..284

8.1.2.2 *Fragment Size from Blasting Tests and the Brittleness Concepts Based on Rock Moduli*……..……...284

8.1.2.3 *Comparison of Fragment Size from Blasting Tests with Brittleness Based on Normalised Stress-Axial Strain Curves and Extension Strain Criterion*……..……..285

8.1.3 Fragment Volumes and Brittleness ……285

8.1.4 Selection of Brittleness Concept Based on Different Measures of Fragmentation…….286

8.1.5 Brittleness Concept for Different Measures of Fragmentation……... 286

8.2 Further Research and Recommendations ……..288

8.2.1 Further Research ……288

8.2.2 Recommendations…….. 289

REFERENCES……291

APPENDICES…….322

APPENDIX 1.1 Rock Specimen Preparation, Water and Density Determination……..…….…322

APPENDIX 1.2 MTS (815) Testing System…….330

APPENDIX 1.3 MPT PROCEDURE TESTING TEMPLATE AND PARAMETERS……..339

APPENDIX 2.1 BRAZILIAN TENSILE TEST, LOAD AND COMPRESSION CURVES…..348

APPENDIX 2.2 CHARACTERISTIC PRE- AND POST-FAILURE CURVES……358

APPENDIX 3.1 COMPARISON OF FRAGMENTATION FROM COMPRESSION AND STATIC MECHANICAL PROPERTIES……377

APPENDIX 3.2 COMPARISON OF FRAGMENTATION FROM COMPRESSION AND BRITTLENESS BASED ON STATIC MECHANICAL PROPERTIES……380

APPENDIX 3.3 COMPARISON OF FRAGMENTATION FROM COMPRESSION AND BRITTLENESS BASED ON MODULI……..382

APPENDIX 3.4 COMPARISON OF FRAGMENTATION FROM COMPRESSION WITH BRITTLENESS BASED ON NSSC AND CRITICAL EXTENSION STRAIN……386

APPENDIX 4.1 TOTAL NUMBER OF FRAGMENTS PER VOLUME OF ROCK AND BRITTLENESS BASED ON STATIC MECHANICAL PROPERTIES……387

ENDIX 4.2 TOTAL NUMBER OF FRAGMENTS PER VOLUME OF ROCK AND BRITTLENESS BASED ON MODULI……..388

APPENDIX 4.3 VOLUMES OF FINES PER VOLUME OF ROCK PRODUCED AND BRITTLENESS BASED ON MODULI……..390

APPENDIX 4.4 VOLUMES OF FINES PER VOLUME OF ROCK PRODUCED AND BRITTLENESS BASED ON NSSC……..392

FIGURES

Figure 1.1 Principles of closed-circuit servo-controlled system (Hudson et al., 1971)……8

Figure 1.2 Classification of rock into Class I and Class II behaviour in uniaxial compression tests (ISRM, 2007)……9

Figure 1.3 Schematic stress-strain curve for constant strain rate loading of a Class I rock (Okubo & Nishimatsu, 1985, p. 324)……10

Figure 1.4 Schematic stress-strain curve of Class II rock (Okubo & Nishimatsu, 1985, p. 324)……10

Figure 1.5 Elastic strain energy per unit volume as the area under the stress-strain curve.11

Figure 2.1 Randomly-spaced cracks, crack propagation and coalescence (Germanovich et al., 1994)……18

Figure 2.2 Stress (σ=compressive, σ_t=tensile) concentrates around the crack tips of enlargement of the circled area in Figure 2.1b (modified by author after Broek, 1986)……18

Figure 2.3 Scheme of brittle fracture processes in rock (Bieniawski, 1967a)……21

Figure 2.4 Stress-strain diagram showing stages in the failure process (Martin, 1993; Martin & Chandler, 1994)……22

Figure 2.5 Mechanism of brittle fracture of rock in compression showing stages in the failure process (Bieniawski, 1967d, p. 426)……23

Figure 2.6 Relationship between axial stress and volumetric strain for South African Quartzite in uniaxial compression tested in a conventional loading machine (a) (Bieniawski, 1967c)……26

Figure 2.7 Stress-strain curves for South African Norite in uniaxial tension (Bieniawski,1967d)……27

Figure 2.8 Effect of specimen diameter on compressive strength of Longmont sandstone (unit adjusted after Hoskins & Horino, 1969)……30

Figure 2.9 Influence of specimen size on the strength of intact rock (Hoek & Brown, 1980).31

Figure 2.10 Uniaxial compressive strength of seven sedimentary rocks tested on specimens at eight different diameters (Hawkins, 1998)……..31

Figure 2.11 Pre-failure and post-failure stress-strain curves for specimens with a certain value of length to diameter ratio 1/3:1, 1:1 and 3:1 but different sizes. (a) Numerical results by EPCA3D (Pan et al., 2009) and (b) laboratory results (Hudson et al., 1972)……..33

Figure 2.12 Pre-failure and post-failure stress–strain curves for different specimen shapes (a) Numerical results by EPCA3D (Pan et al., 2009) and (b) laboratory results (Hudson et al., 1972)……36

Figure 2.13 Relationship between UCS and L/D ratio for the data on Westerly Granite rocks tested by Mogi (2007)……37

Figure 2.14 Relationship between L/D ratio and UCS value for dry Sandstone (John, 1972)……37

Figure 2.15 Influence of the body shape and height-diameter ratio (H/D) on compressive strength (Andreev, 1995)……..38

Figure 2.16 Pre-failure and post-failure axial stress–axial strain curves of marble samples with different flaw geometries (Yang et al., 2009)……..40

Figure 2.17 Simulated strength reductions with end constraint for specimens with different loading platens in terms of Young's modulus using RFPA2D (Tang et al., 2000)……42

Figure 2.18 Relationship between uniaxial strength and length to diameter ratio of rock specimen with different sizes, with and without considering loading platen effect (a & c) EPCA3D simulated result (Pan et al., 2009) and (b) laboratory result (Yang et al., 2005 as contain in Pan et al., 2009)……44

Figure 2.19 Strength of Granite, Limestone, and Sandstone in uniaxial compression at low temperatures (Mellor, 1973)……..47

Figure 2.20 Effect of temperature on deformation parameters and strength values of Granite (Lau et al., 1991)……48

Figure 2.21 Relationships between: (a) the uniaxial compressive strength and the quartz to feldspar ratio, (b) uniaxial compressive strength versus mean grain size (quartz size) (Tugrul & Zarif, 1999)……48

Figure 2.22 Variation of compressive strength with strain rate after Kobayaski (1970) (a) and uniaxial compression tests from earlier studies showing different strain-rate sensitivities of compressive strength (b) (Blanton, 1981)……..50

Figure 2.23 The variation of the Young's modulus and Poisson's ratio with the loading rate (Zhao et al., 1999)……51

Figure 2.24 Energy plotted against strain rate for the variable speed unconfined compressive strength test (Whittles et al., 2006)……52

Figure 2.25 Stress-strain curves for six representative rock types in uniaxial compression (Wawersik & Fairhurst, 1970)……55

Figure 2.26 Normalised stress-strain curves in tension and compression (a) lnada Granite (b) Sanjome Andesite (c) Akiyoshi Marble (d) Tage Tuff (Okubo & Fukui, 1996)……59

Figure 2.27 Stress-strain curve for sandstone tested under servo-controlled machine (Rini & Mord, 2008)……60

Figure 2.28 Stress–strain curve of six different Sandstone specimens tested under later servo-controlled machine (Brijes & Dachao, 2013)……60

Figure 2.29 Stress–strain curve of different Coal specimens tested under servo- controlled machine (Brijes & Dachao, 2013)……61

Figure 2.30 Influence of strain rate on post-failure behaviour of Arkose Sandstone and Charcoal Granite in uniaxial compression in a servo-controlled testing machine (Pan, 1973)……63

Figure 2.31 Predicted stress-strain curves for the Ibbenburen Sandstone model cores with a different strain rate using PFC3D (Jackson et al., 2008)……..64

Figure 2.32 Relationship of fragmentation with P-wave velocity and dynamic elastic modulus (Hossaini et al., 2013)……..66

Figure 2.33 Concentration of increasing rising cracks result in an oblique fracture (Germanovich & Dyskin, 1988; Horii & Nemat-Nasser, 1985)……..78

Figure 2.34 Photograph of the pre- and post-test sample core debris from the Ibbenburen Sandstone and Caldon low Limestone, showing changes in fragments size with strain rate (Whittles et al., 2006)……81

Figure 2.35 Photographs of the pre- and post-test sample core debris from the Melton Ross chalk, showing changes in fragments size with strain rate (Whittles et al., 2006)……..81

Figure 2.36 Quantities participating in brittleness determination in stress-strain curve (Andreev, 1995)……85

Figure 2.37 Illustration of cohesion-loss and frictional strengthening as a function of plastic strain (Hajiabdolmajid & Kaiser, 2003)……..86

Figure 2.38 Stress-strain relationships for elastic perfectly plastic and a rigid plastic material….97

Figure 2.39 Mohr Coulomb's equation from a plot of axial stress against confining pressure…..99

Figure 2.40 Calculation of Energy released at post-peak (Tarasov, 2012)……...101

Figure 2.41 Scale of rock brittleness index, with brittleness increasing from left to right (Tarasov & Potvin, 2013)……..103

Figure 2.42 Estimation of elastic strain energy and rupture energy from pre-failure (a) and post-failure (b) stress-strain curves (Tarasov, 2011)……..105

Figure 3.1 A dual-beam oscilloscope at centre with it main parts enlarged by it sides.116

Figure 3.2 Layout of the electronic component for sonic velocities determination (ISRM, 2007)……..119

Figure 3.3 MTS Criterion 45……121

Figure 3.4 (a) MTS Criterion™ 45 features (b) TestWorks® 4 test window (c) graph review window……..122

Figure 3.5 (a) The press, below it is the specimen-platen arrangement (b) pendulum dynamometer, PD, below it is the pulley system……..124

Figure 3.6 (a) Strain gauge dimensions and (b) strain gauges in Wheatstone bridge connection configuration……128

Figure 3.7 Elastic modulus, *E*, determination……129

Figure 3.8 Schematic diagrams showing (a) open-loop control (b) closed-loop control……130

Figure 3.9 (a) Cross-section of a typical two-stage servo-valve (b) double acting hydraulic actuator (MTS, 1996)……131

Figure 3. 10 Post-failure modulus, *M*, determination for Mottled Anorthosite……133

Figure 3.11 (A) shows the 720 mg electric detonators, (B) shows one detonator inserted into each hole on the rock block, (C) shows the outer view of the blasting chamber and (D) shows the blasting pattern……135

Figure 4.1 XPL photograph of an opaque intragranular vein in sample Gabbro (field of view 2 mm)……141

Figure 4.2 XPL photograph of the relationship muscovite has with other minerals in Granite1 (field of view 2 mm)……142

Figure 4.3 XPL photographs of micro-cracks and vein-lets in Granite2 (field of view 2 mm)……143

Figure 4.4 XPL photographs of the intragranular fractures in Monzo-Granite sample (Granite3) (field of view 2 mm)……145

Figure 4.5 XPL photograph of Alkali Feldspar Granite (Granite4) showing the perthitic texture seen in feldspars (field of view 2 mm)……146
Figure 4.6 XPL photograph of the vague layering within sample of Leucocratic Monzo-Granite (Granite5) (field of view 2 mm)……147
Figure 4.7 XPL photograph of Marble (field of view 2 mm)……148
Figure 4.8 XPL photograph of Mottled Anorthosite (field of view 2 mm)……149
Figure 4.9 XPL photograph illustrating exsolution in pyroxene in Norite1 (field of view 2 mm)……150
Figure 4.10 XPL photograph illustrating the cumulus intercumulus relationship in Norite2 (field of view 2 mm)……151
Figure 4.11 XPL photograph of the intercumulus orthopyroxene in sample Norite3 (field of view 2 mm)……152
Figure 4.12 PPL photograph illustrating the features described in sample Quartz Arenite (field of view 2 mm)……153
Figure 4.13 XPL photograph of Quartzite1 (field of view 2 mm)……154
Figure 4.14 XPL photograph illustrating the cementation of the quartz grains in Quartzite2 (field of view 2 mm)……155
Figure 4.15 XPL photograph of Sandstone (field of view 2 mm)……156
Figure 4.16 XPL photograph of Spotted Anorthosite (field of view 2 mm)……157
Figure 4.17 PPL photograph illustrating the relationship the olivine grains have with one another in Troctolite1 (field of view 2 mm)……158
Figure 4.18 PPL photograph of a cluster of olivine grains in Troctolite2 (field of view 2mm)… ……159
Figure 4.19 Normalized stress-strain curves for Granite1……168

Figure 4.20 Normalized stress-strain curves for Granite2……169

Figure 4.21 Normalized stress-strain curves for Granite3……169

Figure 4.22 Normalized stress-strain curves for Granite4. ……170

Figure 4.23 Normalized stress-strain curves for Granite5. ……170

Figure 4.24 Normalized stress-strain curves for Marble. ……171

Figure 4.25 Normalized stress-strain curves for Norite1……171

Figure 4.26 Normalized stress-strain curves for Norite2……172

Figure 4.27 Normalized stress-strain curves for Norite3……172

Figure 4.28 Normalized stress-strain curves for Quartz Arenite. …… 173

Figure 4.29 Normalized stress-strain curves for Sandstone. ……173

Figure 4.30 Normalized stress-strain curves for Spotted Anorthosite. ……174

Figure 4.31 Normalized stress-strain curves for Trocolite1. ……174

Figure 4.32 Normalized stress-strain curves for Mottled Anorthosite. ……175

Figure 4.33 Normalized stress-strain curves for Quartzite1. ……176

Figure 4.34 Normalized stress-strain curves for Troctolite2……176

Figure 4.35 Normalized stress-strain curves for Gabbro. ……177

Figure 4.36 Normalized stress-strain curves for Quartzite2……178

Figure 5.1 Sieve sizes against cumulative percentages passing for the Class II rocks. ……187

Figure 5.2 Sieve sizes against cumulative percentages passing for Class I rocks……187

Figure 5.3 Comparison of the sieve sizes against the cumulative percentage passing from compression test of the rocks selected for blasting test……189

Figure 5.4 The sieve sizes against cumulative percentage passing for blasting test……190

Figure 5.5 Comparison of X_{50s} for Class I and Class II rocks of similar UCS values……191

Figure 5.6 Comparison of X_{10s} for Class I and Class II rocks of similar UCS values……192

Figure 5.7 Comparison of X_{50s} for Class I and Class II rocks of similar Brazilian tensile strength values……193

Figure 5.8 Comparison of X_{10s} for Class I and Class II rocks of similar Brazilian tensile strength values. ……193

Figure 5.9 The probability density distribution model for the combined sample……194

Figure 5.10 The probability density distribution model for the Class II rocks……195

Figure 5.11 The probability density distribution model for the Class I rocks……195

Figure 5.12 The probability density distribution model for the combined sample……197

Figure 5.13 The probability density distribution model for the Class II rocks……198

Figure 5.14 The probability density distribution model for the Class I rocks……198

Figure 5.15 Elastic modulus and passing sieve size at X_{50s} and X_{10s} for Class II rocks……210

Figure 5.16 UCS and passing sieve size at X_{50s} and X_{10s} for Class II rocks……211

Figure 5.17 BTS and passing sieve size at X_{50s} and X_{10s} for Class II rocks……211

Figure 5.18 P-wave velocity (m/s) against X_{50s} and X_{10s} for Class II rocks……213

Figure 5.19 B_{13} (MPa)^2 against X_{50} and X_{10} for Class II rocks……215

Figure 5.20 B_{14} (MPa)^2 against X_{50} and X_{10} for Class II rocks……215

Figure 5.21 B_{13} (MPa)^2 against post-failure modulus for Class I and Class II rocks……216

Figure 5.22 B_{16} (GPa)^2 against passing sieve size for Class II rocks……217

Figure 5.23 B_{16} (GPa)^2 against passing sieve size for Class I rocks……218

Figure 5.24 Brittleness k against passing sieve size for combined sample……219

Figure 5.25 Brittleness k against passing sieve size for Class I rocks……219

Figure 5.26 Brittleness k_2 against passing sieve size for combined sample……220

Figure 5.27 Brittleness k_2 against passing sieve size for Class I rocks……221

Figure 5.28 Normalised stress-axial strain curve showing rock stiffness……225

Figure 5.29 NSSC Estimation for Spotted Anorthosite……226

Figure 5.30 NSSC and passing sieve size for Class II rocks……227

Figure 5.31 NSSC and passing sieve size for Class I rocks……228

Figure 5.32 Different stress-strain behaviours……229

Figure 5.33 Critical extension strain estimation for Norite3. ……231

Figure 5.34 Critical extension strain for Class II rocks against passing sieve size (mm)……232

Figure 5.35 Critical extension strain for Class I rocks without Marble data against passing sieve size (mm) ……233

Figure 5.36 Critical extension strain against brittleness B_{16} (GPa)^2 ……233

Figure 5.37 Critical extension strain against brittleness NSSC for Class II rocks……234

Figure 5.38 Critical extension strain against post-failure modulus (GPa)……234

Figure 5.39 B_{11} and 50 % passing sieve size for compression and blasting tests……236

Figure 5.40 B_{11} and 10 % passing sieve size for compression and blasting tests……236

Figure 5.41 B_{13} and 50 % passing sieve size for compression and blasting tests……237

Figure 5.42 B_{13} and 10 % passing sieve size for compression and blasting tests……237

Figure 5.43 B_{14} and 50 % passing sieve size for compression and blasting tests……238

Figure 5.44 B_{14} and 10 % passing sieve size for compression and blasting tests……238

Figure 5.45 B_{16} and 50 % passing sieve size for compression and blasting tests for Class II rocks……240

Figure 5.46 B_{16} and 10 % passing sieve size for compression and blasting tests……240

Figure 5.47 Brittleness k and 50 % passing sieve size for compression and blasting tests……241

Figure 5.48 Brittleness k and 10 % passing sieve size for compression and blasting tests……241

Figure 5.49 Brittleness NSSC and 50% passing sieve size for compression and blasting tests……243

Figure 5.50 Brittleness NSSC and 10 % passing sieve size for compression and blasting tests……243

Figure 5.51 Brittleness NSSC and 50 % passing sieve size for compression and blasting tests for class II rocks……244

Figure 5.52 Brittleness NSSC and 10 % passing sieve size for compression and blasting tests for class II rocks……244

Figure 5.53 Brittleness estimated as Critical Extension Strain and 50% passing sieve size for compression and blasting tests for combined sample……246

Figure 5.54 Brittleness estimated as Critical Extension Strain *and* 10% passing sieve size for compression and blasting tests for combined sample……246

Figure 5.55 Brittleness estimated as Critical Extension Strain and 50% passing sieve size for compression and blasting tests for Class II rocks……247

Figure 5.56 Brittleness Critical Extension Strain and 10 % passing sieve size for compression and blasting tests for Class II rocks……247

Figure 6.1 Total number of fragments per volume of rock from both tests and brittleness B_{11}……255

Figure 6.2 Total number of fragments per volume of rock from both tests and brittleness B_{12}……256

Figure 6.3 Total number of fragments per volume of rock from both tests and brittleness B_{16} $(GPa)^2$. ……257

Figure 6.4 Volume of fines per volume of rock produced (mm_3) from both tests and brittleness B_{11}. ……258

Figure 6.5 Volume of fines per volume of rock produced (mm_3) from both tests and brittleness B_{12}. ……259

Figure 6.6 Volume of fines per volume of rock produced (mm^3) from both tests and brittleness B_{13}. ……259

Figure 6.7 Volume of fines per volume of rock produced (mm^3) from both tests and brittleness B_{14} $(MPa)^2$. ……260

Figure 6.8 Volume of fines produced (mm^3) from both tests and brittleness B_{16} $(GPa)^2$……261

Figure 6.9 Volume of fines per volume of rock produced (mm^3) from both tests and Extension Strain Criterion……262

Figure 6.10 Elastic strain energy per unit volume, $(J/mm)^3$ and total number of fragments per volume of rock (mm^{-3}) ……263

Figure 6.11 Elastic strain energy per unit volume, $(J/mm)^3$ and post-failure modulus……263

Figure 7.1 critical extension strain, e_c and X_{50b} passing sieve size (mm)……277

Figure 7.2 critical extension strain, e_c and fragmentation quotient, *fi*.……279

TABLES

Table 2.1 Method of stress threshold identification based on stress-strain curves (Yathavan & Stacey, 2004). ……..……..28

Table 2.2 Effect of moisture on UCS (Obert et al., 1946). ……46

Table 4.1 Percentage of light coloured minerals and dark coloured minerals for rocks selected for blasting tests. ……...……..…140

Table 4.2 Dynamic properties of rocks. ……..…….160

Table 4.3 Static mechanical properties of rock…..…….……..162

Table 4.4 Brittleness indices based on static mechanical properties of rock…..……..180

Table 4.5 Brittleness concepts based on moduli……..…….181

Table 5.1 Comparisons of passing sieve size at X_{50s} and X_{10s} for segregated and combined models…….196

Table 5.2 Comparisons of X_{50b} and X_{10b} for the segregated and combined models…...……...199

Table 5.3 Coefficients of correlation with fragmentation……..……...201

Table 5.4 Correlations……...……202

Table 5.5 Model Summary……..…….203

Table 5.6 ANOVA…….……...203

Table 5.7a Coefficients at 10% passing sieve sizes……..204

Table 5.7b Coefficients at 50% passing sieve sizes……..204

Table 5.8 Collinearity Diagnostics……..…….204

Table 5.9 Excluded Variables……...……....205

Table 5.10 Correlation coefficient of brittleness based on NSSC and e_c with fragments size from compression……...…….249

Table 5.11 Correlation coefficients of the various brittleness concepts with fragmentation (fragments size) for compression and blasting tests. ……..252

Table 6.1 Various Brittleness and Fragment volumes from both compression and blasting tests…..……265

Table 7.1 Relationship between brittleness and fragmentation from the compression tests based on X_{50s} and X_{10s} passing sieve size. ……...267

Table 7.2 Relationship between brittleness and fragmentation from blasting tests based on % passing sieve size. ……...……270

Table 7.3 Various brittleness and fragments volumes from both compression and blasting tests…….272

Table 7.4 Fragmentation and brittleness (based on critical extension strain, e_c) scale…….....…..278

CHAPTER ONE

INTRODUCTION

1.1 Introduction

The main purpose of this research is to provide an understanding about the relationship between fragmentation and brittleness of rocks under steady and dynamic loading conditions. Based on the post-failure characteristic behaviour of rocks, Class II rocks are more brittle than Class I rocks, and in addition these have a self-sustained failure beyond its post-failure region. As a result, this research intended to show whether or not the self-sustained failure of rock during uniaxial compression test relates to its fragmentation. In addition, an attempt was made to demonstrate if the brittleness of rock is related to fragmentation in a blasting application. It was therefore necessary to explore the relationship between fragmentation and brittleness.

The research involved the analyses of fragmentation and brittleness of the rocks in order to establish a connection between them. The method of research was through laboratory determination of the rock's properties according to ISRM (2007) suggested methods and its brittleness, with a practical application of fragmentation of the rocks through laboratory scale blasting tests.

Therefore in this work, brittleness is considered a very important intact rock mechanical property that has a strong influence on the failure process and on the fragmentation of rock. Part of the purpose of this investigation is to determine whether a relationship exist between brittleness and fragmentation. No research have attempted to link brittleness and fragmentation together.

A statistical analysis is done using stepwise multiple regression technique to show whether or not brittleness is related to fragmentation of rock under unconfined uniaxial compressive failure using variety of widely used brittleness concepts in the literature. The relationship between them is also compared under laboratory scale blasting test. Additional analyses were done with other concepts to see the validity of the relationship and provide suitable concept for both compression and blasting tests. The possibility of incorporating this into the Kuz-Ram model is assessed to account for the effect of rock brittleness on fragmentation.

The following sections begin with a statement of the relevance of the subject matter. Thereafter, the research question is provided. The thesis objectives and contribution to knowledge are itemised. Next is the explanation on brittle behaviour to distinguish between Class I and Class II rocks. The brittle behaviour which distinguishes the rocks as Class I or Class II is based on their post-failure regime. In addition, there is an overview of the testing system used to study this behaviour in the laboratory. Lastly, discussion on the brittleness and fragmentation of rock is provided.

1.2 Statement of Problem and Motivation for the Research

This research investigates the relationship between the shattering of brittle rocks under steady and dynamic loads (fragmentation by explosive) and its brittleness. Brittleness is described as a property of material to shatter with little or no ductility (Yarali & Soyer, 2011). This brittleness property of rock to shatter is quantified by Tarasov (2010; 2011) and Tarasov and Potvin (2013) as the capability of the rock to self-sustaining failure. The brittleness quantification depends on the stored elastic energy available in the post-failure region to shatter the rock. Therefore, the shattering of rock or its fragmentation depends on its self-sustaining failure and the energy available in the post-failure region.

Thus, the fragmentation produced under this condition depends to a large extent on the energy available to cause fragmentation and its self-sustaining failure or brittle nature. In the literature, it appears that no research has attempted to link brittleness and fragmentation and the self-sustaining failure behaviour of rocks at the post-peak region. Rock failure under dynamic loading conditions as experienced in blasting, rockbursting, crushing, milling, as well as during conventional unconfined compressive strength testing of rock specimens and the subsequent fragments size distribution is a little-understood phenomenon. The brittleness of a rock has a significant effect on its behaviour under such loading conditions and in the fragments that result.

At present, there is no satisfactory theoretical basis for predicting dynamic failure behaviour, brittleness and fragmentation, and such a prediction could be useful in

the solution to many practical mining and civil engineering problems. For example, effectiveness of all the subsystems in the mining operations (e.g. loading, hauling and crushing) depends on an optimal fragmentation quality prediction (control of fines and oversize of fragmented rocks). In addition, the rapid mining of ore bodies, design of stable structures and the efficiency of rock fragmentation processes can be designed and evaluated with more accuracy.

Therefore, knowledge of the brittleness of the rock and its post-failure characteristics could enable the designer reduce potential hazards in relation to rock failure under compression and better understanding of rock fragmentation. For example, in the evaluation of the potential of rockburst near underground openings, the determination of the post-failure behaviour of rock is required to assess if a possible failure will be gradual or violent (Simon et al., 2003). Furthermore, an evaluation of rock mass response to mining or tunnelling activities as a result of dynamic processes particularly associated with fragmentation and seismicity, the correct determination of brittleness of the rock "at such loading conditions is important to better predict and mitigate these dynamic" and potential catastrophic events (Tarasov & Potvin, 2013, p. 57). These issues motivated this research.

1.3 Research Question

Rocks are classified into Class I or Class II based on the characteristic shape of their post-failure curve. The failure of brittle rock occurs explosively in a conventional testing machine. Stiff testing made it possible to obtain the post-failure stress-strain curve of rock specimen. The characteristic shape of the curves (i.e. the pre-failure and post-failure moduli) is used to determine the brittleness of rock. It appears that no research has attempted to link rock brittleness, post-failure modulus (characterising Class I and Class II rocks) and its corresponding fragmentation under unconfined uniaxial compressive failure. This topic forms the focus of this research work. This research was undertaken to answer the question below:

- ***What is the relationship between brittleness and fragmentation of rock?***

1.4 Objective of Research

In an attempt to answer the research question above, the following was done:

(a) Determination of the intact rock properties (uniaxial compressive strength, post-failure modulus, Brazilian tensile strength, sonic velocities, density, elastic parameters, dynamic parameters and the petrographic examination of rock specimens).

(b) Determination of brittleness of the rocks and analysis of the fragments size distribution produced during blasting and compression tests.

(c) Comparison of the fragmentation of the rocks under compression and blasting tests with their brittleness.

In addition, the research seeks to provide answers to the following questions:

(d) Is there a link between fragmentation and brittleness from the compression tests? Therefore, can fragmentation of rocks be predicted from their brittleness?

In addition, Class II rocks have self-sustaining fracturing response during unconfined uniaxial compression test. Therefore, do Class II rocks relate more to fragmentation than Class I rocks under steady compressive test?

(e) Is there a link between fragmentation and brittleness from the blasting test? Therefore, can fragmentation of rocks be predicted from brittleness under blasting tests?

1.5 Contribution to Knowledge

The study contributed to knowledge by providing:

(a) An understanding of the relationship between the brittleness and fragmentation of rocks,
(b) An acceptable norm for describing the brittleness of rocks for the compression and blasting tests,
(c) Information on Class I and Class II rocks behaviour under steady fragmentation.

1.6 Laboratory Determination of Rock Parameters and Stiff Testing of Rock Specimen

In order to answer the research question and accomplish the set objectives so that the research could contribute to the body of knowledge, a well-planned and meticulous laboratory determination of the rock parameters was required. In addition, the rock samples were selected to include rock types that are homogeneous. The suggested ISRM (2007) standard was followed in the determination of the rock parameters. The reason for the choice of ISRM standard is provided in Chapter 2.

There is difficulty with the laboratory determination of the post-failure curve of rocks using conventional equipment. Rock specimens are often in an unstable state at the point of failure as most testing machines tend to be soft. Rock specimens break explosively at their ultimate strength and no further information could be obtained. Simon et al. (2003) observed that the laboratory determination of the post-failure properties during uniaxial compression test on brittle rocks is often difficult to realise. Shimizu et al. (2010) concurred that there are still complications in achieving post-failure stress-strain curve of brittle rocks in the laboratory experiments.

However, Okubo and Fukui (1996) and recently Brijes and Dachao, 2013 obtained pre-failure and post-failure stress-strain curves for different rocks under uniaxial compression tests with the use of a closed-loop servo-controlled testing machine. A closed loop servo-controlled testing machine is the only practical way

to avoid explosive breakage of a rock specimen when the ultimate strength is reached. Figure 1.1 shows the principle of a closed loop, servo-controlled testing machine. A transducer is attached to the rock specimen. It generates a signal that is compared with the program instruction where constant strain rate or deformation is considered as the control variable. If the transducer signal is not equal to the program instruction value, the hydraulic system automatically adjust the servo-valve until the transducer signal agrees with the program value. The efficiency of the testing machine, therefore depends on the capability of the servo-valve to respond quickly enough to correct the error and prevent release of strain energy after the peak strength of the rock is reached.

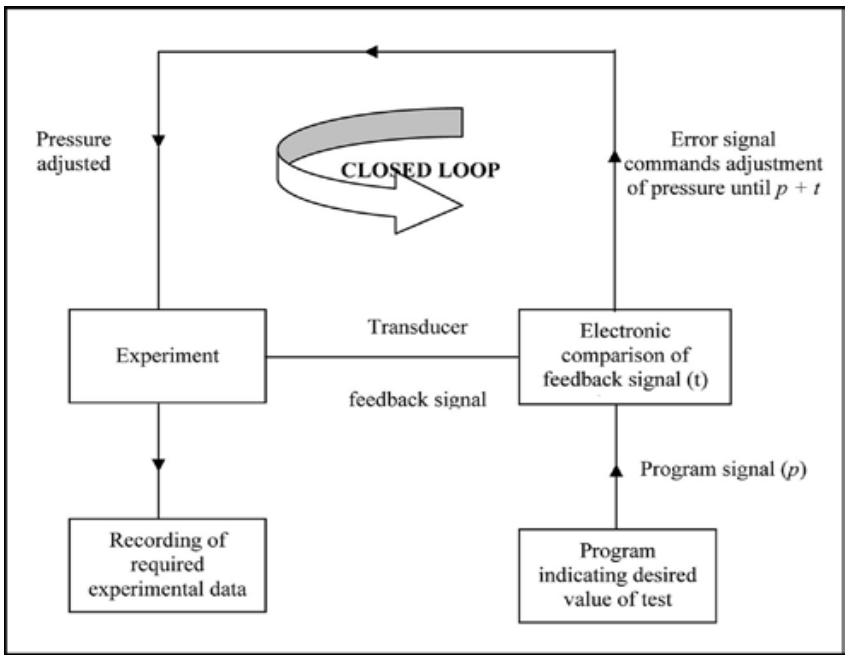

Figure 1.1 Principles of closed-circuit servo-controlled system (Hudson et al., 1971).

1.7 Class I and Class II Rocks

Figure 1.2 shows the pre-failure and post-failure stress-strain curves that were obtained from a closed-loop servo-controlled testing machine. Wawersik and Fairhurst (1970) classified rocks into Class I and Class II according to their failure behaviour in a uniaxial compression tests. Beyond the post-peak region, either the curve increases continuously in strain or it does not. If it increases in strain, it is Class I, if it does not, then it is a Class II rock.

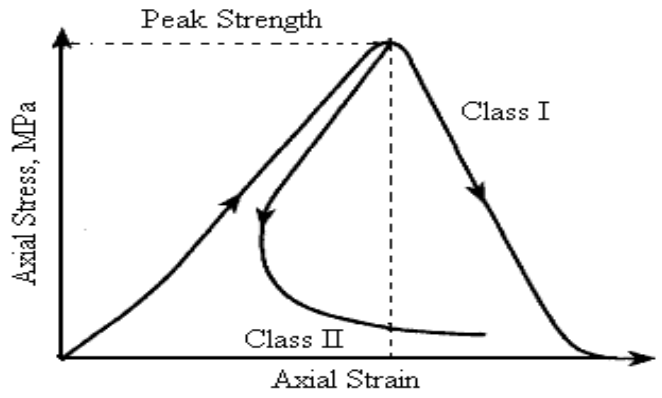

Figure 1.2 Classification of rock into Class I and Class II behaviour in uniaxial compression tests (ISRM, 2007).

Rock specimens that display characteristic curve of Class I are less brittle in nature under axial load and continue to increase in strain. The Class I part of Figure 1.2 is shown in Figure 1.3 (strain increases from a to d). Experiments performed in an axial strain control are usually satisfactory to obtain the Class I behaviour. A different control procedure is important to obtain the Class II curve as the curve does not show a continued increase in strain after the peak strength. Figure 1.4 illustrates the Class II part of Figure 1.2. Strain increases up to the

ultimate strength and decreases with decreasing stress after the ultimate strength was reached. Rock specimens that display Class II behaviour are likely to react in a brittle fashion to axial loading. Such stress-strain curve is characterised by a positive slope in the post-failure region, in contrast to the Class I behaviour with a persistently negative post-failure slope to the stress-strain curve.

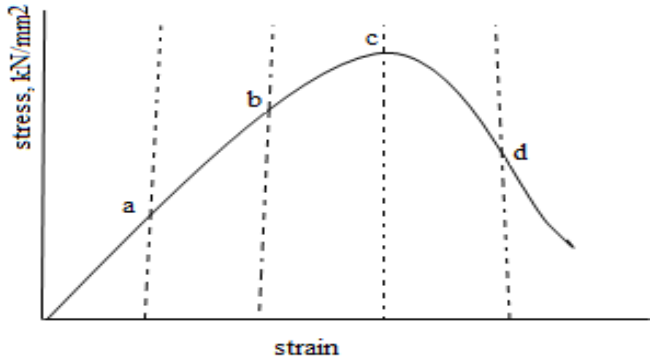

Figure 1.3 Schematic stress-strain curve for constant strain rate loading of a Class I rock (Okubo & Nishimatsu, 1985, p. 324) (strain increases continually from a to c at peak strength and continues to increase to d).

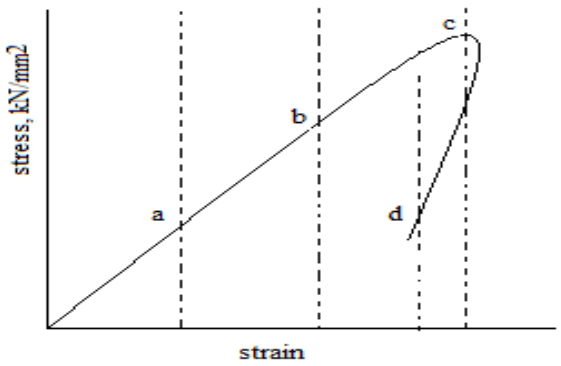

Figure 1.4 Schematic stress-strain curve of Class II rock (Okubo & Nishimatsu, 1985, p. 324) (strain increases from a to c at peak strength and decreases from peak strength to d).

1.8 Elastic Strain Energy

As a rock is deformed under axial load it stores elastic strain energy per unit volume of the rock. Strain energy is stored within the specimen when the specimen is deformed under stress since the load or stress does work on the specimen which it deforms. Without energy losses, the strain energy is equal to the work done on the specimen by the external load or stress. By the principle of conservation of energy, the energy in the specimen is stored as elastic strain energy. Figure 1.5 below shows the stress-strain curve up to the elastic limit.

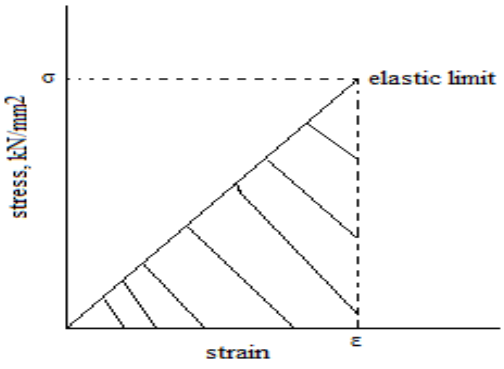

Figure 1.5 Elastic strain energy per unit volume as the area under the stress-strain curve.

When the stress is equal to the specimen's ultimate strength or lower (i.e. the specimen is in the elastic range), the strain energy per unit volume is the area under the stress-strain curve (the shaded area). This is expressed in Equation 1.1:

$$w_e = \tfrac{1}{2}\sigma \times \varepsilon \qquad (1.1)$$

This is the energy absorbed by the specimen with stress, σ in straining the specimen by ε. The accumulated elastic strain energy per unit volume at failure is a direct function of compressive strength, σ and elastic modulus, E and is expressed by.

As $\varepsilon = \sigma / E$, it follows that:

$$w_e = \sigma^2 / 2E \tag{1.2}$$

The equation above reveals that for any given increment in strength, accumulated elastic strain energy per unit volume increases in proportion to the square of the stress. Therefore, the energy required to initiate breakage is proportional to the square of the strength of the material.

1.9 Laboratory Determination of Fragmentation and Brittleness of Rocks

During the determination of uniaxial compression strength of brittle rocks, rock specimens often shatter at their peak load. Unfortunately, the fragments are not usually subjected to thorough analysis. Instead, the fragments are counted or by visual observation. For example, Whittles et al. (2006) and Jackson et al. (2008) determined the effect of strain rate on degree of fragmentation. They determined the degree of fragmentation by counting the number of fragments produced after each test. The method used to estimate fragmentation by these authors appears not to satisfactorily describe the fragments produced in a statistical sense. Instead, in this research the fragments are characterised by sieve analysis and statistical

analysis are used to show the relationship of selected particle size with widely used brittleness definitions.

At present, the term ‘brittleness’ has no clear definition. Different definitions and methods used to determine this term are based on the purpose and its use. Therefore, these values vary from method to method. These include: determination from stress-strain curves, strain ratio, energy ratio, ratio of internal friction and strength ratio. This research assessed different brittleness concepts in order to give a true definition to brittleness based on its characteristic brittle behaviour during unconfined uniaxial compression test.

1.10 Thesis Layout

The thesis contains eight chapters. It begins with an introduction and overview of its contents and provides an explanation of various terminologies framing the thesis topic. Chapter 2 gives detailed explanation of existing theories and experimentation on the brittle failure of rocks. It also reviews past research on brittle failure of rock in unconfined uniaxial compression test. The influence of increased strain rate, rock structure (e.g. grain size, quartz content) and specimen size on the strength parameters and fragmentation of brittle rock are also identified. In addition, the different methods used to determine brittleness are assessed.

Chapter 3 describes the equipment and methodology used to determine the parameters of interest in the analysis. The methodology adopted is contained in the International Society of Rock Mechanics Commission on Testing (ISRM,

2007). Chapter 4 presents the results of the experimentation. The results are presented for discussion in tables and figures. Chapter 5 analyses the results based on fragments size at a certain selected percentage of sieve size for compression and blasting tests.

Chapter 6 further analyse fragmentation in terms of the total number of fragments per volume of rock and the volume of fines per volume of rock as a measure of fragmentation. These are done for both the compression and the blasting tests and are compared with the brittleness of the rocks. Chapter 7 encapsulates the findings in Chapters 5-6 in order to suggest a better concept that can be used to quantify brittleness based on different measures of fragmentation for the compression and the blasting tests. It also provides the links between brittleness and fragmentation. Chapter 8 provides the conclusion based on Chapters 5-7. It includes further research and recommendations.

1.11 Chapter Summary

Rocks are classified into Class I and Class II as a result of their characteristic post-failure curve. A stiff testing system using a closed-loop, servo-controlled testing machine is the only practical method to achieve this. The characteristic post-failure curve of rock is an indication of their brittle nature. As a result, this research intends to show whether or not the self-sustained fracturing behaviour of rock during uniaxial compression test relates its fragmentation. In addition, this research attempts to show if there exist a relationship between fragmentation and brittleness under compression and blasting tests.

The next chapter reviews the theory of brittle failure of rock under compression and the factors that affect the determination of its strength parameters. It reviews the pre-failure and post-failure curves and factors that affect its shape, and discuss various methods of brittleness determination.

CHAPTER TWO

LITERATURE REVIEW

2.1 Introduction

In order to study the relationship between the laboratory determination of rock brittleness and its fragmentation, it is essential to review the factors that can affect their determination. Therefore, this chapter reviews the factors affecting laboratory determination of rock strength parameters (macroscopic investigation). For better understanding of rock's brittleness, the use of a servo-controlled testing machine for classifying rocks into Class I or Class II is discussed. The methods used for assessing fragmentation are identified. In addition, various concepts used to quantify brittleness are assessed. Lastly, studies on brittleness and fragmentation of rocks that are relevant to this research are identified and discussed.

2.2 Micromechanics of Brittle Failure (Microscopic Failure)

All rocks contain some degree of imperfection (i.e. flaws or defects) which can be observed under the microscope. The strength of a rock is affected by the imperfection. The imperfection in rock acts as a zone of weakness which makes it exhibits low integrity compare with other parts. Hence, the presence of cracks in

rock reduces its strength. It is difficult to account for these imperfections in calculations based on laboratory test conducted on rock specimens. Nonetheless, reviewing the effect of the imperfection on the macroscopic deformation of a rock provides information for better understanding of the estimated parameters from laboratory tests.

The cracks or the imperfection in rocks are randomly scattered within the rock body (Figure 2.1a). When a rock is subjected to stress, the stress concentrates around the crack's tip. The crack begins to extend from its tip to other part of the rock. As the stress increases, the crack grows and unites with other cracks growing towards the same direction, thereby forming bigger cracks (Figure 2.1b). When the bigger cracks unite or intersect with other bigger cracks (coalesce) the rock cannot support an increase in load and the specimen fails (Figure 2.1c), and breaks to pieces.

As a consequence, when under compressive load some of the pre-existing and newly opened micro-cracks propagate, coalesce and finally lead to macro-crack. The growth of many cracks triggers interference and perhaps coalescence, both of which are capable of sustaining the growth to the extent to cause failure (Germanovich et al., 1994). In fact, the failure of the specimen starts when a (primary) crack starts to propagate. There are many theories in the literature that relate the failure of rock to cracks propagation.

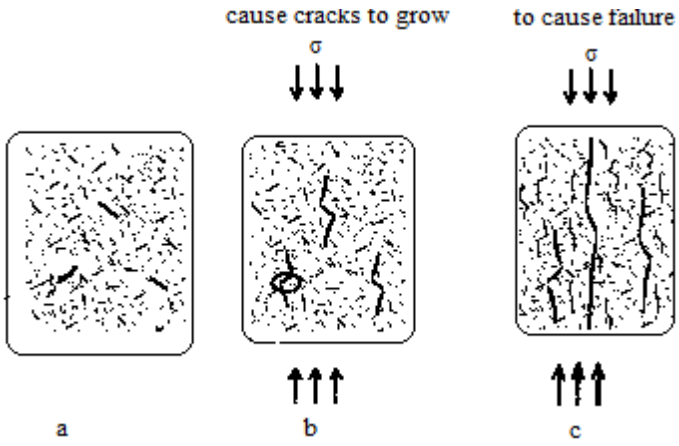

Figure 2.1 Randomly-spaced cracks, crack propagation and coalescence (Germanovich et al., 1994).

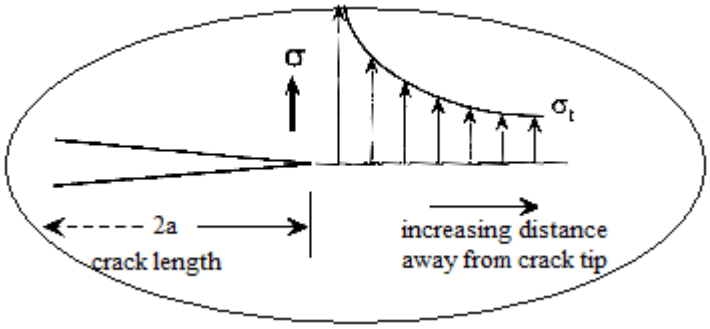

Figure 2.2 Stress (σ=compressive, σ_t=tensile) concentrates around the crack tips of enlargement of the circled area in Figure 2.1b (modified by author after Broek, 1986).

Most prominent of these theories is the Griffith Law. The Griffith Law postulates that when a material is under stress, the stress increases around a crack tip (Figure 2.2). The crack may be stable or unstable. The condition for stability is expressed in the terms of the strain energy gain and surface energy (i.e. the energy needed to disrupt the inter-molecular bonds within a material when a surface of unit area is

created) on the crack tip. In brittle materials, crack propagation and shattering of the specimen results when a critical stress value is exceeded at the crack tip.

Therefore, crack growth arises when surface energy gained during disruption of molecular bonds towards the crack pathway is equal to the net decrease in strain energy. In other words, the system is in a balanced state when the total potential energy (PE) of the system "is balanced by the elastic strain energy stored in the" material "and the surface energy in the free face" of the crack (Bieniawski, 1967c, p. 399). The expression is written as:

$$PE = w_e + w_s \qquad (2.1)$$

The stored elastic strain energy, w_e and surface energy in the free face of the crack, w_s are estimated as follows:

$$w_e = \frac{\pi T^2 \sigma^2}{E} \qquad (2.2)$$

Where T is the crack surface tension and E is the elastic modulus

As $$w_s = 4aT \qquad (2.3)$$

Where 'a' is the half length of the crack

It follows that the applied critical stress, σ which is necessary for stable crack propagation is given by:

$$\sigma \geq \sqrt{\frac{2ET}{\pi a}} \qquad (2.4)$$

Griffith (1924) claimed that a crowd of pre-existing, tiny cracks in a rock play considerable role in its brittle fracture under compression. Therefore, the rocks sampled in this research were, as far as possible, free from observable surface defects or cracks.

The deformation and fracture characteristics of brittle rock have been studied by many researchers (Brace, 1964; Bieniawski, 1967*b*; Wawersik & Fairhurst, 1970; Lajtai & Lajtai, 1974; Martin & Chandler, 1994). The common agreement among them is that the failure process occurs in stages. The stages are determined from stress-strain characteristic curves obtained from axial and lateral deformation measurements during laboratory uniaxial compression test. In the determination of the uniaxial compression strength of the rocks used in this study, it was considered necessary to evaluate these stages in order to assess the process that lead to the failure of the rocks.

2.2.1 Stages in the Deformation Process

Brace et al. (1966) and Bieniawski (1967*a*) evaluated stress-strain behaviour of a deformed material and classified the deformation steps in the brittle fracture process as follows:

- Crack closure,
- Linear elastic deformation,
- Crack initiation and stable crack growth,

- Critical energy release and unstable crack growth and
- Failure and post-peak behaviour.

Figure 2.3 illustrates the steps in a schematic flowchart.

.

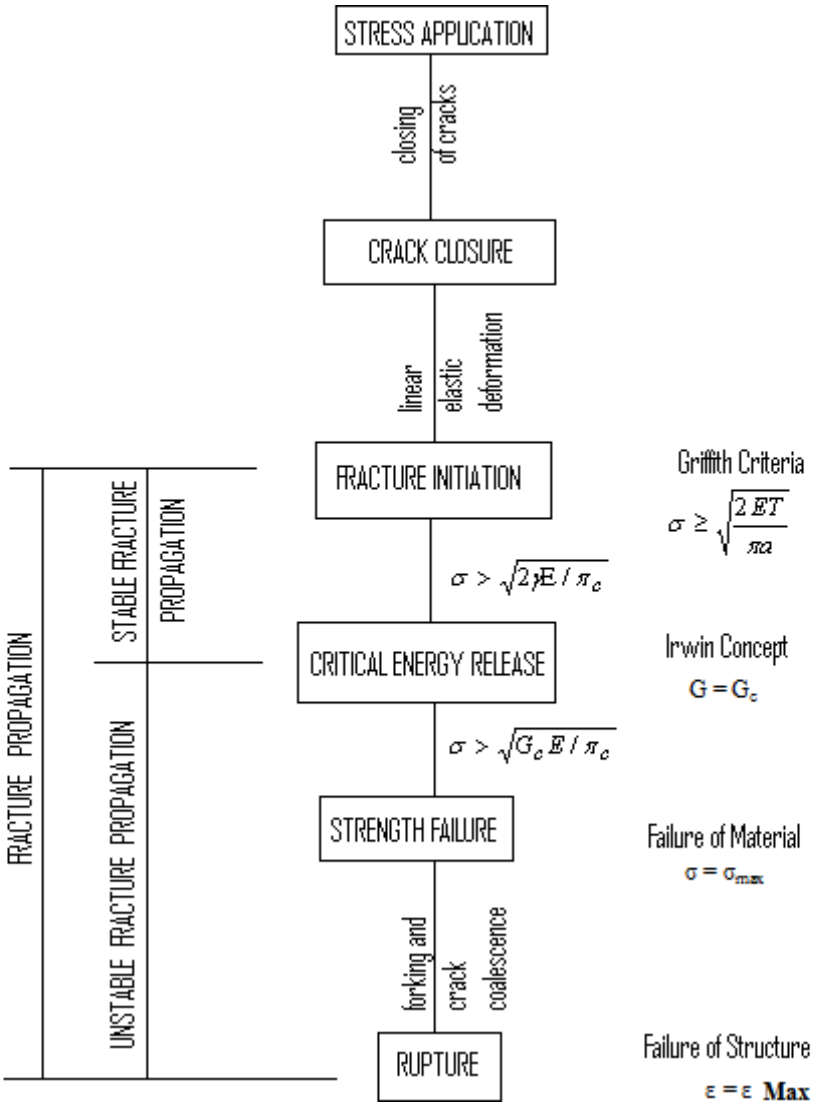

Figure 2.3 Scheme of brittle fracture processes in rock (Bieniawski, 1967a).

In order to evaluate the stages of deformation in rocks, Martin (1993) conducted uniaxial compression tests on cylindrical samples of continuous, homogenous, isotropic, linear and elastic (CHILE) massive Lac du Bonnet Granite obtained from the Underground Research Laboratory (URL) at 420 m below ground surface. The test was carried out to identity a suitable site for the disposal of radioactive wastes. The stages in the failure process are identified in the stress-strain curves (Figure 2.4).

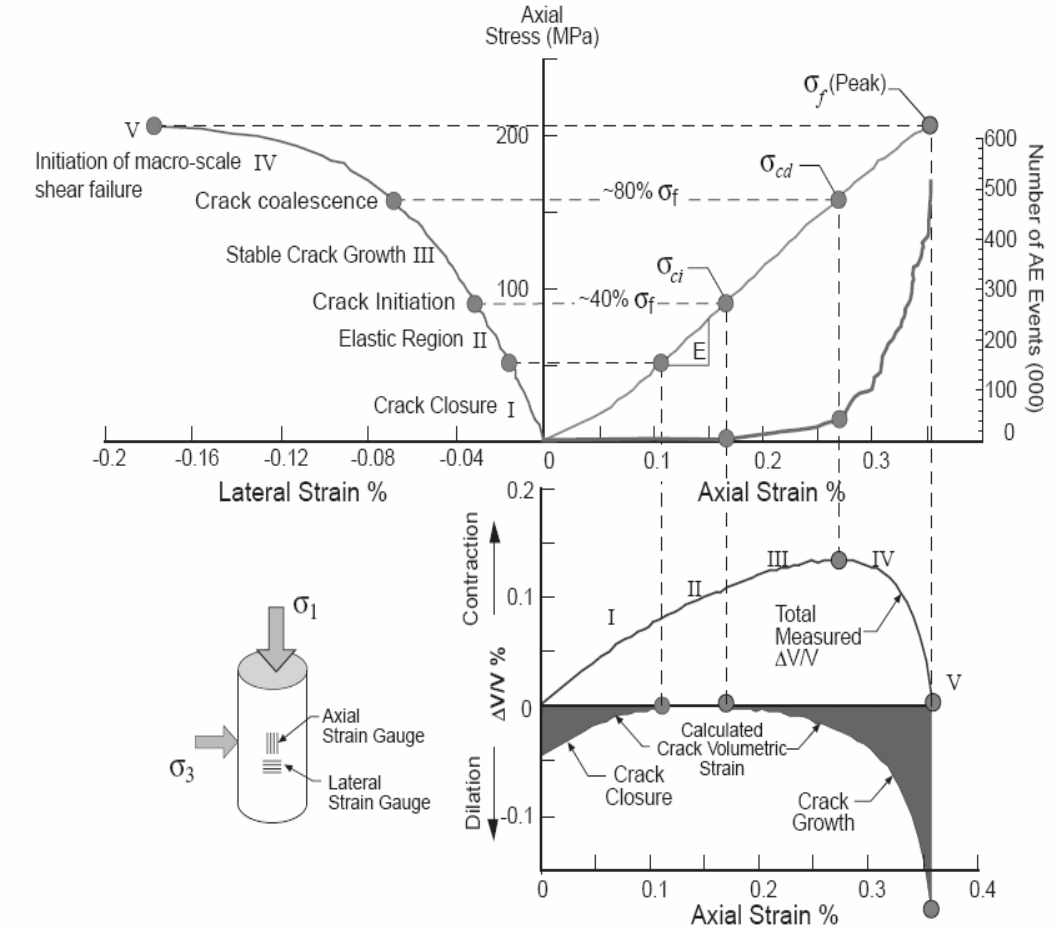

Figure 2.4 Stress-strain diagram showing stages in the failure process (Martin, 1993; Martin & Chandler, 1994).

Similarly, a study of compression tests on two South African hard rocks, namely a Norite (igneous rock) and Quartzite (metamorphosed sedimentary rock) was done in "order to eliminate, for the purpose of" the "investigation, the influence of non-homogeneity and anisotropy on the mechanism of rock" failure (Bieniawski, 1967b, p. 407) (Figure 2.5). It shows that there are similar steps in the failure process (with Figures 2.3 and 2.4). The steps in the failure process in Figure 2.4 and Figure 2.5 are discussed next.

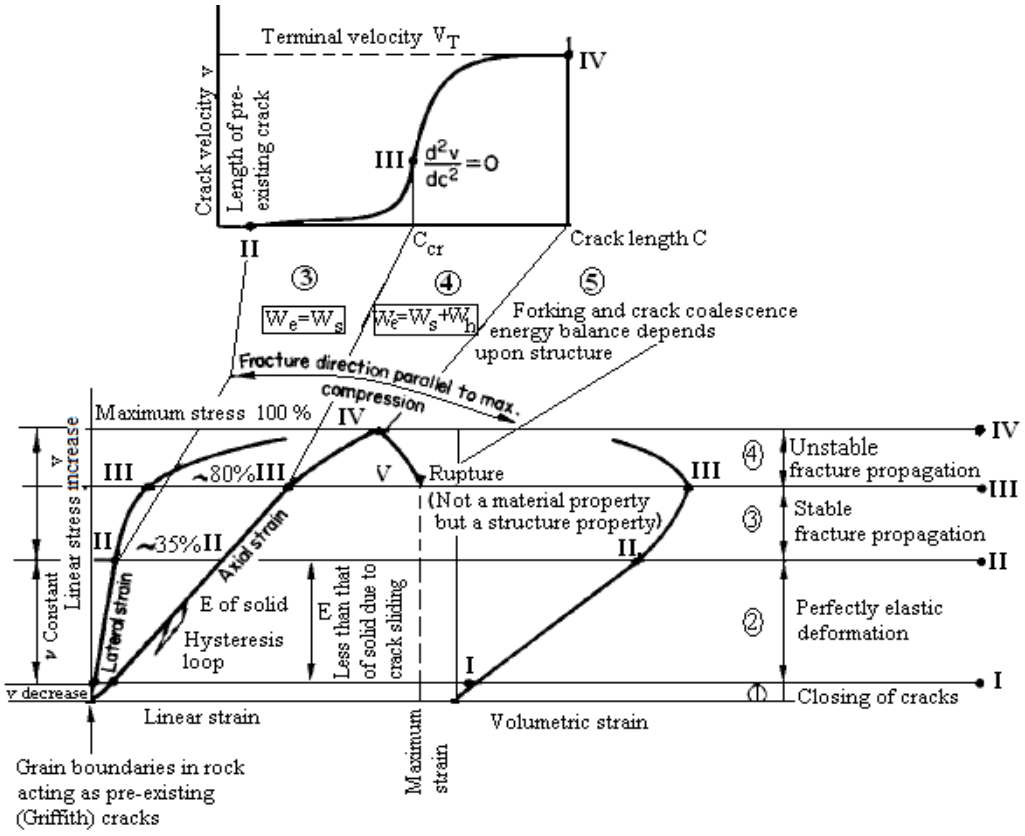

Figure 2.5 Mechanism of brittle fracture of rock in compression showing stages in the failure process (Bieniawski, 1967d, p. 426) (extracted from main diagram by author).

Crack closure occurs during the early stage of loading (crack closure corresponds to Stage 1 in Figures 2.4 and 2.5). At this stage, the stress-strain curve is slightly inclined towards the axial strain. As a result, the pre-existing cracks inclined to the applied load are closed (Eberhardt, et al., 1998). At the crack closure stage, the stress-strain curve is nonlinear and expresses an increase in axial stiffness (i.e. deformation modulus). The size of this nonlinearity depends "on the initial crack density and geometrical characteristics of the crack population" (Eberhardt, et al., 1998. P. 222). After the pre-existing cracks are closed, linear elastic deformation begins.

During the elastic deformation stage, the relationship between stress-strain curves is linear (Stage II in Figures 2.4 and 2.5). The elastic constants (Young's modulus, Poisson's ratio) of the rock are estimated from this linear portion of the stress-strain curve. Crack initiation stress (shown in Figure 2.4) represents the stress level when micro-fracturing begins. Zhang et al. (2011) defined crack initiation as the stress level that marks the start of dilation and crack propagation.

Moreover, crack propagation is considered as either stable or unstable (Martin, 1993). Stable crack (fracture) propagation begins at the end of Stage II while unstable propagation starts at Stage IV. At Stage III, cracks increase by a small quantity as a result of increase in stress level but these do not continue to extend at this stage to form macroscopic failure. Also at this stage (Stage III) fracture propagation is a function of the applied stress. At the beginning of crack propagation Griffith's criteria in Equation 2.4 is obeyed. During the stable condition, crack development can be arrested by the removal of the applied stress.

On the other hand, unstable crack growth occurs at the point of reversal of the volumetric strain curve (Figures 2.4 and 2.5). This stage is known as the point of critical energy release or crack-damaged stress threshold (Martin, 1993). Bieniawski (1967c) defined unstable crack propagation as the condition which occurs when the relationship between the applied stress and the crack length ceases to exist. Therefore, this is when the crack growth velocity, takes over in the propagation process. Unstable fracture propagation starts when the strain energy release rate in Equation 2.4 attains a critical value (Kemeny & Cook, 1986). The cracks continue to extend because of the strain energy stored within the specimen.

In addition, the velocity of the crack propagation increases from Stage III and reaches its maximum (terminal velocity) at Stage IV (Figure 2.5). In the opinion of Craggs (1960), as crack velocity increases, the force needed to uphold crack propagation decreases. Using Craggs analysis, Bieniawski (1967b) claimed that at the onset of unstable fracture propagation, the fracture process is self-sustaining until failure. According to Robert and Wells (1954); Dulaney and Brace (1960); and Bieniawski (1967b), the terminal velocity is given by:

$$V_T = 0.38\sqrt{\frac{E}{\rho}} \tag{2.5}$$

Where V_T is the terminal velocity, E is the modulus of elasticity and ρ is the density of the rock.

Also, the increase in velocity causes general increase in volume (dilation). Figure 2.6 shows dilatancy in Quartzite under uniaxial compression test. Using dilatancy,

failure process was grouped into regions (Bieniawski, 1967d) (Figure 2.6). Bieniawski (1967d) stated that the stages of brittle fracture of rock shown in Figure 2.5 are also valid for the stress-strain curves in tension. In contrast, crack closure is absent in tension. The process of stable and unstable crack propagation has a short duration and, as a result, cracks propagate on their own accord. Figure 2.7 shows the absence of crack closure and fracture propagation, in short-lived stable and unstable crack propagation on a stress-strain curve for South African Norite rock in uniaxial tension test.

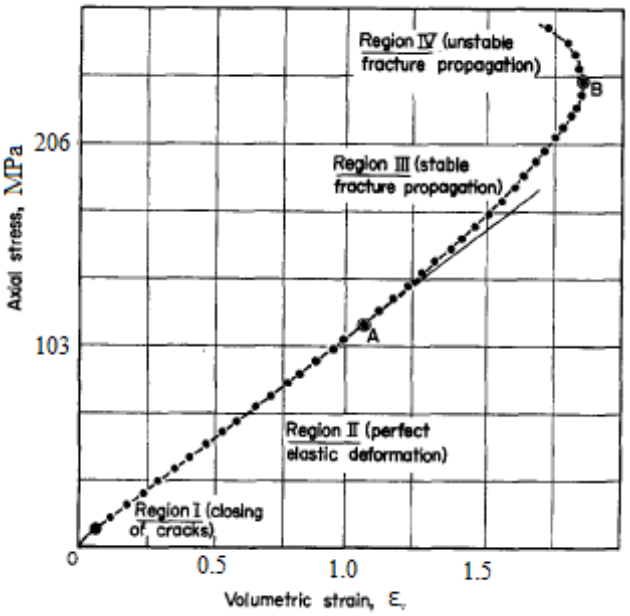

Figure 2.6 Relationship between axial stress and volumetric strain for South African Quartzite in uniaxial compression tested in a conventional loading machine (a) (Bieniawski, 1967c) (units converted by author).

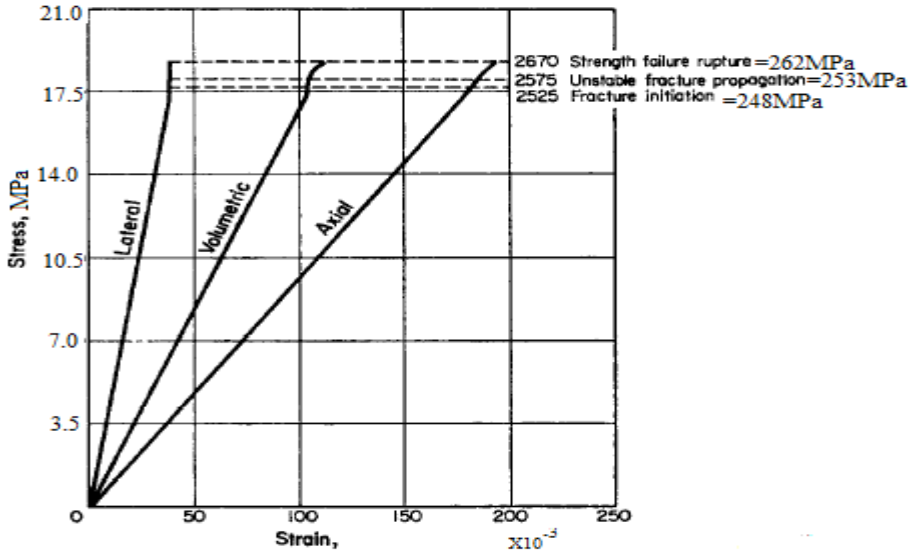

Figure 2.7 Stress-strain curves for South African Norite in uniaxial tension (Bieniawski, 1967d) (units converted by author).

Yathavan and Stacey (2004) summarised the procedure for obtaining the stages of the deformation process from laboratory tests, as shown in Table 2.1. This summary is adopted in this research to plot the stress-strain curves and to identify the stages of deformation. The microscopic studies are based on gaining an understanding on how the imperfections in a rock impact on the macroscopic failure of a rock sample under laboratory conditions. This is discussed in the following sections.

Table 2.1 Method of stress threshold identification based on stress-strain curves (Yathavan & Stacey, 2004).

	Identifying Methods	Crack Closure	Crack Initiation	Crack Damage
Brace, Brace et al. 1963; Bieniawski (1967a, 1967b)	Axial strain	Point of nonlinear zone changes to linear zone		
	Lateral strain		Point of departure from linearity to non-linearity	
	Volumetric Strain		Point of departure from linearity to non-linearity	Point of reversal
Martin and Chandler (1994)	Crack Volumetric strain		Dilation begins after crack volume unchanged during elastic deformation	

2.3 Factors Affecting Laboratory Determination of Mechanical Properties of Rocks (Macroscopic Failure).

There are various standards available to determine the mechanical properties of rocks. The standard tests (methods) can be formalised into three groups: 'branch', 'state' and 'international' standards. For example, the Bulgarian State Standard (BDS) can be regarded as a 'branch' standard. The Soviet State Standard (GOST) as a 'state' standard and the suggested methods of the International Society of Rock Mechanics (ISRM) are an 'international' standard. There are several other testing standards like the British standard (BS) and the American Society for Testing and Materials (ASTM). ISRM methods meet the international standard,

widely accepted and recognised by experts in rock mechanics. For this reason, this research has made use of the ISRM standards.

The strength parameters, especially the UCS, are estimated from the stress-strain curve and are affected by many variables. The effect of the variables on the accuracy and reliability on the measured parameters needs to be understood. It is important to show from the literature which variables influence the parameters to be measured. The variables include: specimen shape and size; specimen-platen contact condition; rate of loading; temperature; mineral composition and heterogeneity.

2.3.1 Effect of Shape and Size of Specimen on the UCS

Contradictory reports exist in the literature about the effect of specimen shape on the UCS. Hodgson and Cook (1970) and Obert et al. (1946) reported that there was no change in rock strength with specimen size (i.e. diameter) while a considerable decrease in strength with the increase of specimen size was reported by Bieniawski (1972), Hoek and Brown (1980), Hoskins and Horino (1969), Hudson et al. (1971), Koifman (1963), Mogi (1962); Protodyakonov et al. (1972) and Van der Merwe (2003).

In addition, Hoskins and Horino (1969) performed the UCS tests on Limestone, Marble, Sandstone, Granite, and Plaster of Paris. The researchers kept the height to diameter ratio constant at 2 while a different diameter was used in the tests. In the graph (Figure 2.8), the UCS increases with an increase in diameter of the rock sample up to a diameter of 50 mm. Then the UCS appears constant between 50

mm to 75 mm diameter of rock sample (Figure 2.8). However, the Hoek and Brown (1980) result shows that UCS decreases with an increase in specimen diameter (Figure 2.9).

Hawkins (1998) carried out similar uniaxial compression tests on sedimentary rocks. In this case, the diameters of the test samples were chosen from 12.5 mm to 150 mm. The result shows that the maximum strength values were for rock cores with diameters of approximately between 40 mm to 60 mm while below and above this diameter, the range of the UCS values was lower (Figure 2.10). Based on their findings, Hoek and Brown (1980) suggested that 50 mm was the optimum diameter to be used in a UCS test while Hawkins (1998) suggested 54 mm diameter (Figure 2.9 and Figure 2.10).

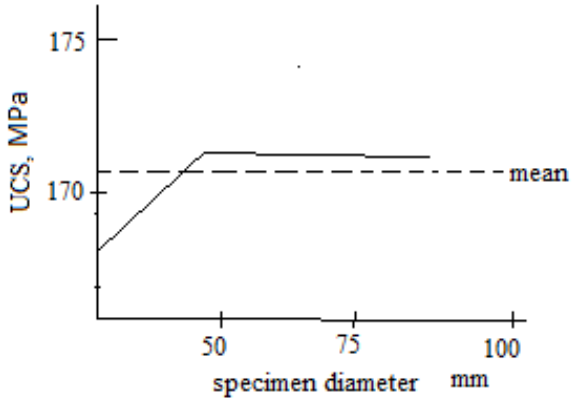

Figure 2.8 Effect of specimen diameter on compressive strength of Longmont sandstone (unit adjusted after Hoskins & Horino, 1969) (units converted from Ibf/in^2 to MPa by author).

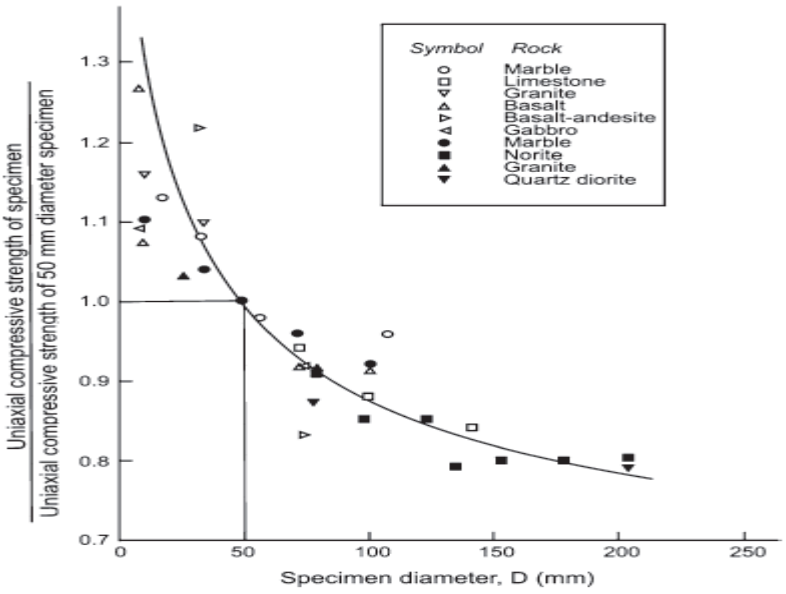

Figure 2.9 Influence of specimen size on the strength of intact rock (Hoek & Brown, 1980).

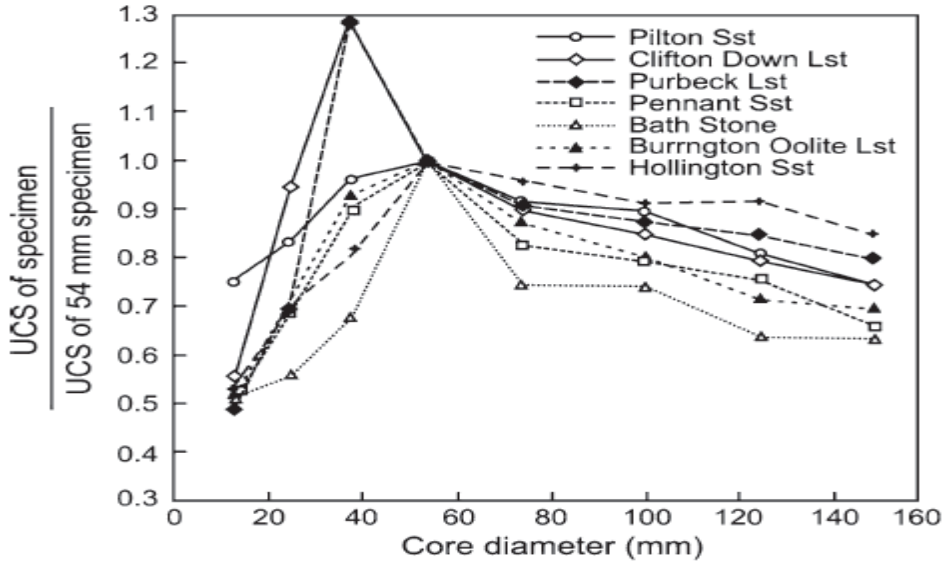

Figure 2.10 Uniaxial compressive strength of seven sedimentary rocks tested on specimens at eight different diameters (Hawkins, 1998). The values at each size have been reduced to dimensionless form relative to the strength of the 54 mm diameter specimen for each rock type.

ISRM (2007) suggested the specimen diameter to be 54 mm while ASTM (2002) suggested that the specimen diameter should be 47 mm. Both values are close to the estimates proposed by Hoek and Brown (1980) who calculated 50 mm and Hawkins (1998) who calculated it as 54 mm. Based on the conclusions of these researchers, it could be stated that diameter between 47-54 mm would be appropriate for most laboratory experiments. Nevertheless, Hawkins' results show that the maximum strength value for rock specimen diameter occurs within 40–60 mm. Therefore, from Figure 2.10 it could be inferred that diameter within 40 mm-60 mm could also be appropriate.

However, Hodgson and Cook (1970) performed the UCS tests on different diameters of cylindrical Quartzite specimens. Their result showed no evidence of the effect of size on UCS after taking the precaution that all of the specimens were subjected to uniform stress. Obert et al. (1946) concurred that shape does not affect rocks under uniaxial compression test. Pan et al. (2009) used a three-dimensional elasto-plastic cellular automaton (EPCA3D) code to simulate the process of failure of rocks when under uniaxial compression tests. They studied the effects of size and shape in the failure process of heterogeneous rocks. They used three different diameters of 101.6 mm, 50.8 mm and 19.05 mm respectively, to obtain a length to diameter ratio of 1:3, 1:1 and 3:1 constant for each test. The result is shown in Figure 2.11a. Even though the specimen was heterogeneous, the effect of size and shape on failure was minimal. The uniaxial strength and deformation behaviour was similar. Hence, the simulation of the characteristic curve of deformation behaviour of the specimens with the same diameter but

different lengths were consistent with the laboratory result obtained by Hudson et al. (1972) in Figure 2.11b. The results show that diameter plays no significant role on the UCS of rocks.

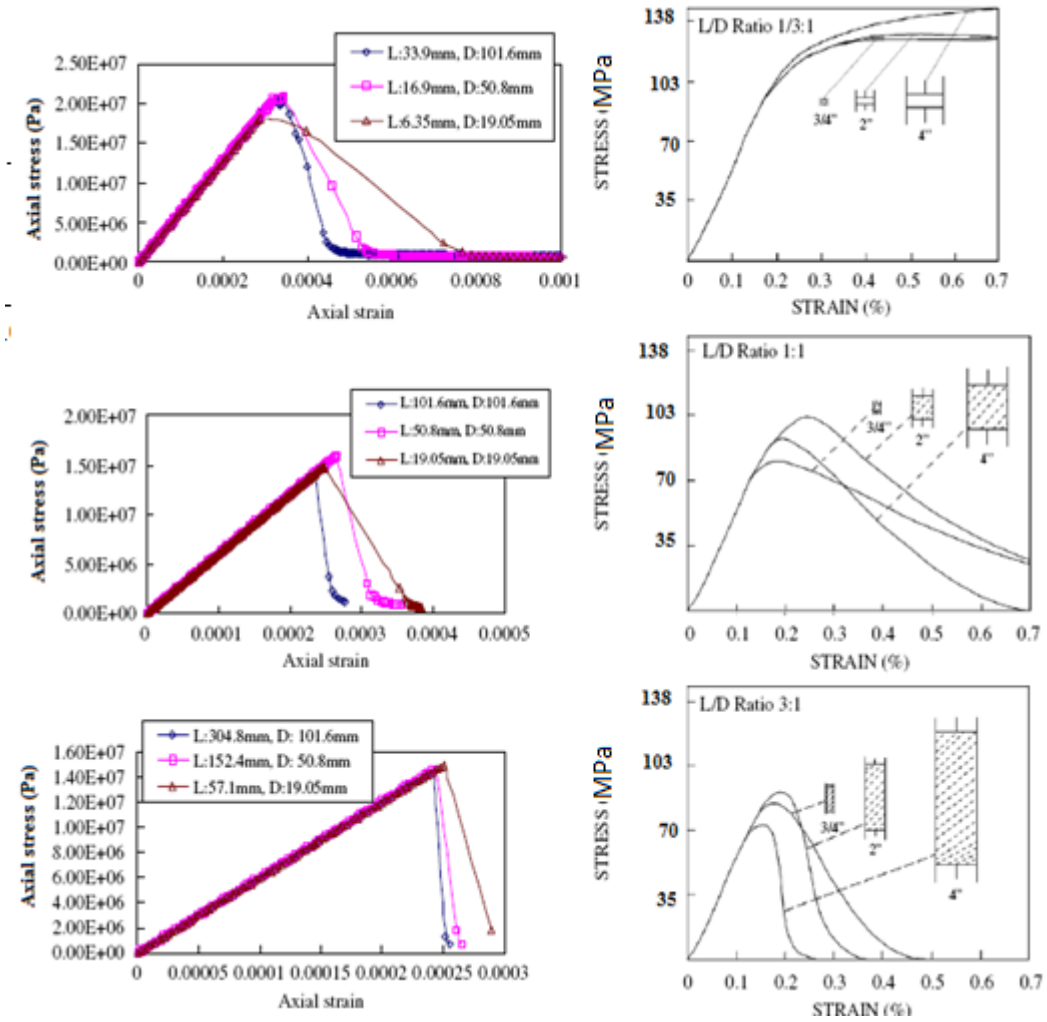

a b

Figure 2.11 Pre-failure and post-failure stress-strain curves for specimens with a certain value of length to diameter ratio 1/3:1, 1:1 and 3:1 but different sizes. (a) Numerical results by EPCA3D (Pan et al., 2009) and (b) laboratory results (Hudson et al., 1972) (units converted by author from psi to MPa in part 'b' of the figure).

The variation in UCS over diameter was as a result of non-uniform distribution of stress within the specimen's volume. An experimental and theoretical analysis of stress and strain in rock and steel cylinders reveals that 'uniaxially-loaded' specimens in most laboratory tests were essentially 'tri-axially stressed' (Pan, 1971). This means that the stress is different in specific direction and they differ from point-to-point within the specimen. This prompted other researchers (Brady, 1971a; Brady, 1971b; Brady, 1971c; Al-chalaby & Hiang, 1974) to look for analytical solutions about stress distribution within the specimen volume. There is common agreement that the basic problem in uniaxial compression test is the specimen to platen contact conditions and height to diameter ratio. This is discussed in the next sections.

2.3.2 Height to Diameter Ratio Effect on the UCS

The ratio of height to diameter of the specimen does have an influence on test results. Stress distribution in a specimen with a low height to diameter ratio tends to be tri-axially stressed and thus it exhibits a high UCS value (Vutukuri et al., 1974). However, a specimen with a large height to diameter ratio (L/D) has low UCS value compared to specimen with a low height to diameter ratio. The low value in UCS is attributed to elastic instability with regards to large specimen. Lastly, the specimen with a height to diameter ratio about 2:1 was found to be elastically stable and the stress distribution within the specimen was uniformly distributed.

In addition, Pan et al. (2009) and Hudson et al. (1972) demonstrated this with the use of EPCA code simulation and laboratory tests on specimens with different height to diameter ratios but with constant diameters. They made use of a diameter to height ratio of 1/3:1, ½:1, 1:1, 2:1 and 3:1 with a constant diameter of 19.05 mm, 50.08 mm and 101.6 mm respectively. Figure 2.12 illustrates this effect. It revealed that with the same height to diameter ratio the effect on UCS was small. However, with different height to diameter ratios (e.g. ratio 1/3:1 and 3:1) the UCS and the curve shape differed widely.

Similarly, Mogi (2007) performed laboratory tests on Dolomite, Granite and Trachyte core specimens with a diameter to height ratio ranging from 1:1 to 4:1. According to the result of this researcher, the UCS value was approximately constant for cores with a length to diameter (L/D) ratio of 2.5:1 or greater (Figure 2.13). However, for the cores with a ratio less than 2.5, the strength was higher. John (1972) agreed that the UCS values obtained from test specimens with an L/D ratio of 2 or greater was approximately constant. For specimen with ratio lower than 2 the UCS value was higher (Figure 2.14). Both John (1972) and Mogi (2007) showed a similar trend in UCS value variation with the height to diameter ratio.

Nevertheless, Andreev (1995) concluded that a test specimen could not be studied without also considering its size. The study suggested that the size of specimen have more significant effect than the shape, but disregarding the shape was illogical. He observed that the height to diameter ratio influences the stress distribution in the loading direction and the diameter affects stress distribution in

the perpendicular direction (Figure 2.15). In other words, with different specimen shapes, stress and strain distributions differ widely in respect to laws of similarity as illustrated in Figure 2.15. Andreev (1995) asserted that size effects are an attribute of brittle fracture and will become more significant with increasing brittleness.

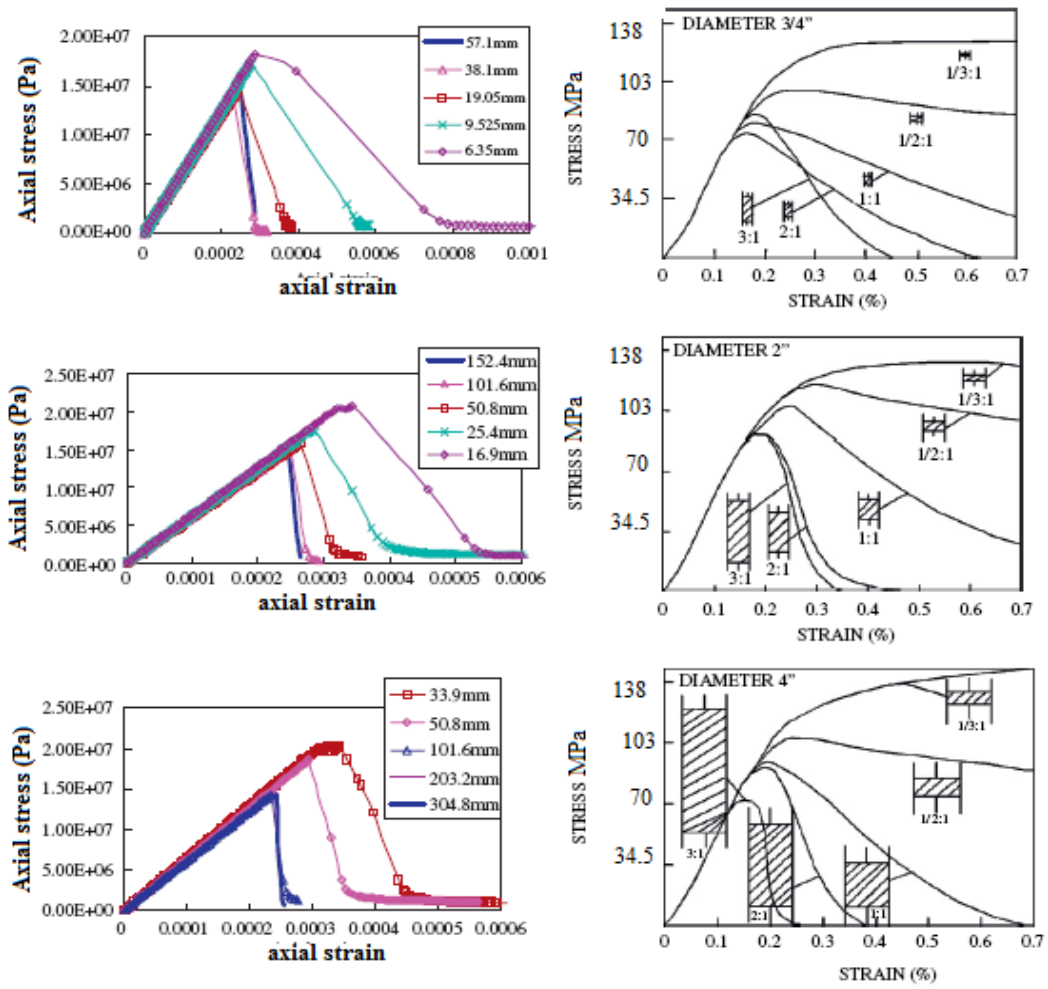

a b

Figure 2.12 Pre-failure and post-failure stress–strain curves for different specimen shapes (a) Numerical results by EPCA3D (Pan et al., 2009) and (b) laboratory results (Hudson et al., 1972). With the same diameters of 19.05 mm, 50.8mm and 101.6mm, but different lengths (units converted from psi in to MPa in part 'b' in the figure by author).

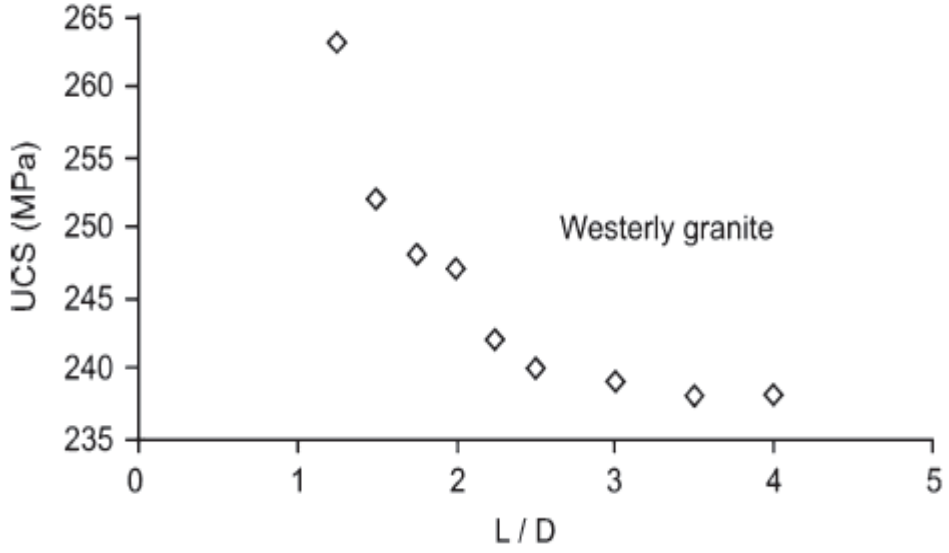

Figure 2.13 Relationship between UCS and L/D ratio for the data on Westerly Granite rocks tested by Mogi (2007).

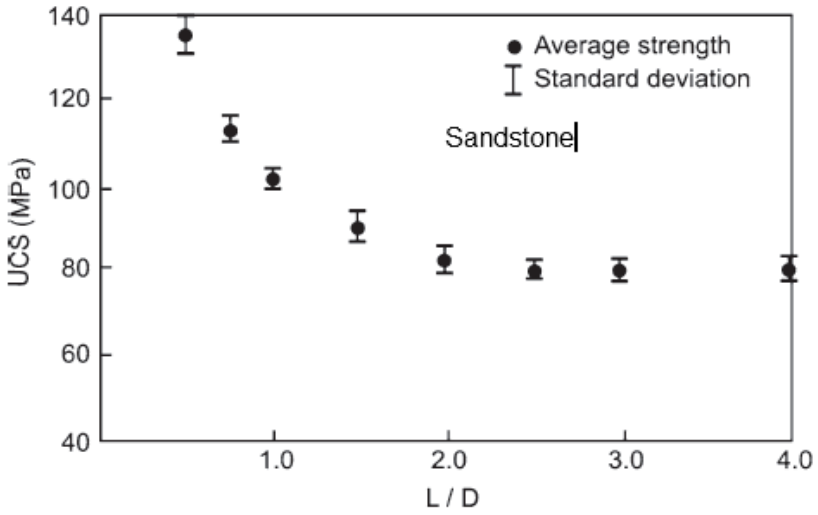

Figure 2.14 Relationship between L/D ratio and UCS value for dry Sandstone (John, 1972).

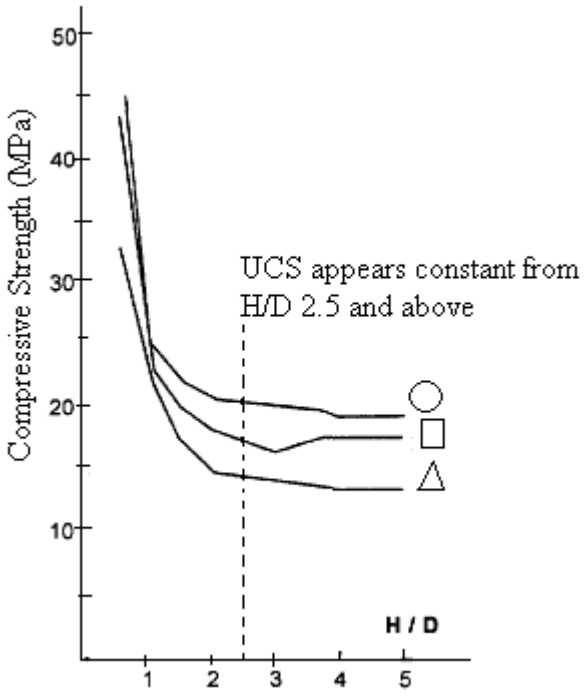

Figure 2.15 Influence of the body shape and height-diameter ratio (H/D) on compressive strength (Andreev, 1995).

ASTM recommended a ratio between 2 and 2.5 while ISRM suggested 2.5 to 3. The researchers in the previous paragraphs detailed that high UCS values are obtained for L/D ratios less than 2 and there was a very slight difference in values between L/D of 2 and 2.5. The UCS remains constant with L/D ratio 2.5:1 and above. The ratio of L/D of 2.5 coincides for both ASTM and ISRM. Therefore, in this research the specimen height to diameter ratio was chosen to be 2.5:1. A ratio of L/D of 2.5 was preferred to a ratio L/D of 3 because the effect of size (height) becomes stronger for brittle rocks in the determination of brittleness.

2.3.3 Non-homogeneity Effect on the UCS

Pan et al. (2009) pointed out that the effect of height to diameter ratio on the UCS of rocks was as a result of the fact that larger specimen contained a low strength element to initiate failure. In other words, the height to diameter ratio effect was as a result of heterogeneity (non-homogeneity) of the rock specimens. Tang et al. (2000) studied the effect of brittle disorder (termed 'heterogeneous') on UCS of rock using the numerical analysis method (2-dimension Rock Failure Process Analysis code). From the numerical simulation they concluded that heterogeneity played an important role in the deformation and strength value of rock specimens. A more homogeneous specimen has higher strength than the heterogeneous one, and has more linear deformation behaviour before peak stress was encountered.

In addition, Yang et al. (2009) agreed with an investigation of the mechanical behaviour of brittle marble samples containing different defects under uniaxial compression tests. They showed that UCS values were higher for intact rocks than heterogeneous specimens and the deformation behaviour of the stress-strain curves also varied (Figure 2.16).

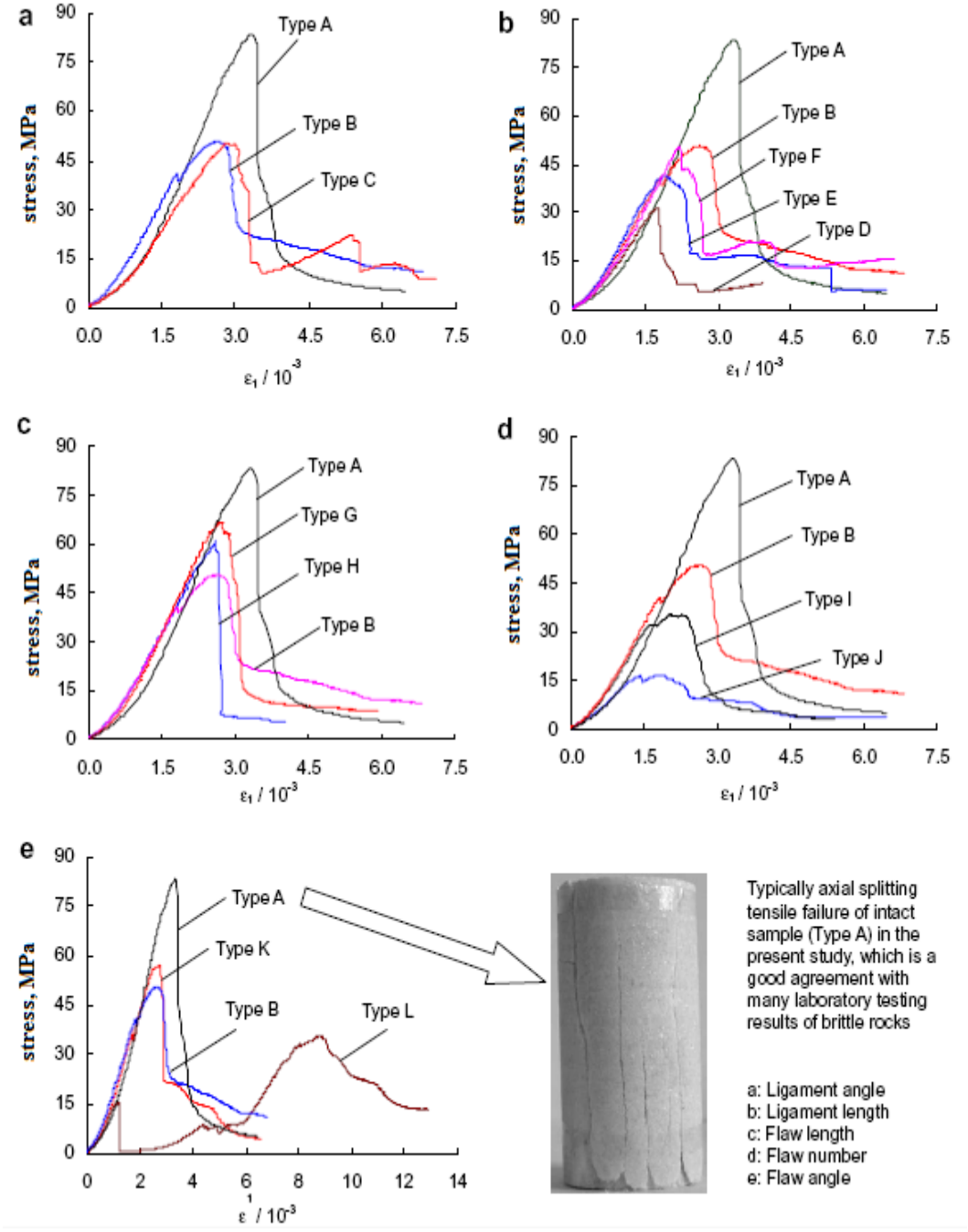

Figure 2.16 Pre-failure and post-failure axial stress–axial strain curves of marble samples with different flaw geometries (Yang et al., 2009). Types A–L under uniaxial compression, in which Type A is an intact sample; however Types B–L has different pre-existing flaws.

2.3.4 Contact Condition between Specimen End Surface and Platen

In the laboratory determination of mechanical properties of rock, it is habitually presumed that loading platen and end surfaces of test specimens are flawless planes. Thus, close contact arises when the two surfaces are mated together in parallel arrangement. Strictly speaking, intimate contact is difficult to achieve in practice. The roughness of the surfaces and foreign particles causes departure from smoothness. This causes non-uniform stress distribution at the contact surfaces. Furthermore, the platens are made of steel, so the Young's modulus and Poisson's ratio are different from those of the rock specimen. During contact, stress distribution between the specimen-platen interfaces is not uniform. This is as a result of their end effects. Many researchers (Bordia, 1971; Brady, 1971a; Pan, 1971) looked for an analytical solution for the stress distribution within the specimen body. The solution varied with the contact condition between the specimen ends and the platen pressing against it.

Accordingly, Brady (1971b) performed an analytical solution (using Fourier series) with radially end-constrained elastic cylindrical specimen that was deformed axially between cylindrical end plates (platen) of different elastic properties (Young's modulus and Poisson's ratio) from those of the specimen. The result showed that the functional form of their elastic properties depends on the diameter of the specimen and platen. Other researchers, including Brady (1971c), Hoek (1977) and Pan (1971; 1972) agreed that the effect of elastic property was as a result of contact frictions between the platen-specimen end contacts. They showed that this effect vanishes if Equation 2.6 was satisfied.

$$\frac{v_s}{E_s} = \frac{v_p}{E_p} \tag{2.6}$$

Where v_s, v_p are Poisson's ratio for specimen and platen and E_s, E_p is elastic modulus for specimen and platen respectively.

Similarly, Tang et al. (2000) performed numerical simulation of uniaxial compression to evaluate the effect of the loading system and specimen geometry on the deformation and failure behaviour of brittle and heterogeneous rock using a 2-Dimension Rock Failure Process Analysis program (RFPA 2D). The numerical model employed a specimen with different Young's modulus of platen to specimen ratios (E_p/E_s) of 0, 0.1, 1, 2, and height to diameter ratios of 0.5, 0.67, 1, 1.5 and 3. The result showed that the UCS was highest when E_p equal E_s (i.e. E_p=E_s=1) (Figure 2.17).

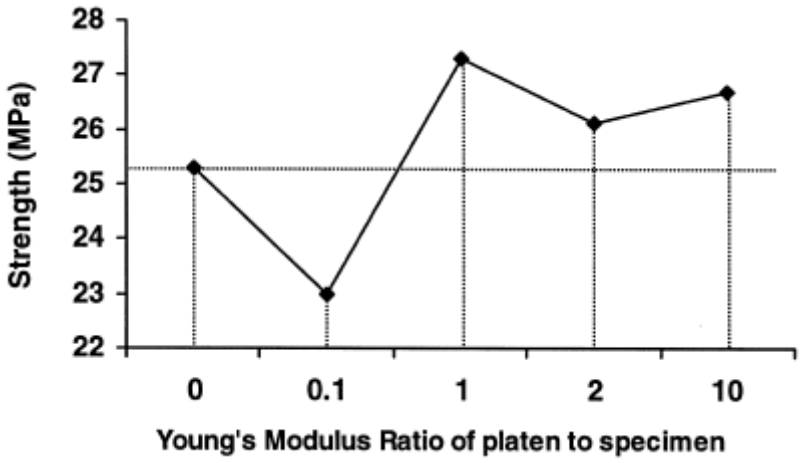

Figure 2.17 Simulated strength reductions with end constraint for specimens with different loading platens in terms of Young's modulus using RFPA2D (Tang et al., 2000).

In addition, the difference between the diameter of the specimen and that of platen also contributes to the deformation mismatch between the two materials in contact. Often the diameter of the platen is bigger than that of the specimen. The effect of the deformation mismatch disappears when the diameters are equal (Equation 2.7) (Brady, 1971d; Jaeger, 1967; Pan, 1971; 1972).

$$D_s = D_p \tag{2.7}$$

where D_s is the diameter of specimen and D_p is the diameter of platen

Pan et al. (2009) used the EPCA3D to simulate the effect of the length to diameter ratio on rock specimens of different sizes with loading platen and without loading platen on uniaxial compressive strength. The result of their simulation is shown in Figure 2.18a. When there was no loading platen, the UCS was constant irrespective of the size of length to diameter ratio. However, with loading platen the UCS rapidly decreases as the length to diameter ratio increases up to a ratio of one. It then decreases slowly and becomes constant from ratio of two and above, when the ratio was large enough.

It is evident that the friction between loading platens and specimen's ends is the factor that was responsible for the shape and size effect discussed in Section 2.3.1. As a result, when the length to diameter ratio is large enough, particularly when the ratio is larger than 2, the end effect of the loading platen can be disregarded. This result was consistent with the laboratory result of Yang et al. (2005) (as found in Pan et al., 2009) on the effect of loading platen friction on the UCS of rock. The result is shown in Figure 2.18b.

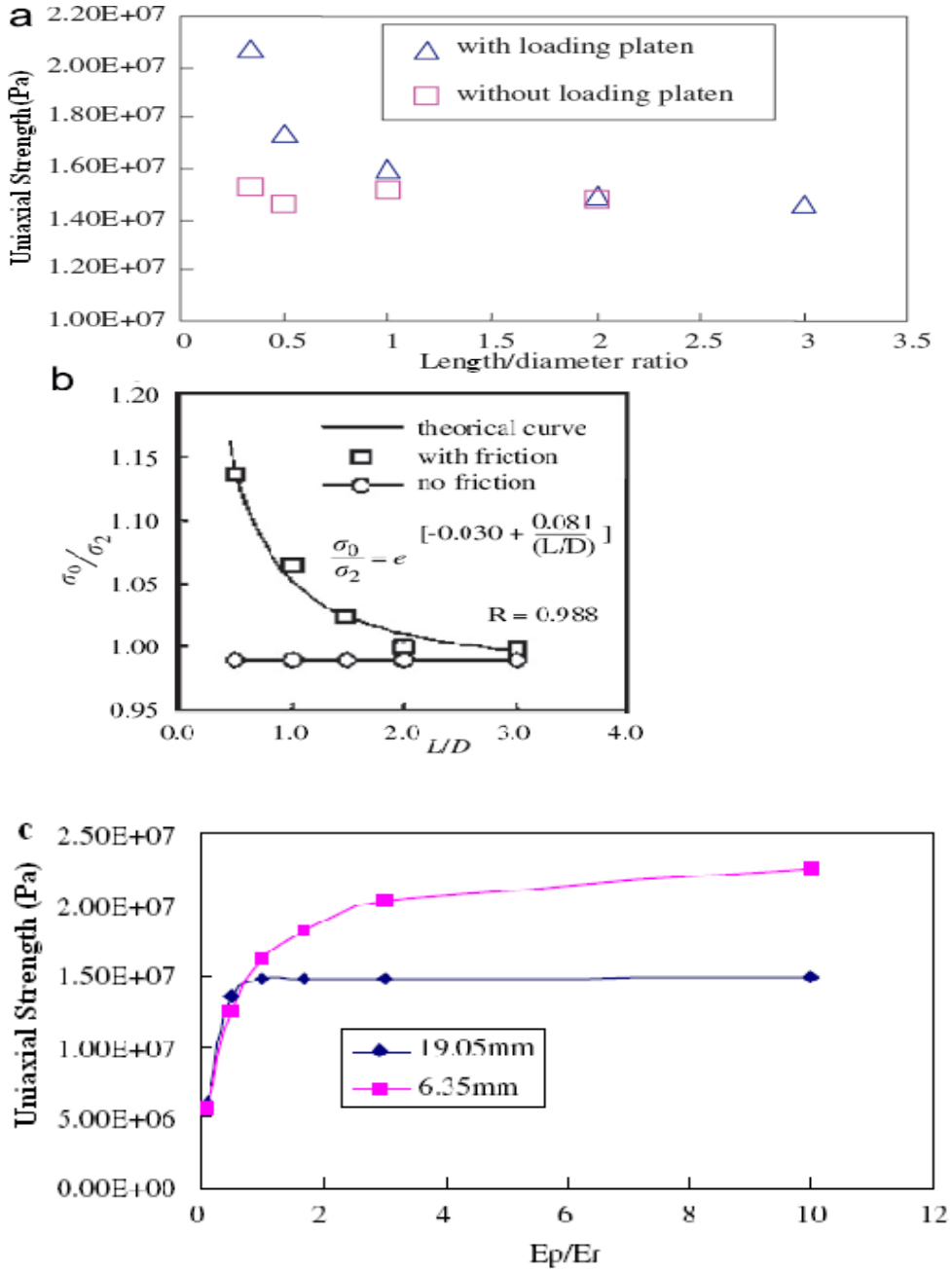

Figure 2.18 Relationship between uniaxial strength and length to diameter ratio of rock specimen with different sizes, with and without considering loading platen effect (a & c) EPCA3D simulated result (Pan et al., 2009) and (b) laboratory result (Yang et al., 2005 as contain in Pan et al., 2009).

This finding was also documented in the laboratory result of Dhir and Sangha (1973). Likewise, Pan et al. (2009) showed that when the specimen length was large enough then the influence of platen and specimen Young's moduli on the UCS may be ignored (Fig 2.18c).

In the laboratory determination of UCS, the ISRM (2007) suggested that the diameter of platen (D_p) is between D_s + 2 mm of specimen. The thickness of the platen is suggested to be at least 15 mm and flatness of 0.005 mm. In this research, the diameter of platen (D_p) was equal to that of specimen (D_s) in the determination of UCS of the rocks. The thickness of the platen was 15 mm and their flatness was 0.005 mm or lesser. But in the determination of the pre-failure and post-failure curves the diameter of the platen was slightly larger than that of the test specimens. This becomes necessary because when rock deformation passes the peak stress the hard brittle rocks begin to crumble at the contacts points between platen and the specimen especially when the two are equal. When the platen was slightly bigger than the specimen then this effect was minimal. This behaviour was noticed during the pre-test done with the rock specimens.

2.3.5 Effect of Moisture, Temperature and Mineralogy on Strength Parameters

At high temperature and moisture levels, the UCS of rocks is lowered. Obert et al. (1946) studied the effect of moisture on different rocks types. The result of their tests is shown in Table 2.2. The table reveals the influence of moisture content on the UCS values of the rocks. However, for this research, since the specimens were tested at room temperature under laboratory condition and with a dry specimen,

the issue of temperature and moisture was found to have no significant role to play. However, the UCS value of rock is influenced by the moisture content of the rocks as a result of the age of the specimen. Therefore, ISRM (2007) suggested that specimens shall be stored for no longer than 30 days, and in such a way to preserve the natural water content.

Table 2.2 Effect of moisture on UCS (Obert et al., 1946).

Moisture Condition	Ratio of oven-dried and saturated UCS to air-dried UCS						
	Marble	Lime-stone	Granite	Sandstone1	Sandstone 2	Slate	Average
Oven-dried	1.01	1.03	1.07	1.01	1.18	1.06	1.06
Air-dried	1.00	1.00	1.00	1.00	1.00	1.00	1.00
Saturated	0.96	0.85	0.92	0.90	0.80	0.85	0.88

Mellor (1973) measured the uniaxial compressive and tensile strength of granite, limestone, and sandstone over a range of temperatures from -197^{0}C to 25^{0}C. For each of the three rock types, the UCS of both air-dry and water-saturated specimens was determined. The researcher observed 35% increase in the compressive strength of the rock between 0^{0}C and -120^{0}C (Figure 2.19). The graph shows constant UCS values for both air-dry and water-saturated specimens between temperatures of about 0^{0}C to 25^{0}C. This reveals that the UCS is constant under room temperature conditions which can be assumed to be between 20^{0}C to 25^{0}C. Lau et al. (1991) concurred that change in specimen temperature of less than 100^{0}C appears to have little effect on ultimate stress, strain and elastic parameters of rocks (Figure 2.20).

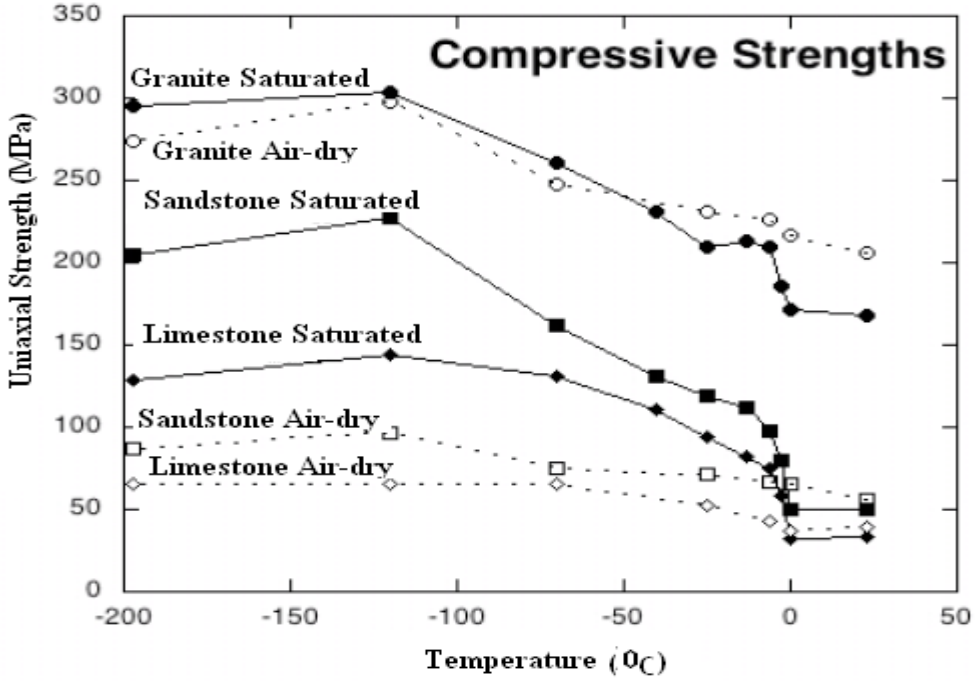

Figure 2.19 Strength of Granite, Limestone, and Sandstone in uniaxial compression at low temperatures (Mellor, 1973).

However, mineral composition, texture (grain size and shape) and fabric (arrangement of minerals and voids) affect the properties of rock (Irfan, 1996). In typical fresh igneous rock, the mineralogy and texture determines the strength and its elastic deformation characteristics (Johnson & De Graff, 1988). In addition, Tugrul and Zarif (1999) used correlation analysis to investigate the relationship between the mineralogical and mechanical properties of granitic rocks. They showed that the UCS values of rock increases with quartz to feldspar ratio and decreases with quartz grain size (Figure 2.21).

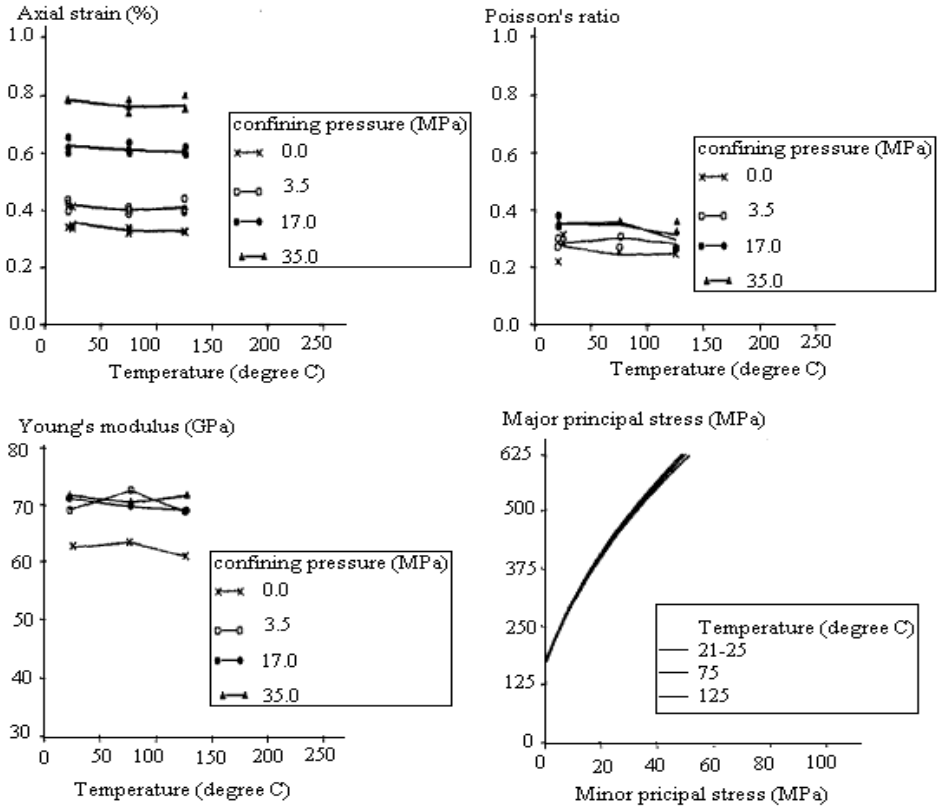

Figure 2.20 Effect of temperature on deformation parameters and strength values of Granite (Lau et al., 1991).

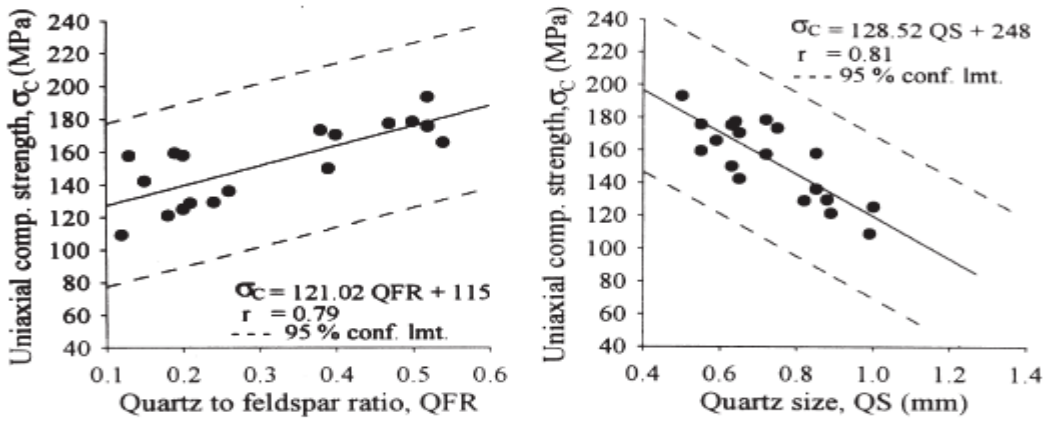

Figure 2.21 Relationships between: (a) the uniaxial compressive strength and the quartz to feldspar ratio, (b) uniaxial compressive strength versus mean grain size (quartz size) (Tugrul & Zarif, 1999).

All the factors listed in the preceding sections, such as specimen shape and size, height to diameter ratio, non-homogeneity, contact surfaces between specimen and platen, mineralogy and water content are related to the rock samples and its preparation. These are the factors that can influence the result of the tests in regards to nature of rock samples and their preparation. On the other hand, one important factor that has not been discussed and which relates to the testing program is the strain rate. The effects of strain rate on a number of parameters determined during the uniaxial compression tests are discussed in the following sections.

2.3.6 Effect of Strain Rate on Strength Parameters

Strain rate affects rock parameters determined under the uniaxial compression test. These parameters are discussed in the later sections. Strain rate is the deformation, $\Delta\ell / \ell$ per unit of time, *t*. It is the time required to build up a given strain. It is expressed in Equation 2.8.

$$\varepsilon_r = \left(\frac{\Delta\ell}{\ell}\right) \Big/ t \qquad (2.8)$$

The UCS of rocks normally increases with an increase in the strain rate. Kobayashi (1970) showed an increase in the value of the UCS of different rocks with an increase in the strain rate (Figure 2.22a). At a lower strain rate of 10^{-6} to 10^{-1} sec^{-1} the increase in the UCS value was gradual. But at a higher strain rate of 10^{-1} to 10^{3} sec^{-1} the UCS of the rocks increases rapidly.

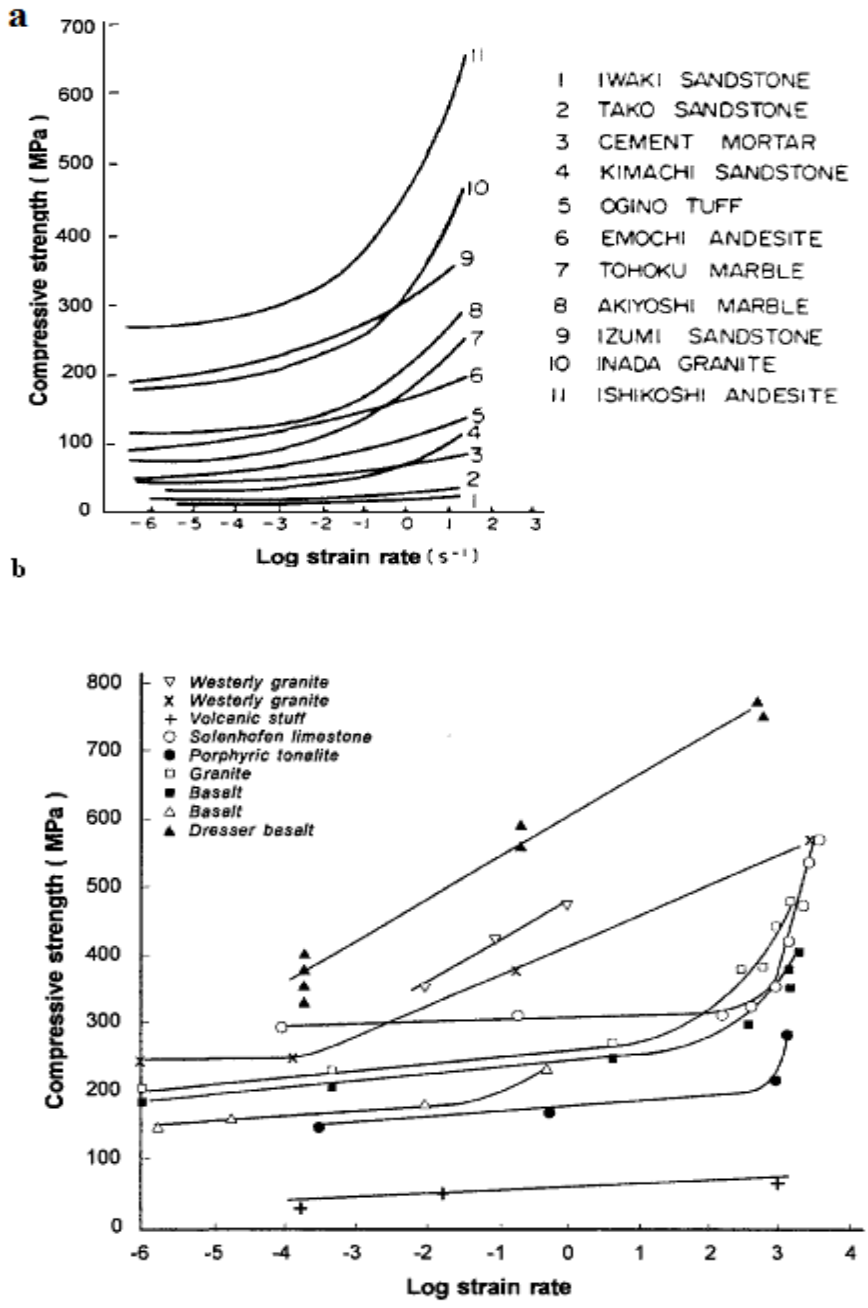

Figure 2.22 Variation of compressive strength with strain rate after Kobayaski (1970) (a) and uniaxial compression tests from earlier studies showing different strain-rate sensitivities of compressive strength (b) (Blanton, 1981).

A similar trend that is consistent with Kobayashi (1970) was given by several other authors (Green & Friedman, 1970; Green & Perkins, 1972; Kumar, 1968; Perkins et al., 1974; Logan & Handin, 1971; Stowe & Ainsworth, 1972 as reported in Blanton, 1981) (Figure 2.22b). Lindholm et al. (1974) result on Dresser Basalt and Green and Perkins' (1972) on Westerly Granite showed a rapid and continuous increase in the UCS with an increasing log strain rate over an interval of strain rates of 10^{-4} to 10^{3} sec^{-1} (Figure 2.22b). However, Zhao et al. (1999) claimed that Young's modulus and the Poisson's ratio of granite are barely affected by changes in the loading rate (Figure 2.23) which implies that changes in strain rate does not affect the rock's elastic properties.

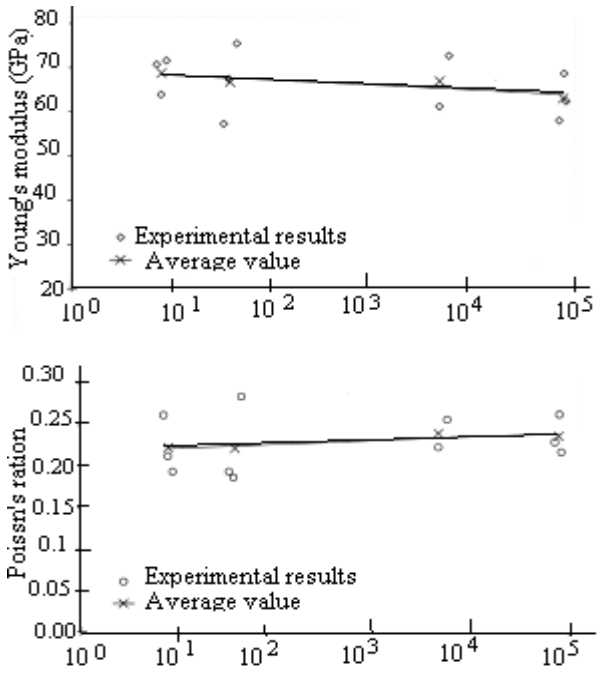

Figure 2.23 The variation of the Young's modulus and Poisson's ratio with the loading rate (Zhao et al., 1999).

Yashima et al. (1983) investigated the effect of strength parameters (Young's modulus and unconfined compressive strength) on the estimate of elastic strain energy during a laboratory compression test on rock specimens with varying strain rates. They found that the elastic strain energy increases over strain rates range of approximately 2 x 10^{-7} to 2.0 x 10^{-1} strain/second. Likewise, Whittles et al. (2006) performed a series of laboratory tests on three different rock types (strong Sandstone, strong Limestone and weak Chalk) over a series of strain rates varying from 2.6 x 10^{-5} to 5.0 x 10^{-2} strain/second. The test was conducted with a RDP-Howden, 1000 kN stiff compression testing machine.

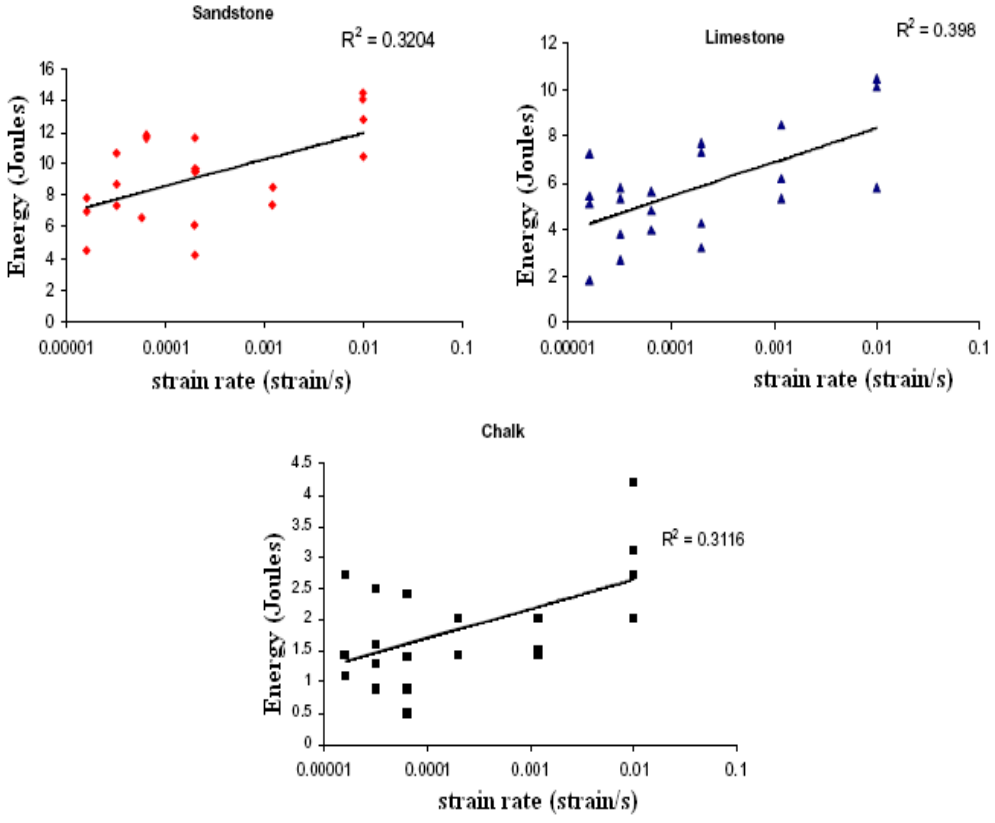

Figure 2.24 Energy plotted against strain rate for the variable speed unconfined compressive strength test (Whittles et al., 2006).

They used the ISRM (1981) method for the determination of unconfined compressive strength. The elastic strain energy was determined in each test as the area under the load displacement curve up to the point of failure. The relationship between the elastic strain energy and the strain rate for each of the three rock types is shown in Figure 2.24. Although the correlations are weak, this shows that there is an increase in the elastic strain energy over an increase in the strain rates in each of the three rock types.

In the laboratory determination of UCS, the rate of loading is constrained to certain limits in order to give a reasonable amount of time to carry out the test. The ISRM (2007) recommended a continuous loading at a constant stress rate such that failure occurs within 5-10 minutes of loading. This suggestion was applied with caution. It was found that the strength of the rocks used in this study is far apart. For instance, Quartz Arenite is about 35 MPa while Quartzite2 is over 500 MPa. To achieve a consistent and even strain rate becomes what is relevant. This is because Quartz Arenite has to be loaded slower than Quartzite2 such that it fails within 5-10 min. This becomes necessary so that the strain rate of Quartzite2 is not much faster than the soft rocks. This ensures that the strain rates for the rock' specimens are close to each other. Since a higher strain rate raises the UCS, at the same time it increases the degree of fragmentation and affects the post-failure behaviour of the rock as discussed in the next sections.

2.4 Rock Classification

When the ultimate strength of a rock is reached, there is progressive departure from elastic behaviour as the load bearing capacity of the rock passes through the peak stress and then decreases. The behaviour of the pre-failure curve of rocks is more or less similar. However, the post-failure behaviour differs. The post-failure behaviour of rocks after the peak stress is ascribed to two different classes. It is classified as Class I and Class II behaviour (Wawersik & Fairhurst, 1970).

2.4.1 Post-Failure Characteristic Curves of Rock under Uniaxial Compression

As has been discussed, the specimen's height to diameter ratio influences the characteristic shape of the post-failure part of stress-strain curves. This was illustrated in Figure 2.12 (as discussed in Section 2.3.2). Recent research corroborates the fact that specimen length influences post-failure shape. Tarasov and Potvin (2013) emphasised that the same rock with a different specimen length has different post-failure behaviour. They claimed that the amount of elastic energy stored within the specimen at the peak stress was proportional to the specimen length, as a result, it affects the post-failure characteristic curve. The effect of elastic energy stored in a specimen and its brittleness is discussed further in Section 2.6.5.

In Class I rock, the behaviour exhibited demonstrated a gradual reduction in the load carrying capacity of the rock after the peak load is reached. On the other hand for Class II rock, there is a rapid reduction in the load-carrying capacity immediately after the peak load is exceeded. Wawersik and Fairhurst (1970)

observed that stable fracture propagation is a characteristic of Class I behaviour. A further reduction in the load-carrying ability of Class I rock requires work to be done on the specimen, thus retains some strength after the peak load. In the case of Class II rock behaviour, at peak stress the elastic strain energy stored in the specimen is sufficient to maintain fracture propagation to the residual strength (i.e. is self-sustaining). Fracture propagation can only be arrested if the strain energy is extracted from the test specimen.

Figure 2.25 shows the post-failure behaviour of Charcoal Grey Granite, Indiana Limestone, Tennessee Marble, Solenhofen Limestone and Basalt (Wawersik & Fairhurst, 1970). All of the rock specimens are homogeneous and of a length-to-diameter ratio of 2:1 while specimen diameters varied between 25.4 mm and 50.8 mm. From the graph, the pre-failure behaviour of the slopes appears to be similar for the rocks but the post-failure behaviour slopes are quite different.

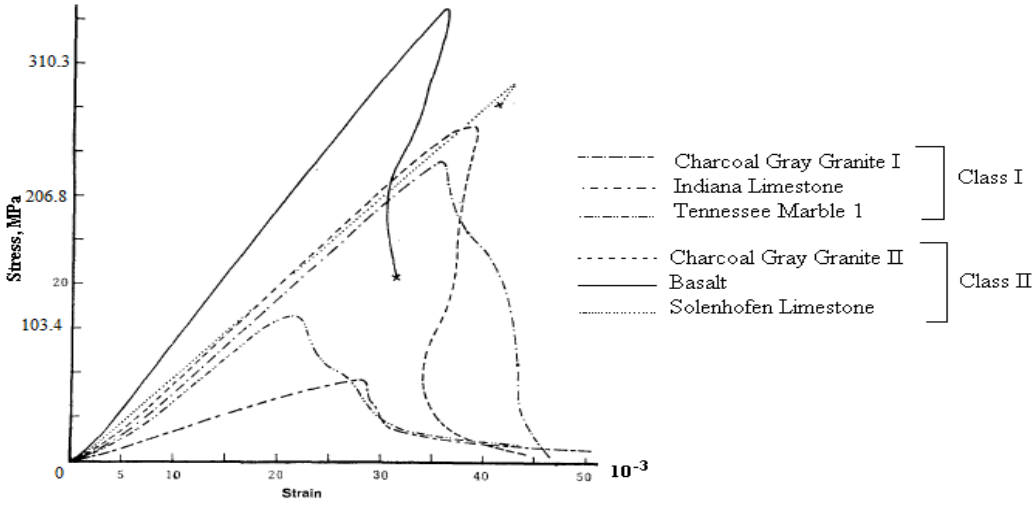

Figure 2.25 Stress-strain curves for six representative rock types in uniaxial compression (Wawersik & Fairhurst, 1970)**.** Unit converted from psi to MPa by author for possible comparison.

He et al. (1990) demonstrated that the striking difference between Class I and Class II types was due to the increase in non-elastic strain. Both Class I and Class II rocks tend to decrease in elastic strain in the post-failure region with a decrease in the load-bearing capacity. They showed that the difference between Class I and Class II was the magnitude of the non-elastic strain. In other words, if the decrease in elastic strain is accompanied by a faster increase in non-elastic strain, the rock demonstrates Class I, otherwise it shows Class II behaviour.

In addition, Class II rock behaviour is characterised by localised fractures in fairly homogeneous rock (Pan et al., 2006; Chen et al., 2006). They observed that the pre-failure and post-failure stress-strain curves are influenced by the heterogeneity of the rocks and rock with higher homogeneity behave more like Class II rocks in the post-peak region. Pan et al. (2006) and Chen et al. (2006) also observed that homogeneity or heterogeneity of the rocks played a major role in the post-peak fragmentation of brittle rocks in two respects in that it affects the peak strength and determines how cracks initiate and develop into singular faults. The methods used to determine the post-failure curves of Class II rocks are examined in the next section.

2.4.2 Studies on Class II Behaviour of Rocks

The elastic strain energy stored in the specimen during loading and released during unloading to supply growing fractures with surface energy causes the two classes of stress-strain curves (Cook, 1965). The Class I curve increases continuously in axial strain, an experiment conducted in axial strain control is

sufficed to show this behaviour. In contrast, Class II rock does not show a linear increase in axial strain even with a stiff machine, therefore, a different control method is required to avoid an uncontrolled specimen failure.

Many researchers reported different methods used to achieve Class II behaviour of rocks. Wawersik and Fairhurst (1970) determined Class II behaviour of rock with the use of a thermal contraction machine. They achieved pre-failure and post-failure stress-strain curves from the envelope of unloading-reloading loci. Soon after, many researchers attempted to find alternative and easier methods to obtain the pre-failure and post-failure stress-strain curves by using a servo-controlled testing machine. Hudson et al. (1971) achieved pre-failure and post-failure stress-strain curves for different rocks in uniaxial compression with servo-controlled testing machines by using lateral displacement as a feedback signal.

Besides, other authors tried alternative methods programmed to obtain Class II behaviour by controlling other rock parameters such as: a linear combination of stress and strain (Okubo & Nishimatsu, 1985), the acoustic emission rate (Terada et al., 1984) and the dilatant volumetric strain (Sano et al., 1982). However, few pre-failure and post-failure stress-strain curves were reported (He et al., 1990). Nishimatsu et al. (1981) and Saito et al. (1983) extended the idea of Hudson et al. (1971) with the use of lateral strain as the feedback signal for the determination of stress-strain curves. Nevertheless, smooth pre-failure and post-failure stress-strain curves were not achieved because the local lateral failure makes it problematic to correctly determine the lateral strain in the post-failure regime (Okubo & Nishimatsu, 1985).

Hudson et al. (1971) and Hudson et al. (1972) opined that the use of a constant lateral strain rate as the feedback signal in programming the stress-strain curves was the most effective method. This is because it continuously increases all through the failure process and in that case the axial strain can be separately controlled. The use of servo-controlled testing machines allows the failure behaviour of rock in the post-failure region to be studied.

However, Simon et al. (2003) observed that the laboratory determination of the post-failure properties during uniaxial compression tests of brittle rocks is often difficult to realise. Shimizu et al. (2010) concurred that there are still complications to achieve post-failure stress-strain curves of brittle rocks in laboratory experiments. They pointed out that at present the Class II post-failure characteristic curve is not sufficiently clarified.

Nevertheless, Okubo and Fukui (1996) obtained pre-failure and post-failure stress-strain curves for various rocks under compression and tension with the use of a closed-loop servo-controlled testing machine. They achieved it with a linear combination of stress and strain as the feedback signals (Figure 2.26). Rini and Mord (2008) obtained pre-failure and post-failure stress-strain curves for Sandstone under uniaxial compression with the use of a closed-loop servo-controlled testing machine using axial strain control (Figure 2.27). Also, Brijes and Dachao (2013) obtained post-failure stress-strain curves for different Sandstone and Coal specimens under lateral strain control with the use of a closed-loop servo-controlled testing machine in uniaxial compression tests (Figure 2.28 and 2.29).

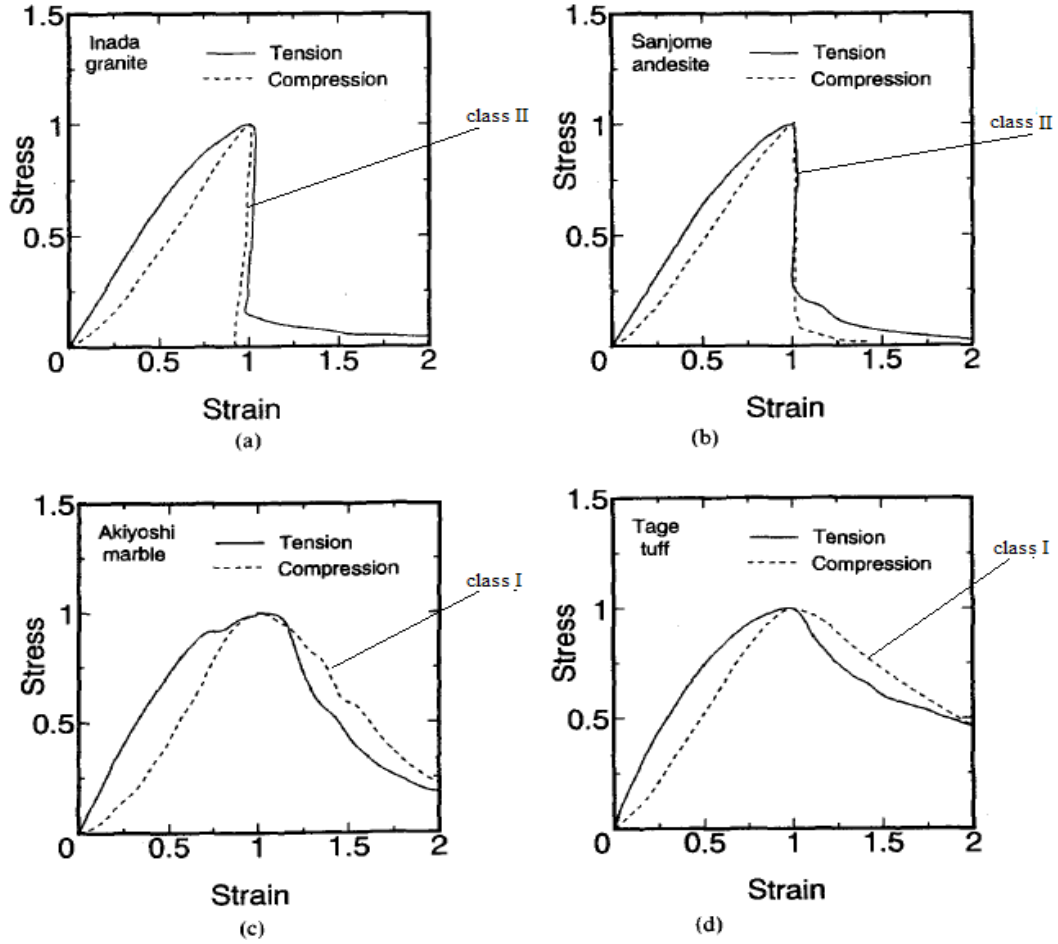

Figure 2.26 Normalised stress-strain curves in tension and compression (a) lnada Granite (b) Sanjome Andesite (c) Akiyoshi Marble (d) Tage Tuff (Okubo & Fukui, 1996).

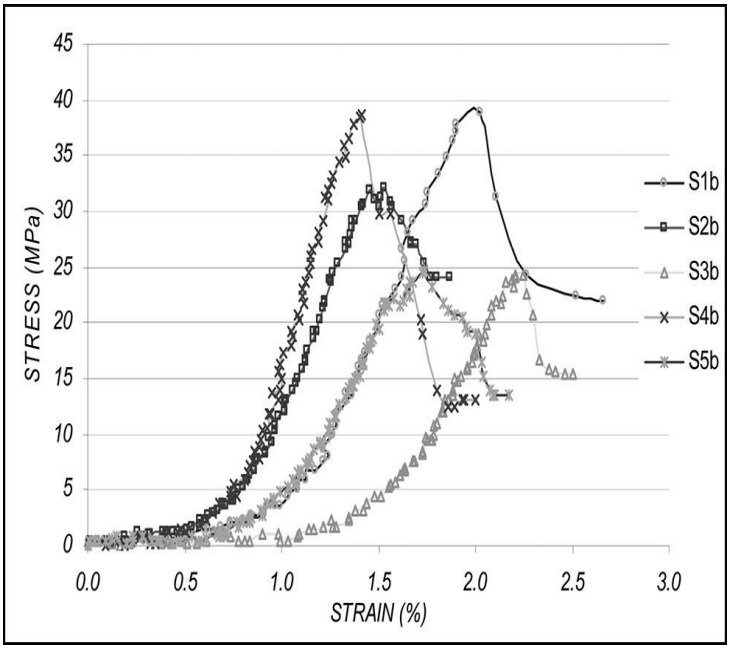

Figure 2.27 Stress-strain curve for sandstone tested under servo-controlled machine (Rini & Mord, 2008).

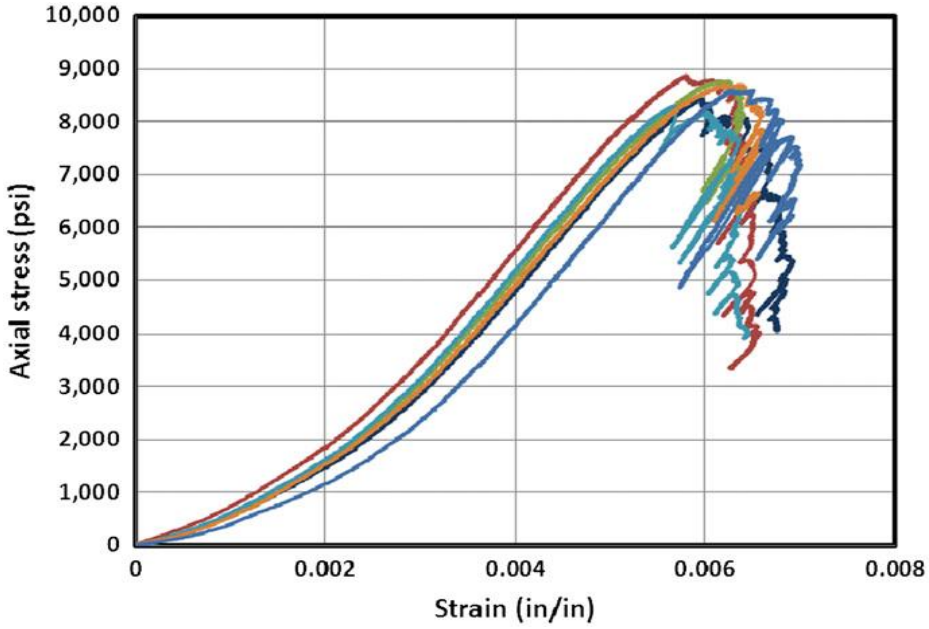

Figure 2.28 Stress–strain curves of six different Sandstone specimens tested under later servo-controlled machine (Brijes & Dachao, 2013).

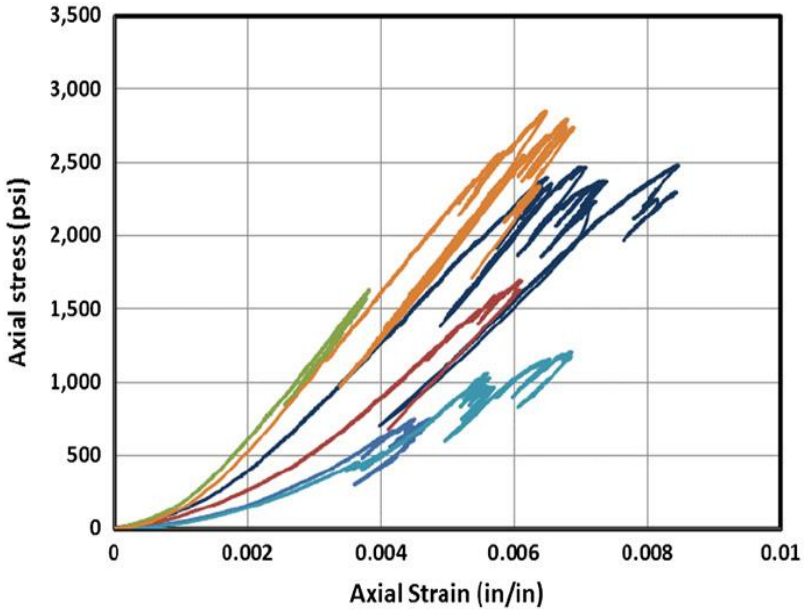

Figure 2.29 **Stress–strain curves of different Coal specimens tested under servo-controlled machine** (Brijes & Dachao, 2013)

2.4.3 Effect of Strain Rate on the Post-failure Behaviour of Rock in Uniaxial Compression

The post-failure curve tends to fall more rapidly with a steeper slope as the strain rate is decreased. The peak stress is reached at a smaller value of strain with a decrease in the strain rate. A laboratory-based study of the post-failure curve of Arkose Sandstone and Charcoal Granite with the use of a servo-controlled testing machine at various strain rates illustrates this (Pan, 1973). The sample was prepared to meet the ASTM standard of 31.7 5 mm diameter and 63.5 mm length. The stress-strain curve is shown in Figure 2.30. This behaviour was also observed in other rocks, like: Granite; Limestone and Marble (Pan & Podnieks, 1972; Rummel & Fairhurst, 1970; Wawersik, 1973).

It was consistent with Jackson, et al.'s (2008) laboratory work and numerical (using Particle Flow Code in 3 Dimensions, PFC 3D Version 3.0 produced by Itasca, 2003) techniques. They performed a series of laboratory tests on three different rock types (Sandstone, Limestone and Chalk) with strain rates varying from 2.6×10^{-5} strain/sec to 5×10^{-2} strain/sec in order to examine the effect of strain rate on the breakage behaviour of rocks. The post-failure behaviour of the rocks changes with the different strain rates (Figure 2.31) and as the strain rate increases, the degree of fragmentation and the UCS increases. The effect of the strain rate on the degree of fragmentation is discussed in the next section.

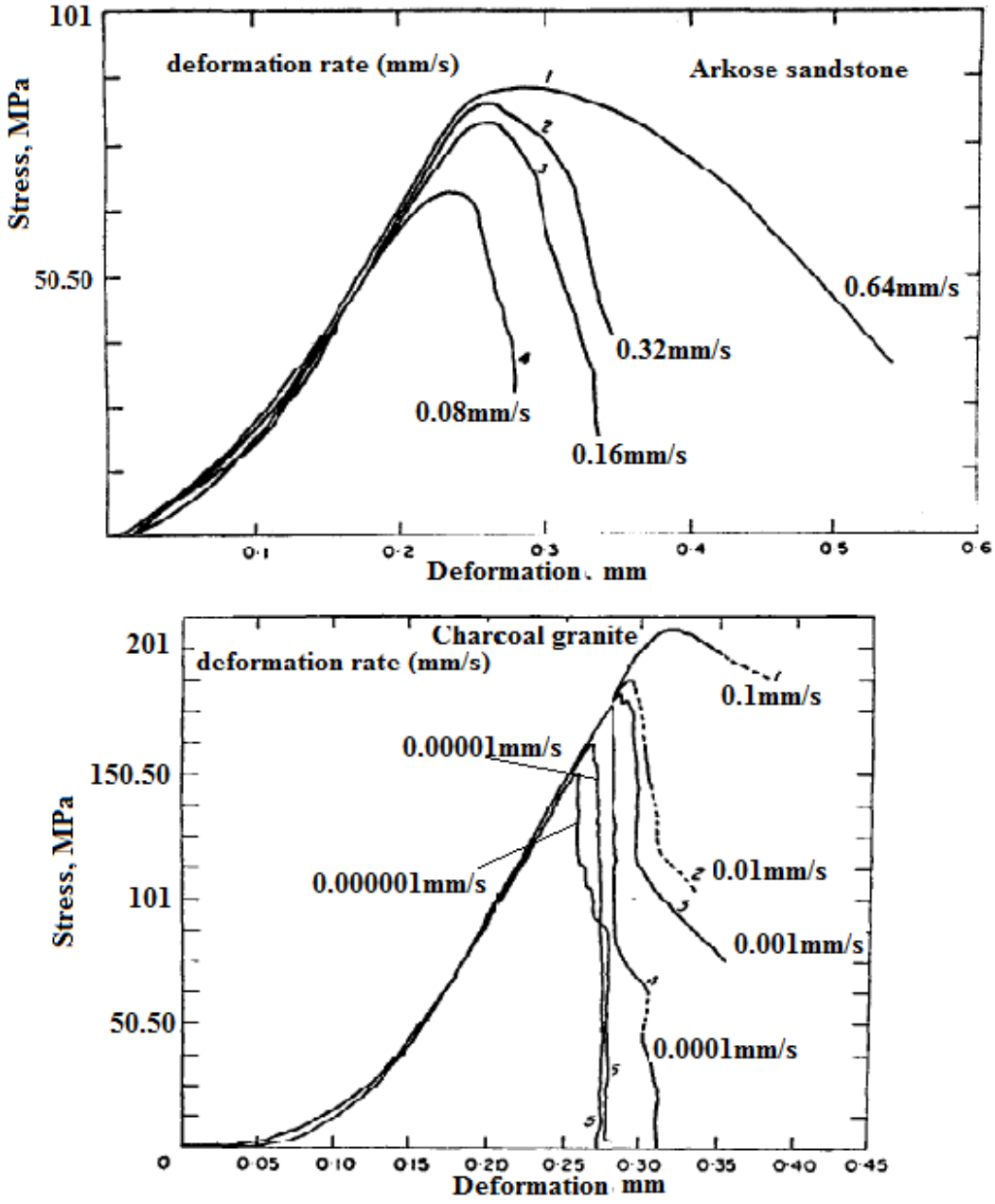

Figure 2.30 Influence of strain rate on post-failure behaviour of Arkose Sandstone and Charcoal Granite in uniaxial compression in a servo-controlled testing machine (Pan, 1973). Load normalised to stress using specimen diameter (31.75 mm) for possible comparison by the author.

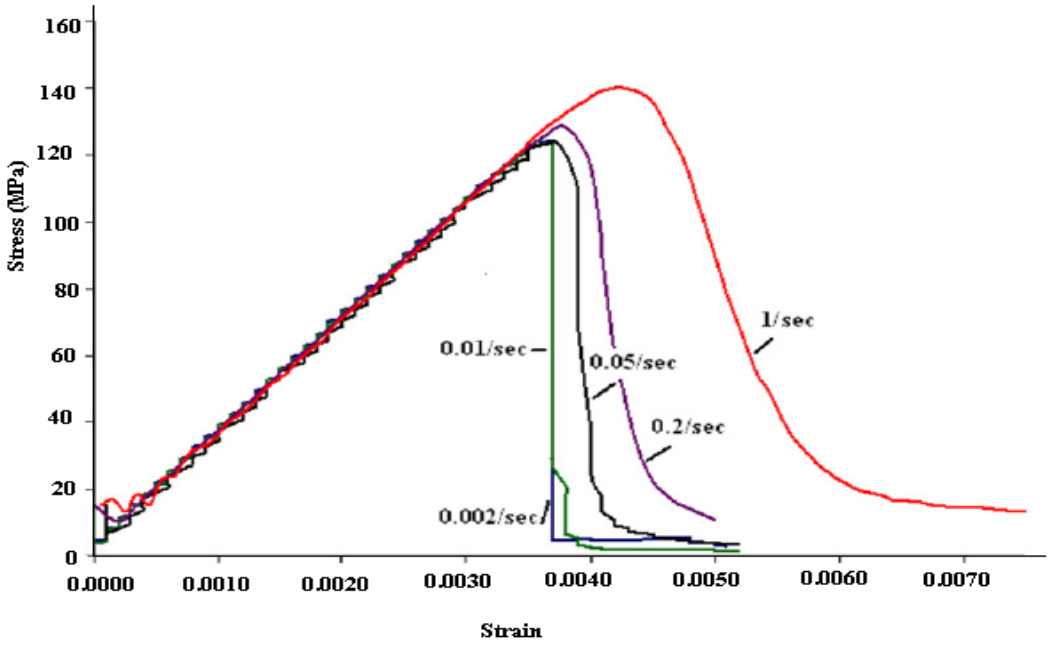

Figure 2.31 Predicted stress-strain curves for the Ibbenburen Sandstone model cores with a different strain rate using PFC3D (Jackson et al., 2008).

2.5 Rock Fragmentation

Rock breakage is traditionally achieved either by mechanical means or using explosives. However, other novel practices of rock fragmentation include heat, high pressure, water jets and hydraulic. Under these processes, rocks are fragmented into various sizes and yield a characteristic distribution when analysed through sets of sieves. This is seen particularly during the steady loading of rock to determine its mechanical strength properties with a soft loading machine (e.g. Amsler Rock Testing Machine). Different rock types exhibit different fragments size distributions. This is also applicable in rock fragmentation using explosives.

2.5.1 Rock Fragmentation under Explosive or Dynamic Loading

Moser et al. (2000) suggested that the particle size distribution of blasted materials is based on the natural breakage characteristics of the rock. They opined that there exists a comparable and material specific characteristic of particle size distribution from 0.1 mm to 10 mm for both full scale and laboratory-scale blasting tests. It was also observed that the characteristic curves of particle size distribution does not change because of energy input or for a specific charge used for blasting but can only shift their position on a log-log graph.

Worsey and Rustan (1987) as contained in Sergey (2003) claimed that the tensile strength of rock (estimated from Brazilian tensile strength, BTS) is related to the blasting performance while compressive strength of rock has no significant influence on rocks' fragmentation. This is because, often rock breakages occur in tensile failure. This occurs as the shock waves from explosive detonation, passes through the rock body thereby causing tensile failure around the plane of weakness in the rock, while compressive failure only occurs around the charge holes. Thus, the tensile strength of rock is an important factor for determination of rock resistance to blasting. Gupta et al. (1990) suggested a relationship that estimates the charge factor for the rock using the effective burden and Protodyakanov strength index. They defined the Protodyakanov strength index using the compressive strength of rock and modulus of elasticity.

On the other hand, the dynamic properties of rocks are used to estimate rock fragmentation. Recent research indicated that the mean fragments size passing at 50% depends on the dynamic properties of the rock, and increases with an

increase in the P-wave velocity and dynamic modulus (Figure 2.32). The researchers concluded that the relationship is introduced for mine blasting practice in central Iran (Hossaini et al., 2013).

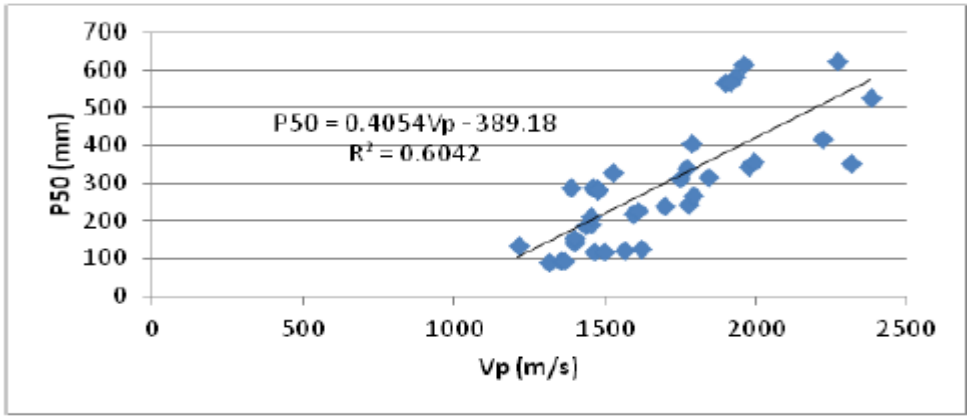

A Fragmentation versus P wave velocity

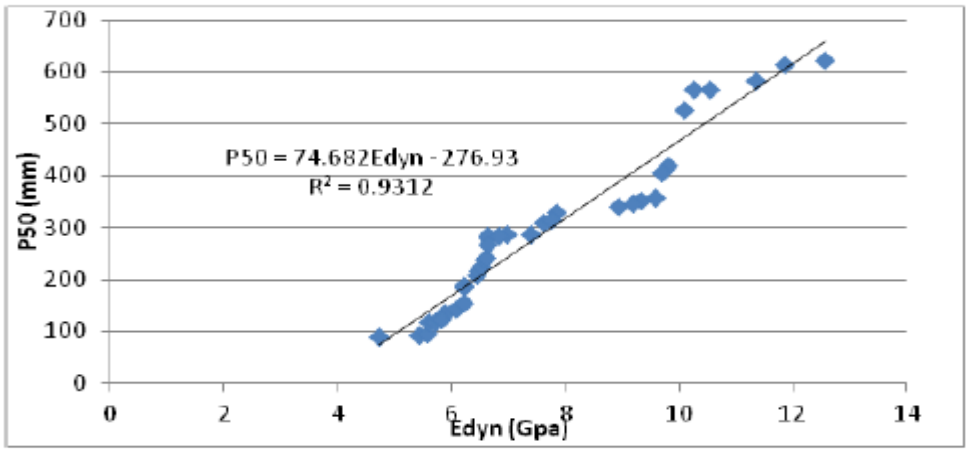

B Fragmentation versus dynamic elasticity modulus

Figure 2.32 Relationship of fragmentation with P-wave velocity and dynamic elastic modulus (Hossaini et al., 2013).

High-quality fragmentation is important to successful mining operations and equipment maintenance. It is advantageous to have a uniform distribution of

fragments size, to avoid both fines and oversize. According to Gheibie et al. (2009) two different mechanisms are used to analyse rock fragmentation. The coarse part is produced by tensile fracturing, and the Kuz-Ram model is used to predict this part of the size distribution. In addition, Moser et al. (2000) claimed that the Kuz-Ram model predicts the coarse part of the fragmentation size distribution with good accuracy. Djordjevic (1999) predicted rock fragmentation based on the assumption that the zone close to the borehole produces the fines material i.e. failure through shearing and in the outer zone medium- to large-sized material. Djordjevic (1999) show a good correlation between blasting results and predicted results. More recent works agreed that it is vital to consider the rock fragmentation in the crushed zone to correctly understand the partitioning of the energy delivered by the explosive (Sellers et al., 2012a and Sellers et al., 2012b).

However, both fines and coarse material are predicted with reasonable accuracy using the Rosin-Rammler distribution function. The Rosin-Rammler distribution function and Kuz-Ram model are widely used prediction models occurring in the literature on blasting. The Kuznetsov function, in combination with the Rosin-Rammler distribution function is known as the Kuz-Ram and is often used to predict the fragments size distribution from blasting (Cunningham, 1983). It has been a generally recognised method for giving a reasonable description of fragmentation of blasted rocks. Equation 2.9 is proposed by Rosin and Rammler (1933).

$$R_m = 1 - e^{-\left(\frac{X}{X_c}\right)^n} \tag{2.9}$$

where R_m is the proportion of material passing the screen, x is the screen size (cm), x_c is the characteristic size (cm), and n is the index of uniformity.

The characteristic size x_c is one through which 63.2% of the particle passed. Equation 2.9 is rearranged for the characteristic size to yield:

$$X_c = \frac{X}{\sqrt[n]{-\ln(1-R_m)}} \tag{2.10}$$

Since the Kuznetsov formula gives the screen size, X_m for which 50% of the material could pass, therefore, substituting the values $X = X_m$ and $R_m = 0.5$ into Equation 2.10 gives:

$$X_c = \frac{X_m}{\sqrt[n]{0.693}} \tag{2.11}$$

Kuznetsov (1973) developed a relation between the mean fragments size (k_{50}, cm) and the explosive quantity used per unit volume, as a function of rock type categorised as 'medium-hard', 'hard and fissure' and 'weak' rocks. The model is used to predict fragmentation from blasting in terms of the mass percentage passing versus the fragments size. Kuznetsov's equation is given in Equation 2.12

$$X_m = A\left(\frac{V_o}{Q_e}\right)^{0.8} Q^{1/6} \tag{2.12}$$

where X_m is the mean fragments size (cm), A is the rock factor, (7 for 'medium-hard' rocks, 10 for 'hard, highly fissured' rocks, 13 for 'hard, weakly fissured' rocks), V_o is the rock volume broken per blast hole (m^3), and Q_e is the mass of TNT

containing the energy equivalent of the explosive charge in each blasthole (kg) and the relative weight.

Hence, Equation 2.12 based upon ANFO instead of TNT can be written as

$$X_m = A\left(\frac{V_0}{Q_e}\right)^{0.8} Q_e^{1/6}\left(\frac{S_{anfo}}{115}\right)^{\frac{-19}{30}} \tag{2.13}$$

Where Q_e is the mass of explosive being used (kg) and S_{anfo} is the relative weight strength of the explosive to ANFO.

Given that,

$$\frac{V_0}{Q_e} = \frac{1}{K} \tag{2.14}$$

Where K is the powder factor (kg/m^3),

Therefore,

$$X_m = A(K)^{-0.8} Q_e^{1/6}\left(\frac{115}{S_{anfo}}\right)^{\frac{19}{30}} \tag{2.15}$$

The Kuz-Ram ability in predicting fragmentation has been questioned by many authors that necessitated its modifications by several authors. Even at present the problem has not been completely resolved. Some improvements made to the model include modification to the rock factor. The rock mass categories defined by Kuznetsov (1973) are very wide and need more precision. Therefore, Cunningham (1983) developed a model to improve the Kuz-Ram model for the

estimation of rock factor ‘A’ to vary between 0.8 and 22, depending on hardness and structure (Equation 2.16).

$$A = 0.06\ (RMD + RDI + HF) \quad (2.16)$$

Where *RMD* is the rock mass description, *RDI* is the rock density influence and *HF* is the hardness factor, the values for these parameters being derived as follows:

RMD, A number is assigned according to the rock condition; Powdery/friable = 10; massive formation (joints further apart than blasthole) = 50 and jointed rock factor.

The vertically jointed – derive jointed rock factor (JF) is derived as follows:

$$JF = (JCF\ JPS) + JPA \quad (2.17)$$

Where JCF is the joint condition factor, JPS is the joint plane spacing factor and JPA is the joint plane angle factor.

The hardness factor *(HF)* is estimated as:

If $Y < 50$, $HF = Y/3$; If $Y > 50$, HF = UCS/5

Where Y = elastic modulus, GPa; UCS = unconfined compressive strength, MPa.

In addition, Cunningham (1987) provided technique for the estimation of the uniformity index in the Rosin-Rammler formula as indicated in Equation 2.18, to further improve the Kuz-Ram prediction ability. Cunningham (1987) used Blastability Index earlier proposed by Lilly (1986) to fill this gap.

$$n = (2.2.-14Bd/\ d)((1/md)\ /\ 2)0.5\ (1-W/\ Bd)(abs(((lb-lc)\ /\ Lch)\ +0.1)0.1(Lch/Hb) \quad (2.18)$$

Where n is index of uniformity; Bd is burden in drilling (m), d is blast hole diameter (mm), md is spacing to burden ratio while drilling; W is standard deviation of accuracy in burden while drilling (m); abs is the absolute value; lb is base charge length (m); lc is column charge length (m); Lch is total charge length (m); Hb is bench height (m).

After Cunningham (1987), major research works toward improving the Kuz–Ram model has been in the area of estimating fines. Prominent research addressing this has been done probably by Kanchibotla et al. (1999), Djordevic (1999), Ouchterlony (2005a), Spathis (2004) and Ouchterlony (2005b). The researchers noticed that the Kuz-Ram model is deficient in predicting fines and come out with modifications as discussed in the following paragraphs.

Kanchibotla et al. (1999) presented the crushed zone model (CZM) to improve the Kuz-Ram model in estimation of fines. The CZM uses two functions; one describes the fines part while the second describes the coarse part of the curve. The coarse part is expressed in Equation 2.19. The coarsest particle size is assumed to be 1 mm and the characteristic size X_C ranges from X_{50} for strong rocks to X_{90} for very soft rocks.

$$P(x) = 1 - e^{\left(\ln(1-P(X_c)) - \left(\frac{X}{X_c}\right)^{n_{coarse}}\right)} \tag{2.19}$$

Where:

$P(X)$ is percentage of material passing sieve size X

$P(X_C)$ is percentage of material passing characteristic size X_C

X is sieve size, X_c is characteristic size

The n_{coarse} is the uniformity index for the coarse part of the curve and is expressed in Equation 2.20;

$$n_{coarse} = \left(2.2 - 14 * \left(\frac{B}{D}\right)\right) * \sqrt{\left(\frac{1 + S/B}{2}\right)} * \left(\frac{L_{tot}}{H}\right) \tag{2.20}$$

Where:

B is burden (m), D is drillhole diameter (mm), S is spacing (m), H is bench height and L_{tot} (m) is the total charge length.

Similarly, the fine part of the size distribution curve is given in Equation 2.21

$$P(x) = 1 - e^{\left(\ln(1 - P(X_c)) - \left(\frac{X}{X_c}\right)^{n\,fine}\right)} \tag{2.21}$$

Where,

N_{fine} is the uniformity index for the fine part of the curve and express as follows;

$$n_{fine} = \frac{\ln\left(\frac{\ln(1 - F_c)}{\ln(1 - P(x_c))}\right)}{\ln\left(\frac{1}{x_c}\right)} \tag{2.22}$$

Where F_c is fraction of crushed material, $P(X_c)$ is percentage of material passing characteristic size X_c, X_c is characteristic size and n_{fine} is the uniformity index for the fine part of the curve

Djordevic (1999) work attributed the excess of fines to the crush zone around each blasthole, and introduces a term to incorporate into the Kuz–Ram model. The fragmentation curve is given by Equation 2.23. The Kuz-Ram model parameters X_{50} and n are similar to a and b in the CZM.

$$P(x) = 100 * \left[1 - (1 - F_c) * e^{-\ln 2 \left(x/a \right)^b} - F_c * e^{-\ln 2 \left(\frac{x}{c} \right)^d} \right] \quad (2.23)$$

Where,

$P(X)$ is percentage of material below size X, X is size material (m), F_c is fraction of crushed material while a and b are mean fragments size (m) and uniformity coefficient outside the crushed zone; c and d are mean fragments size and uniformity coefficient within the crushed zone.

Ouchterlony (2005a) recognised that the Rosin–Rammler curve has limited ability to follow the various distributions from blasting, and introduces the more adaptable Swebrec function, which is able to define fines better. It is called KCO model, an extension of Kuz-Ram model. It contains three parameters, the median fragments size x_{50}, the maximum fragments size x_{max} and an undulation parameter b, which is similar to n in the Kuz-Ram model, as expressed in Equation 2.24. The

expression for X_{50} is the same for the Kuz-Ram model while the Swebrec function is given in Equation 2.25.

$$b = \left[2 * \ln 2 * \ln\left(\frac{x_{\max}}{x_{50}} \right) \right] * n \tag{2.24}$$

Where b is the curve undulation parameter, x_{max} is the maximum insitu block size (cm), X_{50} is 50% passing size and is the same as given in Kuz-Ram model (cm) and n is the uniformity index as given in the Kuz-Ram model.

$$P(X) = \frac{1}{\left[1 + \left(\frac{\ln\left(X_{\max} / X \right)}{\ln\left(X_{\max} / X_{50} \right)} \right)^{b} \right]} \tag{2.25}$$

Where $P(X)$ is the percentage of material passing sieve size X.

However, Spathis (2004) noticed that Ouchterlony (2005a, Spathis cited the wok before been published in EFEE conference proceedings) use of the X_{50} term in the Kuznetsov equation was at odd with the definition of the Rosin–Rammler 50% passing term. Spathis demonstrated that, for low values of n, i.e. the uniformity index in the Kuz-Ram model (which lies between 0.8 and 2.2), the characteristic sizes of the original model are in error of 179% and 105% respectively thereby showing a large deviation between the values.

In addition, Spathis proceeded that the Cunningham (1983) expressions for the Kuznetsov mean size and the Rosin-Rammler 50% passing size yields an incorrect expression for the characteristic size, X_c^* given in Equation 2.26

$$X_c^* = \frac{d_k}{(\log_e 2)^{1/n}} \tag{2.26}$$

Where d_k is the mean size

As a result of this, Spathis presented the correct expression for the characteristic size, X_c, of the Rosin-Rammler distribution, given the mean size, d in Equation 2.27 as presented in the original Kuznetsov's analysis

$$X_c = \frac{d}{\Gamma(1 + 1/n)} \tag{2.27}$$

Where Γ is the gamma function

Furthermore, Spathis demonstrated that the difference between the scaling factors in Equations (2.26) and (2.27) is substantial. The correction is given in Equation 2.28, when d=d_K

$$X_c^* / X_c = \Gamma(1 + 1/n) / (\log_e 2)^{1/n} \tag{2.28}$$

Therefore, Ouchterlony (2005b) applied the correction pointed out by Spathis to the Kuz-Ram model as given below:

$$X_{50} = \left(\frac{(\log_e 2)^{1/n}}{\Gamma(1 + 1/n)} \right) * A * \left(\frac{1}{K^{0.8}} \right) * Q^{1/6} * \left(\frac{115}{S_{anfo}} \right)^{19/30} \tag{2.29}$$

With the correction incorporated into Kuz–Ram model, the expression shifts the fragments size distribution to smaller values for X_{50} accounting for more fines

fraction. The modifications applied to the Kuz–Ram model has been largely towards fitting of size distribution curve into the fines.

It is evident from the above literature that the Kuz-Ram empirical fragmentation model is based on the fact that increased levels of explosive energy result in increased fragmentation. In addition, high strength rocks require more explosive energy than the lower strength rocks. However, the fragments size may not only depend on the explosive energy input but may also depend on the rock resistance to fragmentation or its brittleness.

The model inherently assumed that the brittleness behaviour of rocks is the same. As indicated above, there are modifications to the formulation of the equation due to its deficiency in accommodating fines in the fragmentation curve, but these do not consider the effects of rocks resistance to fragmentation or the brittleness behaviour of rocks.

Therefore, in this work brittleness is considered a very important intact rock mechanical property because it has a strong influence on the failure process and on the rock mass response to fragmentation activities. No research had ever attempted to link the two. Part of the purpose of this investigation is to determine the influence of rock brittleness on fragmentation. A statistical analysis is developed using stepwise multiple regression technique to show whether or not brittleness is related to fragmentation of rock under unconfined uniaxial compressive failure using variety of widely used brittleness concepts in literature.

The various brittleness concepts are also compared with fragmentation by laboratory scale blasting tests. Relationships between them are established.

Additional analyses are done with different brittleness concepts to see the validity of the relationship and provide suitable concept for describing brittleness of rock under compression and blasting tests. The relationship between brittleness and fragmentation by blasting test is analysed and the possibility of incorporating it into the Kuz-Ram model is assessed to account for the effect of rock brittleness on fragmentation.

2.5.2 Rock Fragmentation under a Compression Loading Condition

The fragmentation of rock under compression involved series of mechanisms that occur within the rock body during loading and results in splitting it into smaller pieces. A rock specimen under compression or tensile loading condition fails when the stress applied exceeds the strength of the rock specimen. Rocks fail across the slip surface in the form of shear failure, axial splitting and extension fracture. Extension of fracture occurs in a uniaxial tensile test as the specimen splits or divides normal in the direction of the applied tensile stress. The axial splitting or axial cleavage is the predominant fracture form during the uniaxial compression and Brazilian tensile tests.

The magnitude of randomly growing cracks (like the one shown in Figure 2.1 Section 2.2) is capable of influencing the result of fracture appearance. For instance, several authors (Dey & Wang, 1981; Wong, 1982; Du & Aydin, 1991; Lockner et al., 1992) observed that at a low concentration (i.e. the mean distance

between the cracks is large enough to prevent crack interaction) of cracks, they have enough spaces to extend. Subsequently, the task of crack's interference increases the chances of crack growth and results in axial splitting of the sample. They observed that when the concentration of cracks is high, their interaction produces disorder in the stress field which result to a bigger crack restricted by a thin band slanting to the orientation of the axial stress. They concluded that it may ultimately result in an oblique (shear) fracture even though the sample is under uniaxial loading and the stress distribution is uniform (Figure 2.33).

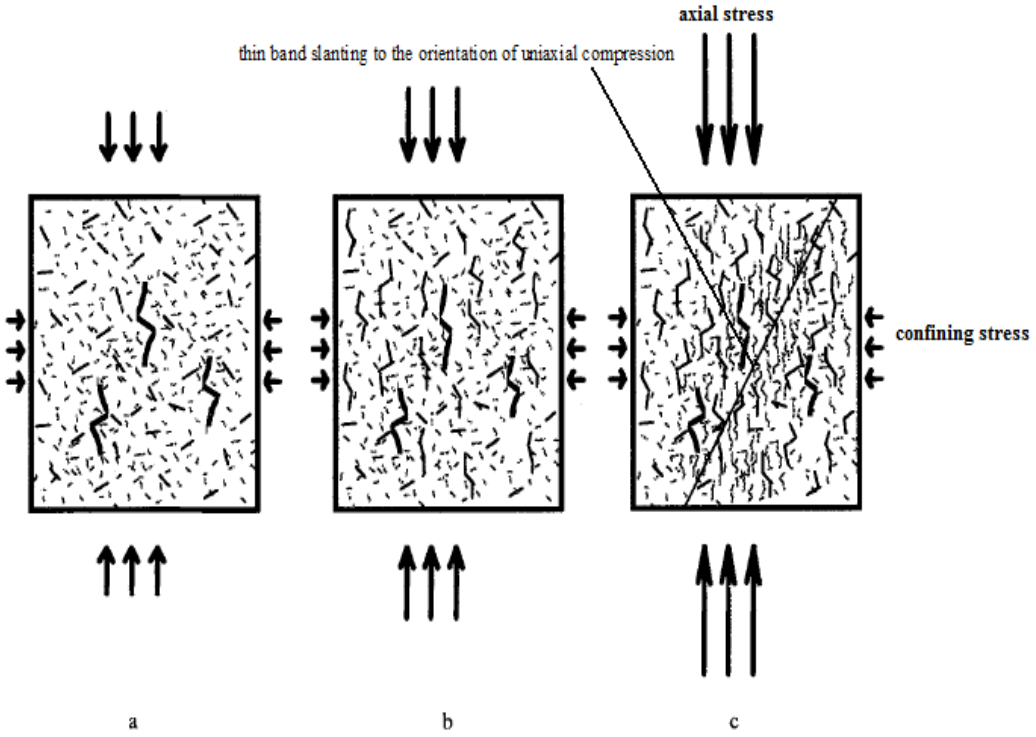

Figure 2.33 Concentration of increasing rising cracks result in an oblique fracture (Germanovich & Dyskin, 1988; Horii & Nemat-Nasser, 1985).

In Figure 2.33 (a) the presence of lateral pressure hampers growth of the largest cracks and, therefore, these cracks can no longer cause the fracture; (b) as the load increases, the smaller cracks can start to grow; (c) at the final stages of loading,

the initiation of new growing cracks is localised within an inclined band which eventually produces the shear failure indicated by a solid line (Germanovich & Dyskin, 1988; Horii & Nemat-Nasser, 1985)

Ozkahraman (2010) opined that the brittle fracture of rock is basically grouped into two: ‘tensile fracturing’ and ‘compressive-shear’ failure depending on the level of the applied stress. The form of fractures and their orientation is influenced by the distribution of stress across the specimen, the nature of the material, and whether the applied stress is in tension or in compression (Ozkahraman, 2010). It was observed in previous sections that the behaviour of brittle rocks in compression is affected by strain rate, structure of the rock, heterogeneity and the extent of its internal damage. These factors also influence the degree of fragmentation produced under compression loading.

Yang et al. (2009) showed that heterogeneity played an important role in the deformation characterisation of rock. This is illustrated in Figure 2.16 in Section 2.3.3. Hajiabdolmajid and Kaiser (2003) also observed that in brittle fracturing, the rock type, grain size, pre-existing cracks, pore and the occurrence of flaky, soft and altered minerals influence the brittleness of rock (this is discussed further in Section 2.6.3).

Donald et al. (1974) described a procedure for predicting fragments size distribution for rock under dynamic loading condition. They showed that fragmentation behaviour could be predicted from a few measurable rock properties using controlled impact experiments on Novaculite. Also Bohloli and

Hoven (2007) selected for laboratory testing four rock types: Amphibolites, Diabase, Diorite and Gneiss and, performed a series of Brazilian tensile tests on each of these. They established that there is a relationship between the percentage of fines produced and the tensile strength of the specimens.

2.5.3 Fragmentation and Effect of Strain Rate

Whittles et al. (2006) and Jackson et al. (2008) revealed the effect of strain rate on the degree of fragmentation. They determined the degree of fragmentation by counting the number of fragments produced after each test. They showed that the test at the lowest strain rate produce two main fragments, separated along a single shear plane. An increase in strain rate increases the number of fragments. This is illustrated in Figures 2.34 and 2.35 with the highest fragmentation at the highest strain rate for all the rock types. The increase in rock fragmentation with an increase in strain rates was in agreement with the findings of other researchers who observed that the degree of fragmentation varies as a function of strain rate (Brace & Byerlee, 1967; Grady & Kipp, 1987).

Figure 2.34 Photograph of the pre- and post-test sample core debris from the Ibbenburen Sandstone and Caldon low Limestone, showing changes in fragments size with strain rate (Whittles et al., 2006).

Figure 2.35 Photographs of the pre- and post-test sample core debris from the Melton Ross chalk, showing changes in fragments size with strain rate (Whittles et al., 2006).

2.6 Concept of Rock Brittleness

A general theory with regard to rock brittleness states that a more brittle rock will break under very little deformation (Gong & Zhao, 2006). Rock brittleness simply means the absence of ductility. The ductility of a material is the ability of the material to tolerate a large inelastic deformation with no loss of its load-carrying capacity. In contrast, the brittleness of a material is demonstrated by its decrease in load-carrying capacity as the strain increases with little or no inelastic deformation. This differs from the failure of ductile materials where shear slip surfaces form in such a way that continuity of material contact is maintained. However, brittle failure is a process whereby continuity is dislocated to create chunks or blocks that are separated with feasible failure modes (Hajiabdolmajid & Kaiser, 2003).

A material can be considered brittle or ductile with respect to its mechanical properties as well as with respect to its behaviour under the loading conditions (Andreev, 1995). Since the definition of brittleness is described by deformation behaviour of rock and failure subject to the loading condition, the measurement of brittleness is not yet standardised (Gong & Zhao, 2006). An earlier work by Hucka and Das (1974) agreed that the notion of brittleness is not yet completely defined. They stated that with higher level of brittleness, the following is observed: low value of elongation, fracture failure, formation of fines, high ratio of compressive to tensile strength, high resilience, and a high angle of internal friction and formation of cracks on indentation. Ramsey (1967) defined brittleness as a loss of internal cohesion in rock, when this happen the rock is said to be

brittle. Obert and Duvall (1967) described brittleness of a material such as cast iron and brittle rocks to end by fracture at or after the yield stress. Brittleness is also defined as a property of a material that shatters or fractures with slight or absent of plastic flow (Yarali & Soyer, 2011).

At present there is no clear cut method accepted by the mining community to quantify brittleness. Therefore, its meaning is vague. However, there are number of methods to determine it in the literature. Different definitions and methods that are used to determine it are based on the purpose and the use. Definitions that appeared in the literature are coined from the methods of its determination. Some of the lists of the definitions in the literature are discussed in the next section.

The following brittleness indices (referred to in this research as B_i where B stands for brittleness and 'i' is the number of various brittleness' indices that exist in literature; i takes a whole number based on the sequence it appears in this section) exist in the literature with their method of estimation. The indices are subdivided into 'dimensionless' (without any form of unit) and 'dimensional' (with a sort of unit). The different concepts for brittleness measurement are discussed in the following sections.

2.6.1 Dimensionless Brittleness Indices

Baron (1962) estimated brittleness as a percentage of the reversible energy from pre-failure and post-failure stress-strain curve (Figure 2.36 with "o" as the origin). This figure shows the pre-failure and post-failure curves under deviator stress (σ

$_1$-σ_3), axial strain (ε_1) and total volumetric strain (ε_v). The maximum stress is denoted as R_m .The brittleness is estimated as follows:

$$B_1 = areaDCF \big/ areaOCF \qquad (2.30)$$

where B_1 is the brittleness estimated from this concept.

According to Coates (1966), brittleness is the ratio of the reversible strain to the total strain at the point of failure. Brittleness, B_2 (brittleness from ratio of strain) is estimated from Figure 2.36 as follows:

$$B_2 = DF \big/ OF \qquad (2.31)$$

Andreev (1995) used various concepts to estimate brittleness from pre-failure and post-failure stress-strain curves in Figure 2.36. This is discussed as follows.

Brittleness, B_3 is determined from the ratio between the difference in peak strength and residual strength deviator, R_m-σ_3, and R_r-σ_3 in Equation 2.32 (Andreev, 1995). The parameter used is in Figure 2.36.

$$B_3 = \frac{(R_m - \sigma_3) - (R_r - \sigma_3)}{R_m - \sigma_3} \qquad (2.32)$$

Andreev (1995) also determined brittleness (B_4) as the ratio of residual, R_r to peak stress R_m. In addition, brittleness, B_5 is determined from initiation stress, σ_{1i} to peak strength, R_m using Figure 2.36 in Equation 2.33 and Equation 2.34.

$$B_4 = \frac{R_r}{R_m} \qquad (2.33)$$

$$B_5 = \frac{\sigma_{1i}}{R_m} \tag{2.34}$$

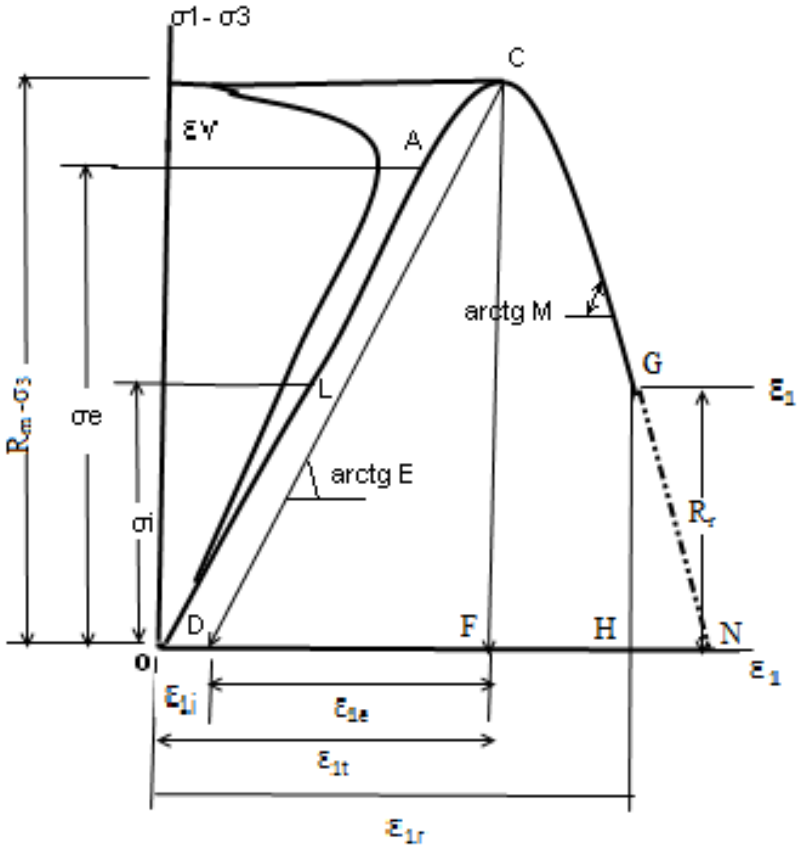

Figure 2.36 Quantities participating in brittleness determination in stress-strain curve (Andreev, 1995).

Brittleness, B_6 is estimated from the ratio of residual strain, ε_{1r} to post-peak strain, ($\varepsilon_{1r} - \varepsilon_{1t}$) from Figure 2.36 in Equation 2.35 below (Andreev, 1995).

$$B_6 = \frac{\varepsilon_{1r}}{\varepsilon_{1r} - \varepsilon_{1t}} \tag{2.35}$$

Bergman and Stille (1983), and Stavrogin and Protossenia (1985) as contained in Andreev (1995) estimate brittleness, B_7 from the ratio of post-peak modulus, M to the pre-peak modulus, E (i.e. modulus of elasticity) from Figure 2.36 in Equation 2.36.

$$B_7 = \frac{M}{E} \approx \frac{OACD}{FCN} = \lambda \tag{2.36}$$

Furthermore, the ratio of M to the sum of M and E is used to estimate brittleness, B_8 (Batougina et al., 1983; Stavrogin & Protossenia, 1985; as contained in Andreev, 1995). The ratio is expressed in Equation 2.37.

$$B_8 = \frac{M}{E+M} \approx \frac{DCF}{OACF + FCN} \tag{2.37}$$

They suggested that material turns out to be brittle when the value of $B_8 > 0.5$. They opined that in such a case B_8 is expressed in Equation 2.38 for B_9 (Manjikov et al., 1983; as contained in Andreev, 1995).

$$B_9 = \frac{E\varepsilon_{1e}}{E\varepsilon_{1e} + M\left(E\varepsilon_{1r} - E\varepsilon_{1e}\right)} \tag{2.38}$$

Brittleness is determined from strain-dependent strength mobilisation (cohesive and frictional strength components). Hajiabdolmajid and Kaiser (2003) introduced a strain dependent brittleness index, B_{10}. It is expressed by Equation 2.39 with plastic strain limits $\varepsilon_f^p, \varepsilon_c^p$ in Figure 2.37 using plasticity theory and the concept of strain-dependent strength mobilisation.

$$B_{10} = \frac{\varepsilon_f^p - \varepsilon_c^p}{\varepsilon_c^p} \tag{2.39}$$

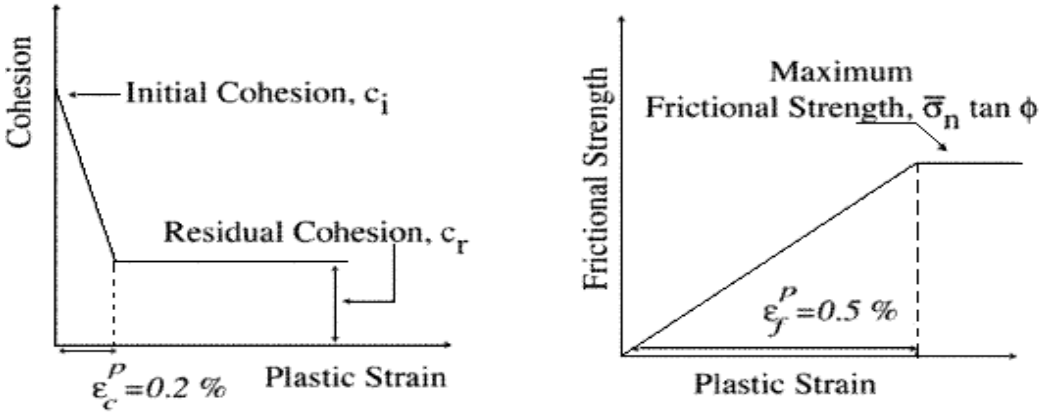

Figure 2.37 Illustration of cohesion-loss and frictional strengthening as a function of plastic strain (Hajiabdolmajid & Kaiser, 2003).

Brittleness is estimated from Brazilian tensile and uniaxial compressive strength of rock (Gong & Zhao, 2007; Kahraman, 2002; Altindag, 2002; Yagiz, 2009). Using the ratio of Brazilian tensile, σ_t and uniaxial compressive, σ_c strength of rock, brittleness, B_{11} and $B12$ are estimated as follows:

$$B_{11} = \frac{\sigma_c - \sigma_t}{\sigma_c + \sigma_t} \tag{2.40}$$

$$B_{12} = \sigma_c / \sigma_t \tag{2.41}$$

2.6.2 Dimensional Brittleness Indices

In addition, using the product of uniaxial compressive strength and Brazilian tensile strength of rock, brittleness, B_{13} is estimated as follows:

$$B_{13} = {\sigma_c * \sigma_t}/{2} \quad (\text{MPa})^2 \tag{2.42}$$

Additionally, a brittleness concept is proposed as the square root of brittleness B_{13} (Altindag, 2008 as contained in Altindag & Guney, 2010).

Yarali and Soyer (2011) proposed a new brittleness, B_{14} concept as a result of their study on the effect of mechanical properties of rock on drillability. The relation is expressed is Equation 2.43.

$$B_{14} = (\sigma_c \times \sigma_t)^{0.72} \ (\text{MPa})^2 \tag{2.43}$$

Brittleness, B_{15} is estimated and is based on the absolute irreversible longitudinal (parallel to σ_1) strain, ε_{1i} at failure in Figure 2.36.

$$B_{15} = \varepsilon_{1i} \times 100\% \quad (\%) \tag{2.44}$$

Based on this brittleness estimation, rocks are classified as follows:

$\varepsilon_{1i} <$ 3% brittle rock

3% < ε_{1i} <5% brittle-ductile transition

ε_{1i} > 5% ductile

Similarly, brittleness is determined as a product of pre-peak modulus, E and post-peak modulus, M from Figure 2.36 as shown in Equation 2.45 (Batougina et al., 1983; as contained in Andreev, 1995). They opined that a rock specimen is unstable and accordingly it is brittle if B_{16}< 1.

$$B_{16} = EM \quad (\text{GPa})^2 \tag{2.45}$$

Brittleness is determined from the measurement of the oblique shear in the Mohr envelope. Hucka and Das (1974) estimated brittleness from Mohr's 'Theory of Strength' in which the maximum resistance to deformation is given by Equation 2.46:

$$r = c + \sigma_n \tan\phi \tag{2.46}$$

Where r is the resistance to deformation at failure, σ_n is the normal stress, c is cohesion and angle of friction, ϕ. From Equation 2.46, ϕ is given by the equation below:

$$\phi = \arctan\left(\partial r / \partial \sigma_n\right) \tag{2.47}$$

It follows that B_{17}

$$B_{17} = \sin\phi = \left(\partial r / \partial \sigma_n\right) / \left(1 + \partial r / \partial \sigma_n\right) \quad \text{(degree)} \tag{2.48}$$

Also, according to Hucka and Das (1974), brittleness is estimated from the oblique shear. The oblique shear, α is the inclination of the failure plane to the principal stress, σ_1. The relationship between friction angle and oblique shear is given by:

$$2\alpha = \pi/2 - \phi \tag{2.49}$$

Therefore, B_{18} is given by:

$$B_{18} = \alpha = \frac{\pi}{4} - \frac{\phi}{2} \tag{2.50}$$

Brittleness, B_{19} is also determined from the amount of fines formed during an impact test for estimating the rock's strength. Protodyakonov (1963) estimated brittleness from the percentage of fines (-28 mesh) formed in the Protodyakonov impact test. The relation below is used:

$$B_{19} = q\sigma_c \quad \text{(MPa)} \tag{2.51}$$

Where q is the percentage of fines formed in the Protodyakonov impact test and σ_c is uniaxial compressive strength.

Blindheim and Bruland (1998) estimated brittleness in Equation 2.52 from the percentage of fines (<11.2 mm) formed in an impact test for TBM (Tunnel Boring Machine) performance prediction with the NTNU (Norwegian University of Science and Technology) model. The brittleness, B_{20} determined here is a measure of the ability of the rock to resist crushing by repeated impacts.

$$B_{20} = S_{20}(\%) \tag{2.52}$$

Where S_{20} is the percentage of fines (<11.2 mm) formed in an impact test for TBM performance prediction with the NTNU model.

The brittleness value S_{20} equals the percentage of material that passes the 11.2 mm mesh after the aggregate has been crushed by 20 impacts in a mortar. The brittleness value is the mean of 3 to 5 parallel tests (Dahl, 2003).

Brittleness is determined from hardness and toughness values. The brittleness is estimated from the difference between macro-indentation hardness and micro-indentation hardness. The difference in the values is used to quantify brittleness. Macro-indentation hardness means hardness is determined from the experiment carried out with a macro or large size indenter or small size indenter as with micro-indentation hardness (Honda & Sanada, 1956). The relation for B_{21} is given by Equation 2.53:

$$B_{21} = \frac{H_{\mu} - H}{K} \quad (\text{N/mm}^2) \tag{2.53}$$

where H_{μ} is micro-indentation hardness, H is macro-indentation hardness and K is a constant. Using Vickers's micro and macro-hardness, K = 2.6.

Quinn and Quinn (1997) proposed brittleness, B_{22} for ceramic materials from hardness (H), Young's modulus (E) and fracture toughness (K_{ic}) in Equation 2.54:

$$B_{22} = \frac{HE}{K_{ic}^2} \quad (\text{MPa m}^{0.5}) \tag{2.54}$$

Fracture toughness is defined $K_{ic} = \left[\frac{2E\gamma_f}{(1-\nu^2)}\right]^{1/2}$, as ν is Poison's ratio and γ_f is the effective fracture surface energy.

Lawn and Marshall (2006) determined brittleness, B_{23} as a ratio of hardness, H (resistance to deformation) to toughness, K_c (resistance to fracture) in Equation 2.55:

$$B_{23} = \frac{H}{K_c} \quad (\text{MPa}) \tag{2.55}$$

Yagiz (2009) proposed a brittleness concept, B_{24} from the result of a punch penetration test as given in Equation 2.56:

$$B_{24} = \frac{F_{\max}}{P} \quad \text{(kN/mm)} \tag{2.56}$$

where B_{24} is the brittleness estimated from the slope of force and displacement curve in a punch penetration test. F_{max} is the force on the specimen (kN), and P is the penetration at ultimate force (mm).

Brittleness, B_{25} is also determined from the crushing of rocks. The rock brittleness is estimated as a ratio of work done, w in rock crushing to Brazilian tensile strength σ_t as given in Equation 2.57 (Andreev, 1995):

$$B_{25} = \frac{w}{\sigma_t} \quad \text{(J/MPa)} \tag{2.57}$$

Brittleness, B_{26} is also determined from rock core drilling. "After sound drilling, very often the core is divided into discs with a thickness h and a diameter d" (Andreev, 1995, p.127). The relation is given below:

$$B_{26} = h \leq \frac{d}{3} \quad \text{(mm)} \tag{2.58}$$

If the relation above holds, the rock is assumed to be brittle.

2.6.3 Factors Influencing Brittleness Determination

The twenty-six brittleness indices determined from various concepts are listed in the previous section. Brittleness determination that are similar in concept and theory but differ only with the symbols are omitted to avoid duplication.

However, the list of 26 different meanings and equations used to quantify rock brittleness shows that the determination of brittleness is not clear. The reason for this is that brittleness is affected by many factors. These factors include the rock properties, the geometry and size of specimen and the loading conditions. These factors create conditions under which it is difficult to use a general meaning and equation that embraces all of the above factors.

Rock properties like: hardness, grain size and mineral composition, influence brittleness determination. For instance, hard rock is more brittle than soft rock. Hajiabdolmajid and Kaiser (2003) opined that different rocks have different indices of brittleness as a result of their distinctive textural and mineralogical constituent. As shown in Figure 2.21 in Section 2.3.5, UCS decreases with an increase in grain size of rock. Several researchers also show that the UCS of granitic and other rock types decreases with the increase in the mean grain size (Fredrich et al., 1990; Hugman & Friedman, 1979; Olsson, 1974; Onodera & Kumara, 1980; Prikryl, 2001). Yilmaz et al. (2009) stated that the grain size influences their relative brittleness index values in granitic rocks. Generally, rock brittleness index increases with increasing grain size (Gong & Zhao, 2006).

In addition, Onodera and Kumara (1980) showed that the proportion of boundary connected cracks (inter-granular cracks) decreases with increasing grain size whereas the number of intra-granular cracks increases. Therefore, Hajiabdolmajid and Kaiser (2003) suggested that for fine-grained polycrystalline rocks, the inter-granular cracks are more profuse than in the coarse-grained rocks. Consequently, fine-grained rocks are more brittle than coarse-grained rocks. Goktan and Yilmaz

(2005) showed that for a given rock group, an increase in the brittleness index is accompanied by an increase in uniaxial compressive strength (Equation 2.59):

$$B = 2.065 + k_i (\log \sigma_c)^2 \quad (2.59)$$

Where B is brittleness, k_i is dependent on rock type as grouped by Hoek (1983) taking values from 0.170 to 0.659, and σ_c is compressive strength expressed in kilopascals.

Hajiabdolmajid and Kaiser (2003) demonstrated in their work that the mineralogical composition of rock affects its brittleness. They showed that the occurrence of a small proportion of flaky, soft and distorted minerals tends to increase the rock's brittleness and lower its strength. Quartz mineral in rock affects the strength predominantly due to the interlocking structure between its grains. The presence of cleavable minerals (such as feldspars) in rocks leads to reduction in the strength and results in a higher brittleness index. Hence, the ratio of quartz to feldspar contents can be considered as a signal for higher brittleness (Liu et al., 2004). This is perhaps as a result of the comparatively weak bonds along the cleavage planes in feldspars which apparently have substantive and negative effect on the brittleness of the rock (Liu et al., 2004).

In addition, a mica-poor rock exhibits higher brittleness (Liu et al., 2004). Therefore, mica is a mineral that affects the brittleness properties of a rock in a similar way as the basic mineralogy does. An inverse effect is seen with an increase in the mica content of a rock on brittleness, it becomes less brittle. Since

mica is a soft mineral, it is likely that an increase in its content might have a significant negative effect on the brittleness of the rock (Liu et al., 2004)

Hajiabdolmajid and Kaiser (2003) observed that rock's brittleness is influenced by the loading rate and size (i.e. geometry) of the rock. As shown in Figure 2.12, the longer the specimen length, the more brittle the specimen becomes after the peak stress. This shows that rock specimen with longer length but the same diameter has a higher brittleness value than those with shorter lengths. The lower the loading rate, the more brittle rock becomes (Figure 2.30). Therefore, the brittleness of a rock increases with a decrease in the loading rate (time dependent) and an increase in the size of the sample (size dependent).

Earlier research by Kaiser and Morgenstern (1981) explained that a lower loading rate advances a more brittle behaviour as loads are distributed in a different way between cracking elements. The reduction in the loading rate advances the period for more cracks to proliferate. Therefore, a lower loading rate promotes brittleness. Temperature is another factor that influences the brittleness of a material. However, since this test is conducted under room temperature, this is not a concern in this research.

2.6.4 Assessment of the Various Brittleness Concepts

The factors in the previous section explained the reasons for the variability in brittleness determinations. However, most of the determinations and methods used to quantify brittleness do not express the real meaning or definitions of brittleness. The reason for this is that the definitions of brittleness expressed in

Section 2.6 point to the fact that brittleness is a mode of fracture accompanying material deformation. For instance brittleness B_{15} expresses absolute irreversible strain before failure. Also B_1 and B_2 estimate the percentage of reversible strain and the energy before failure. It gives an ideal of brittleness but what happens at post-failure regime is unknown. However, brittleness based on extension strain is analysed in this research as a brittleness concept.

Brittleness B_3 and B_4 expresses the ratio of strength at peak to residual strength. The physical meaning of these parameters does not explain the meaning of the brittleness concept of rock. For example, during a uniaxial compression test, the equation suggests that if the residual strength is equal to zero then B_3=1 and B_4=0 which may suggests for example 'perfect' brittleness or absolute brittleness (while Tarasov, 2010 assumed that absolute brittleness=0 at over 300MPa confining pressure). Nevertheless, brittleness based on strength ratios are analysed in this research as a brittleness concept.

The theoretical meaning of B_5 is uncertain as it expresses the ratio of fracture stress initiation to peak strength. It is a fact that the more brittle a material is the later micro-fracturing begins (Andreev, 1995). Brittleness, $B_{6,}$ give an idea about brittleness but not sufficient information. It can be seen that when ε_{1r} becomes smaller, the brittleness decreases. However, according to Andreev (1995) brittleness is supposed to increase with elastic-brittle behaviour. Brittleness B_7, B_8, B_9 and B_{16} give an idea of brittleness of rock but the parameter of estimation (pre-failure modulus and post-failure modulus) is expressed as an angle and not as a stress or strain. Therefore, their value depends on the scale adopted to plot the

values on the stress-strain graphs. However brittleness based on pre-failure modulus and post-failure modulus expressed as a stress and strains is analysed in this research as a brittleness concepts.

Brittleness B_7, B_8 and B_9 are ideas of stability based on Drucker's postulation (for the postulate see Romanov, 2001). The postulate is applied to the stability condition for plastic materials (e.g. metals). There are two categories of deformation of the material for this purpose, either 'elastic plastic' or 'rigid plastic' (Figure 2.38). The postulate applied the theory of plasticity. All materials are stable in Drucker's sense. There is nothing that suggests that a real material like rock could satisfy Drucker's stability. Drucker provides a link between material behavior (during plastic deformation) and the mathematics and it has nothing to do with the understanding of the brittleness of rock.

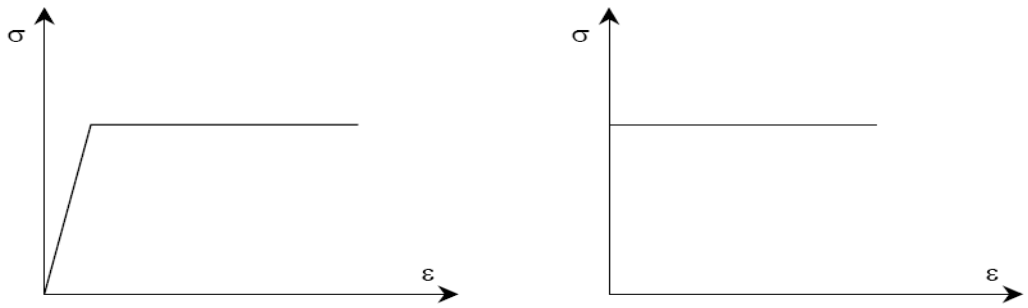

a) Elastic perfectly plastic *b) Rigid plastic*

Figure 2.38 Stress-strain relationships for elastic perfectly plastic and a rigid plastic material.

Brittleness B_{10} used the old theory of plasticity for its determination. The stresses are calculated in-situ using back analysis of stresses. The stresses are input into

the Mohr-Coulomb failure criterion called the ‘cohesion weakening-frictional strengthening model’ to capture the failure mechanism involved during brittle failure of an underground opening. The model is then used to estimate the parameters to determine its brittleness. The parameters might not be of interest here in the determination of brittleness using a stress-strain curve based on laboratory work. Moreover, Mohr-Coulomb does not give any information about brittleness of a rock. It contains no information on the post-failure characteristics of the rock. It is a combination of mechanisms used to estimate the strength of material. The envelope is drawn to fulfil the following requirement:

a. The circle is drawn to pass through the principal stresses
b. A line to touch all the Mohr circles
c. The line to touch the effective tensile stress circle i.e. uniaxial tensile

Brittleness B_{17} and B_{18} are also based on Mohr-Coulomb envelopes as explained in the previous paragraph. It has nothing to do with the brittleness of rocks. It is about strength behaviour rather than failure behaviour. Mohr Coulomb depicts rock strength against confining pressure (Figure 2.39).

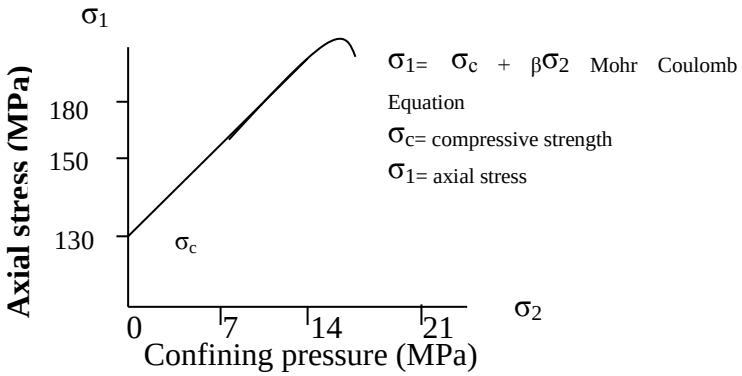

Figure 2.39 Mohr Coulomb's equation from a plot of axial stress against confining pressure.

The concepts from plasticity and Mohr's envelope discussed above are based on shear stresses. The concept used to analyses brittleness must satisfied the test condition since brittleness is subject to the loading condition. This is explained further in Chapter 5 Section 5.11. Brittleness B_{19}, B_{20} and B_{25} give a relationship between the impact of crushing on the compressive strength, tensile strength of rock and quantities of crushed rock passing through a particular sieve size. It measures the ability of the rock to resist crushing by repeated impacts. It gives no information about the behaviour of rock under brittle deformation. Brittleness B_{21}, B_{22}, and B_{23} give an indication of the hardness of a material by impact of an indenter or resistant to fracture toughness. It has no relationship with the deformation of material under brittle failure in compression. The author is investigating only the relationship between drillability and the parameter of interest, hardness of rock and fracture toughness.

B_{11}, B_{12}, B_{13} and B_{14} do not give any information about the failure mechanism. These are simply strength ratios or products. This was discussed and criticised by

Altindag (2000, 2002, 2003 and 2010b). The researcher pointed out that the ratio and products of rock strengths are basically intended to investigate their influence on rock drillability. These brittleness concepts are estimated from the static mechanical properties and are frequently used in many studies as a brittleness index. However, the researcher claims that this parameter is not 'brittleness', because it has nothing to do with the relation between elastic to plastic strain and pre and post-failure behaviour. However, this brittleness expressed as a stress ratio and products is analysed in this research as a brittleness concepts. Brittleness B_{26} is meaningless. It's just a diameter of drill core divided by 3. It has nothing to do with the rock's property or behaviour.

In summary, instead of the stress-strain curve in Figure 2.36 a normalised stress-axial strain version is used. The normalised stress-axial strain curves of the tested rocks are evaluated as a brittleness concept (chapter 5 section 2.10).

2.6.5 Brittleness and Fragmentation in Relation to the Research Study

All the brittleness indices discussed in the previous section do not consider the brittle behaviour of the rock characterising the post-failure stress-strain curve from which a rock could either be classified as Class I or Class II on a classification scale to show when a rock is brittle or appear to be 'ductile' or less brittle apart from B_{16} (with Class I having negative sign and Class II positive). Similarly, brittleness k has a classification scale as discussed in the following paragraph.

The modulus of the post-failure curve is used by many scholars to quantify brittleness as shown in brittleness B_7, B_8 and B_{16}. In addition, Tarasov (2010; 2011; 2013) introduce a new brittleness concept ''*k*''. This brittleness, *k*, was quantified as the capability of the rock to self-sustaining failure due to the elastic strain energy that accumulates in the material body during loading and available for rupture development in the post-peak region. Tarasov derived the relation below to estimate brittleness index, *k*. The formulation involves energy balanced at the post-peak response of the rock.

It is based upon, the balance between the post-peak elastic energy withdrawn from the specimen body at the rupture development with the rupture energy and the excess (released) energy that are associated with the failure process at post-peak (Figure 2.40). In Figure 2.40, the failure process between points *B* and B^i illustrates the variation in the energy balance at post-peak, where *E* and *M* are the pre-failure and post-failure moduli.

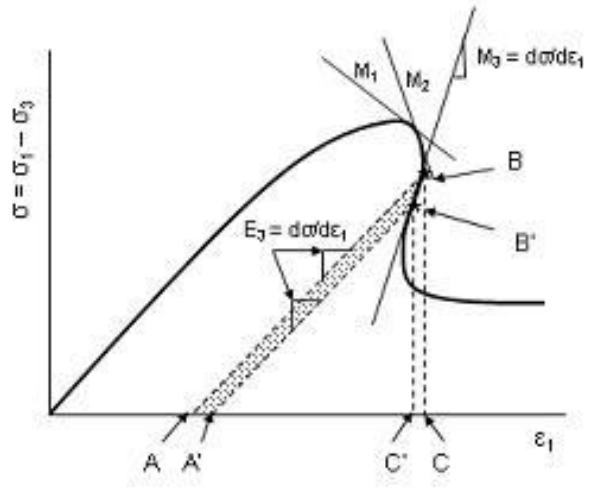

Figure 2.40 Calculation of Energy released at post-peak (Tarasov, 2012).

The elastic energy withdrawn, *dWe* from the material body corresponds to the area ABCC^{i}BiA^{i}. The corresponding rupture energy, *dWr* represent the area ABB^{i}A^{i}. The area C^{i}B^{i}BC represents the excess (released) energy, *dWa*. The energy are given by the following equations:

$$\delta W_e = \frac{\sigma^2{}_B - \sigma^2{}_{B^i}}{2E} \tag{2.60}$$

$$\delta W_a = \frac{\sigma^2{}_B - \sigma^2{}_{B^i}}{2M} \tag{2.61}$$

$$\delta W_r = \delta W_e - \delta W_a = \frac{\sigma^2{}_B - \sigma^2{}_{B^i}\left(M - E\right)}{2EM} \tag{2.62}$$

Tarasov (2012) mentioned that the energies are calculated on the basis of elastic modulus, *E* and post-peak modulus, *M* as given below:

$$k_1 = \frac{dw_r}{dw_e} = \frac{M - E}{M} \tag{2.63}$$

Brittleness" *k*" takes into account the sign of post-peak modulus *M* for Class I and Class II behaviour as expressed in Equation 2.64.

$$-k_1 = -\frac{dw_r}{dw_e} = -\frac{M - E}{M} = \frac{E - M}{M} = k \tag{2.64}$$

The brittleness index k_2 represents the ratio between the excess (released) and the withdrawn elastic energy as expressed in Equation 2.65.

$$k_2 = -\frac{dw_a}{dw_e} = -\frac{E}{M} \tag{2.65}$$

The brittleness concepts, k, k_1, k_2 are able to represent brittleness on a scale, with brittleness increasing from Class I rock to Class II rock (Figure 2.41), except for brittleness k_1.

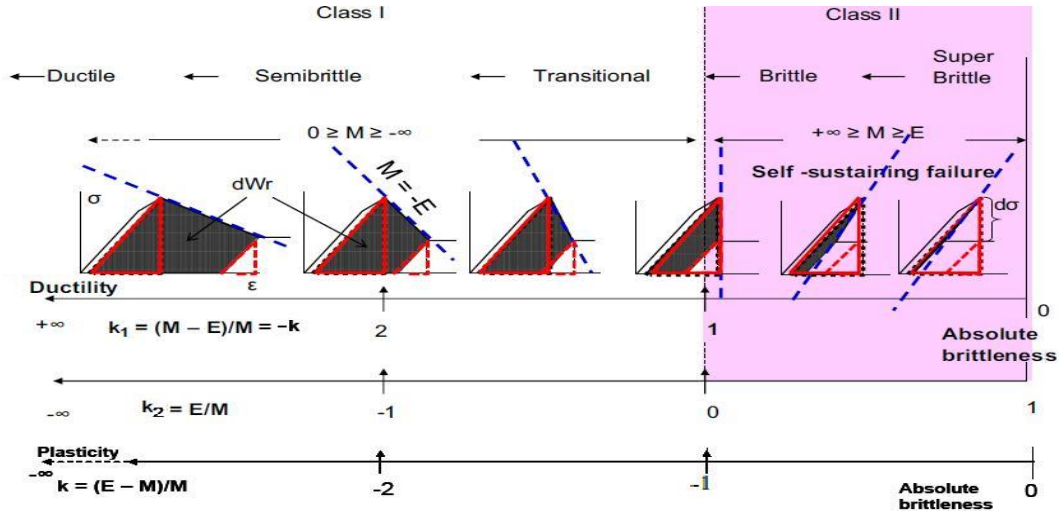

Figure 2.41 Scale of rock brittleness index, with brittleness increasing from left to right (Tarasov & Potvin, 2013).

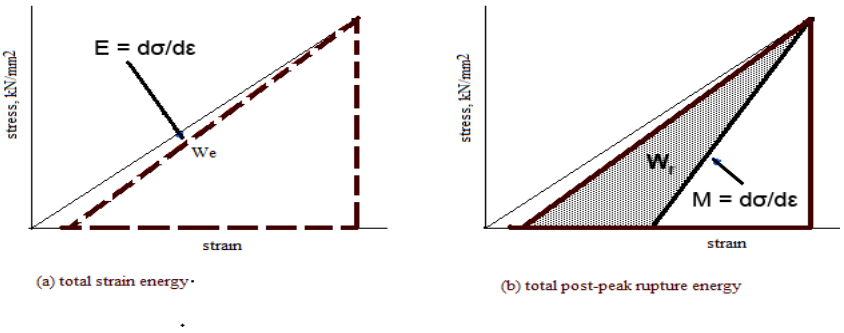

Figure 2.42 Estimation of elastic strain energy and rupture energy from pre-failure (a) and post-failure (b) stress-strain curves (Tarasov, 2011).

All of the parameters in the equations are determined from the pre-failure and post-failure stress-strain curves in Figure 2.41. The area of the triangle is outlined with dotted lines and corresponds to the strain energy density w_e stored within the rock material at the peak stress. The post-peak parts of the curves differ for different curves while the pre-failure curves are similar. The shaded area is the strength reduction at failure from the peak stress to the residual strength. Figure

2.42 illustrate how w_e and w_r are estimated. Within the range of brittleness index -1< k< 0 the elastic energy, w_e available in the material exceeds the rupture energy, w_r and provides energy for the self-sustaining failure.

The physical justification that implies the Tarasov brittleness measurements are direct measures of the energy released can be inferred from Griffith energy balance concept. Fundamentally, Griffith postulate form the basis of brittle failure process as discussed at the beginning of this chapter (Section 2.2, micromechanics of brittle failure). Griffith's idea is based upon fundamental physics to model a static crack as a reversible thermodynamical system. Griffith thought about the energy required to create new crack surface area, U_s (measured in Joules per metre^2, J/m^2) and the change in the mechanical energy (U_m) that resulted from this. The mechanical energy is the sum of the stored elastic energy (U_e) and the potential energy of the applied loading system (U_a) under compression, U is the total energy as expressed in Equation 2.66.

$$U = U_m + U_s \tag{2.66}$$

At equilibrium between the testing system and the specimen when there no crack extension or contraction. At infinitesimally increase in crack length, ∂C, there is no overall change in energy. Thus, the Griffith energy balance concept can be expressed thus:

$$\frac{\partial U}{\partial C} = 0 \tag{2.67}$$

It can be stated by the comparison that the Griffith energy balance concept and Tarasov brittleness measurements are similar. The elastic energy withdrawn, dW_e from the material body and the excess (released) energy, dW_a can be regarded as

the summed mechanical energy (U_m) while rupture energy, dW_r represent the energy for breaking crack.

Therefore, as shown in Equation 2.66, applying the first law of thermodynamics, Tarasov brittleness energy concept can be written as

$$U = U_m + dW_r \tag{2.68}$$

Therefore, at equilibrium between the testing system and the specimen when there is no crack extension or contraction. At infinitesimally increase in rupture energy, dW_r, there is no overall change in energy. Thus, as ∂W_r tends to zero this can be compared with Griffith energy balance concept and can be expressed as:

$$\frac{\partial U}{\partial W_{r\to 0}} = 0 \tag{2.69}$$

However, there was inconsistency in the behaviour of this brittleness concept as a result of changes in confining pressure, because brittleness of a rock is subject to the loading condition. The increase in the confining pressure changes the post-failure characteristic curves of the rock from Class I to Class II and then to Class I again or vice versa. For hard and brittle rocks, the instability and brittleness increases even at low confinement but they become controllable under high confining pressure since all rocks become ductile under high confinement.

Usually, the failure process associated with tensile crack formation is considered as brittle while shear rupture development is treated as ductile behaviour. At low confining pressures specimens failed with the formation of a number of long tensile cracks. At higher confining pressures, the failure mode changes to one with a shear plane inclined to the specimen axis. So, the gradual transition from one fracture mode to the other is accompanied by increasing instability of the failure

process as a whole (Santarelli and Brown, 1989). Such dual rupture mechanism creates conflicting results when samples are tested under triaxial compression.

For instance, at an early stage of testing an increase in confining pressure leads to an increase in brittleness but at a certain high confining pressure it decreases and increases again at very high pressure reaching absolute brittleness (absolute brittleness=0 as defined by Tarasov, 2010). This variation in confining pressure changes the angle of shear rupture orientation in relation to the specimen axis. Therefore, it becomes necessary to correct the value of the brittleness index, post-peak properties, and energy balance as a result of failure localisation at a specific angle (Tarasov & Potvin, 2013). As a result of the inconsistency in brittleness determination under confining pressure, this research therefore investigates the brittleness of rock under unconfined uniaxial compressive test since brittleness is subject to the loading condition.

Sections 2.4.3 and 2.5.3 show how the strain rate relates to a number of parameters. For example, an increase in strain rate causes an increase in the elastic strain energy and fragmentation of the rock. On the other hand, a decrease in the strain rate makes the post-failure characteristic curves of the rock more brittle. The quantification of brittleness depends more on the post-failure modulus of the rock (Equation 2.64). In addition, the elastic strain energy is also used to quantify the brittleness of rocks (brittleness k). Hence, elastic strain energy appears to be related to brittleness.

Therefore, it appears that fragmentation and brittleness may be connected with the strain rate. Fragmentation is linked to the elastic strain energy and the brittle nature of the rock. Whittles et al. (2006) stated in their work on the laboratory and numerical investigation into rock fragmentation that as the strain rate increases both the energy requirement for breakage and the degree of fragmentation of the samples also increases. This is in agreement with dynamic fragmentation process as suggested by Li et al. (1992). Li et.al (1992) also stated that there is a certain relationship between the degree of fragmentation and energy consumption in that the higher the energy, the greater the degree of rock fragmentation. Later research by Hong et al. (2009) concurred that the higher the energy, the finer the fragmentation and better the graduation of fragmentation of rocks.

Wang and Park (2001) claimed that elastic strain energy is a key factor that induces rockburst in mines. They estimated the elastic strain energy in Equation 1.2 from a laboratory experiment using a closed loop servo-controlled testing machine (MTS815). They related elastic strain energy (w_e) to rockburst as follows:

- w_e =50 kJ/m^3, then the rockburst hazard is very low;
- 50< w_e =100 kJ/m^3, then the rockburst hazard is low;
- 100< w_e =150 kJ/m^3, then the rockburst hazard is moderate;
- 150< w_e =200 kJ/m^3, then the rockburst hazard is high; and
- w_e >200 kJ/m^3, then the rockburst hazard is very high.

In addition, they related brittleness (B) to rockburst as follows:

- B>40, then no rockburst;
- B=40-26.7, then weak rockburst;
- B=26.7-14.5, then strong rockburst; and
- B<14.5, then violent rockburst.

Therefore, brittleness might be related to strain rate. The brittleness, B is estimated from the ratio of UCS to Brazilian tensile strength of the rocks as given in Equation 2.41. Therefore, rocks have the potential to store elastic strain energy under load (which is shown to relate to brittleness in Equation 2.41 and also shown to relate with "k" in Equation 2.64) and release this energy at failure which is usually accompanied with rock fragmentation. Therefore, the brittleness indices based on these concepts (on the static mechanical properties, UCS and the Brazilian tensile strength, B_{11}, B_{12}, B_{13} and B_{14}) are evaluated in this study and other concepts based on rock moduli (E and M) i.e. k, k_2 B_7, B_8 and B_{16}.

In the review of literature, it appears that no research has attempted to link brittleness and fragmentation in a quantified manner. Rock failure under dynamic loading conditions as experienced in blasting, rockbursting, crushing, milling, and also during conventional unconfined compressive strength testing of rock specimens and the subsequent distribution of fragments sizes is a little understood phenomenon. At present, there is no satisfactory understanding of the theoretical or experimental basis to explain the phenomenon responsible for fragmentation during uniaxial compression failure and the dynamic failure of rock from blasting.

Understanding the relationship between brittleness and fragmentation could be useful in the solution to many practical mining and civil engineering problems. For example, recent research concurs that in the evaluation of a rock mass response to mining or tunnelling activities as a result of dynamic processes particularly associated with fragmentation and seismicity, the correct determination of brittleness under such loading conditions is important to better predict and mitigate these dynamic catastrophic rockbursts events (Tarasov & Potvin, 2013).

Furthermore, effectiveness of all the subsystems in mining operations (e.g. loading, hauling and crushing) is dependent on the quality of the prediction of the fragmentation. The production of fines and oversize in rock breakage processes (such as in blasting, crushing etc.) impose additional problems. For instance, fines from blasting and crushing in the aggregate industry have a low value while oversize incurs additional cost during secondary blasting. Moreover, understanding this relationship might result in better efficiency of rock fragmentation processes. This will lead to optimised mining of ore bodies and design of stable structures with more accuracy. Therefore, the knowledge of the brittleness of the rock and its post-failure characteristics curve can guide the designer to reducing any potential hazards concerning rock failure under compression and aid mining engineers in understanding rock fragmentation.

2.7 Chapter Summary

The behaviour of brittle rock under microscopic and macroscopic failure has been reviewed. Under a compressive load, some of the pre-existing microcracks initiate crack propagation, coalesce and finally macroscopic fracture of the rock. The stages of failure are identified based on the microscopic failure.

In this research, the specimens are tested within 30 days of collection in a way to preserve the natural water content. In addition, a 42 mm diameter of specimen is selected as it falls within the range of 40-60 mm (from the results of Hawkins, 1998). A specimen diameter of 42 mm is large enough to remove the influence of grain size. Again, shorter specimens contain fewer defects and therefore contain a higher degree of homogeneity. In addition, a ratio of L/D of 2.5 is preferred to a ratio L/D of 3 because the effect of size (length) becomes stronger for brittle rocks in the determination of brittleness. The amount of elastic energy stored within the specimen at the peak stress is proportional to the specimen length; as a result it affects the post-failure characteristic curve (Tarasov & Potvin, 2013). The loading rate was selected such that the failure of the rocks occurs within 5-10 minutes of loading. The diameter of platen was equal to that of specimen in the determination of UCS of the rocks.

However, in the determination of the pre-failure and post-failure curves the diameter of the platen was a little bigger than that of the test specimen. This becomes necessary because as the rock deformation passes the peak stress hard brittle rocks begin to reduce in area at the contacts between platen and the

specimen especially when the two are equal. When the platen was slightly bigger than the specimen this effect was minimised. This behaviour was noticed during pre-tests done with the rock specimens. The literature reviewed suggested a closed-loop servo-controlled testing machine as the only practical laboratory test program to obtain a post-failure stress-strain curve for different rocks in compression. Various concepts used for the determination of brittleness are reviewed. The ability of the concepts to determine brittleness is assessed and their shortcomings identified. At present, there is no universally accepted concept to describe brittleness. However, brittleness concepts estimated from the rock moduli are able to classify the whole brittle failure process on a scale of brittleness for Class I and Class II rocks and will be assessed. In addition, brittleness concepts estimated from strength parameters are frequently used in the literature to quantify brittleness and these concepts are also evaluated in this study.

The method used to determine the fragmentation of rock specimens under compressive failure is identified. The method used to estimate fragmentation (counting of fragments produced) from the literature appears not to satisfactorily describe fragments produced in a statistical sense. Instead, in this research the fragmentation is characterised by sieve analysis. The fragmentation produced under this condition depends to a large extent on the energy available to cause fragmentation. From the literature, it appears that no research has attempted to link brittleness and fragmentation. It was pointed out that the determination of brittleness and fragmentation are influenced by the loading rate, specimen diameter to height ratio, specimen-platen contact condition and heterogeneity. The

possible influence of these factors was avoided by proper choice of materials, equipment and methods. The procedural experimental set up was meticulously carried out. This is discussed in the next chapter.

CHAPTER THREE

TEST MATERIALS DESCRIPTION AND EXPERIMENTAL SET UP

3.1 Introduction

In order to examine under laboratory conditions the connection between fragmentation and brittleness, different rock parameters need to be determined. Therefore, rock specimens are subjected to axial load in order to fragments them under compressive failure. The rocks were also subjected to dynamic failure with the use of explosives. The fragmentation produced were analysed. This also made it possible to estimate both the static and dynamic parameters of rocks. The brittleness of the rocks was estimated from the static mechanical properties and rock moduli. It was shown from the literature reviewed, that a closed-loop servo-controlled testing machine is the only practical laboratory test program to obtain post-failure modulus of brittle rocks in compression.

The literature review showed that rock strength is affected by strain rate, specimen geometry, anisotropy, heterogeneity and moisture. These influences were avoided by following the suggestion in the literature review and by meticulously adhering to the suggested ISRM (2007) methods. This research makes use of the ISRM standard as guidelines for sample preparation, equipment/instrumentation as the testing procedure. Where the method was not

applicable the method used was described. The tests were performed at the Genmin Laboratory (Rock Engineering Laboratory) facilities of University of the Witwatersrand while the post-failure curve determination was done at the Rock Engineering Laboratory, Aalto University, Finland. The blasting tests were conducted at AEL (Ltd) Mining Services.

The following sections provide the description of the rock specimens and methods used to prepare them. The description of the rock specimens' and their preparation is contained in Appendix 1.1. The following sections is a short description of the test facilities and test controlling methods for the determination of the parameters of interest. The testing procedures and equipment description information provided in this thesis are contained in the manuals of the manufacturer of the testing machine (e.g. MTS), ISRM suggested methods and pre-tests done with the rock specimens.

3.2 Description of Rock Specimens

The rock samples were selected such that they cover all rock types, igneous, sedimentary and metamorphic. In addition, the choice of the rocks was such that the strength varies from low, to intermediate and very high strength rocks. The texture varied from fine-grained, to medium-grained and to coarse-grained rocks. The rocks were free from visible cracks and without any surface alteration or defects.

3.2.1 Petrographic Examination of Rock Sample and Equipment Description

Petrographic examination of rock samples is necessary to identify the rocks based on their mineral composition. It was pointed out in Section 2.6 that different rocks differ in their brittleness characteristics as a result of their distinctive textural and mineralogical constituents. Since grain size and mineral composition influence the brittleness determination. Therefore, it is pertinent to indicate the grain size and mineral composition of rock specimens.

The equipment items used for the determination of mineral composition includes a petrographic microscope and materials for thin section preparation. The material used to prepare the thin section includes a diamond saw with a saw blade size 150 mm in diameter; cast iron plate of size 250 x 250 x 20 mm and two glass plates of size 250 x 250 x 20 mm for rough grinding. Silicon carbide grinding powder of grain numbers 180 or 220 was used to improve the surface roughness which was produced from rough grinding. Silicon carbide grinding powder of 600 size grit was used for the fine grinding and 1200 (6.5 μm) and 3000 (3.5 μm) grit sizes for finishing. Other material includes glass slides of approximate size of 25 x 45 mm and thickness of l mm on top of which the thin section of the rock specimen was placed. An epoxy resin was used for mounting the rock specimen on the glass slide. Stains were impregnated into the thin section to distinguish minerals when placed under a petrographic microscope. This method is easy to interpret and is dependable.

3.2.1.1 *Procedure for Petrographic Examination of Rock Specimen*

Petrographic examination of rock specimens under a microscope was done to reveal the microstructure, composition, texture and mineralogy of the rocks. A high energy beam of electrons was used to scan the surface of the thin section to reveal its mineral constituents. The ground surface of the specimen was then cut into a thin section. The ground surface of the specimen was further re-sectioned with a diamond wafering saw. A thin section from the specimen was prepared by additional grinding and polishing with finer abrasives of 1200 (6.5-μm) and 3000 (3.5-μm) grit sizes respectively. Before cementing the thin section onto the glass slide of the petrographic microscope, it was cleaned and dried to avoid interference during scanning with the microscope.

3.3 Sonic Velocities Determination and Equipment Description

Sonic velocity is the measurement of velocity of propagation of elastic waves through laboratory rock specimens. Sonic velocities are used to estimate the dynamic moduli of rock specimens. Since fragmentation is a dynamic process, it was considered necessary to compare fragmentation with dynamic properties such as sonic velocities and dynamic moduli.

To study the propagation of elastic sonic waves through rock, a dual-beam cathode ray oscilloscope (i.e. two oscilloscopes in one cabinet) type 565 was used. The cabinet is 43.18 cm width, 34.29 cm height, 58.51 cm depth and it weighs 28.12 kg. The cathode ray tube (CRT) is the type T5650-2-1 aluminised tube with its face coated with phosphor-type P2 standard fluorescent material. The dual-

beam oscilloscope generates two beams: an upper beam and a lower beam (Figure 3.1).

Figure 3.1 A dual-beam oscilloscope at centre with it main parts enlarged by it sides.

The dual beam oscilloscope was connected to a Portable Ultrasonic Non-destructive Integrity Testing (PUNDIT) device. This connection made it possible to detect and record the arrival time of the wave form with greater accuracy.

3.3.1 Procedure for Determination of Sonic Velocities of Rock Specimens

The electronic arrangement for the propagation of elastic sonic waves through rock specimens in order to determine the sonic velocities is shown in Figure 3.2. The transmitter was coupled to one end of the specimen by a thin layer of grease. It was pressed by a stress of about 10 N/mm^2 with a cylindrical disc perpendicular to the plane of direction of wave propagation. The receiver was positioned at the opposite end of the specimen to the plane to which the transmitter was pressed in a similar arrangement.

The sensitivity of the oscilloscope, voltage output of the pulse generator, counter and the gain of the amplifier were amplified to an optimal level with a higher pulse front to promote a precise time reading. The wave that first arrived on the oscilloscope screen from the transmitter was the longitudinal, P-wave while the transverse wave was the first change in the wave amplitude. The travel time was measured to precision and accuracy of 1 part in 100. The velocities of P (v_p) & S-waves were determined from the measured distance between the transmitter and the receiver (d) divided by the travel time (t) for the waves using Equation 3.1. Five tests was performed per rock type.

$$v_p = d/t \tag{3.1}$$

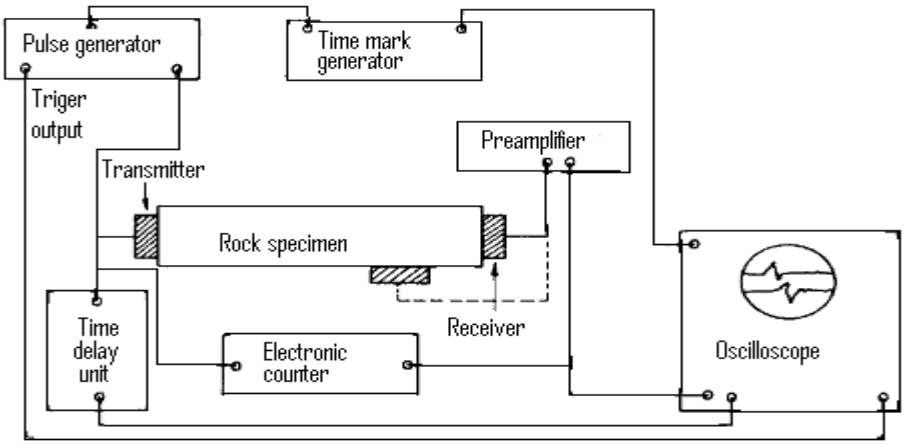

Figure 3.2 Layout of the electronic component for sonic velocities determination (ISRM, 2007).

3.4 Brazilian Tensile Strength Determination and Equipment Description

It is necessary to correlate fragmentation with the strength of rock in tension. In the literature, several authors estimated the brittleness of rock from ratio of tensile strength to the uniaxial compressive strength (as discussed in the Literature Review, Section 2.6).

The testing machine used was MTS Criterion® Model 45. It was recently installed and calibrated. The machine is shown in Figure 3.3 while its features are shown in Figure 3.4a. The platens are designed to withstand dynamic compressive stress of 276 MPa and the static compressive stress of 690 MPa on the contact area. The handset was used to perform standard functions (Figure 3.4a). The machine was connected to a computer with force and displacement recorder software (Testworks® software 4). This machine made it possible to monitor the load

deformation curve. Therefore, the load at failure was easily detected and with more accuracy than other machines without X-Y recorders.

3.4.1 Procedure for Determination of Brazilian Tensile Strength of Rock Specimens

The procedure for the determination of the Brazilian tensile strength of the rock specimens is as follows: one level of masking tape was wrapped around the end of the test specimen. It was inserted securely into the Brazilian test fixture in a way that the curved spherical seated platen centre coincides with the specimen diameter and the axes of rotation of the apparatus.

The fixture with the specimen was placed between the upper and lower compression platen of the MTS Criterion® machine. The load was applied by clicking on the start icon. The software has an on-screen real-time auto-scaling graphics that display the test in a Testworks® Virtual Control Panel (Figure 3.4c). The load and displacement curves were monitored during the tests so that the peak load at failure is correctly detected. The load applied, was at a constant rate of 200 N/s until failure occurs within 15-30 sec. Ten valid tests were done per rock sample (see for Appendix 2.1 for compression-extension curves). The Brazilian tensile strength is calculated as expressed in Equation 3.2 and average result reported.

$$\sigma_t = 0.636P \big/ Dt \quad \text{(MPa)} \tag{3.2}$$

Where P is the load at failure (N), D is the diameter of the test specimen (mm), t is the thickness of the test specimen measured at the centre (mm).

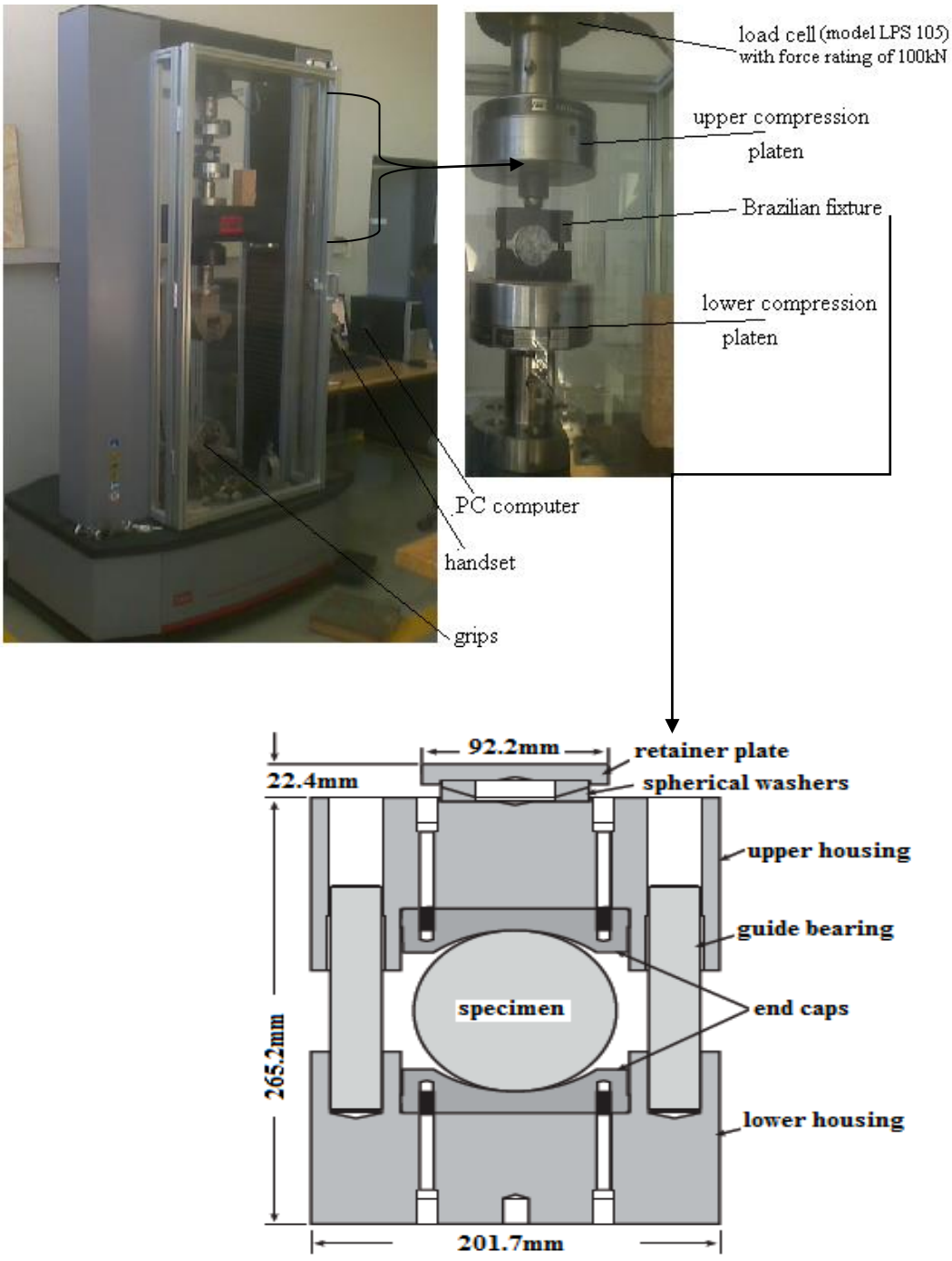

Figure 3.3 MTS Criterion 45.

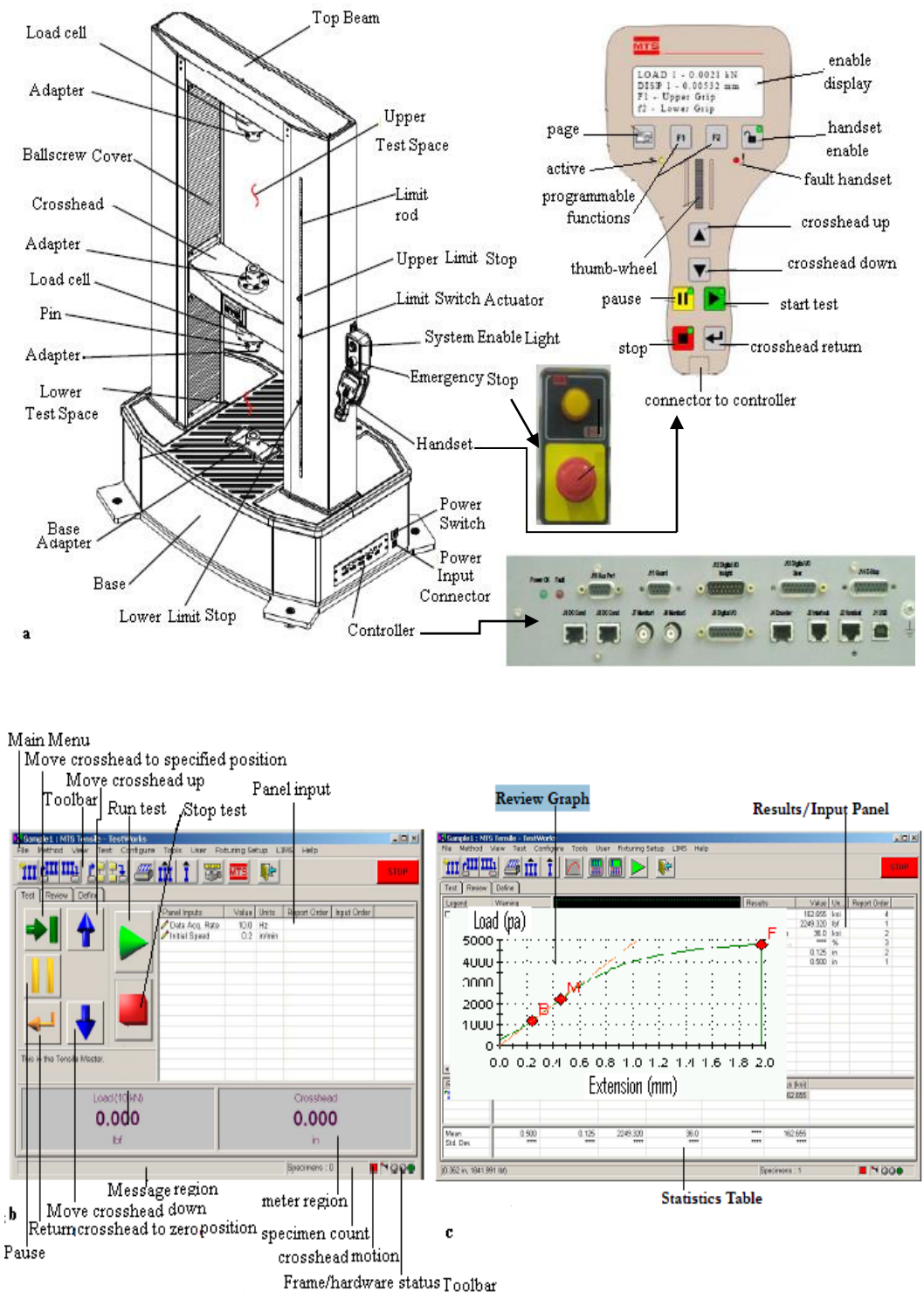

Figure 3.4 (a) MTS Criterion™ 45 features (b) TestWorks® 4 test window (c) graph review window.

3.5 Description of Uniaxial Compressive Strength Determination and Equipment

Uniaxial compressive strength was used to estimate the elastic strain energy stored in the test specimen and brittleness based on static mechanical properties. The uniaxial compression tests were performed on the test specimens using the Amsler Rock Testing Machine type 200 DB 76. The operation of the machine was by hydraulic transmission of load on the test specimens to a separate house load indicator. A complete unit of the testing machine consists of two separate parts; the press and the pendulum dynamometer (Figure 3.5). A brief description of the testing machine and its control method is given below.

Figure 3.5a shows the press. It consists of the hydraulic loading cylinder with two straight threaded steel columns. The movement of the cross-head was done by pressing the up and down buttons on the pendulum dynamometer (PD) type PM 103 (Figure 3.5b). The spherical seat of the upper platen was lightly lubricated with mineral oil so that it locks after the deadweight of the cross-head is picked up. Its diameter was the same as the diameter of the test specimens.

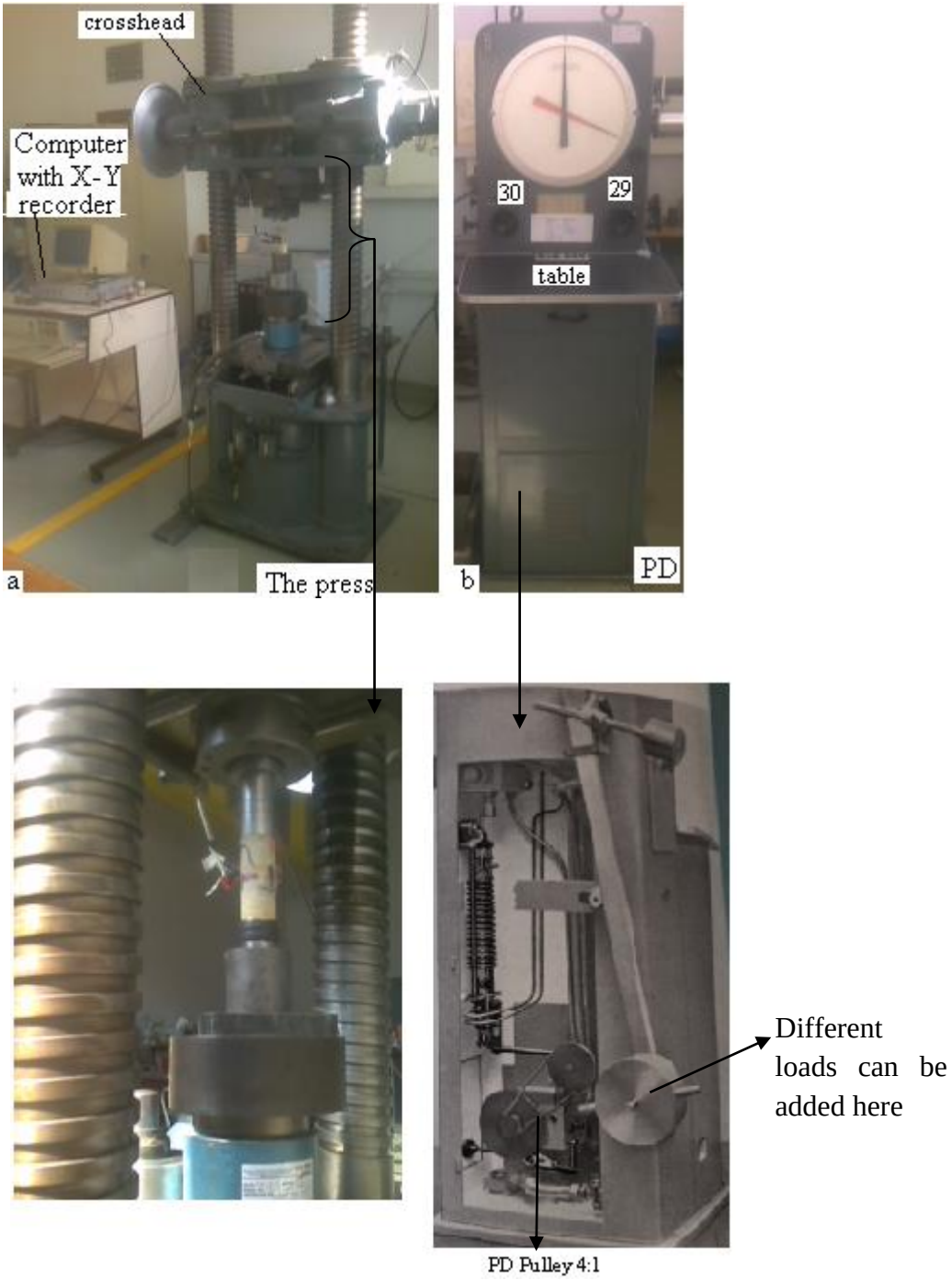

Figure 3.5 (a) The press, below it is the specimen-platen arrangement (b) pendulum dynamometer, PD, below it is the pulley system.

The specimen, the platens, the spherical seats and the loading ram are precisely centred such that the curvatures of their centres coincide. This arrangement is to lessen the effect of elastic property and non-uniform stress distribution as a result of contact friction between the platen-specimen end interfaces. In addition, the diameter of specimen and that of loading platens used are equal. The effect of deformation mismatch disappears as the diameters are the same. The spherical seats compensate for the initial misalignment of the specimen ends thereby minimising specimen bending.

The configuration of the machine can be changed without compromising its integrity. This becomes necessary to suit some peculiar situations. For instance, the rocks used in this research vary from very soft Quartz Arenite to very hard Quartzite2. The machine configuration was changed in case of Quartz Arenite and Sandstone to 100 kN scale so that a very small fractions in load could be read. In the case of Quartzite2 and Mottled Anorthosite, the configuration was changed to 2000 kN in order to apply enough load to cause the failure of the rocks, see Figure 3.5b. This is not possible with some other testing machines. The machine is periodically calibrated to ensure reliability.

3.5.1 Procedure for Determination of Uniaxial Compressive Strength of Rock Specimen

Before conducting the test, the pointer on the PD was set to zero. Both the delivery regulating valve and the release or return valves were closed. When the two valves are closed, oil from the pump by-passes the testing machine to the

reservoir. The delivery valve was opened slowly so that some quantity of oil passes to the cylinder of the testing machine. This forces the ram upwards and thus stresses the specimen. The hand-wheel of the delivery regulating valve is provided with a scale which makes it possible to read off fractions of a turn on the delivery regulator. The loading rate was selected for each different rock type so that failure occurred within 5-10 minutes of loading. Five specimens are tested per rock sample and average result reported. The Uniaxial compressive strength is calculated as given in Equation 3.3 and average result reported for each rock sample.

$$\sigma = \frac{P}{A_o} \tag{3.3}$$

Where, P is the compressive force on the specimen, and A_o is the initial cross-sectional area. In this test procedure, compressive stresses and strains are considered positive.

Axial strain, ε_a, is calculated as

$$\varepsilon_a = \frac{\Delta l}{l_o} \tag{3.4}$$

Where, Δl is the change in measured axial length (positive for a decrease in axial length) and l_o the axial length of specimen prior to loading.

The diametric strain, ε_d, is calculated as

$$\varepsilon_d = \Delta d \big/ d_o \tag{3.5}$$

Where Δd is the change in diameter (negative for an increase in diameter) and d_o the diameter of the specimen prior to loading.

3.6 Deformation Parameters and Equipment Description

This test was intended to determine the deformation parameters (Young's modulus and Poisson's ratio) from the stress-strain curves. The Young's modulus was used to estimate the stored elastic strain energy in the test specimen prior to its failure or at peak stress. Additional testing materials to the one described in the previous section (i.e. under determination of uniaxial compressive strength) are needed to determine the deformation parameters. This includes an electrical resistance strain gauge and an apparatus for recording the load and deformation. The strain gauge used (in Figure 3.9a) was a bonded metallic gauge of 120 Ω with a constantan wire grid embedded in a phenolic resin backing (i.e. carrier). The carrier enables attachment of the strain gauge directly to the test specimen.

3.6.1 Procedure Used for Determination of the Deformation Parameters of the Rock Specimens

Two circumferential and two axial electrical strain gauges with strain sensitivity of the order of 5×10^{-6} were installed with adhesive (glue) at an equally spaced distance along the axis and circumference of the test specimen. This was installed in such a way that the length of the gauges (axial and circumferential or diametric) does not encroach within half a diameter of the specimen ends. The four strain gauges (two axial and two circumferential) were connected in series (i.e. Wheatstone bridge connection) by soldering one end of the axial together and the

other ends of circumferential together. This was done carefully so that the wires do not touch each other or overlap. With Wheatstone bridge connection the bridge were balanced as in Figure 3.6b.

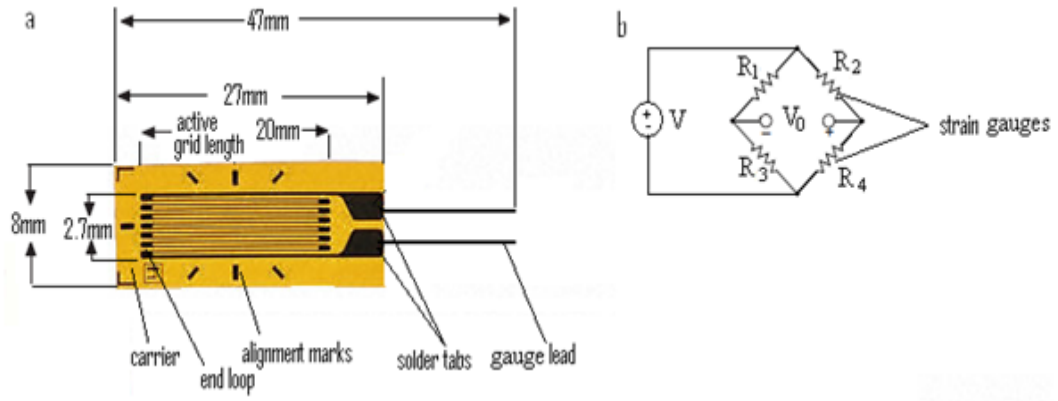

Figure 3.6 (a) Strain gauge dimensions and (b) strain gauges in Wheatstone bridge connection configuration.

The specimen with the strain gauges was centred with respect to the platens and the loading machine. The free ends of the strain gauges were then connected using jockeys to a computer with software capable of automatically plotting each increment in stress and strain. The loading rate was selected for different rock types so that failure occurs within 5-10 minutes of loading. Five tests were done per specimen and average result reported. The elastic modulus (also referred to as pre-failure modulus) is calculated as given in Equation 3.6 and average result reported. Elastic modulus, *E*, is measured at a stress level of 70% to 30% of the ultimate strength (Figure 2.7)

$$E = \Delta\sigma / \varepsilon_a \qquad (3.6)$$

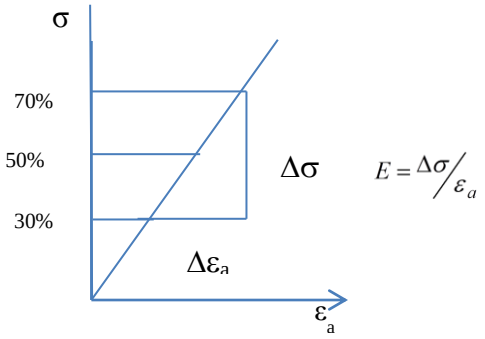

Figure 3.7 Elastic modulus, E, determination

Poisson's ratio, υ, is calculated from the equation below

υ = (slope of axial stress-strain curve, E) divided by (slope of diametric stress-strain curve)

Where the slope of the diametric stress-strain curve is calculated in the same manner the elastic modulus is calculated

3.7 Description of the Determination of Pre-failure and Post-failure Stress-Strain Curves in Uniaxial Compression and Equipment

The post-failure modulus was used to estimate the brittleness of the rock based on rock moduli. It was also used to classify the rocks into Class I or Class II. A closed-loop servo-controlled testing system was used to accomplish this test. Firstly, before discussing the working principle of this machine it is relevant to explain the testing machine (i.e. closed-loop servo-controlled system).

A closed loop control is a procedure by which a desired output is constantly obtained by adjusting its input through a controller to result in a stable system. Figure 3.8b illustrates a closed loop control in which the measured output from

the system is monitored by the controller through a feedback signal. The efficiency of the deformation process thus depends on the sensitivity of the controller to respond quickly enough to correct the measured error and prevent the release of strain energy after the peak strength, thereby, ensuring stable specimen failure. A closed-loop control contains the input variable, controller, system and feedback (Figure 3.8b). It is the absence of feedback in open-loop control that differentiates it from closed-loop control (Figure 3.8a).

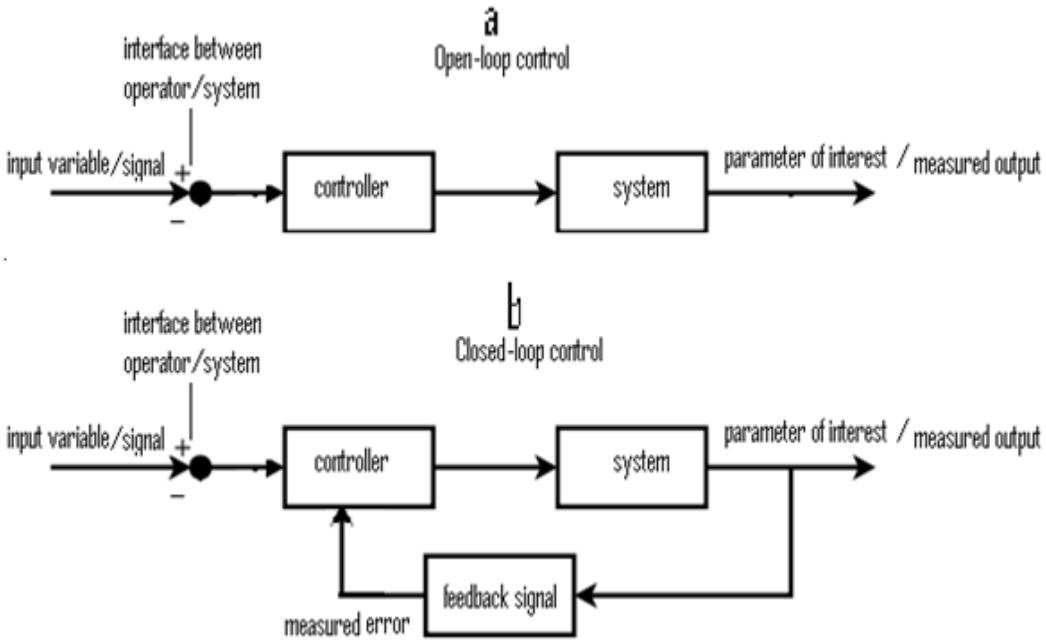

Figure 3.8 Schematic diagrams showing (a) open-loop control (b) closed-loop control.

The controller then compares the feedback signal with system programmed instructions. The difference between the two gives the measured error. The error is used to manipulate the system until the two signals are equal. This manipulation involved the control of the applied load through a series 252.xx servo-valve (i.e.

servo-controlled). The servo-valve does this through its inlet and outlet connection with the two pressure chambers of the actuator (Figure 3.9). The working principle of the MTS machine is discussed in Appendix 1.2

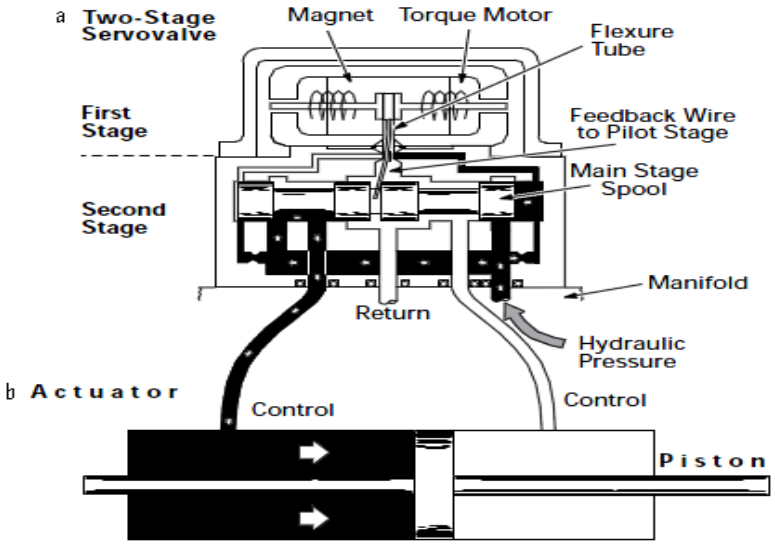

Figure 3.9 (a) Cross-section of a typical two-stage servo-valve (b) double acting hydraulic actuator (MTS, 1996).

3.7.1 Procedure for the Determination of Pre-failure and Post-failure Stress-Strain Curves for the Rocks in Uniaxial Compression

During uniaxial compressive testing to determine the pre-failure and post-failure stress-strain curves using the servo-controlled testing machine, the following control steps were employed:

The axial extensometer was installed at 120^0 apart and contacts the specimen at 25% and 75% of its full length while the circumferential extensometer was located at mid-height of the specimen. The specimen was then installed on the lower platen of the load unit assembly.

A small preload was applied with the force cell drive to contact the specimen in force control mode using the output of the axial force as the feedback signal. This made the specimen 'seat' to the lower loading platen and the upper loading platen becomes spherically seated. The readings of both axial, radial extensometer and axial force were reset to zero. The procedure template for determination of the pre-failure and post-failure of the rocks is shown in Appendix 1.3. The template is modified each time the tests were conducted.

Ductile (i.e. less brittle) specimens were continuously loaded at an axial strain rate of 0.001 mm/mm/sec. This was continued up to 70% of the predetermined peak load of the specimen. After this point the loading rate was reduced by switching to a lower strain rate of 0.000001 mm/mm/sec. The loading continued at an axial strain rate of 0.000001 mm/mm/sec until the applied load drops close to 50% of its peak load. At this point, a pre-failure and post-failure load-deformation curve was obtained.

In the case of specimens with a brittle behaviour, the control switch over method is as follows. The control mode was switched from axial force to axial strain control mode. The specimens were continuously loaded at an axial strain rate of 0.001 mm/mm/sec. This was continued up to 70% of the predetermined peak load of the specimen. At 70% of peak load, instead of a slower or reduced axial strain rate, the control mode was switched to circumferential control mode at a rate of 0.0001 mm/mm/sec. This continued until the applied load reduces to about 50% of peak load. At this point a pre-failure and post-failure load-deformation curve

was obtained. Five tests were performed per each rock type and the average result reported.

The post-failure modulus, M, is determined from the peak stress to 70% of the peak stress, the linear part of the descending curve (Figure 3.10 and Equation 3.7).

$$M = \frac{\Delta\sigma}{\Delta\varepsilon_a} \tag{3.7}$$

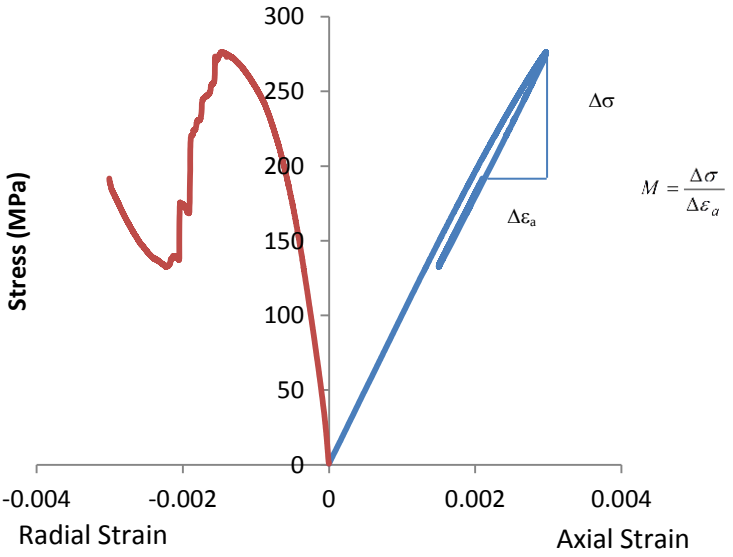

Figure 3. 10 Post-failure modulus, M, determination for Mottled Anorthosite

3.8 Fragmentation by Blasting and Equipment Used for Analysis of Fragments

Blocks of rocks measuring 150 mm in length, 100 mm in height and 100 mm in width were prepared from dimensional stones of Granite1, Granite2, Quartz Arenite, Sandstone, Norite1, Gabbro and Marble. The blocks were cut to dimension using a diamond cutting machine. A template was prepared measuring

150 mm length x 100 mm width. On the template 4 holes were cut with a spacing of 44.7 mm between 2 holes on a row and 28 mm across holes forming a rectangular pattern. With the template taped on the rock block surface, a drilling machine with a 8 mm diameter drill bit was used to drill into the blocks to the depth of 80 mm. The template ensures that the holes in the rocks' blocks are of identical geometry.

A 720 mg electric detonator with two lead wires was inserted into each of the holes in the block of rock that had been prepared for blasting. Therefore, each hole contained one 720 mg electric detonator thereby ensuring consistent charge per hole and per rock block. Each lead wire was connected to the lead wire by the side's holes in series. The two free ends of the lead wires were connected to an instantaneous electric exploder. This arrangement was performed inside a large cylindrical steel blasting chamber measuring 2 m in diameter and 4 m in height at AEL (Ltd) Mining Services, see Figure 3.11. The inside of the chamber was encircled with thick rubber mats in order to reduce secondary fragmentation as a result of the blasted fragments hitting the wall of the chamber. The firing of the rock block was done outside the blasting chamber. After firing all fragments from each rock block were gathered and screened using a vibrating sieve shaker.

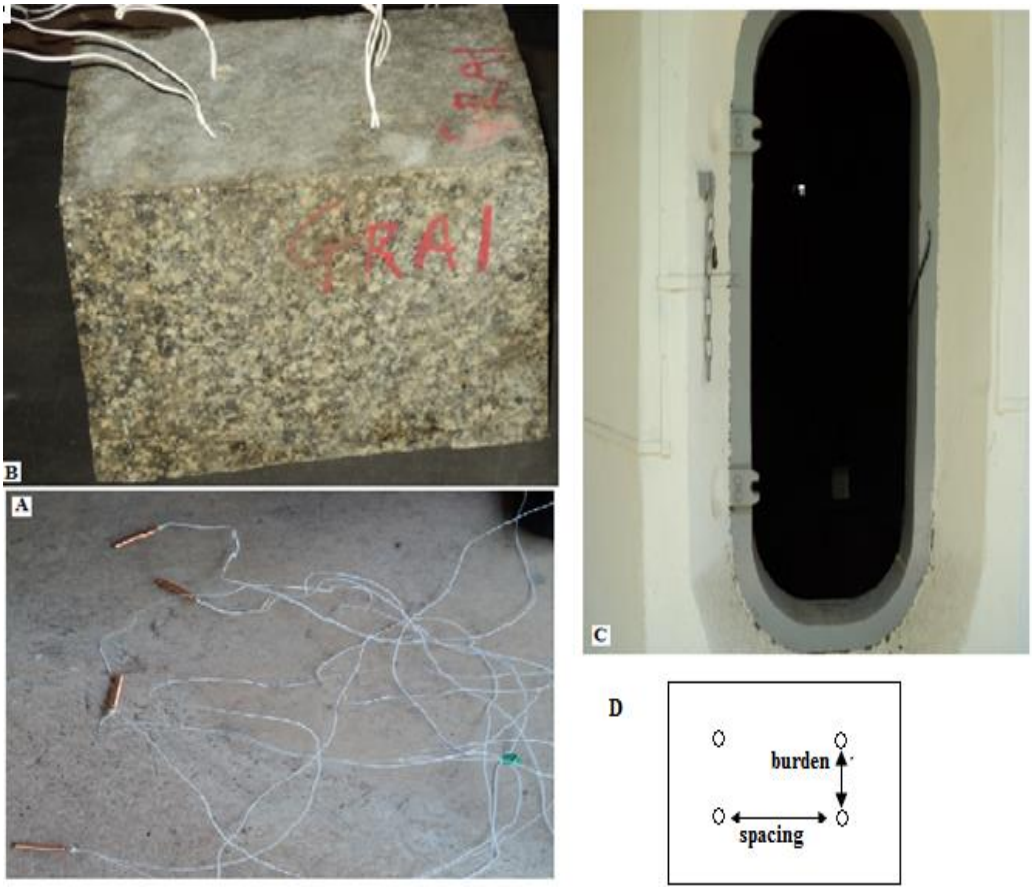

Figure 3.11 (A) shows the 720 mg electric detonators, (B) shows one detonator inserted into each hole on the rock block, (C) shows the outer view of the blasting chamber and (D) shows the blasting pattern.

3.9 Procedure for Estimating Fragmentation by Sieve Analysis

Sieve analysis was used to classify the rock fragments produced during explosive and compression failure of the samples. The screen sizes were selected on the basis of the diameter of the rock specimen (from the compression test). The following screen sizes were selected as a percentage of the diameter of specimen.

- 1% of 42 mm diameter of rock specimen, (0.5 mm screen size selected since 0.42 mm screen size was not available),
- 2.5% of 42 mm (screen 1mm selected),
- 5% of 42 mm (2 mm screen selected since 2.1 mm was not available),
- 15% of 42 mm (6.3 mm screen selected),
- 30% of 42 mm (13.2 mm screen selected because 12.6 mm screen was not available),
- 45% of 42 mm (19 mm screen selected, 18.9 mm screen was not available),
- 60% of 42 mm (25 mm screen selected, 25.2 mm screen was not available),
- 75% of 42 mm (31.5 mm screen selected),
- 90% of 42 mm (37.5 mm screen selected).

A total of 10 screens were used for the size screening. The screens were arranged with an additional bigger screen which had an aperture larger than the specimen diameter (45mm screen), placed on top of the screens of a Powermatic sieve shaker.

3.10 Chapter Summary

The specimens from each rock type were meticulously and carefully prepared to meet the suggested ISRM (2007) standard. All the deformational tests (Brazilian tensile test, UCS tests and control damage tests i.e. pre-failure and post-failure

stress-strain curves) could be used to plot the stress-strain curves from a load-deformation recorder.

Considerable effort was made to minimise the effect of non-uniform stress distribution as a result of contact friction between the platen-specimen end interfaces. The specimen, the platens and the loading ram were precisely centred so that the curvatures of their centres coincided. Again, to minimise the effect of deformation mismatch, the loading platen used and the specimen are equal in diameter. The spherical seats of the platens compensate for the initial misalignment of the specimen ends thereby minimising specimen bending. However, in the case of the determination of the post-failure curves, the platen used was a little larger in diameter than the specimen diameter. This was necessary in order to minimise size reduction at the specimen ends. This was observed when specimen and platen diameters were equal.

It was shown that the use of MTS axial and circumferential direct contact extensometers has an advantage over other deformation measuring instruments (Appendix 1.2). These are easy to install and reusable for a large number of test specimens. As for the LVDT, it does not measure directly the actual deformation of the test specimen. In addition, it was difficult to use the LVDT to control post-failure of Class II rocks as a result of its slow response to a closed-loop control rate.

The axial extensometers were attached at 120^0 apart and contact the specimen at 25% and 75% of full length. The gauge length of the axial extensometer was large

enough to give a representative average value. The circumferential extensometer was located at the specimen mid-height. The circumferential extensometer measures change in chord length rather than change in specimen circumference. The correction equation was given.

At the beginning of the determination of pre-failure and post-failure stress-strain curves for both Class I and Class II rocks, the control rate and feedback signal were the same. The specimen was loaded at an axial strain rate of 0.001 mm/mm/sec. This was continued up to 70% of the predetermined peak load of the specimen. After this point, the loading rate was reduced by switching to a lower strain rate of 0.000001 mm/mm/sec for the less brittle rock. Instead of a slower or reduced axial strain rate, the control mode for brittle rock was switched to circumferential control mode at a rate of 0.0001 mm/mm/sec. The tests are meticulously carried out and the results are presented for discussion in Chapter 4.

CHAPTER FOUR

RESULTS OF THE LABORATORY WORK

4.1 Introduction

This chapter presents the results of the tests described in Chapter 3. It starts with a description of the rock specimens used for the tests. It is followed by results obtained from the non-destructive and the destructive tests. Finally, the brittleness indices based on static mechanical properties is followed with brittleness indices based on moduli.

4.2 Rock Specimen Description

The thin sections of the rocks were examined under a petrographic microscope. The objective of this examination was to provide a semi-quantitative analysis of the rocks samples. This was done to identify the mineral composition (%), grain sizes and shapes, the degree of packing, any fabrics or textures and micro-cracks in each rock specimen. In addition, estimates of the amount of dark minerals relative to light minerals were reported along with the estimated proportions of the minerals in the sample. This includes the ratio of quartz to feldspar and where applicable the ratio of multiple feldspar varieties. The rocks were then identified based on their mineral composition as contained in the subsequent sections.

The summary of the percentages of the dark-coloured and the light-coloured minerals of the rocks selected for blasting tests are shown in Table 4.1 and are also contained in the description of the rock specimens used in the study. Marble does not fit into this category as it contains entirely $CaCO_3$ (over 99% calcite).

Table 4.1 Percentage of light coloured minerals and dark coloured minerals for rocks selected for blasting tests.

Rocks	Light coloured minerals (%)	Dark coloured minerals (%)	Quartz content (%)	Feldspar content (%)
Gabbro	30.00	70.00	10.00	20.00
Granite1	75.00	25.00	35.00	35.00
Granite2	85.00	15.00	40.00	40.00
Norite1	60.00	40.00	15.00	45.00
Quartz Arenite	95.00	5.00	90.00	3.00
Sandstone	90.00	10.00	85.00	5.00

4.2.1 Gabbro

Based on its mineralogy, this sample is a Gabbro. The sample is composed of dark minerals such as plagioclase, amphibole, and olivine. The remaining minerals are pyroxene in form of orthopyroxene and clinopyroxene (which average 1-2 mm in size), biotite laths (some with a high iron-titanium oxide concentration), and hornblende and opaque minerals which formed later and therefore are irregularly shaped. These minerals are referred to as the intercumulus phase. The sample is severely altered (Figure 4.1). The sample also exhibits some iron staining caused by oxidation of the heavy minerals.

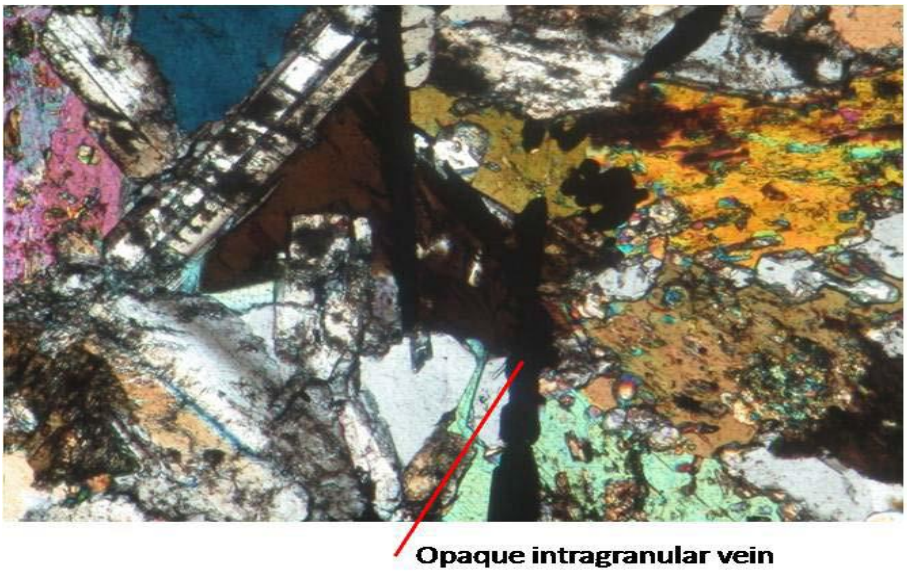

Mineral preferred fabric – none; degree of alteration – major

Micro-cracks or fractures – intragranular veins of either the opaque mineral or chlorite

Figure 4.1 XPL photograph of an opaque intragranular vein in sample Gabbro (field of view 2 mm).

4.2.2 Granite1

This rock sample is a Tonalite. It is a medium-grained rock with a granular texture (meaning that the minerals are equally developed). Hence, roughly equal proportions of quartz and feldspar of ±35% respectively and muscovite (±5%). It is composed of ±25% of the darker minerals which are biotite with high iron concentration (±15%), hornblende (±5%), chlorite (±2%) and opaque minerals (±3%). The euhedral (well-formed) mineral is plagioclase which is on average 2-3 mm in size, as well as the smaller biotite (±0.5 mm). In addition, there are smaller

and less abundant muscovite laths which can be found around the edges of the quartz and feldspar grains (Figure 4.2).

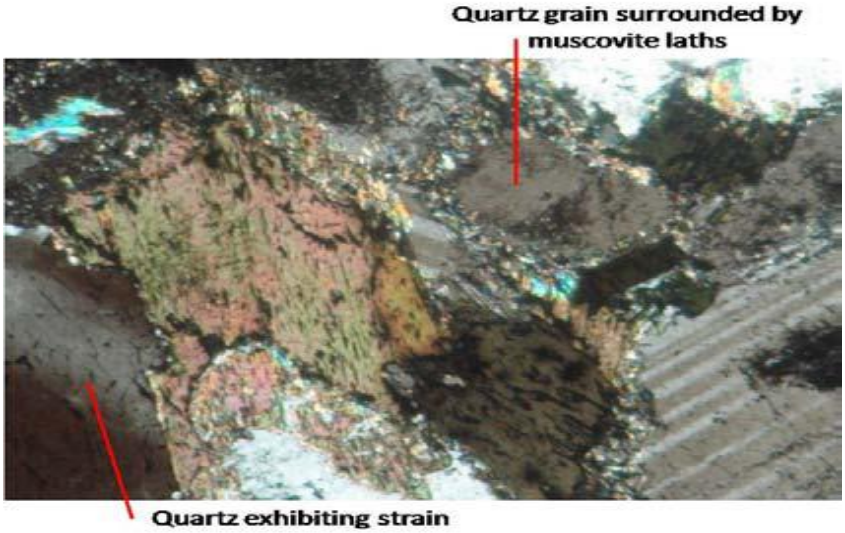

Mineral preferred fabric – none; micro-cracks or fractures – none

Degree of alteration – major

Figure 4.2 XPL photograph of the relationship muscovite has with other minerals in Tonalite (Granite1) (field of view 2 mm).

The quartz tends to be more irregularly shaped and shows evidence of possible strain but is essentially the same size as the feldspar. The opaque minerals on the other hand form a cracked hexagonal shape; the largest are ±0.5 mm in size. This sample is affected by weathering in the form of alteration of the feldspar to sericite (a fine-grained muscovite), and by the alteration of hornblende to chlorite (Figure 4.2).

4.2.3 Granite2

This sample is a medium-grained Syeno-Granite because of the higher proportion of microcline to plagioclase among the feldspars. The thin section is shown in Figure 4.3. This is illustrated by the slight pinkish colouration of the sample, which is due to the higher proportion of alkali feldspar. The sample also exhibits a granular texture as well as isolated instances of intergrowths between quartz and feldspar indicating that the sample is made up of roughly equal proportions of the two minerals.

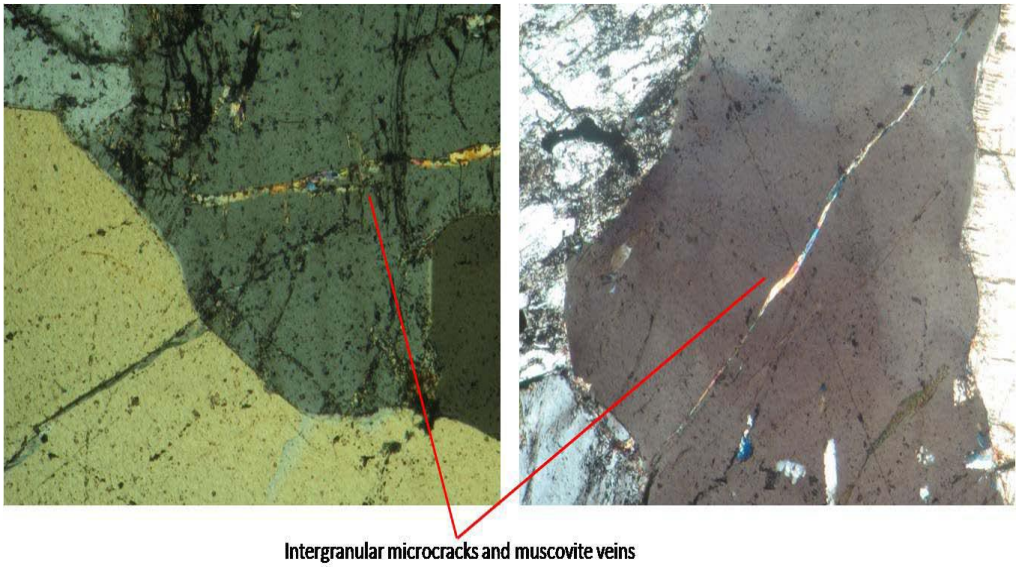

Mineral preferred fabric – none; degree of alteration – intermediate

Micro-cracks or fractures – some of the quartz contains intergranular muscovite veins a few microns wide

Figure 4.3 XPL photographs of micro-cracks and vein-lets in Syeno-Granite (Granite 2)(field of view 2 mm).

The quartz and the feldspars are both irregularly shaped and vary between 1-2 mm in size; together they make up ±85% of the sample (with ±40% quartz, ±10% plagioclase feldspar and ±30% microcline feldspar). Both minerals have been variably altered to sericite. The remainder of the sample is composed of muscovite ±5% and dark minerals which are made of biotite laths (±8%) and irregularly shaped grains of hornblende (±3%) both of which range in size between 0.5-1.5 mm. In addition there are roughly cubic opaque minerals (±4%) which appear silvery to the naked eye.

4.2.4 Granite3

This sample is a coarse-grained Monzo-Granite with phenocrysts (large grains in a finer-grained matrix) of microcline and plagioclase feldspar which reach sizes of 5 mm or larger. The feldspar phenocryts not only show a graphic texture indicating that the quartz and feldspar grew simultaneously but also show replacement by sericite. The sample is also leucocratic (light-coloured) because of the larger proportion of quartz (±40%) and feldspars (microcline and plagioclase of equal proportion, contributing around 50% of the sample). The dark mineral is a small amount of biotite (±8%) and opaque minerals (±2%). There are intergranular veins of either muscovite or fine-grained quartz which are a few microns wide in both the quartz and feldspar minerals. There are also narrow intra-granular fractures (as seen in Figure 4.4) that run the length of the thin section around the quartz and through the feldspar.

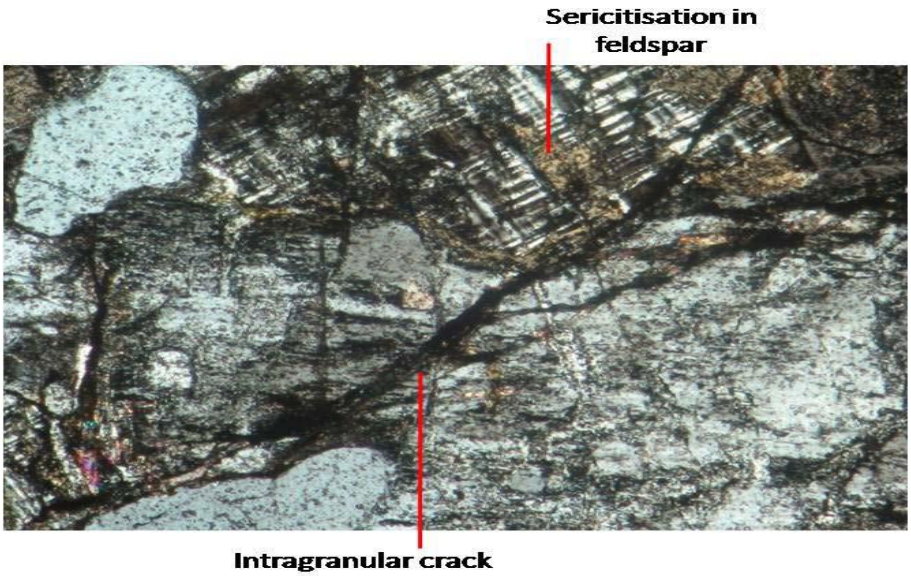

Degree of alteration – minor; mineral preferred fabric – none

Figure 4.4 XPL photographs of the intragranular fractures in Monzo-Granite sample (Granite3) (field of view 2 mm).

4.2.5 Granite4

This sample is Leucocratic Alkali Feldspar Granite due to a large constituent of the sample being made up of perthitic orthoclase feldspar grains which are roughly 3 mm in size. The perthitic texture is the result of exsolution of separation or un-mixing of a homogeneous mineral by solid solution into its component minerals. This can be the result of slow cooling; an example of this texture is seen in Figure 4.5.

The sample is made up of ±40% feldspar (±10% plagioclase, ±30% orthoclase) and ±40% quartz (averaging 1-2 mm) giving the sample a medium-grained granular texture. The sample has also experienced alteration (in the form of

sericitisation of the feldspar) and possibly strain. At least 20% of the sample is made up of dark minerals such as biotite laths (±10%) and irregular grains of hornblende (±5%) which show evidence of alteration to chlorite (±5%) with their size range from 0.5-1 mm.

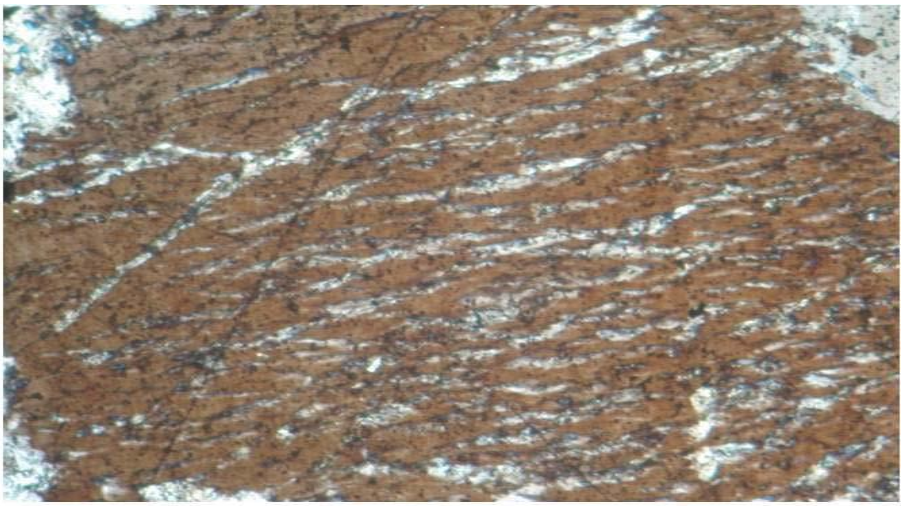

Perthitic texture in feldspar with intergranular cracks

Mineral preferred fabric – none; degree of alteration – intermediate

Micro-cracks or fractures – randomly orientated intergranular fractures in the quartz

Figure 4.5 XPL photograph of Alkali Feldspar Granite (Granite4) showing the perthitic texture seen in feldspars (field of view 2 mm).

4.2.6 Granite5

This sample is a fine-to-medium-grained Leucocratic Monzo-Granite. It has a granular texture with roughly equal proportions of feldspar and quartz (±40%) as well as between the two feldspars: plagioclase (±20%) and microcline (±20%). It

also contains about 10% muscovite. Both the feldspar and quartz are irregularly shaped and can be found in two different sizes, namely ±1 mm and < 0.5 mm.

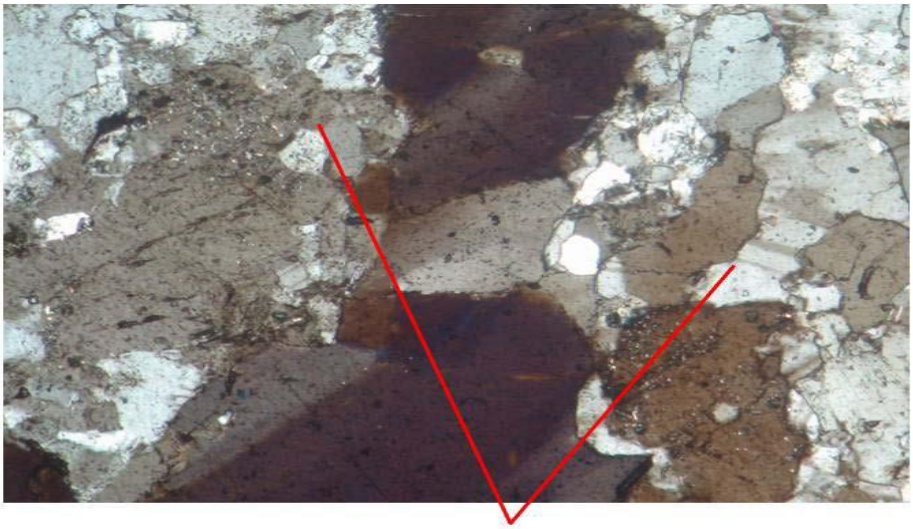

Fine-grained quartz on either side of coarse-grained quartz

Mineral preferred fabric – there is a vague alternating grouping of coarse and fine grains; micro-cracks or fractures – intergranular fractures in the coarse-grained quartz and feldspar. Degree of alteration – major

Figure 4.6 XPL photograph of the vague layering within sample of Leucocratic Monzo-Granite (Granite5) (field of view 2 mm).

The quartz in particular looks like it has been recrystalised. The feldspar shows evidence of sericitisation with some slightly coarser grained muscovite at the grain boundaries. The dark minerals contain small clusters of fine-grained biotite with possible chlorite make up ±10% of the sample. The thin section is shown in Figure 4.6.

4.2.7 Marble

This rock is a Marble with about 99% calcite. Other minerals may be present but not noticeable. Calcite makes up the whole rock with no (or very little) matrix. It contains no impurity with high order interference colours (birefringence) resulting in pure white rock. It was originally a calcite dominated limestone but has undergone metamorphism and/or diagenesis. It is very well packed with interlocking grains/crystals. It has no significant alteration. The thin section is shown in Figure 4.7.

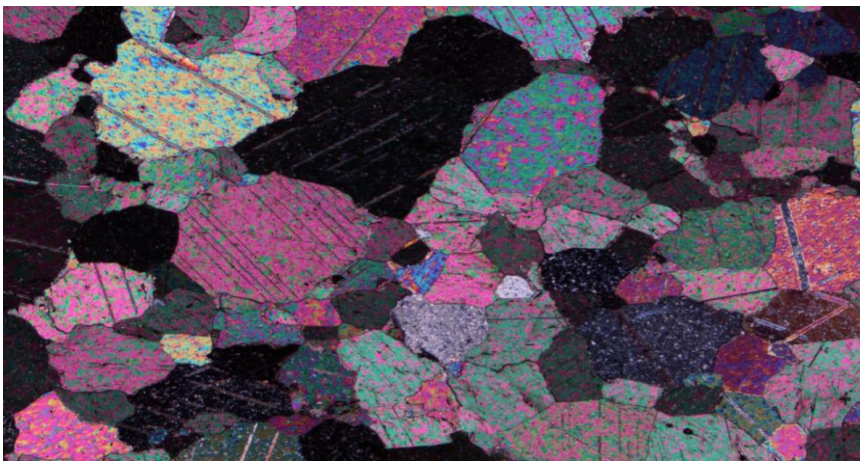

Figure 4.7 XPL photograph of Marble (field of view 2 mm).

4.2.8 Mottled Anothosite

This Anorthosite is a crystalline igneous rock. It is mafic and fairly coarse-grained, consisting 90% of plagioclase feldspar, 5% othopyroxene and 4% clinopyroxene (Figure 4.8). The pyrite, chalcopyrite and the ilmenite together make up to 1%. The plagioclase crystals are subhedral to euhedral with crystal sizes vary from <1 mm to ~4 mm with small alteration but noticeable.

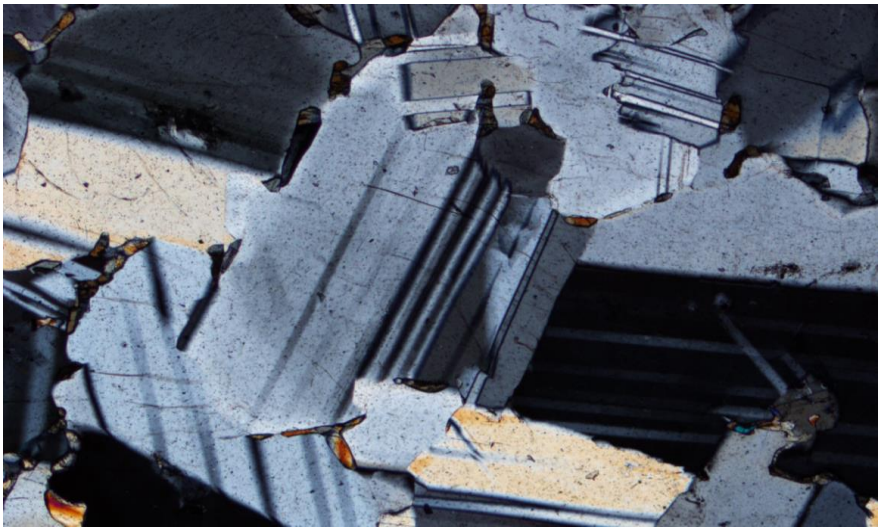

Figure 4.8 XPL photograph of Mottled Anorthosite (field of view 2 mm).

The orthopyroxene crystals are anhedral to subhedral in shape and vary in size but generally between 4-6 mm. The smaller crystals (still coarse) are 2-3 mm in size. The clinopyroxene crystals are anhedral but not abundant. The crystal sizes are between 1 and 3 mm. No major signs of alteration, but likely to be altered in some way (this includes metamorphism).

4.2.9 Norite1

Based on the greater proportion of orthopyroxene (±25%) to clinopyroxene (±15%), this sample is a Norite. The sample consists of cumulus phenocrysts of plagioclase and orthoclase feldspar, ranging between 2-3 mm in size with some as large as 6 mm (Figure 4.9). Cumulus minerals are more or less euhedral in shape and indicate that it was formed early; the cumulus to intercumulus relationship is also depicted in Figure 4.10.

Mineral preferred fabric – the pyroxenes form an interconnected network of grains

Micro-cracks or fractures – intergranular cracks that are in the feldspars but do not go the length of the grain; degree of alteration – minor

Figure 4.9 XPL photograph illustrating exsolution in pyroxene in Norite1 (field of view 2 mm).

The phenocrysts have been affected by sericitisation and possible strain as well as having formed around the same time as some of the quartz. Both varieties of pyroxene show exsolution (see Figure 4.9) and grow between the cumulus minerals because of their irregular shapes; they range between 1-2 mm in size. The proportion of dark minerals makes up to 40% of the sample whereas the rest is predominantly feldspar (±30% plagioclase, ±15% orthoclase) with some quartz (±15%).

4.2.10 Norite2

This sample is also a Norite (Figure 4.10).

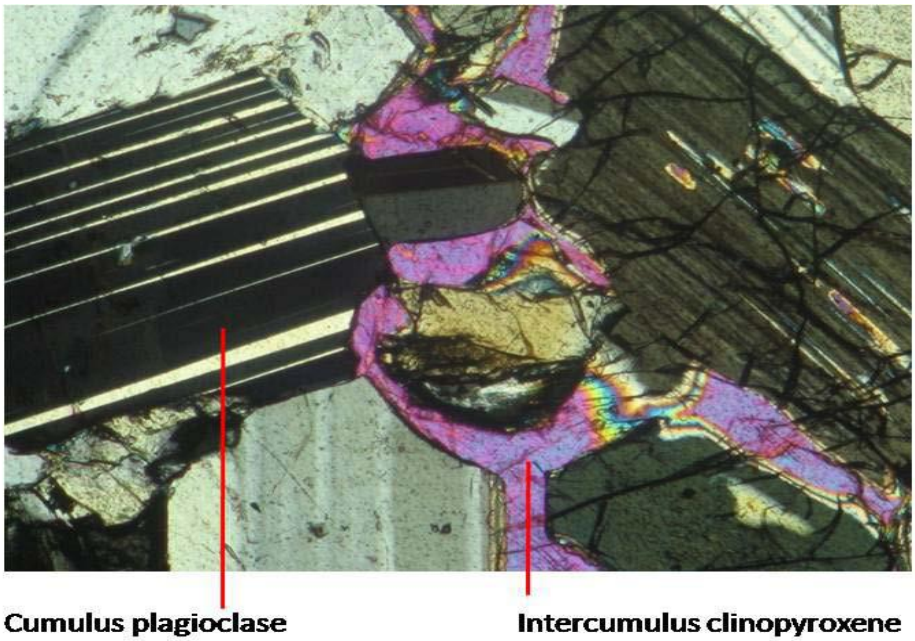

Mineral preferred fabric – none; degree of alteration – minor

Micro-cracks or fractures – minor amounts of intergranular cracks in feldspar

Figure 4.10 XPL photograph illustrating the cumulus intercumulus relationship in Norite2 (field of view 2 mm).

A high percentage of the sample is made up of plagioclase (±40%) and orthoclase feldspar (±10%) as well as some quartz (±10%) which together amounts to at least 60% of the sample with the remaining 40% constituting the dark minerals (±20% orthopyroxene, ±10% clinopyroxene, ±5% olivine and ±5% biotite) (Figure 4.10).

The feldspar grains which are on average ±1 mm form the cumulus phase (Figure 4.10) and occur as tightly packed grains with sutured edges. The olivine and orthopyroxene grains are up to 3 mm in size and are semi-rounded. The latter

mineral is more abundant than the intercumulus clinopyroxene and biotite. Both pyroxenes exhibits ex-solution and are enclosed in some smaller quartz or feldspar crystals.

4.2.11 Norite3

This sample of Norite has cumulus plagioclase (±30%) and orthoclase (±10%) which is affected by sericitisation and possible strain. There are also isolated instances of intergrowth between the feldspar and quartz (±10%) meaning that they are formed at roughly the same time.

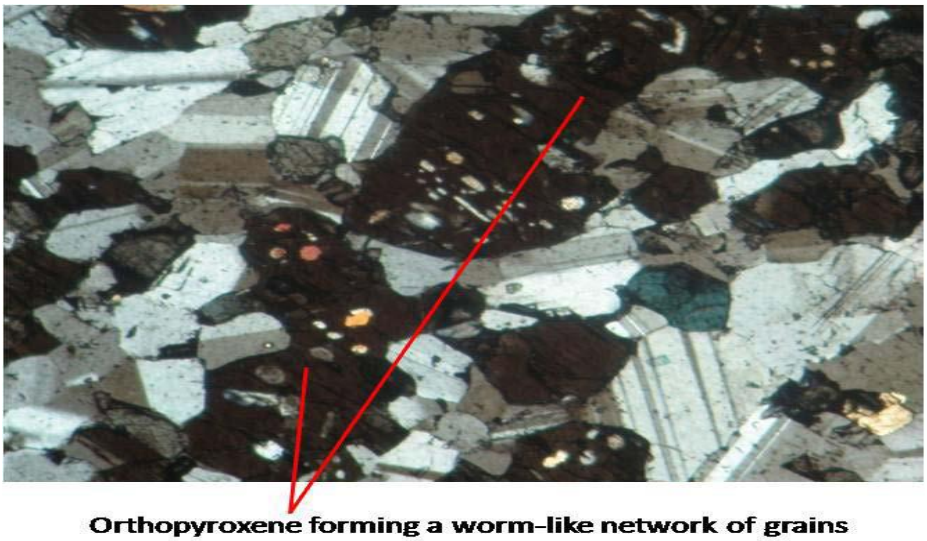

Mineral preferred fabric – none; micro-cracks or fractures – none

Degree of alteration – minor

Figure 4.11 XPL photograph of the intercumulus orthopyroxene in sample Norite3 (field of view 2 mm).

The sample contains orthopyroxene (±30%) and clinopyroxene (±20%), both of which show exsolution. Clinopyroxene is less abundant than the orthopyroxene which forms at least two different phases of a worm-like network of irregularly shaped grains as shown in Figure 4.11.

4.2.12 Quartz Arenite

This rock sample is classified as Quartz Arenite based on its mineralogy. It consists of at least 90% quartz. It also contains ±3% plagioclase feldspar, 5% opaque minerals and 2% lithic fragments.

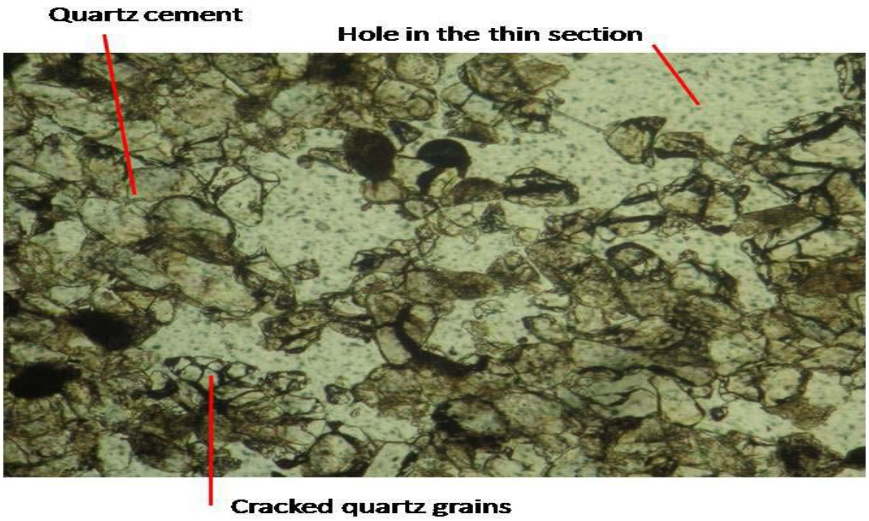

Mineral preferred fabric – none; degree of alteration – intermediate

Micro-cracks or fractures – yes, but likely due to the thin section making process

Figure 4.12 PPL photograph illustrating the features described in sample Quartz Arenite (field of view 2 mm).

The sample has two types of cementing minerals; quartz and haematite. The latter is because of the oxidation of the heavy minerals which makes the thin section

look brown. Some of the quartz grains are cracked, angular in shape and are on average < 0.5 mm in size and moderately sorted, see Figure 4.12. The opaque minerals are fine-grained, whereas, the lithic fragments are made up of clusters of igneous quartz grains and are also < 0.5 mm in size.

4.2.13 Quartzite1

This rock consists of 95% quartz, 1% muscovite, 3% sericite. The quartz is rounded to sub-round but there are some sub-angular grains. It size range between 0.1-3.5 mm. Its grains exhibits 120^0 triple junction in lots of places (metamorphism indicator of recrystallization as shown in Figure 4.13). Its matrix comprises of polycrystalline quartz (fine-grained) and sericite.

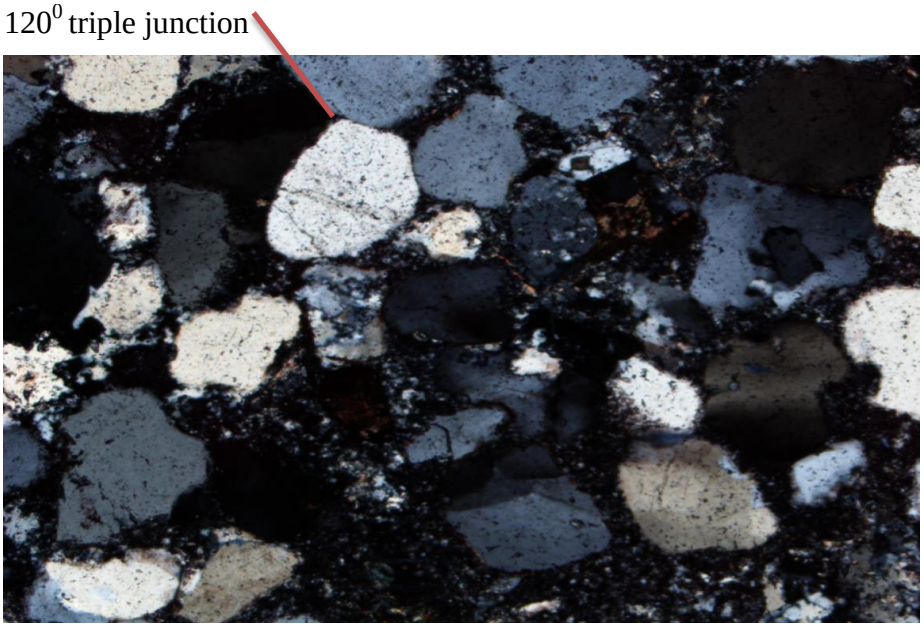

Figure 4.13 XPL photograph of Quartzite1 (field of view 2 mm).

Undulating extinction is common with the quartz grains which suggest that the grains have undergone stress (deformation) at some point. The muscovite is less

abundant with mottled extinction. This sample is meta-sedimentary, it was a sediment before but is now metamorphosed. The sericite fine-grained muscovite is formed because of alteration. There is presence of minor haemitisation (Fe-alteration) but it is not significant. The rock has a moderate to well-packed grain.

4.2.14 Quartzite2

The protolith of this sample is Quartz Arenite before it was metamorphosed into a Quartzite. This is because of the high proportion of quartz (±90%) in the sample, with minor amounts of muscovite (about 5%) and lithic fragments (about 5%).

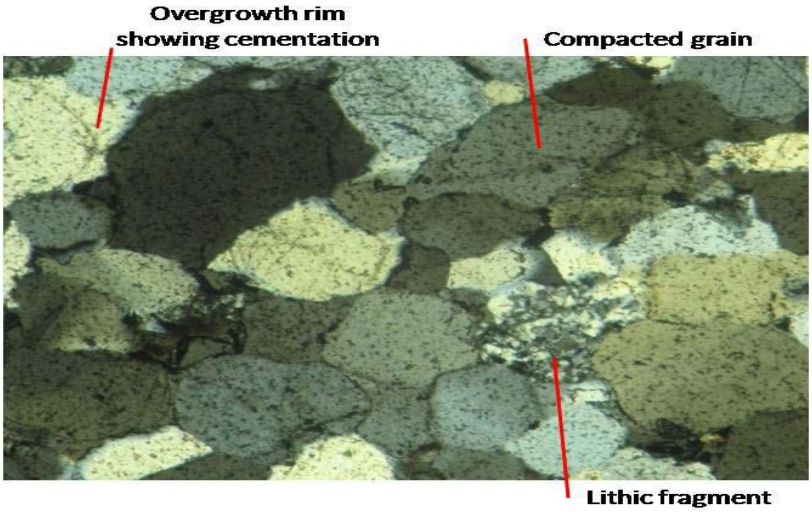

Mineral preferred fabric –compaction of the grains likely due to metamorphism

Micro-cracks or fractures – none; degree of alteration – minor

Figure 4.14 XPL photograph illustrating the cementation of the quartz grains in Quartzite2 (field of view 2 mm).

The quartz grains are roughly 0.5 mm in size, sub rounded and is well sorted; this includes the lithic fragments, which are rounded clusters of igneous quartz

cemented by haematite. The quartz grains are fused together by a quartz cement during metamorphism (see Figure 4.14), which may have also produced the muscovite (which is ±0.25 mm in size) that can be found along the grain boundaries. This sample has a high degree of packing because of how the grains are sorted which is then enhanced by the cementation of the grains.

4.2.15 Sandstone

This Sandstone is similar to the Quartz Arenite in Section 4.2.12 except that it contains less than 90% quartz. It is immature or sub-mature Sandstone. The thin section is shown in Figure 4.15.

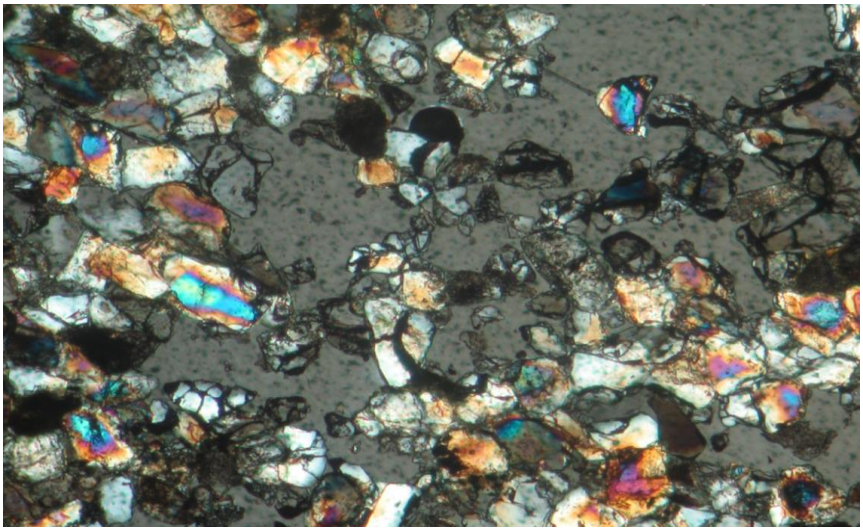

Figure 4.15 XPL photograph of Sandstone (field of view 2 mm).

4.2.16 Spotted Anorthosite

The descriptions for this sample are identical with the Mottled Anorthosite except for proportion of othopyroxene which is lesser. The thin section is shown in Figure 4.16.

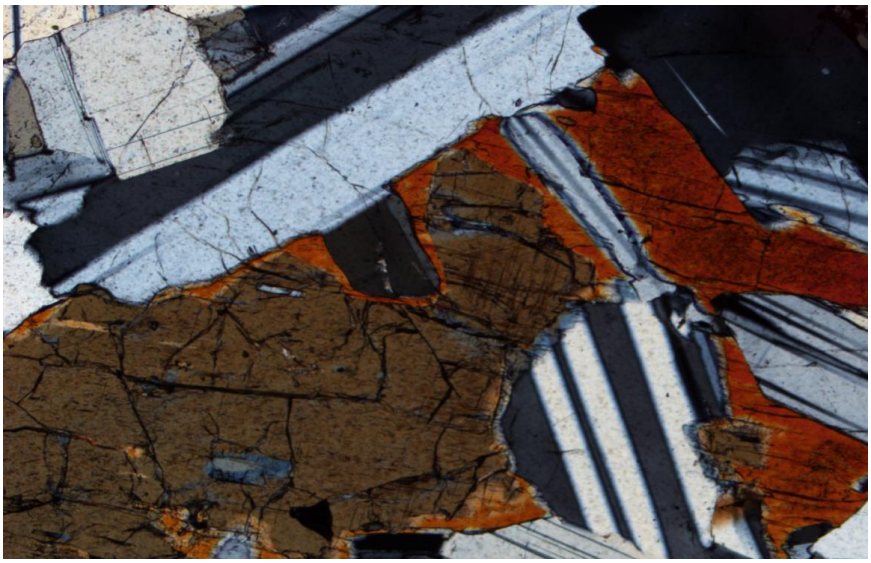

Figure 4.16 XPL photograph of Spotted Anorthosite (field of view 2 mm).

4.2.17 Troctolite1

This sample of Troctolite has a similar composition to Norite except for reduced amount of pyroxenes (±15% orthopyroxene, ±5% clinopyroxene) with the addition of more feldspar (±40%) and (more) olivine (±15%). The sample contains cumulus plagioclase feldspar with semi-rounded olivine (Figure 4.17) and orthopyroxene. The plagioclase grains range from 0.5-1 mm and show possible strain whereas the olivine and orthopyroxene are ±0.5 mm and between 0.5-1.5 mm in size respectively. The intercumulus phases and accessory minerals

include quartz, clinopyroxene (which is less abundant than the orthopyroxene and also exhibits exsolution) and magnetite. Together with the magnetite, the dark minerals making up ±40% of the sample.

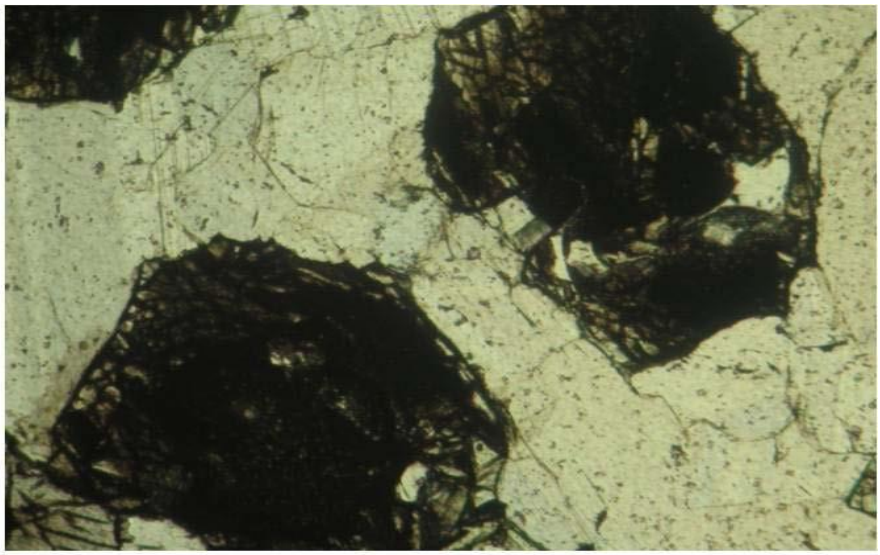

Isolated semi-rounded olivine grains with the cores partially replaced by magnetite

Mineral preferred fabric – none; degree of alteration – intermediate

Micro-cracks or fractures – small intergranular cracks in the feldspars

Figure 4.17 PPL photograph illustrating the relationship the olivine grains have with one another in Troctolite1 (field of view 2 mm).

4.2.18 Troctolite2

This Troctolite sample contains cumulus plagioclase feldspar (±50%) and sub-angular olivine (±10%) and orthopyroxene (±15%), all of which range between 2-3 mm with some of the orthopyroxene being larger than 3 mm. Other minerals include quartz, ±10% (which has inter-grown with the feldspar in some areas) and clinopyroxene (±15%), which like the orthopyroxene shows ex-solution but is

very irregularly shaped since it is an intercumulus phase and tends to surround other minerals (Figure 4.18).

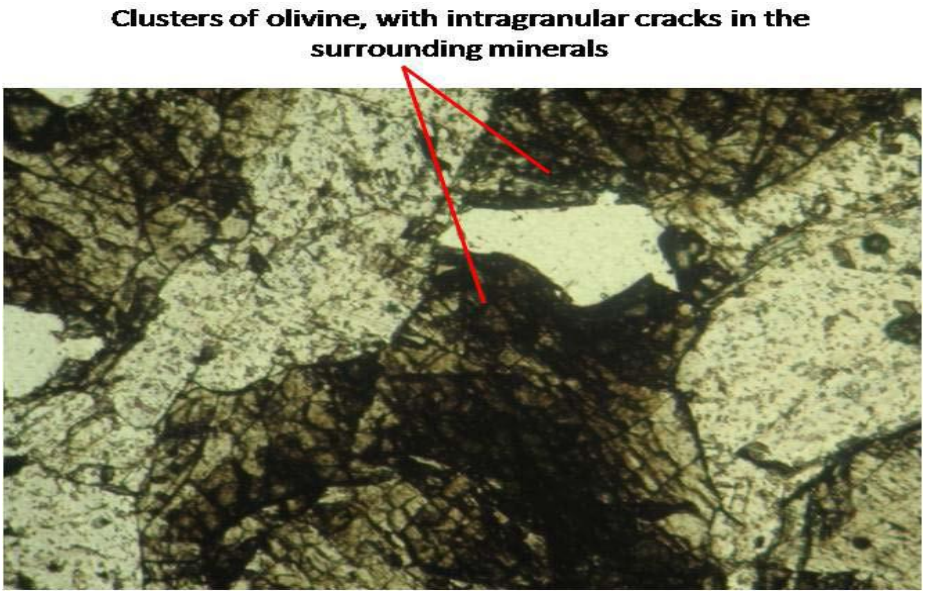

Figure 4.18 PPL photograph of a cluster of olivine grains in Troctolite2 (field of view 2 mm).

Approximately 40% of the sample is composed of the dark minerals, therefore, the rest is mostly plagioclase with minor quartz. It contains intragranular cracks around the olivine grains and in the feldspar. Figures 4.17 and 4.18 illustrate how (clusters of) olivine can affect the surrounding minerals by either expansion (formation of cracks) or alteration.

4.3 Sonic Velocities and Dynamic Parameters

This is a non-destructive test. The estimation of the dynamic properties of the rock are presented in Table 4.2 (the rocks are grouped in the table according to the sign of their post-failure modulus, negative for Class I and positive, Class II.). This table shows that the arrival time of the P-wave of the rocks varies from 14.900 μs to 44.300 μs while the S-wave varies from 24.000 μs to 75.200 μs.

Table 4.2 Dynamic properties of rocks.

Rocks	P waves (μs)	S waves (μs)	P wave Velocity (m/s)	S wave Velocity (m/s)	Dynamic Modulus (GPa)	Dyn. Mod. of Rigidity (GPa)	Acoustic Impedance (Kg/sm^2)
Gabbro	17.900	27.900	5832.402	3741.935	95.080	41.332	17.216
Quartzite2	17.700	31.400	5898.305	3324.841	71.169	28.083	14.984
Class II							
Granite1	18.800	31.900	5553.191	3272.727	71.230	28.863	14.965
Granite2	19.400	36.400	5381.443	2868.132	56.385	21.66	14.169
Granite3	18.700	36.500	5582.888	2860.274	55.232	20.889	14.255
Granite4	21.700	36.100	4811.060	2891.967	53.233	21.868	12.580
Granite5	20.700	33.300	5043.478	3135.135	59.816	25.236	12.949
MottledAnorthosite	14.900	25.700	7006.711	4062.257	112.551	45.134	19.164
Norite1	16.400	31.100	6365.854	3356.913	84.858	32.453	18.333
Quartzite1	22.400	37.900	4660.714	2754.617	49.246	19.993	12.280
Quartz Arenite	37.400	60.200	2791.444	1734.219	15.183	6.402	5.943
Troctolite1	15.100	25.400	6913.907	4110.236	124.109	50.586	20.703
Troctolite2	14.900	25.400	7006.711	4110.236	119.737	48.372	20.062
Class I							
Marble	16.900	28.600	6177.515	3650.350	88.449	35.903	16.645
Norite2	15.300	26.100	6823.529	4000.000	114.574	46.266	19.731
Norite3	15.400	24.000	6779.221	4350.000	133.684	58.121	20.823
Sandstone	44.300	75.200	2356.659	1388.298	10.262	41.57	5.083
SpottedAnorthosite	15.200	25.700	6868.421	4062.257	116.644	47.171	19.764
minimum	14.900	24.000	2356.659	1388.298	10.262	6.402	5.083
maximum	44.300	75.200	7006.711	4350.000	133.684	58.121	20.823

The dynamic modulus has the smallest value for Sandstone (10.262 GPa) and highest value for Norite3 (133.684 GPa). Also Norite3 has the highest value of dynamic modulus of rigidity (58.121 GPa) and acoustic impedance (20.823 kg/sm^2). Quartz Arenite has the lowest value (6.402 GPa) for dynamic modulus of rigidity while Sandstone has lowest value for acoustic impedance (5.083 kg/sm^2).

4.4 Static Mechanical Properties of Rock

The static mechanical properties of the rocks are presented in Table 4.3. The rocks are grouped in the table according to the sign of their post-failure modulus, negative for Class I and positive Class II. The Brazilian tensile strength of the rocks range from 2.617 MPa for Quartz Arenite to 27.609 MPa for Quartzite2. The compression-extension curves for the rocks are shown in Appendix 2.1. The failure modes are identical for the Brazilian tensile tests with an extension fracture across the specimen (Appendix 2.1). Quartzite2 has the highest UCS value of 514.244 MPa and elastic strain energy density of 1530.701 kN/mm^2. On the other hand, Quartz Arenite has the lowest UCS of 35.228 MPa while Marble has the lowest strain energy density of 44.848 kN/mm^2. Sandstone has the lowest modulus of elasticity and highest Poisson's ratio.

Table 4.3 Static mechanical properties of rock.

Rocks	Brazilian Tensile Strength (MPa)	UCS (MPa)	Elastic Modulus (GPa)	Strain Energy (kN/mm^2)	Post. Failure Modulus (GPa)	Poison's ratio
Gabbro	22.029	390.463	94.389	807.622	-	0.264
Quartzite2	27.609	514.244	86.381	1530.701	-	0.178
Class II Rocks						
Granite1	13.971	238.560	70.387	404.271	81.137	0.292
Granite2	12.679	192.804	68.957	269.540	118.269	0.274
Granite3	9.151	129.615	62.841	133.671	74.524	0.344
Granite4	11.728	193.501	59.525	314.512	97.931	0.276
Granite5	12.664	180.708	45.262	360.737	71.255	0.294
Mottled Anorthosite	16.804	276.307	96.772	394.461	96.949	0.322
Norite1	14.599	220.194	91.035	266.301	106.595	0.302
Quartzite1	15.666	249.880	62.359	500.650	79.908	0.215
Quartz Arenite	2.617	35.228	10.742	57.764	16.770	0.409
Troctolite1	16.796	225.960	102.499	249.065	130.687	0.297
Troctolite2	16.852	215.682	109.175	213.047	111.265	0.275
Class I Rocks						
Marble	5.555	76.819	65.790	44.848	-7.126	0.329
Norite2	12.278	186.208	97.306	178.167	-151.644	0.293
Norite3	15.977	205.492	107.194	196.965	-40.584	0.247
Sandstone	2.940	40.326	10.640	76.419	-14.095	0.490
Spotted Anorthosite	13.866	201.321	98.831	205.048	-73.468	0.273
Minimum	2.617	35.228	10.64	44.848	-151.644	0.178
maximum	27.609	514.244	109.175	1530.701	130.687	0.490

The post-failure modulus ranges from -151.644 MPa to 130.687 MPa. The results show a wide spread in properties. The post-failure modulus with negative values are the Class I rocks while those with a positive values are Class II rocks. In addition, the water content for most of the rocks varies from 0.05 to 0.070. The extreme values are 0.020 for Quartzite2, 0.196 for Quartz Arenite and 0.393 for Sandstone. The values for the post-failure moduli of Gabbro and Quartzite2 could

not be determined because specimen failed abruptly as result of their higher strength.

4.5 Pre-failure and Post-failure Curves

The pre-failure and post-failure moduli of the test rocks are shown in Table 4.3. The tests were calibrated by testing with a material with a known property. An aluminium specimen of 56 mm diameter and 105 mm length was tested to determine its elastic constants: elastic modulus, E and Poisson's ratio, *v*. The result was found to be in agreement with the property of the material. The experimental set up and characteristic curve is shown in Appendix 2.2. Photographs of the rock specimens were taken before and after each test and are also contained in the appendix. The failure modes and characteristic curves for the rocks are discussed in the following paragraphs.

The pre-failure and post-failure curves for the Granites are shown in Appendix 2.2.3 to 2.2.7. Tonalite (Granite1) failed with a vertical crack extending from its bottom and close to the top of the specimen. The characteristic post-failure curve is Class II. On the other hand, Syeno-Granite (Granite2), Monzo-Granite (Granite3), Alkali Feldspar Granite (Granite4) and Leucocratic Monzo-Granite (Granite5) show failure modes that are different to the mode of failure in Tonalite (Granite1). These specimens failed with spalling (i.e. small fragments falling out) from the sides. The spalls from Syeno-Granite (Granite2) and Monzo-Granite (Granite3) occurred at the mid height of the specimens around the circumferential chain. The Alkali Feldspar Granite (Granite4) and Leucocratic Monzo-Granite (Granite5) spalls occurred close to the specimen top at the point of contact with

one of the axial extensometers. All of the granites displayed post-failure curves that are characteristic of Class II rocks (Appendix 2.2.3 to 2.2.7).

However, Norite1, Norite2 and Norite3 unlike the granites show different post-failure curves (Appendix 2.2.10 to 2.2.12). Both Norite2 and Norite3 show the characteristic shape of Class I while Norite1 shows the characteristic behaviour of Class II. Norite1 failed with vertical cracks extending from top to bottom of the specimen. Norite2 failed with a big spall close to specimen top. As for Norite3 it failed in a shear mode with a crack extending from the bottom and close to the top of the specimen.

Remarkably, Norite1, Norite2 and Norite3 belong to different classes of rocks. However, this is not unexpected because the brittleness of rocks depends much on their distinctive textural and mineralogical constituents (Hajiabdolmajid & Kaiser, 2003). The Class II Norite1 contains larger grain size of about 6 mm minerals of plagioclase and orthoclase feldspars. The phenocryst (i.e. large grains) of feldspars was responsible for the Class II behaviour. It has already been established that grain size influences the brittleness of the rock because rock brittleness index increases generally with increasing grain size (Gong & Zhao, 2006; Yilmaz, et al., 2009). With an increase in grain size, the number of intra-granular cracks increases and gives the mineral a preferred fabric/matrix (refer to Figures 4.9 to Figure 4.11 for the photo-micrograph of these thin sections). In addition, the higher value of the UCS of Norite1 contributed to the brittle behaviour. Since the increase in the uniaxial compressive strength is accompanied by increase in the brittleness index (Goktan & Yilmaz, 2005).

Similarly, Quartz Arenite and Sandstone have different post-failure characteristic curves (Appendix 2.2.13 and 2.2.16). From the Appendix, it can be seen that the Sandstone exhibits shear failure and has the characteristic curve of Class I. However, the Quartz Arenite, which is another type of Sandstone at the stage of metamorphosing into Quartzite, exhibits different failure behaviour. The characteristic curve of Quartz Arentite is Class II with the failure mode more or less an axial splitting.

The Mottled Anorthosite and Spotted Anorthosite also exhibit different post-failure curves. Mottled Anorthosite has a characteristic Class II curve while Spotted Anorthosite has a curve characteristic of Class I (shown in Appendix 2.2.9 and 2.2.17). The post-failure curve for Mottled Anorthosite was difficult to obtain because of the abruptness of the specimen failure immediately after the curve reached the peak strength. The specimen shattered into pieces causing damage to the extensometers. However, it was much easier with Spotted Anorthosite. In this case, the post-failure curve descended from the peak strength and increases in strength again. Just before the peak strength the specimen failed with spalling at the point of contact with the circumferential chain.

Both Troctolite1 and Troctolite2 rocks showed the same behaviour that is characteristic of Class II. Troctolite1 and Troctolite2 specimens and the characteristic curves are shown in Appendix 2.2.18 and 2.2.19. When Troctolite1 failed there was a small spall from the top of the specimen and Troctolite2 had a big spall from the bottom of the specimen. Because the specimen failure was close to the circumferential chain, it resulted in large increase of circumferential

displacement which exceeded the extension limit of the chain. This leads to the test being terminated as a result of program interlock.

A typical Class I curve is shown for Marble and the specimen before and after failure is shown in Appendix 2.2.8. Although it was easy to obtain the characteristic curve for Marble, the radial strain exceeded the circumferential chain extension limit and also resulted in terminating the test because of program interlock. The failure mode was ductile.

The curve of Gabbro is shown in Appendix 2.2.2. It was not possible to obtain the post-failure curve for this rock. The specimen failed abruptly and catastrophically on reaching the peak strength with the specimen shattering into pieces of almost equal sizes. The failure was accompanied by damage of the metal knife holding the circumferential chain and also to the extensometer springs. Several attempts were made with reduced circumferential control rates and with smaller specimen sizes, and in addition under low confinement pressure (up to15MPa) without success.

It was also practically difficult to obtain the characteristic curves for Quartzite1 and Quartzite2. Although, the Quartzite1 characteristic curve was obtained after several attempts, it was just impossible for Quartzite2. In the case of Quartzite1, there was lot of cracking noise and small pieces of spall falling from the specimen when load was close to the peak. This is characteristic of Class II behaviour (Appendix 2.2.14).

For Quartzite2, the specimen tends to reduce in area often from the bottom and top of specimen at the point of contact with the platens and failed suddenly at peak load. The attempts made after several failed post-failure tests to control Quartzite2 was to reduce the length to diameter ratio to 2 and then at much slower circumferential control rate. Nevertheless, the specimen failed explosively and damaged the system (Appendix 2.2.15). In another attempt, 4 MPa confinement was applied with the triaxial control system after the system was fixed back on. Similar series of attempts of testing under confinement up to 15 MPa was done. However, when the load of the specimen was about 530 MPa it produced loud cracking noises. The system was terminated to prevent damaging the test equipment again.

4.6 Stress-Axial, Radial and Total Volumetric Strain Curves

An attempt was made to determine why it was easy to control the post-failure behaviour of some rocks, especially the Class I rocks while others were difficult to control, e.g. Gabbro and Quartzite2 as described in the two previous paragraphs. Stress-axial, radial and total volumetric strain curves were constructed according to Martin and Chandler (1994) and Bieniawski (1967a) to show the stages in the deformation process as discussed in Section 2.2.1 of the literature review. Three types of curves were identified. The first type has a negative total volumetric strain and with a point of reversal at crack damage stress. The second type has positive total volumetric strain with reversal point at crack-damaged stress and the third type has a positive total volumetric strain without a reversal point.

The difficulty in obtaining the post-failure curves increases as the total volumetric strain approaches a positive value. In other words, difficulty in obtaining the post-failure curves increases from the first type to the second type and finally the third type. For the first and second types, the four stages of deformation process are identifiable while only three stages of deformation process can be identified with the third type. For rocks that exhibit the first type of deformation process the stress-axial, radial and total volumetric strain curves are shown in Figures 4.19 to 4.31.

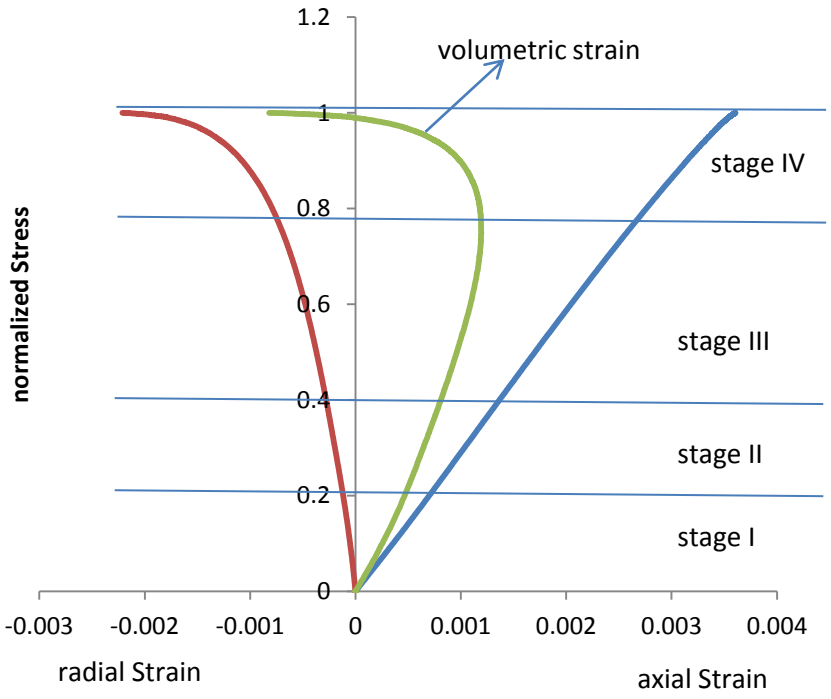

Figure 4.19 Normalized stress-strain curves for Granite1.

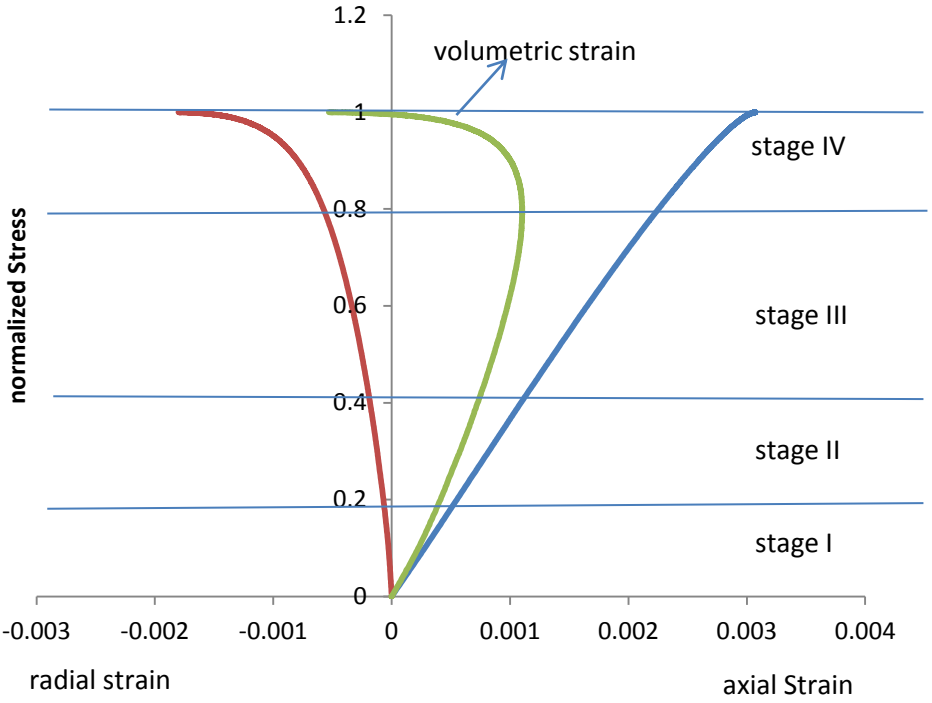

Figure 4.20 Normalized stress-strain curves for Granite2.

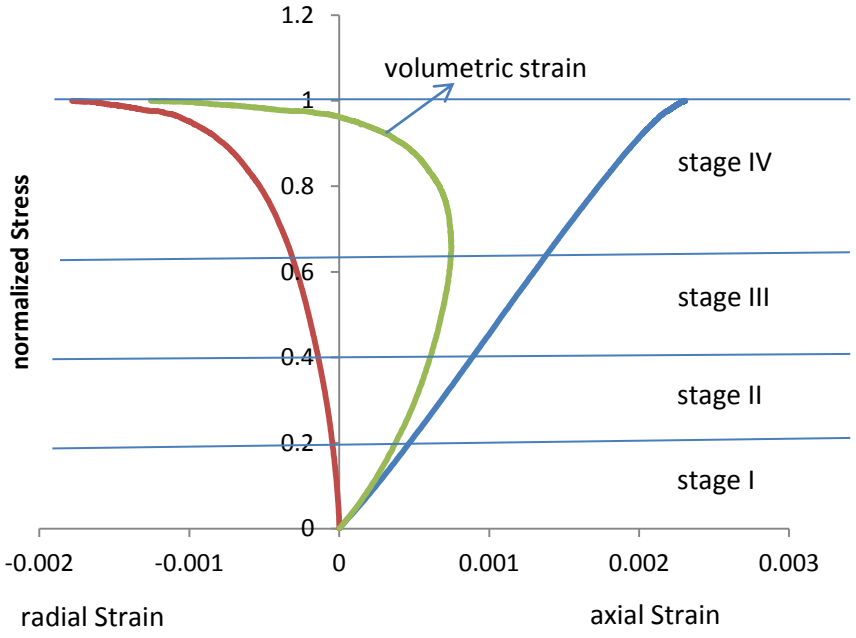

Figure 4.21 Normalized stress-strain curves for Granite3.

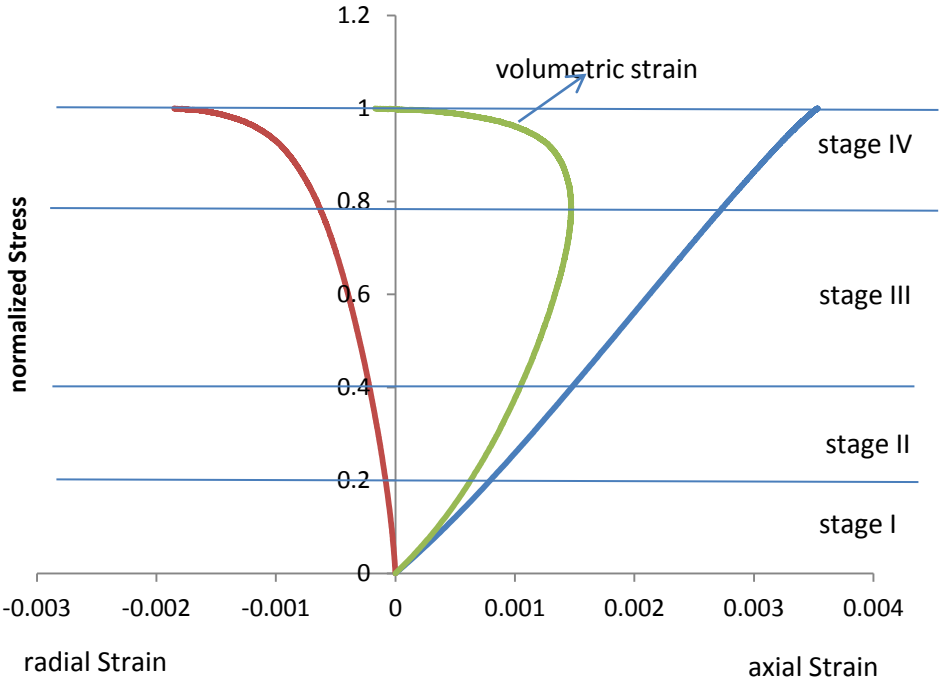

Figure 4.22 Normalized stress-strain curves for Granite4.

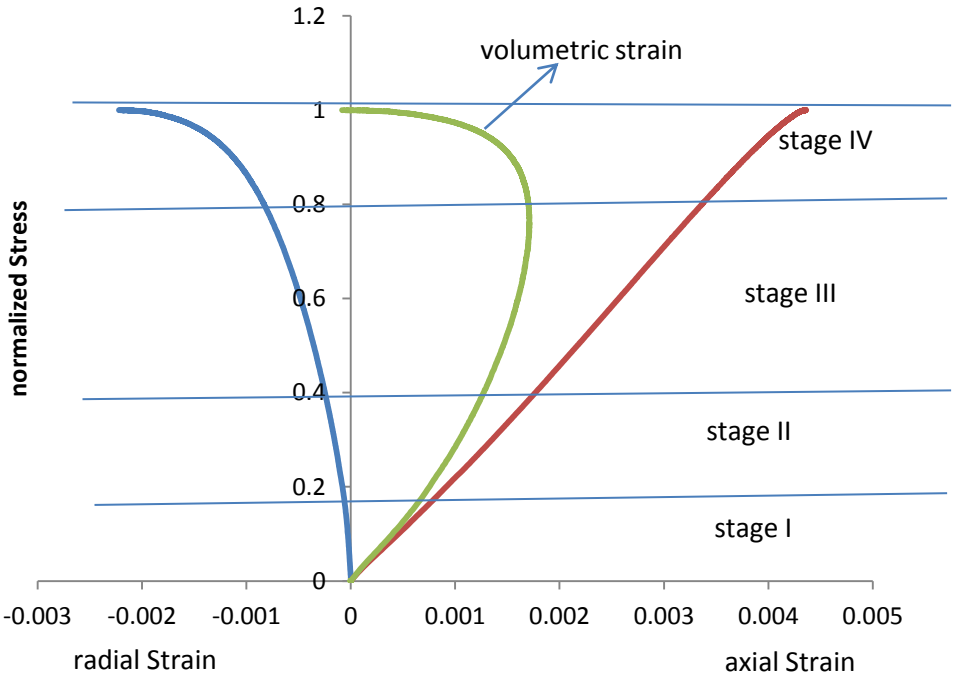

Figure 4.23 Normalized stress-strain curves for Granite5.

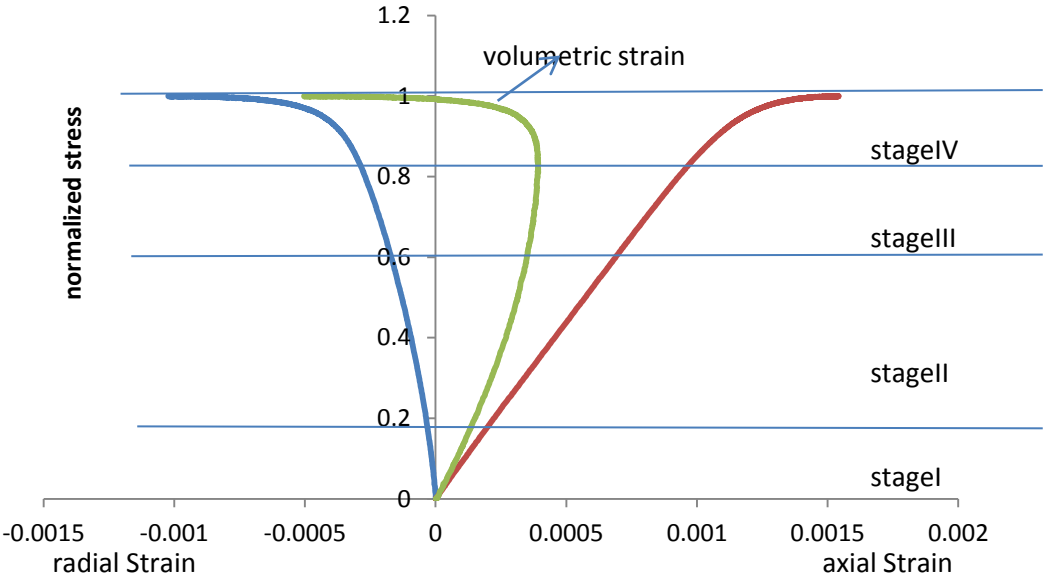

Figure 4.24 Normalized stress-strain curves for Marble.

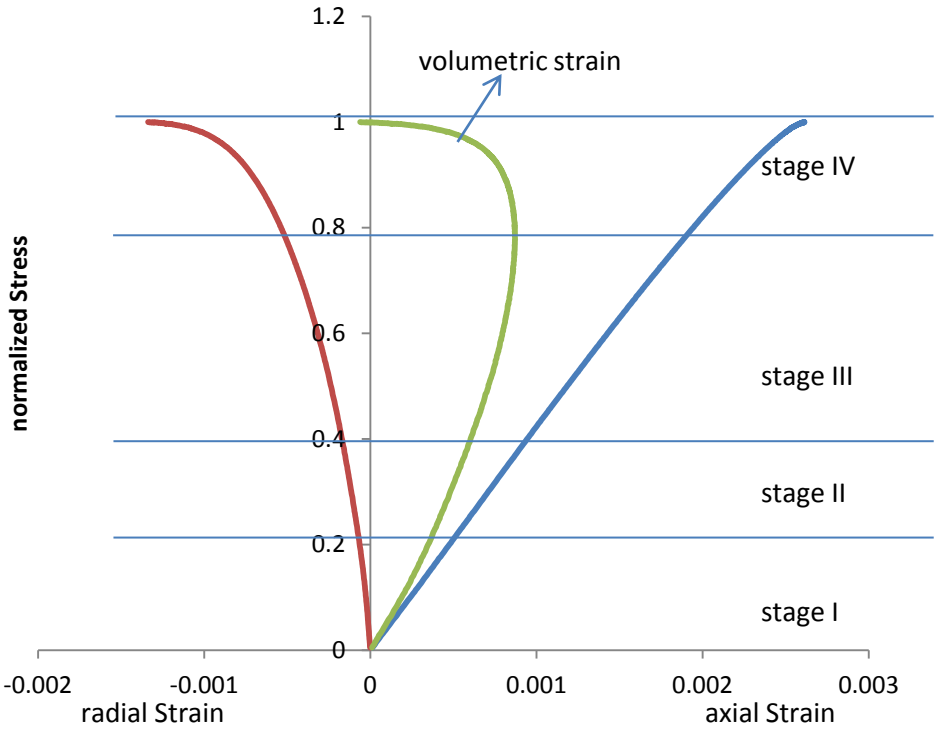

Figure 4.25 Normalized stress-strain curves for Norite1.

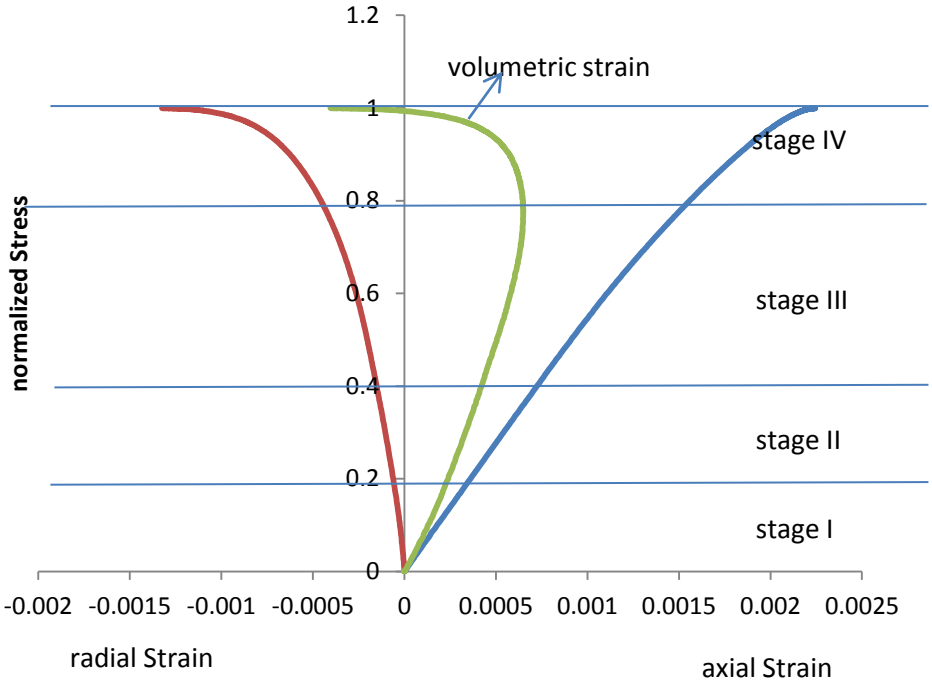

Figure 4.26 Normalized stress-strain curves for Norite2.

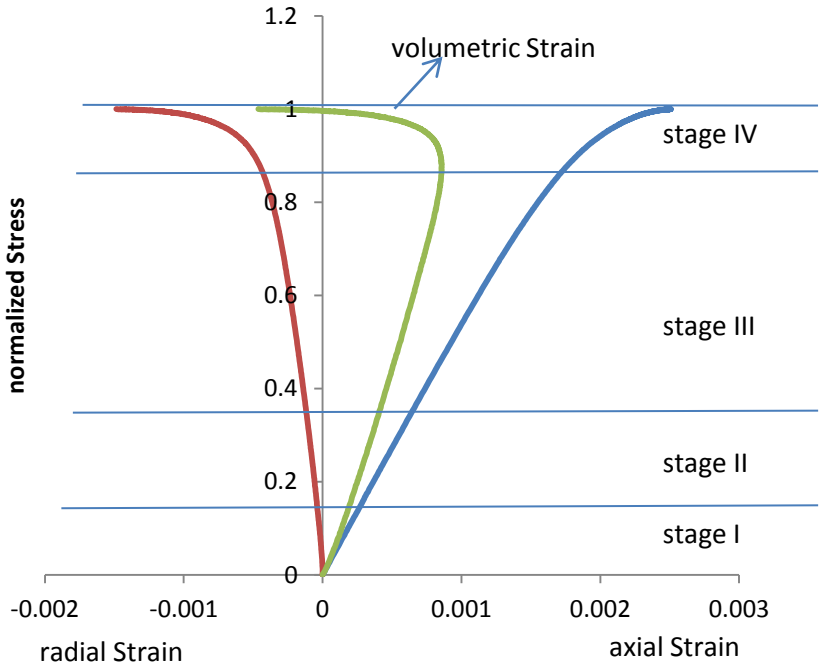

Figure 4.27 Normalized stress-strain curves for Norite3.

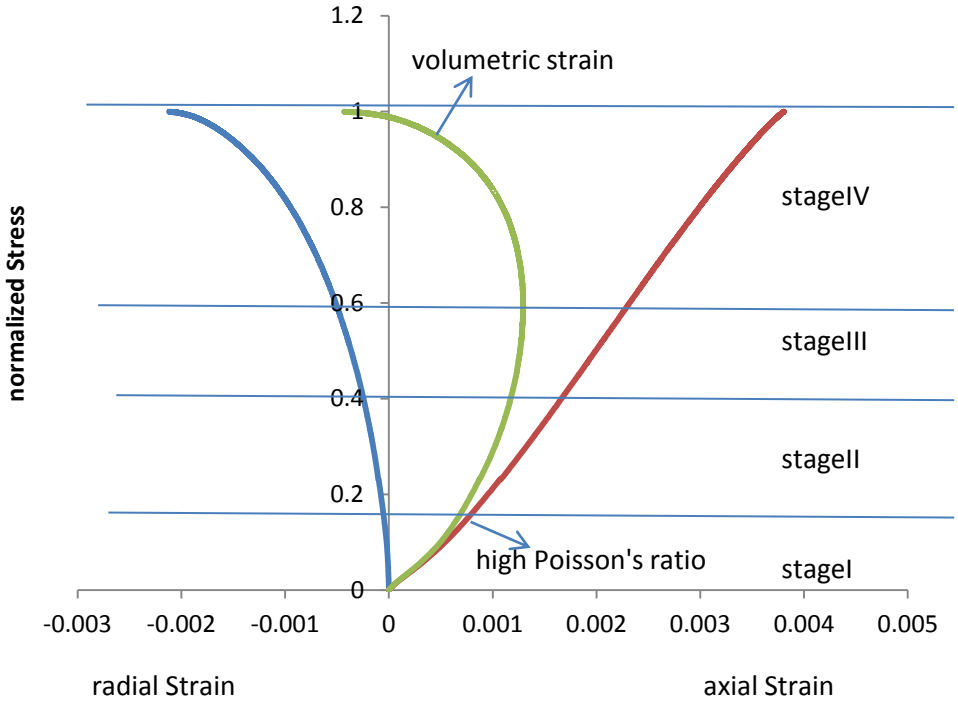

Figure 4.28 Normalized stress-strain curves for Quartz Arenite.

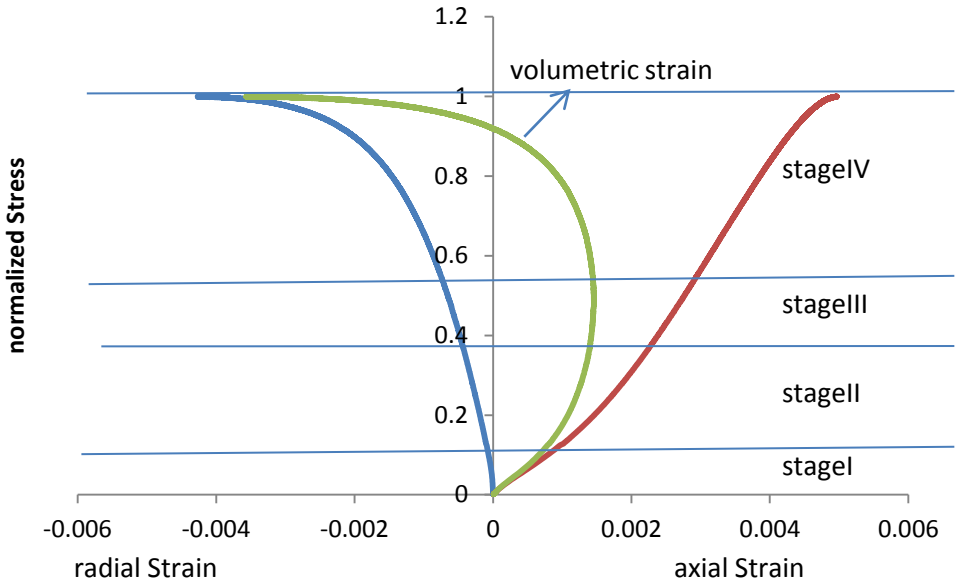

Figure 4.29 Normalized stress-strain curves for Sandstone.

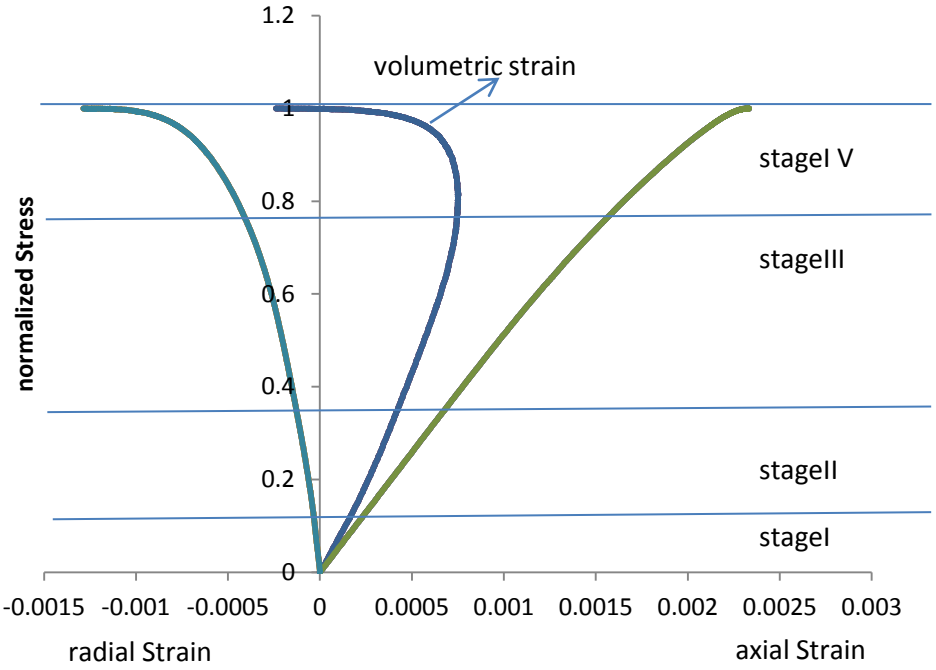

Figure 4.30 Normalized stress-strain curves for Spotted Anorthosite.

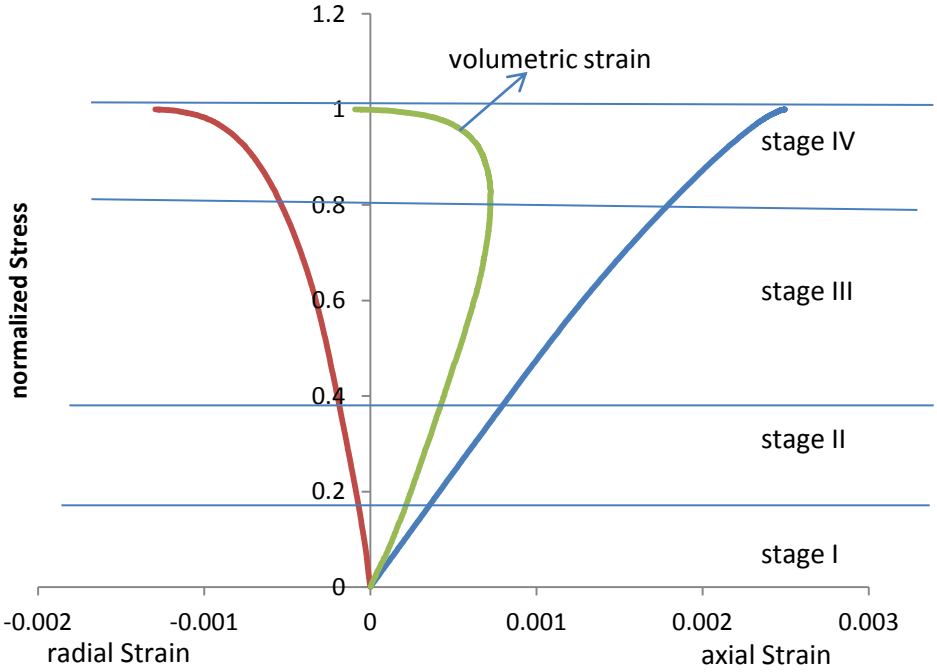

Figure 4.31 Normalized stress-strain curves for Trocolite1.

Figures 4.32 to 4.34 show the second type and the stages of deformation process. For this type of stress-axial, radial and total volumetric strain curves, the process of unstable crack propagation (stage IV) has a small duration and for this reason cracks propagate by their own accord. Thus, the rocks exhibit a higher velocity of micro-crack propagation. This made it difficult to control the post-failure curves than the type one stress-axial, radial and total volumetric strain curves because of the short duration of the crack damage stress threshold to rupture.

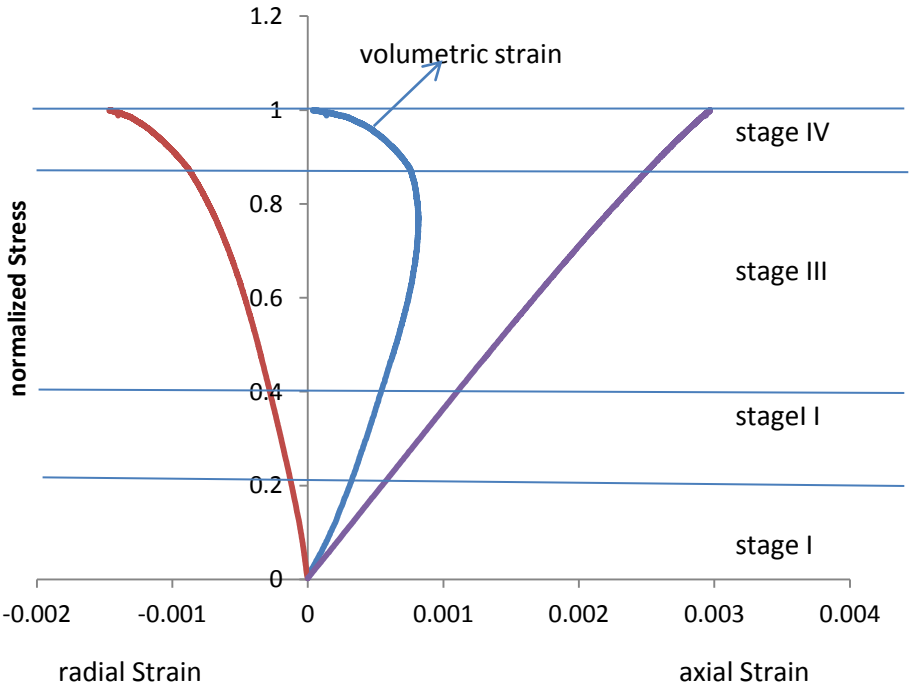

Figure 4.32 Normalized stress-strain curves for Mottled Anorthosite.

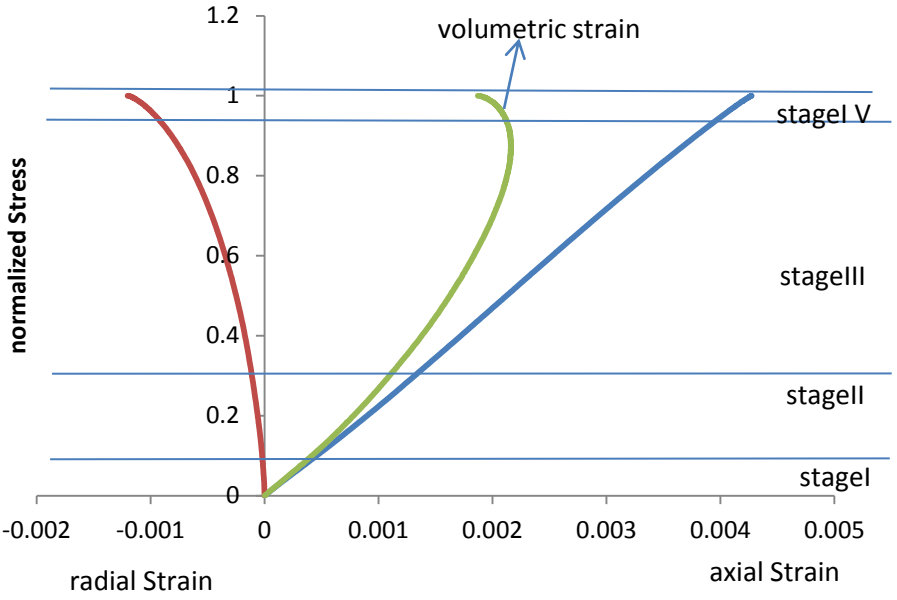

Figure 4.33 Normalized stress-strain curves for Quartzite1.

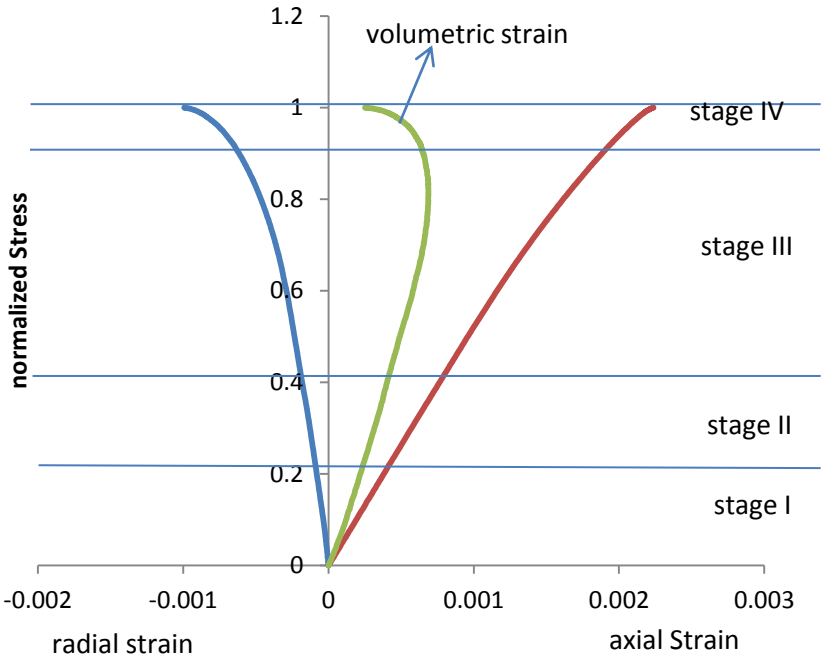

Figure 4.34 Normalized stress-strain curves for Troctolite2.

In the third type of stress-axial, radial and total volumetric strain curves, the crack induced stress and the structural failure of the rock specimen occurred together (Figures 4.35 and 4.36). There was no reversal of the total volumetric strain so there was continued decrease in rock volume. The control feedback, the circumferential strain, does not continuously increase with the applied load after the peak load. Instead, the deformation became a self-sustaining failure and, as a result the micro-cracking of the material continued on its own accord.

Furthermore, unstable crack growth occurs at the onset of the crack initiation stress. The critical energy release rate or crack damage stress threshold started much earlier for this type of curve than observed with others. Under this condition, the relationship between the applied stress and the crack length ceases to exist and other parameters, such as the crack growth velocity, take control of the propagation process.

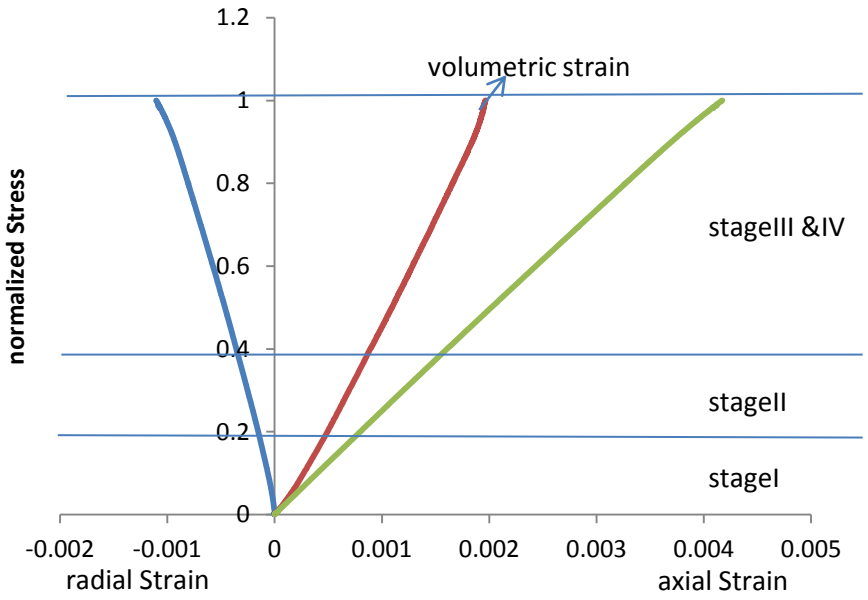

Figure 4.35 Normalized stress-strain curves for Gabbro.

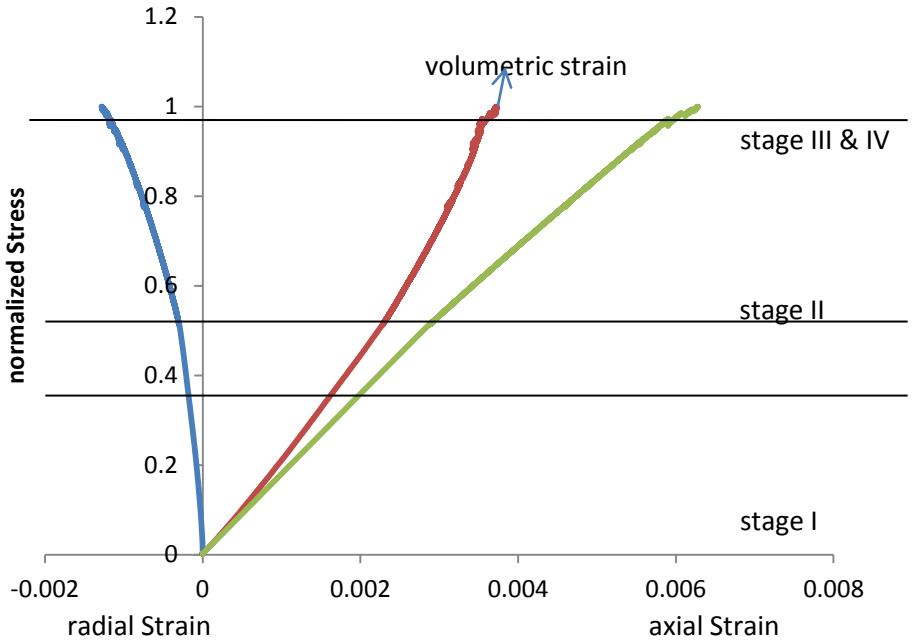

Figure 4.36 Normalized stress-strain curves for Quartzite2.

These specimens exhibit high micro-crack propagation velocities at peak strength. The velocity increases rapidly to reach terminal velocity as unstable crack growth continued to the point where the many micro-cracks coalesce and the rock can no longer support an increase in load. This eventually leads to the rupture of the specimen.

Although the load was reduced, the fracture continues to propagate since the stored elastic strain energy release rate has attained the critical value. The cracks continued to extend because the elastic strain energy stored within the specimen is released. As a result of the high UCS of the rocks, the elastic strain energy accumulated in the system during loading and available for rupture development in the post-failure region was higher than the work that the specimen can do at the post-failure phase. It leads to the violent failure of the rocks with a complete loss

of cohesion. This is what contributed to the difficulty of following the post-failure regime on the stress-strain curve.

4.7 Brittleness Based on Static Mechanical Properties of Rock

Table 4.4 shows the various brittleness indices based on the static mechanical properties of rock (The rocks are grouped in the table according to the sign of their post-failure modulus, negative for Class I and positive, Class II). From the table, letter 'B' with number subscripts are different brittleness concepts and the equations used to estimate them are shown above them. This was discussed in Section 2.6 of the Literature Review. From the values of the various brittleness concepts it was not just possible to identify or classify the rocks as either Class I or Class II except with the use post-failure modulus sign.

For example B_{11} values are almost the same, around 0.8, for both Class I and Class II rocks. The other concepts as well have no clear cut way to classify the rock brittleness. For instance Troctolite2 has minimum brittleness index for B_{11} and B_{12}. On the other hand with brittleness B_{13} and B_{14}, Quartz Arenite has the minimum brittleness index. From the laboratory results, Marble was least brittle while Troctolite2 and Quartz Arenite rocks are actually brittle in behaviour. The post-failure moduli of the rocks reveal the same.

Table 4.4 Brittleness indices based on static mechanical properties of rock.

Brittleness concepts	(σc-σt)/(σc+σt)	(σc*σt)/2	σc/σt	(σc*σt) 0.72
Rocks	B_{11}	B_{13}	B_{12}	B_{14}
Gabbro	0.875	4300.755	15.001	767.480
Quartzite2	0.898	7098.881	18.626	976.334
Class II				
Granite1	0.889	1666.461	17.075	343.902
Granite2	0.877	1222.281	15.207	275.109
Granite3	0.868	593.053	14.164	163.444
Granite4	0.886	1134.690	16.499	260.767
Granite5	0.869	1144.243	14.269	262.346
Mottled Anorthosite	0.885	2321.531	16.443	436.616
Norite 1	0.876	1607.306	15.083	335.068
Quartzite1	0.882	1957.310	15.950	386.133
Quartz Arenite	0.862	46.096	13.461	25.976
Troctolite1	0.862	1897.612	13.453	377.617
Troctolite2	0.855	1817.337	12.799	366.046
Class I				
Marble	0.865	213.365	13.829	78.291
Norite2	0.876	1143.131	15.166	262.163
Norite3	0.856	1641.573	12.862	340.196
Sandstone	0.864	59.279	13.716	31.134
Spotted Anorthosite	0.871	1395.758	14.519	302.695
minimum	0.855	46.096	12.799	25.976
maximum	0.898	7098.881	18.626	976.334

4.8 Brittleness Based on Moduli

Table 4.5 shows the different brittleness concepts based on the moduli for the different rocks (the rocks are grouped in the table according to the sign of their post-failure modulus, negative for Class I and positive, Class II). These concepts were discussed in Section 2.6 of the Literature Review. From the values of the different concepts, it is obvious that the concepts have clearly classified the rocks into Class I and Class II, except for B_8 with no clear cut difference between Class I and Class II rock types. For instance, B_{16} and B_7 show that values with a negative

sign are Class I, while values with a positive sign are Class II rocks. If that is the case, then B_{16} for example, index -14755.871 for Norite2 is at the extreme end of the scale of Class I behaviour, i.e. it is the least brittle. Likewise, the value of 13395.287 for Troctolite1 is at the extreme end of the scale for Class II behaviour i.e. it is the most brittle. Similarly, for B_7, -1.558 value for Norite2 is most Class I and 1.715 value for Granite2 is the highest in Class II. This value shows that these rocks are the strongest in their classes.

Table 4.5 Brittleness concepts based on moduli.

		Brittleness Concepts				
Rocks	Rock Class	B_8 M/(E+M)	B_{16} EM	B_7 M/E	K (E-M)/M	K_2 E/M
Granite 1	Class II	0.535	5710.990	1.153	-0.132	0.868
Granite2	Class II	0.632	8155.475	1.715	-0.417	0.583
Granite3	Class II	0.543	4683.163	1.186	-0.157	0.843
Granite4	Class II	0.622	5829.343	1.645	-0.392	0.608
Granite5	Class II	0.612	3225.144	1.574	-0.365	0.635
Mottled Anorthosite	Class II	0.500	9381.949	1.002	-0.002	0.998
Norite 1	Class II	0.539	9703.876	1.171	-0.146	0.854
Quartzite1	Class II	0.562	4982.983	1.281	-0.220	0.780
Quartz Arenite	Class II	0.610	180.143	1.561	-0.359	0.641
Troctolite1	Class II	0.560	13395.287	1.275	-0.216	0.784
Troctolite2	Class II	0.505	12147.356	1.019	-0.019	0.981
Marble	Class I	-0.121	-468.820	-0.108	-10.232	-9.232
Norite2	Class I	2.791	-14755.871	-1.558	-1.642	-0.642
Norite3	Class I	-0.609	-4350.361	-0.379	-3.641	-2.641
Sandstone	Class I	4.080	-149.971	-1.325	-1.755	-0.755
Spotted Anorthosite	Class I	149.842	-9833.190	-1.007	-1.993	-1.345
minimum		-0.609	-14755.871	-1.558	-10.232	-9.232
maximum		149.842	13395.287	1.715	-0.002	0.998

All the values in brittleness in concept k are negative, so it can not follow the sign convention used above. However, the author (Tarasov, 2011) of the concept has

defined brittleness index k to range from $-\infty<k<0$. Using this definition, then -10.232 values for Marble indicates that it is the least brittle or Class I behaviour while -0.002 value for Mottled Anorthosite is most brittle Class II. The closest value to Mottled Anorthosite on the table is Troctolite2 and to Marble on the Class I side is Norite3 and so on for all the other samples. This is also applicable to brittleness k_2 with Marble rating -9.232 and Norite3 having -2.641 as least brittle, also Mottled Anorthosite with brittleness 0.998 and Troctolite2 with brittleness 0.981 as most brittle Class II. Therefore, brittleness k and k_2 appear to be more convincing than B_7 and B_{16} (refer to Appendix 2.2 for photographs of post-failure curves for the rock specimens).

4.9 Chapter Summary

The results of the laboratory work are presented in this chapter. The rock samples were identified on the basis of their mineral composition. Destructive and non-destructive tests were performed to determine the rock properties. Post-failure moduli of the rocks were determined and subsequently used to classify the rocks into Class I and Class II. The same rock type can be classified as Class I or Class II depending on its textural characteristics, as shown in Norite1-3.

Stress-axial, radial and volumetric strain curves were constructed according to Martin and Chandler (1994) and Bieniawski (1967a) in order evaluate the stages of the deformation process. In addition, this was done to see why it was difficult to obtain the post-failure curves for some rocks.

From the assessments, three types of deformation stages were observed. Type one has negative total volumetric strain and with a point of reversal at crack damage stress. The second type has positive total volumetric strain with a reversal point at crack damage stress while the third type has a positive total volumetric strain without a reversal point at the crack damage stress. It was observed that there was difficulty in obtaining the post-failure curves when the total volumetric strain approaches a positive value. The second type has Class II post-failure behaviour. Gabbro and Quartzite2 rocks tested in this work belong to the difficult type (third type) to determine.

It was observed on the basis of the brittleness concepts based on static mechanical properties of rock that it was difficult to classify the rocks into either Class I or Class II. The brittleness concepts based on moduli classify the rocks into the two different classes particularly B_{16}, B_7, k_2 and k. However, the concept of brittleness described as k_2 and k appear to be more logical than the other brittleness concepts in grouping the rocks into these classes.

CHAPTER FIVE

ANALYSIS OF FRAGMENTS SIZE FROM THE COMPRESSION AND BLASTING TESTS

5.1 Introduction

The goal of this research is to investigate a possible relationship between fragmentation and brittleness. Therefore, the analysis involves the comparison of results of laboratory work (in Chapter 4) for both the compression and the blasting tests. As stated previously, fragmentation was obtained in two ways: by steady compression of the samples and by laboratory scale blasting tests as described in Chapter 4. The rocks blasted were Granite1 and Granite2 (Class II rocks), Norite1 (Class II), Sandstone (Class I), Quartz Arenite (Class II), Marble (Class I) and Gabbro. It was not possible to determine the post-failure modulus of Gabbro as a result of abrupt specimen failure due to its high strength, 390 MPa. Therefore, cannot be classified into either Class I or Class II, so its data was not used in the analysis, this is explained in the next sections.

As there is no universally accepted definition of the term 'brittleness', fragmentation is compared with brittleness according to a number of definitions, split into those based on static mechanical properties and those based on the moduli. In addition, the normalised stress-axial strain curve and the extension

strain criterion were evaluated and compared with both the fragmentation results of steady (also refer to as static) compression and by blasting tests.

To overcome the problem of comparing brittleness, a single number, with fragmentation, which is a distribution, fragmentation is viewed as the aperture at which selected percentages of the fragmented material passed through the sieves. Using just a single point, e.g. the commonly used 50% passing sieve size or X_{50} index, could be misleading. Therefore, 50% and 10% or X_{10} passing sieve size are considered. This will make it possible to compare fragmentation at smaller fragments size with brittleness. Henceforth, X_{50} and X_{10} are used in place of 50% and 10% passing sieves size. In order to distinguish the percentage passing for static, also refer to in this work as steady, the subscript 's' for static and 'b' for blasting were used. For example, X_{50s}, X_{50b} stand for 50% passing sieve size for static and blasting tests respectively.

The following comparisons were investigated:

- Brittleness concepts based on static mechanical properties with fragments size from compression and blasting tests.
- Brittleness concepts based on moduli with fragments size from compression and blasting tests.

These two brittleness concepts were used for comparison with the fragments size because it has been shown in the Literature Review that static mechanical properties are frequently used in the literature to quantify brittleness. Brittleness concepts based on moduli on other hand made it possible to characterise the

brittleness of the rocks into Class I or Class II. This will also allow evaluating the self-fracturing behaviour of Class II rocks under compressive test.

The analyses are discussed in the following sections. It begins with an overview analysis of the fragments size distribution for both the static and blasting tests using probability density distribution models. Following is a statistical analysis to investigate a possible relationship of fragmentation with the rock properties and their brittleness (based on the concepts of static mechanical properties and moduli) under compressive failure for the combined rock sample. As it will be shown latter, brittleness concepts estimated from the normalised stress-axial strain curve and the extension strain criterion show no relationship with the combined sample. The relationship between fragmentation (both static and blasting) and various brittleness concepts were investigated.

5.2 Fragments Size Produced During Uniaxial Compression Test

The fragments produced from failed specimens during uniaxial compression tests were examined by plotting the sieves size against the cumulative percentage passing. For the Class II rocks, Mottled Anorthosite was more fragmented (because higher percentage of the fragments was passed at each sieve size) than the rest of the rocks and next to it was Troctolite2. Likewise for the Class I rocks, Marble was found to be least fragmented (Figures 5.1 and 5.2). Mottled Anorthosite is the most brittle while Marble is least brittle among the rocks tested (using brittleness *k* in Table 4.5 in Chapter 4, show similar trend). Next to Mottled

Anorthosite on the side of Class II rocks is Trotolite2, Figures 5.1 and 5.2 actually reveal the same.

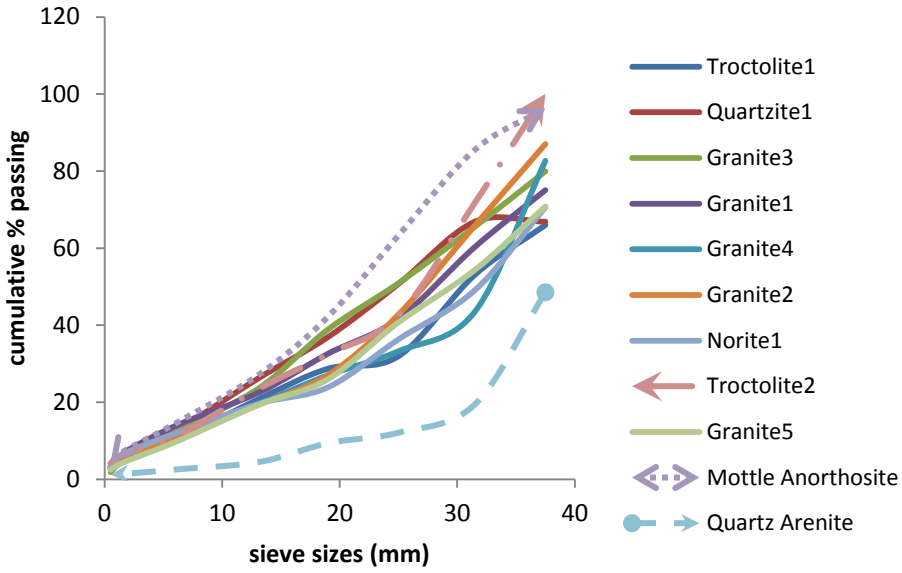

Figure 5.1 Sieve sizes against cumulative percentages passing for the Class II rocks.

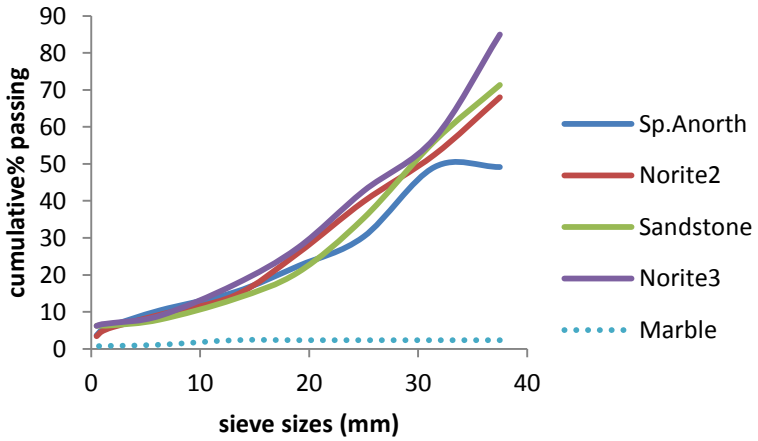

Figure 5.2 Sieve sizes against cumulative percentages passing for Class I rocks.

The cumulative percentage passing against the sieves size from compression tests for the rocks that were selected for blasting tests are shown in Figure 5.3A. For the Gabbro sample the percentage passing under the compression test lies between the Class I and the Class II rocks. For the blasting tests, it was least fragmented, Figure 5.4A. It was observed that the difficulty in the determination of the post-failure modulus for Gabbro was principally due to its high strength.

From Figure 5.3B, it can be seen that the Class II rocks are more fragmented than the Class I rocks. Since Marble is least brittle, its fragments (which are two separated lumps with little fines) were retained on the top screen. Sandstone was also poorly fragmented. The curves show that Class II rocks are more fragmented.

The sieves size against the cumulative percentage passing for the blasting tests are shown in Figure 5.4B. Marble was again poorly fragmented when compared with the other rocks. The higher fragmentation of Sandstone was because of its lower strength. Despite, Quartz Arenite (35.23Mpa, see Table 4,3) of similar strength with Sandstone (40.32Mpa but Class II) is more fragmented than Sandstone. It can therefore be stated that by breaking rocks under the same loading conditions, the Class II rocks tend to be more fragmented than the Class I rocks. This in a sense qualified the self-fracturing nature of the Class II rocks.

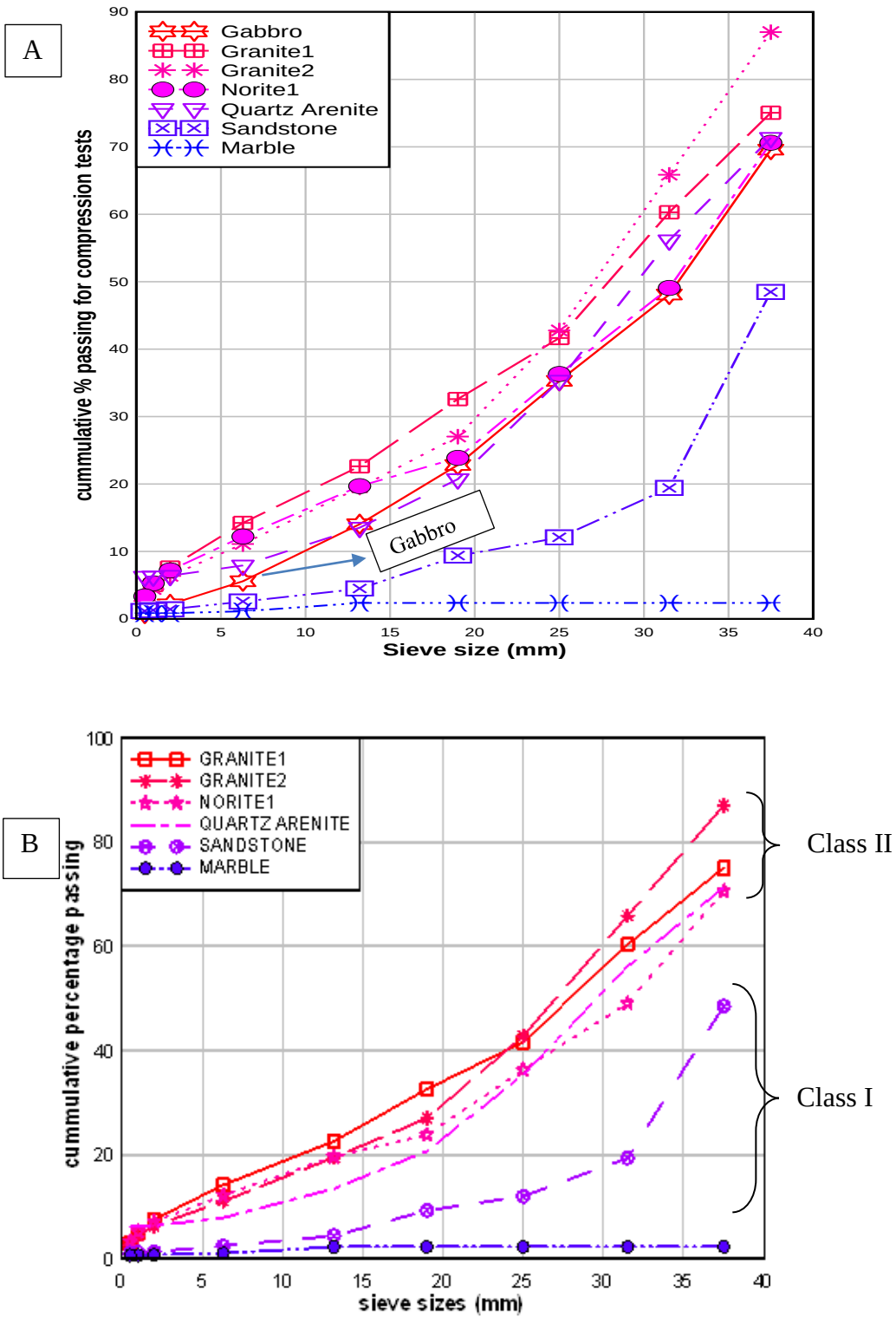

Figure 5.3 Comparison of the sieve sizes against the cumulative percentage passing from compression test of the rocks selected for blasting test.

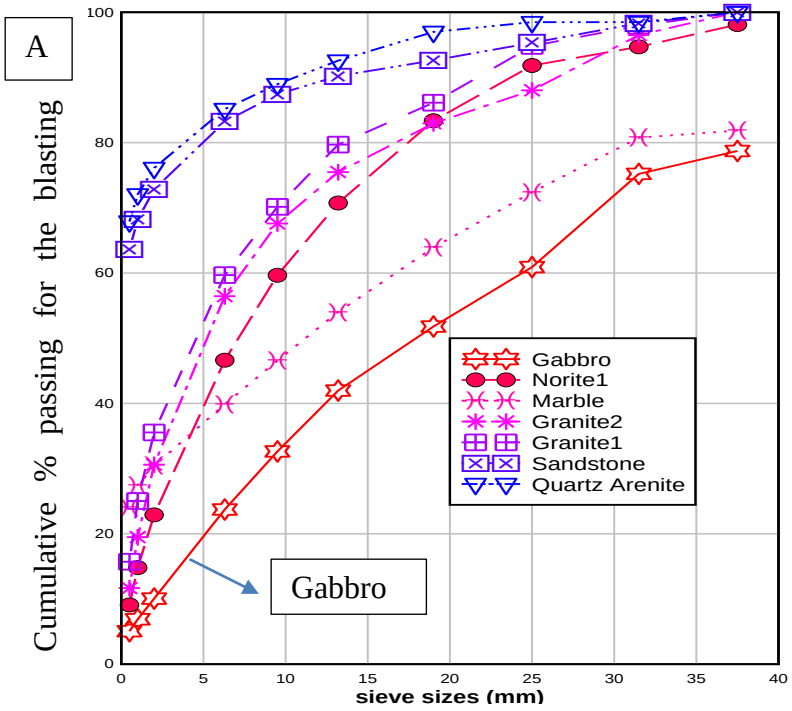

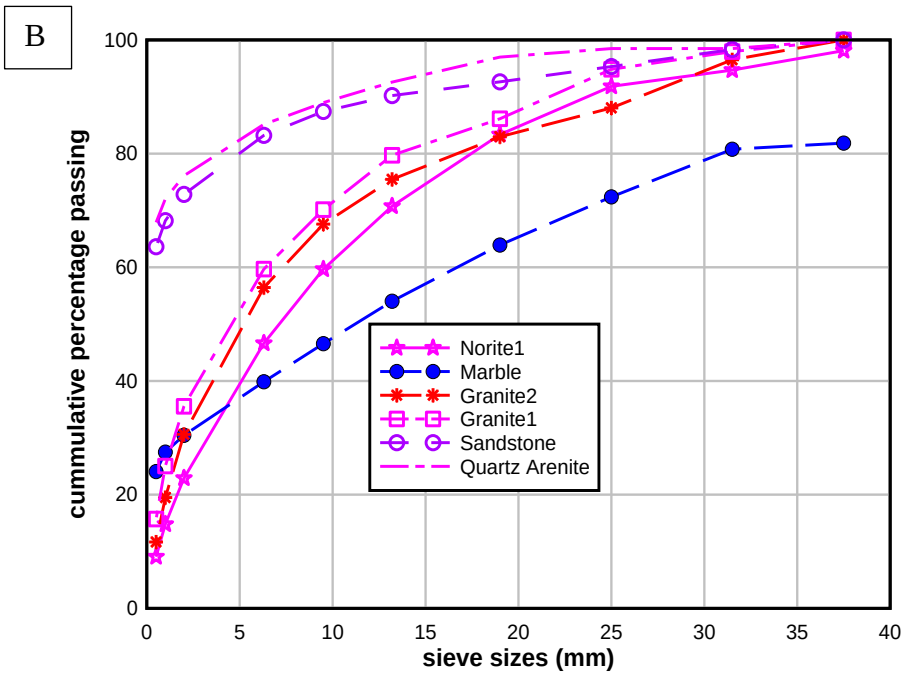

Figure 5.4 The sieve sizes against cumulative percentage passing for blasting test.

5.3 Comparison of Percentage Passing for Steady Compression Tests for Rocks of Similar Strength

The percentage passing (at both X_{50s} and X_{10s}) for the Class I and Class II rocks were compared. The comparison was done for rocks of similar strength using their UCS value for the pairing. Figure 5.5 and 5.6 show that more fragments are passed at X_{50s} and X_{10s} for Class II rocks than the Class I rocks. The differences in the percentage passing become larger as the difference in the value of their brittleness k increases. For instance there is much difference between the percentage passing for Marble which is towards the extreme Class I (brittleness k -10.232) and Granite3 (brittleness k -0.157) which is more brittle Class II rock. This analysis show that much of X_{50s} and X_{10s} are passed for the Class II rocks than the Class I rocks, therefore the Class II rocks are more fragmented.

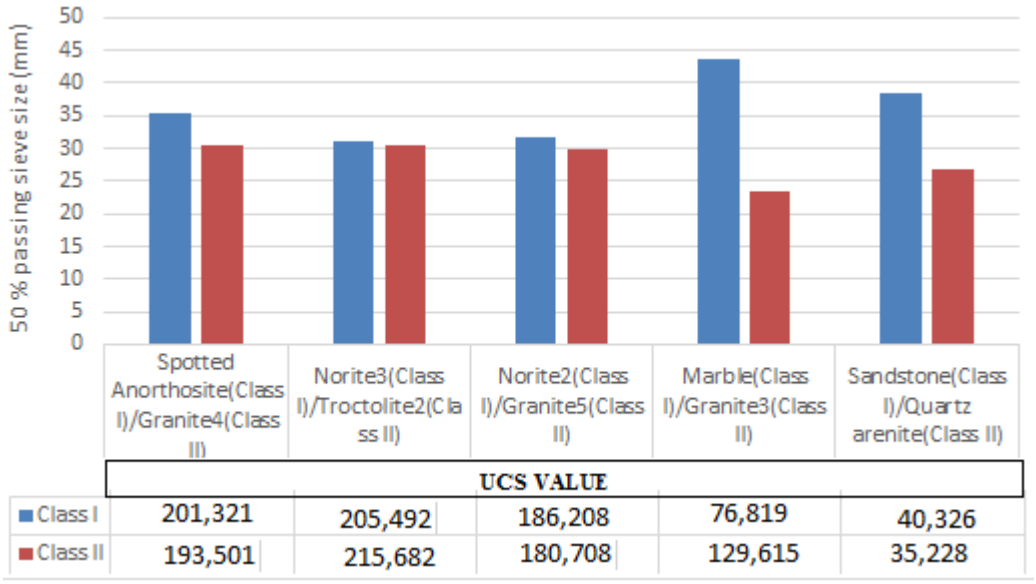

Figure 5.5 Comparison of X_{50s} for Class I and Class II rocks of similar UCS values.

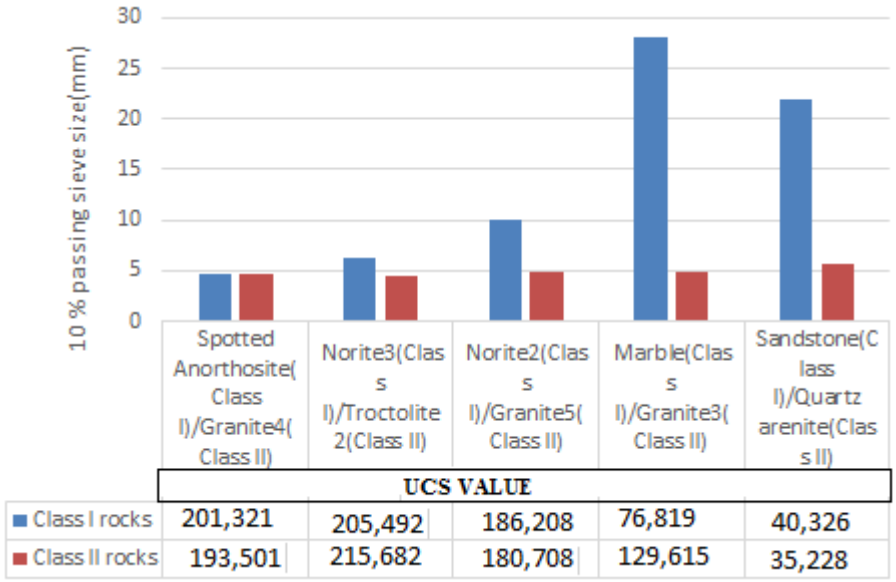

Figure 5.6 Comparison of X_{10s} for Class I and Class II rocks of similar UCS values.

A similar trend is observed when close Brazilian tensile strength (BTS) value for Class I and Class II rocks are used. The comparison shows that more fragments are passed at X_{50s} and X_{10s} for Class II rocks than Class I rocks (Figure 5.7 and 5.8). Also the differences in their percentage passing become larger as the difference in the value of their brittleness *k* increases. This analysis show that much of X_{50s} and X_{10s} are passed for the Class II rocks than the Class I rocks of similar strength (using BTS value), therefore the Class II rocks are more fragmented. This may also in a sense qualify the self-fracturing nature of Class II rocks under compressive failure. It can therefore be stated that by breaking rocks under steady loading conditions, the Class II rocks tend to be more fragmented than the Class I rocks of similar strength.

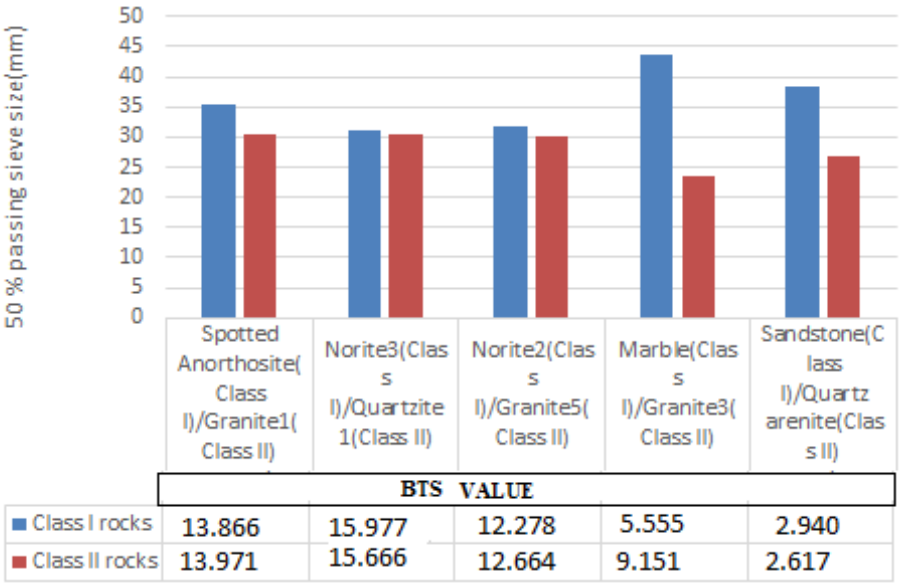

Figure 5.7 Comparison of X_{50s} for Class I and Class II rocks of similar Brazilian tensile strength values.

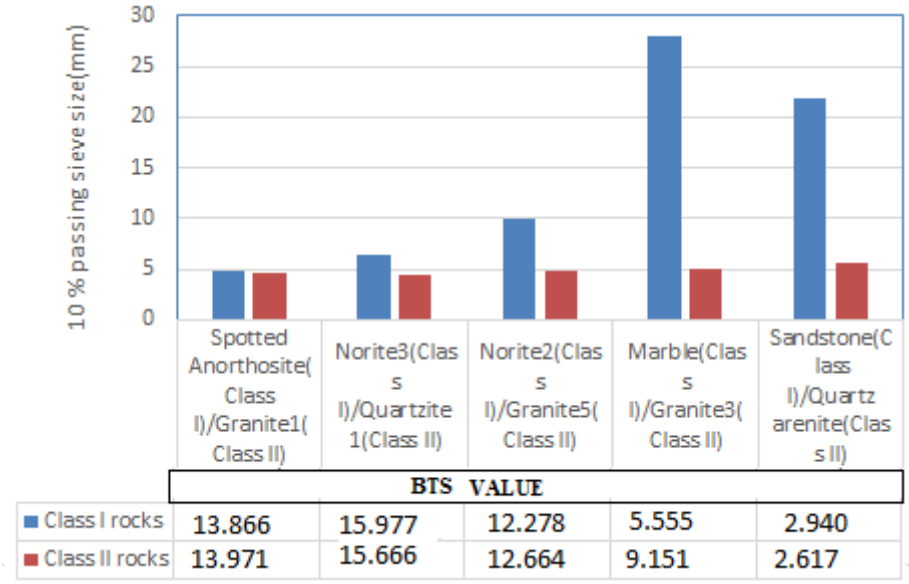

Figure 5.8 Comparison of X_{10s} for Class I and Class II rocks of similar Brazilian tensile strength values.

5.4 Analysis of Fragments Size from Compression Using Probability Density Distribution Models

Probability density distribution models were constructed to show the difference in the fragments size for the Class II and the Class I rocks for the steady compression tests. The distributions show a lognormal distribution that are positively skewed. The calculated probability of the distribution for X_{50s} and X_{10s} for the combined and segregated samples (Class I and Class II rocks) are compared. The calculated probabilities of the distribution at X_{50s} and X_{10s} for the segregated models and the combined model are shown in Figures 5.9 to 5.11 and are summarised in Table 5.1.

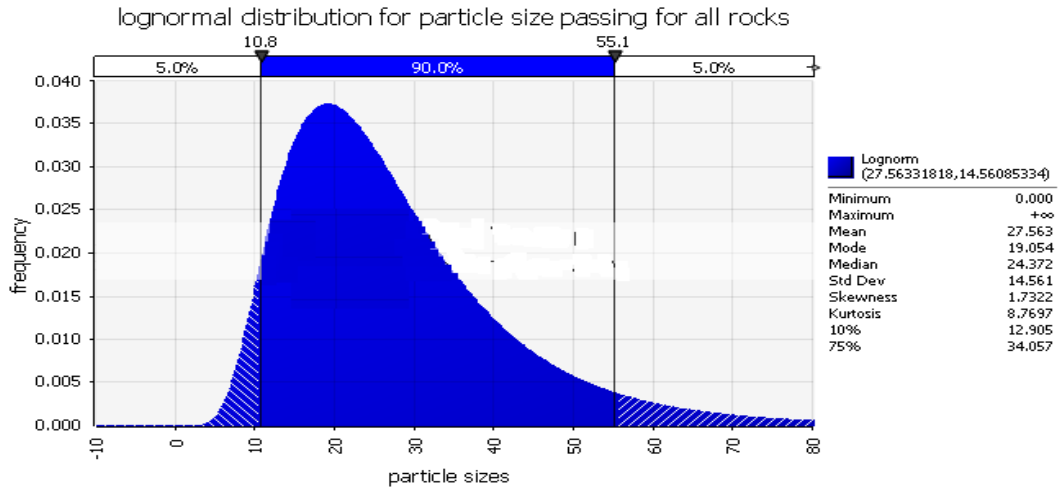

Figure 5.9 The probability density distribution model for the combined sample.

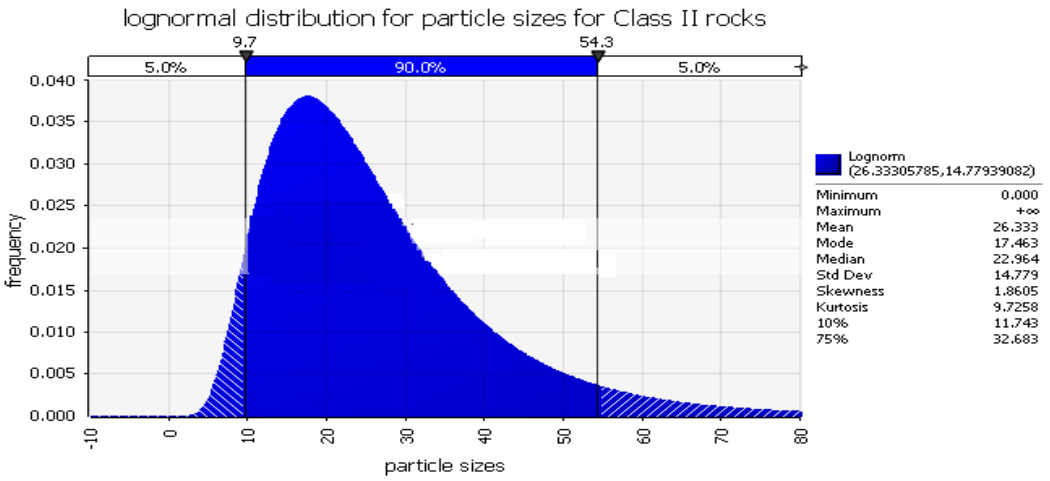

Figure 5.10 The probability density distribution model for the Class II rocks.

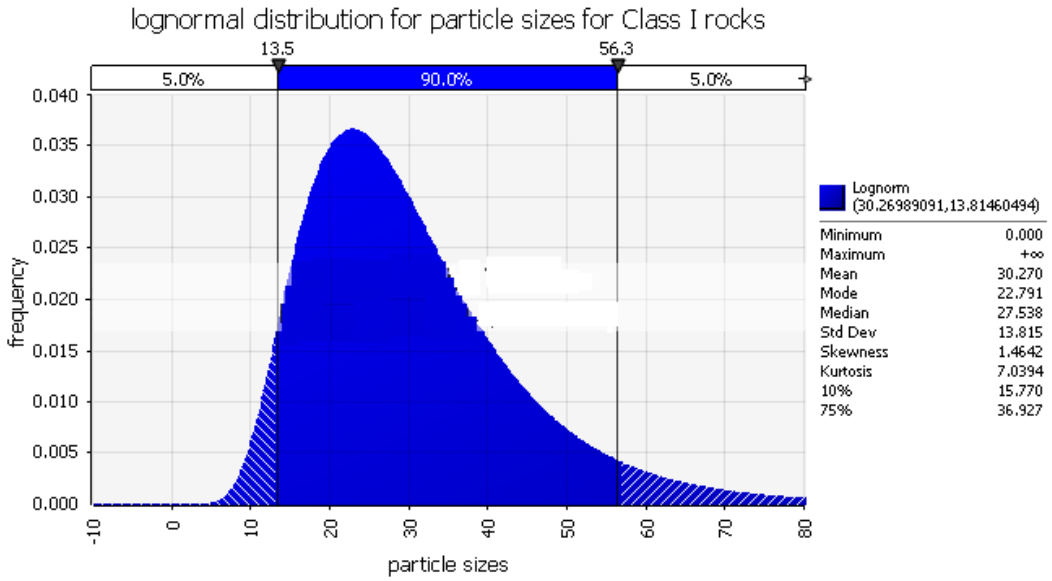

Figure 5.11 The probability density distribution model for the Class I rocks.

Table 5.1 Comparisons of passing sieve size at X_{50s} and X_{10s} for segregated and combined models.

	Combined sample	Class I only	Class II only
X_{10s} (mm)	12.91	15.77	11.74
X_{50s} (mm)	27.56	30.27	26.33

Although the differences are not substantial, this overall view indicates that both the X_{50s} and X_{10s} points are reached at smaller apertures for the Class II rocks than the Class I rocks, therefore the Class II rocks are more finely fragmented.

5.5 Analysis of Fragmentation from Blasting Using Probability Density Distribution Models

Probability density distribution models were constructed to show the difference in the fragmentation of Class I and Class II rocks for the blasting test. The distribution (lognormal distribution) is positively skewed. As expected, the rocks are more finely fragmented for the blasting tests than the compression tests. The distribution becomes more positively skewed with the skewness greater than 5.5 (Figure 5.12) compared with the compression results, with skewness of less than 2.0. The X_{50b} for the combined sample model is 10.954 mm (compared with the compression tests at 27.563 mm) while the X_{10b} is 2.011 mm (compared with compression at 12.905 mm), see Figure 5.12.

The calculated probabilities of the distribution at X_{50b} and X_{10b} for the Class I and Class II rocks are compared. The calculated probabilities of the distribution at X_{50b} and X_{10b} for the segregated models and the combined model are shown in Figures 5.12 to 5.14 and are summarised in Table 5.2. The result shows that the Class II rocks are more fragmented.

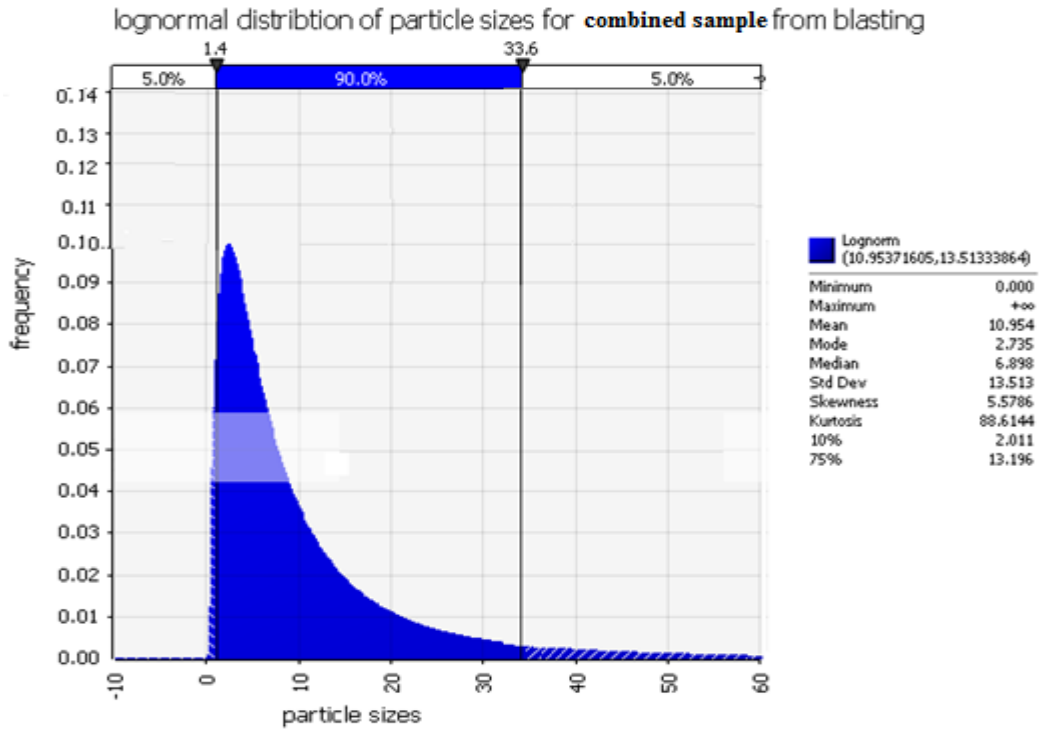

Figure 5.12 The probability density distribution model for the combined sample.

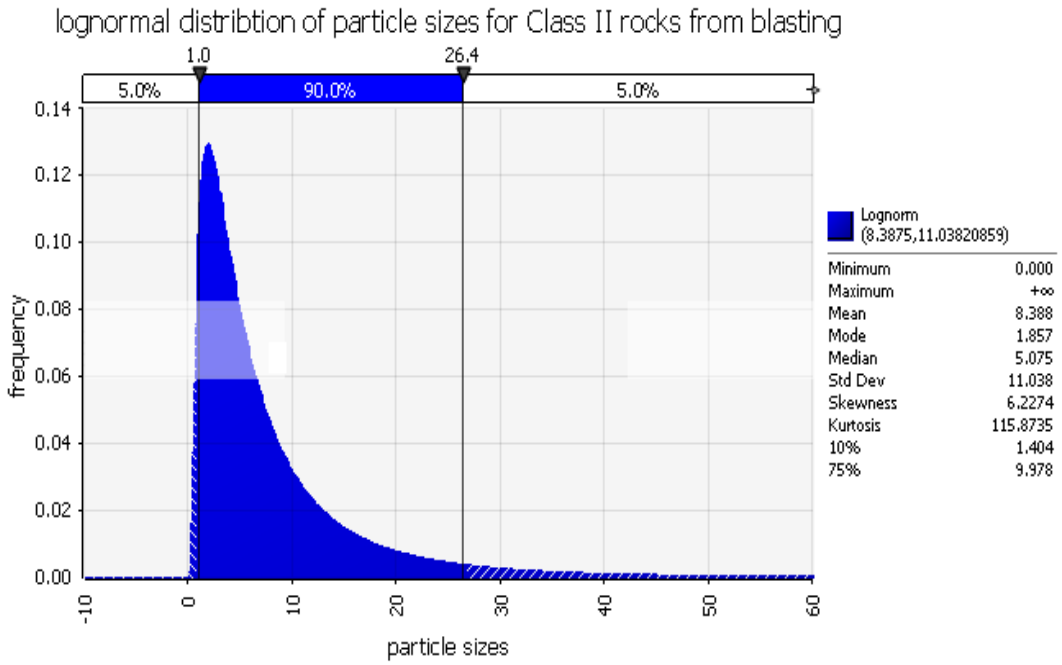

Figure 5.13 The probability density distribution model for the Class II rocks.

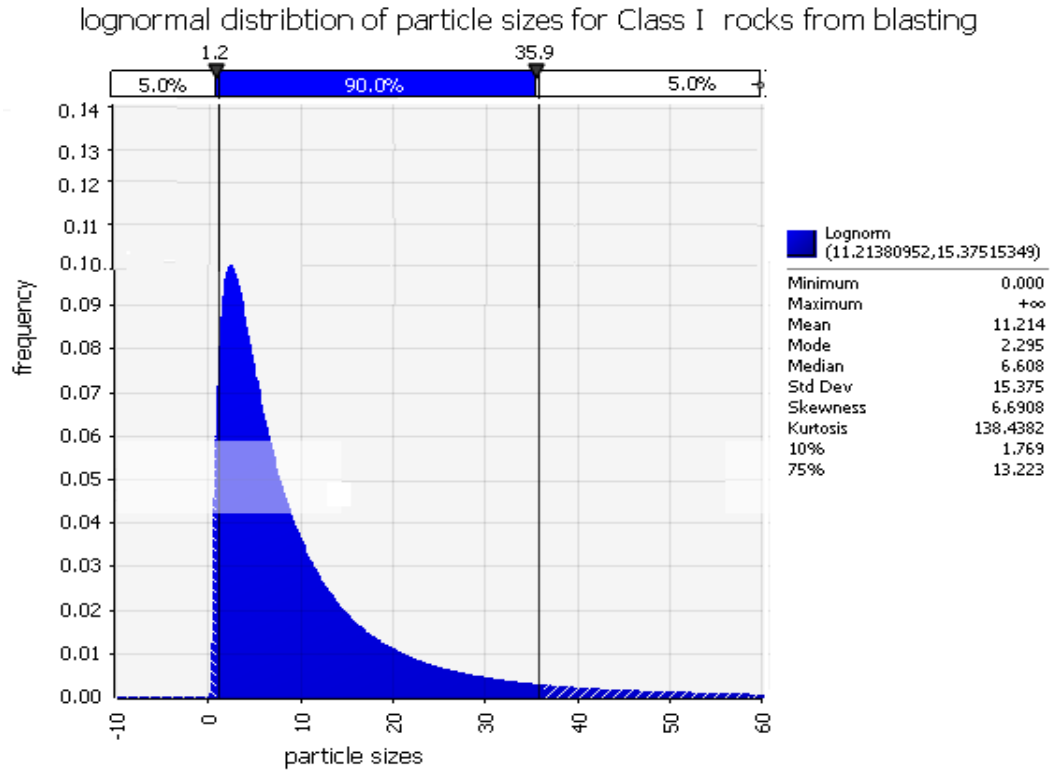

Figure 5.14 The probability density distribution model for the Class I rocks.

Table 5.2 Comparisons of X_{50b} and X_{10b} for the segregated and combined models.

	Combined sample	Class I only	Class II only
X_{10b} (mm)	2.01	1.77	1.40
X_{50b} (mm)	10.95	11.21	8.39

Although the differences is not large, this overall view indicates that both the X_{50b} and X_{10b} points are reached with smaller apertures for the Class II rocks than the Class I rocks, therefore, the Class II rocks are more finely fragmented. It is expected that the X_{10b} for the combined sample would be between the two segregated samples but this is not the case. The reason for this is not clear, but may be due to the nature of the lognormal probability distribution and, of course due to the fact that there were only 2 Class I samples.

5.6 **Assessment of the Relationship of Brittleness Concepts, Rock Parameters and Fragmentation Using Statistical Analysis**

Firstly, to address the aim of the research, that is to show whether a relationship exists between brittleness and fragmentation of rock. The relationship between Fragmentation and brittleness is assessed using statistical analysis. Fragmentation is compared with all the rock properties from mechanical, dynamic and widely used brittleness concepts using multiple regression technique with a statistical

package (SPSS version IBM 18). The first thing is to analyse altogether the relationship of the various brittleness concepts with fragmentation in order to reveal the dependence of fragmentation on the various brittleness concepts. Later a stepwise multiply regression technique is done to screen out potentially interrelated independent brittleness concepts from the model.

Table 5.3 shows the summary of coefficients of correlation of the various properties with fragmentation. From the table dynamic modulus of rigidity and post-failure modulus has the highest correlation and are the most significant parameters from both static mechanical properties and dynamic mechanical properties influencing fragmentation by steady compression. Similarly, brittleness concepts k and k_2 are next to the two properties showing the same correlation coefficients.

Table 5.3 Coefficients of correlation with fragmentation

Model		t	Sig.	Correlation	Collinearity Statistics
					Tolerance
1	B_{11}	-1.520	.226	-.660	.740
	B_{13}	-3.452	.041	-.894	.651
	B_{12}	-1.290	.288	-.597	.761
	B_{14}	-3.491	.040	-.896	.617
	Brazilian Tensile strength	-3.752	.033	-.908	.565
	UCS	-3.112	.053	-.874	.594
	Elastic Modulus (Gpa)	-3.425	.042	-.892	.154
	Strain Energy (kN/mm^2)	-2.077	.129	-.768	.814
	Post. Modulus(Gpa)	-6.038	.009	-.961	.827
	Poison's ratio	2.101	.126	.772	.339
	Mod. Rigidity (Gpa)	-3.527	.039	-.898	.169
	Dynamic Mod. Rigidity (GPa)	28.585	0.000	.998	977
	P waves (us)	2.060	.131	.765	.090
	S waves (us)	1.453	.242	.643	.085
	P wave Velocity (m/s)	-2.484	.089	-.820	.042
	S wave Velocity (m/s)	-.782	.491	-.411	.014
	Dynamic Modulus (GPa)	-1.854	.161	-.731	.003
	Acoustic impedance.(Kg/sm^2)	-3.016	.057	-.867	.051
	B_8	.472	.669	.263	.500
	B_{16}	-5.256	.013	-.950	.791
	B_7	-2.092	.128	-.770	.942
	k	-5.651	.011	-.956	.824
	k_2	-5.650	.011	-.956	.824

Dependent Variable: 0.5

Moreover, Table 5.3 shows that brittleness estimated from rock moduli have higher correlation coefficients, tolerance and are more significant than brittleness estimated from static mechanical properties. Therefore brittleness from rock moduli is used in further analysis..

A further analysis is done in order to establish a relationship that contribute most between brittleness concepts based on moduli and fragmentation since they all show some degree of correlation with fragmentation. From the analysis, the model summary, Table 5.4 shows the coefficient of correlations of various brittleness

concepts from moduli with fragmentation. From the coefficients table brittleness k has the highest value and significant with p<0.5. Brittleness k contributes most to the relationship.

Table 5.4 Correlations

		0.50	Sig. (1-tailed)	
Pearson Correlation	0.50	1.000	0.10	.
	B_8	-.097	B_8	.366
	B_{16}	-.161	B_{16}	.283
	B_7	-.197	B_7	.241
	k	-.929	k	.000
	k_2	-.923	k_2	.000

5.6.1 Stepwise Statistical Analysis of Brittleness k with Fragmentation from Compression

The relationship between fragmentation and brittleness k estimated from the rock moduli are modelled using stepwise multiple regression technique. Stepwise multiple regression technique allows for screening of a number of potentially interrelated independent variables (predictors) to separate those few variables that contribute most to the model. The variables or predictors included in the model are the static mechanical and dynamic properties. Since all these parameters are interconnected or related to fragmentation, the outcome resulted into high multicollinearity problem. It is therefore necessary to lessen data redundancy by removing parameters whose influence are taken over by other parameters. The results of the analyses are shown in Table 5.5 to Table 5.9.

Table 5.5 Model Summary

Model	R	R Square	Adjusted R Square	Std. Error of the Estimate	Change Statistics				
					R Square Change	F Change	df1	df2	Sig. F Change
1	.929a	.863	.852	1.9666885	.863	81.882	1	13	.000
2	.963b	.927	.915	1.4948854	.064	10.501	1	12	.007

a. Predictors: (Constant),

b. Predictors: (Constant), Post. Modulus(GPa)

Table 5.6 ANOVA

Model		Sum of Squares	df	Mean Square	F	Sig.
1	Regression	316.710	1	316.710	81.882	.000a
	Residual	50.282	13	3.868		
	Total	366.992	14			
2	Regression	340.176	2	170.088	76.113	.000b
	Residual	26.816	12	2.235		
	Total	366.992	14			

Table 5.7a Coefficients at 10% passing sieve sizes

Model		Unstandardized Coefficients		Standardized Coefficients	t	Sig.	Correlations			Collinearity Statistics	
		B	Std. Error	Beta			Zero-order	Partial	Part	Tolerance	VIF
1	Constant	.435	.581		.748	.468					
		-1.798	.199	-.929	-9.049	.000	-.929	-.929	-.929	1.000	1.000
2	Constant	-.649	.554		-1.172	.264					
		-2.042	.169	-1.055	-12.097	.000	-.929	-.961	-.944	.800	1.250
	Post. Modulus (GPa)	.017	.005	.283	3.240	.007	-.189	.683	.253	.800	1.250

Table 5.7b Coefficients at 50% passing sieve sizes

Model		Unstandardized Coefficients		Standardized Coefficients	t	Sig.	Correlations		
		B	Std. Error	Beta			Zero-order	Partial	Part
1	(Constant)	28.744	1.180		24.351	.000			
	k	-1.391	.417	-.666	-3.339	.005	-.666	-.666	-.666

a. Dependent Variable: 0.5

Table 5.8 Collinearity Diagnostics

Model	Dimension	Eigenvalue	Condition Index	Variance Proportions		
				(Constant)	(E-M)/M	Post. Modulus (GPa)
1	1	1.486	1.000	.26	.26	
	2	.514	1.701	.74	.74	
2	1	1.616	1.000	.16	.09	.08
	2	1.120	1.201	.00	.26	.29
	3	.264	2.472	.84	.65	.62

Table 5.9 Excluded Variables.

Model	Beta In	t	Sig.	Partial Correlation	Collinearity Statistics		
					Tolerance	VIF	Minimum Tolerance
1. Brazilain Ten. σ_t (MPa)	-.118[a]	-.995	.339	-.276	.744	1.343	.744
UCS (MPa)	-.071[a]	-.555	.589	-.158	.689	1.452	.689
Elastic Modulus (GPa)	-.150[a]	-1.535	.151	-.405	.997	1.003	.997
Strain Energy (kN/mm^2)	.100[a]	.770	.456	.217	.651	1.537	.651
Post. Modulus(GPa)	.283[a]	3.240	.007	.683	.800	1.250	.800
Poison's ratio	.046[a]	.434	.672	.124	.982	1.018	.982
Mod. Rigidity (GPa)	-.159[a]	-1.641	.127	-.428	.996	1.004	.996
P waves (m/s)	.035[a]	.326	.750	.094	.999	1.001	.999
S waves (m/s)	.057[a]	.535	.602	.153	.995	1.005	.995
P wave Velocity (m/s)	-.100[a]	-.969	.352	-.269	.993	1.007	.993
S wave Velocity (m/s)	-.145[a]	-1.452	.172	-.387	.977	1.023	.977
Dynamic Modulus (GPa)	-.184[a]	-1.958	.074	-.492	.980	1.021	.980
Dyn. Mod. Rigidity (Gpa)	-.200[a]	-2.180	.050	-.533	.974	1.027	.974
Acost. Imp.(Kg/sm^2)	-.138[a]	-1.386	.191	-.371	.993	1.007	.993
2. Brazilain Ten. σ_t (MPa)	-.152[b]	-1.822	.096	-.482	.736	1.359	.651
UCS (MPa)	-.110[b]	-1.175	.265	-.334	.678	1.474	.614
Elastic Modulus (GPa)	-.123[b]	-1.677	.122	-.451	.984	1.016	.789
Strain Energy (kN/mm^2)	.012[b]	.116	.910	.035	.599	1.669	.599
Poison's ratio	.064[b]	.800	.441	.234	.977	1.023	.793
Mod. Rigidity (GPa)	-.129[b]	-1.783	.102	-.474	.981	1.019	.787
P waves (m/s)	.054[b]	.669	.517	.198	.993	1.007	.796
S waves (m/s)	.067[b]	.850	.414	.248	.993	1.007	.794
P wave Velocity (m/s)	-.084[b]	-1.075	.305	-.308	.989	1.011	.796
S wave Velocity (m/s)	-.115[b]	-1.527	.155	-.418	.963	1.039	.788
Dynamic Modulus (GPa)	-.139[b]	-1.908	.083	-.499	.941	1.062	.769
Dyn. Mod. Rigidity (Gpa)	-.152[b]	-2.150	.055	-.544	.930	1.075	.764
Acost. Imp.(Kg/sm^2)	-.111[b]	-1.484	.166	-.408	.981	1.019	.790

a. Predictors in the Model: (Constant),

b. Predictors in the Model: (Constant), Post. Modulus (GPa)

The model summary is shown in Table 5.5. It reports the strength of the relationship between the model and the dependent variable. The multiple correlation coefficients are the linear correlation between the observed and model-predicted values of the dependent variable. Its large value indicates a strong relationship. The coefficient of determination, R^2 is the square value of the multiple correlation coefficients. The adjusted R-squared compensates for model complexity to provide a fairer comparison of model performance. Table 5.5 shows that 86.3% of the variation in fragmentation is explained by model 1 with brittleness *k* as the predictor. As a further measure of the strength of the model, the standard error of the estimation in the model is important. From the summary table, the standard error of estimation is 1.967.

However, the model could perform better. To know which predictor could improve the model, the second stage involves the analysis of the input parameters or predictors in Table 5.9, Model 1. The remaining predictors are analysed to determine which, if any, is the most suitable for inclusion at the next step. To choose the best variable to add to the model, the values of partial correlation of the predictors are considered. The partial correlation is the linear correlation between the proposed predictor and the dependent variable after removing the effect of the current model. Thus, post-failure modulus is chosen statistically as the next parameter that improves the model because it has the highest correlation of 0.683 (Table 5.9). Also the significant values are considered, which must be less than 0.05; for post-failure modulus its value is 0.007. The remaining predictors are not fit to be included in the model except for dynamic modulus of

rigidity, which is on the border line of the cut-off (0.05), but has the smallest t-statistic of less than -2.

Another vital parameter to consider is the t-statistic. From Table 5.9, post-failure modulus has the highest t-value of 3.240, so fit for inclusion in the next model. Beta In is the value of the standardized coefficient for the predictor, if it is included next in the model. After the inclusion of post-failure modulus into the model, the remaining predictors have significant values greater than 0.05. As a result, none of the remaining predictors could improve the model if included, as they are all insignificant. The inclusion of post-failure modulus improves the second model, which accounted for variability of the outcome of about 92%. The standard error of estimation also becomes lower. The residual, which is the difference between the observed and model-predicted values of the dependent variable, also becomes smaller (Table 5.6).

Table 5.6, the ANOVA table, test the suitability of the model from a statistical point of view. The regression row displays information about the variation that is accounted for by the model. The residual row displays information about the variation that is not accounted for by the model. For the first model, the regression sums of squares are approximately six times residual. This indicates that over 86% of the variation in fragmentation by steady compression is explained by model1. The significance value of the F statistic is less than 0.05, which means that the variation explained by the model is not due to chance (pb< 0.001). The F statistic is significant (<0.001), and the residual sum of squares, which is the difference between the model and the observed data, becomes lower. This implies

that the second model now accounts for more of the residual values. The result shows that the new model 2 with the extra predictor, post-failure modulus, improves its ability.

Table 5.7a and 5.7b are the coefficients of correlations. The values of the correlations of the predictors rise sharply from the zero-order correlation. This means, for example, that much of the variance in the predictors cannot be explained by other variables. The tolerance is the percentages of the variance in a given predictor that cannot be explained by the other predictors. Thus, the high tolerance shows that 80% of the variance in a given predictor cannot be explained by the other predictors. Statistically, variance inflation factor (VIF) greater than 2 is usually considered problematic, however none of the predictors' values are up to 2.

Table 7.5a and 7.5b show the correlation of fragmentation by steady compression at X_{10s} and X_{50s} with brittleness k of the rocks. From the tables, the relationship between fragmentation by steady compression at X_{10s} and X_{50s} with brittleness k can be expressed as given by Eqn. 5.1 and 5.2.

$$X_{10s} = -1.798k + 0.435 \tag{5.1}$$

$$X_{50s} = -1.391k + 28.744 \tag{5.2}$$

The collinearity diagnostics (Table 5.8) confirm that there is no problem with multicollinearity. The Eigen values are greater than zero, indicating that the predictors are not intercorrelated. Condition index values greater than 15 indicate a possible problem with collinearity and greater than 30, a serious problem. None

of the condition indices is larger than 30, suggesting no problem with collinearity. There are no Eigen values close to zero, and all of the condition indices are much lesser than 15. Therefore, from the statistical point of view, the fragmentation of a rock under steady compression is related to its brittleness. It depends more on brittleness k and improve with the post-failure modulus of the rock for the combined rock sample.

5.7 Fragmentation Produced During Uniaxial Compression Tests and Rock Properties

The statistical analysis shows that fragmentation from compression test relate to the rock strength and their dynamic properties. However, the relationship depends more on post-failure modulus of the rocks. The Brazilian tensile strength, elastic modulus and the dynamic properties show close to average correlation with fragmentation. These relationships are further investigated by comparing the individual rock properties with the fragmentation. The comparisons are done at X_{50s} and X_{10s} respectively. These analyses are compared for the combined and the segregated samples.

5.7.1 Comparison of Fragmentation from Compression and Static Mechanical Properties

The static mechanical properties investigated include UCS, Brazilian tensile strength (BTS) and elastic modulus (E). The relevance of the analysis is to show the effect of static mechanical properties on fragmentation, because a number of definitions of brittleness are based on static mechanical properties.

The strength parameters poorly correlated with the combined sample and Class I rocks at both X_{50s} and X_{10s} percentage passing (see Appendix 3.1). However, they are more closely correlated with the Class II rocks as a group (Figure 5.15 to Figure 5.17). The correlation was stronger at both X_{50s} and X_{10s} for elastic modulus than shown for both UCS and BTS (Figure 5.15 to 17). The correlations improve at finer fragments size (X_{10s}).

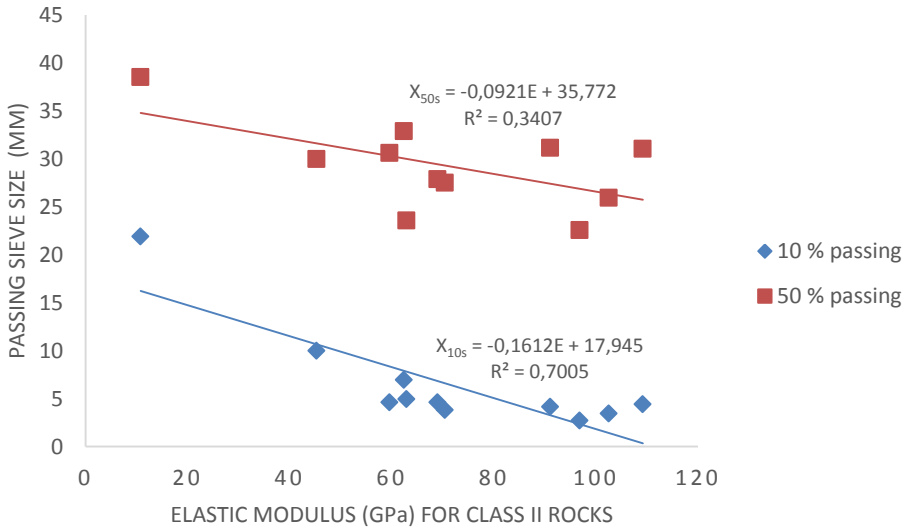

Figure 5.15 Elastic modulus and passing sieve size at X_{50s} and X_{10s} for Class II rocks

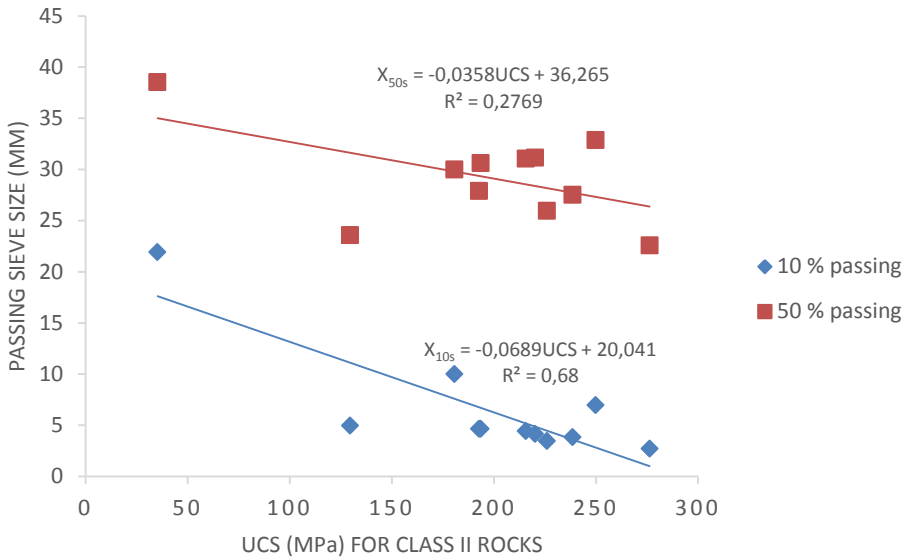

Figure 5.16 UCS and passing sieve size at X_{50s} and X_{10s} for Class II rocks

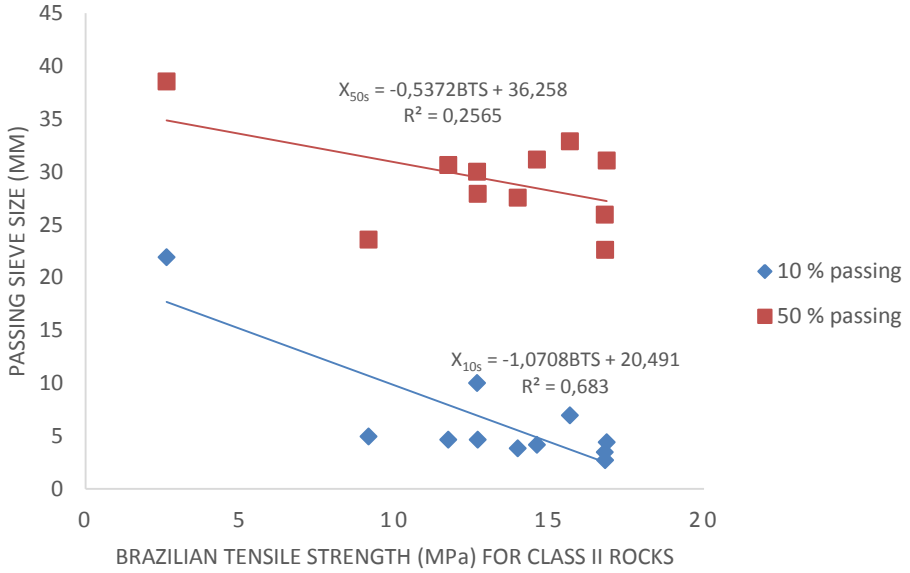

Figure 5.17 BTS and passing sieve size at X_{50s} and X_{10s} for Class II rocks

The graphs show that increase in rock strength increases the degree of fragmentation for the Class II rocks but the same cannot be said for the Class I rocks. This in a sense qualifies the self-fracturing behaviour of the Class II rocks. Fragmentation of high strength rock is explosive at the point of failure. The stored elastic strain energy increases with rock strength and is made available at failure stress to shatter the rock.

5.7.2 Fragmentation from Compression and Dynamic Properties

Similar to strength parameters, the P-wave velocity shows that fragmentation from compression test correlates better with the Class II rocks (Figure 5.18). It may be argued that as the dynamic properties of rocks increases, the fragmentation becomes finer for Class II rocks but the same cannot be said for Class I rocks. The P-wave velocity shows good correlation coefficients of 0.558 and 0.810 at both X_{50s} and X_{10s} for the Class II rocks. This may also qualify the self-fracturing behaviour of the Class II rocks.

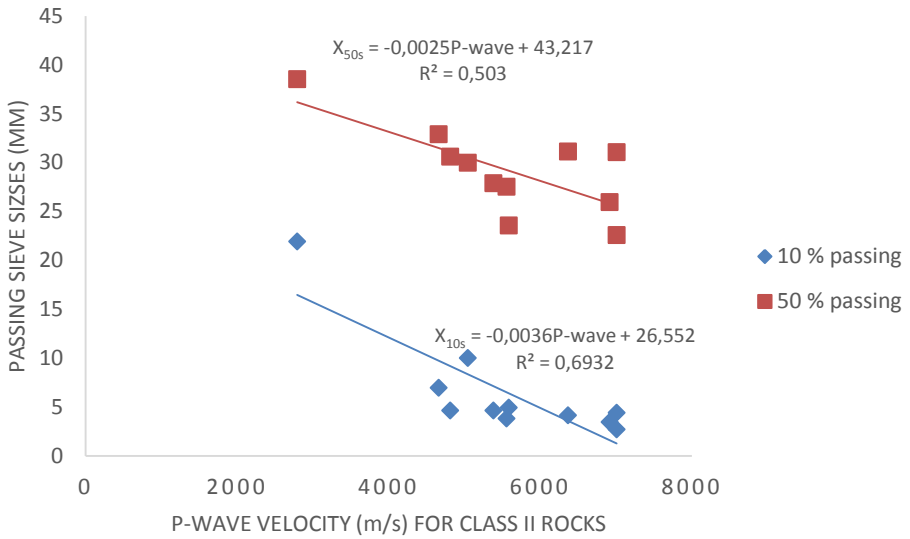

Figure 5.18 P-wave velocity (m/s) against X_{50s} and X_{10s} for Class II rocks

5.8 Fragmentation and Brittleness According to Selected Definitions

Fragmentation is compared with the brittleness indices based on static mechanical properties and moduli of the rocks. The comparisons are done again for X_{50s} and $X_{10s.}$ These comparisons are done for the combined sample, Class I and Class II rocks for each of the brittleness concepts.

5.8.1 Fragmentation and Brittleness Based on Static Mechanical Properties

The relevance of the analysis is to show the relationship between rock brittleness estimated from the concept and fragmentation. It was indicated in Section 5.8.1 that there are certain correlations between individual rock characteristics and fragmentation from compression, and this will evaluate a possible relationship with the combined characteristics.

As shown in Chapter 2 in Section 2.6.1, brittleness B_{13} and B_{14} are defined as:

$$B_{13} = (\sigma_c \times \sigma_t)/2 \quad (5.3)$$

$$B_{14} = (\sigma_c \times \sigma_t)^{0.72} \quad (5.4)$$

Figures 5.19 to 5.20 show the relationship between the brittleness B_{13} and B_{14} with fragmentation at X_{50s} and X_{10s}. Brittleness B_{14} appears to correlate with the post-failure modulus of the Class II rocks but poorly correlated with that of Class I rocks (Figure 5.21). Therefore, B_{14} appears to be related with the post-failure modulus of the rocks. Thus, could be used to quantify brittleness for Class II rocks.

B_{13} and B_{14} show correlation with fragmentation from compression while other concepts based on static mechanical properties are poorly correlated (Appendix 3.2). The correlations show there is a link between brittleness and fragmentation. Brittleness B_{13} and B_{14} show better correlation with fragments size at both X_{50s} and X_{10s} for Class II rocks while the other brittleness concepts did not correlate with either X_{50s} or X_{10s} for the combined samples and Class I rocks. In addition, fragmentation becomes finer with increase in the brittleness B_{13} and B_{14} at lower percentage passing for the Class II rocks. The relationship shows that as the brittleness indices increases, fragmentation becomes finer at both X_{50s} and X_{10s} for the Class II rocks but the same cannot be said for the Class I. It may be stated that at higher brittleness, fragments size becomes finer for the Class II rocks under compressive failure.

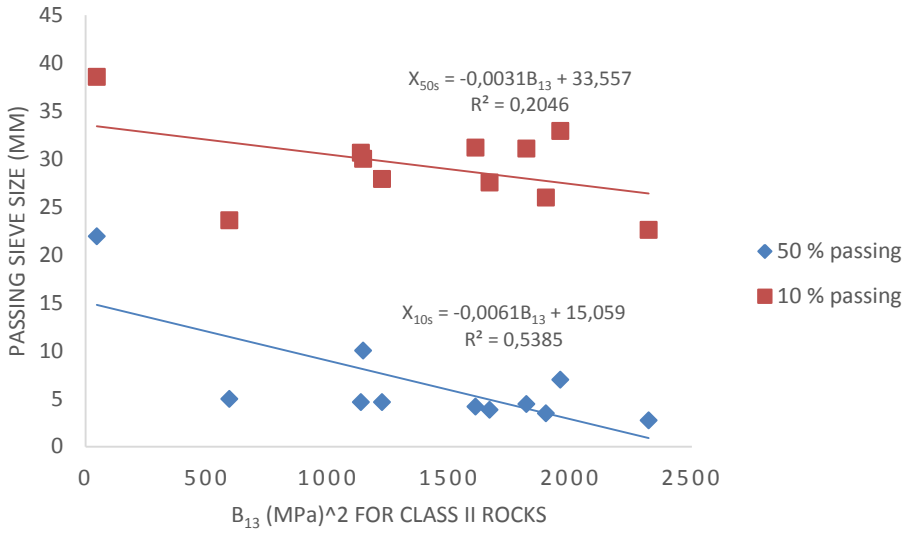

Figure 5.19 B_{13} (MPa)^2 against X_{50} and X_{10} for Class II rocks

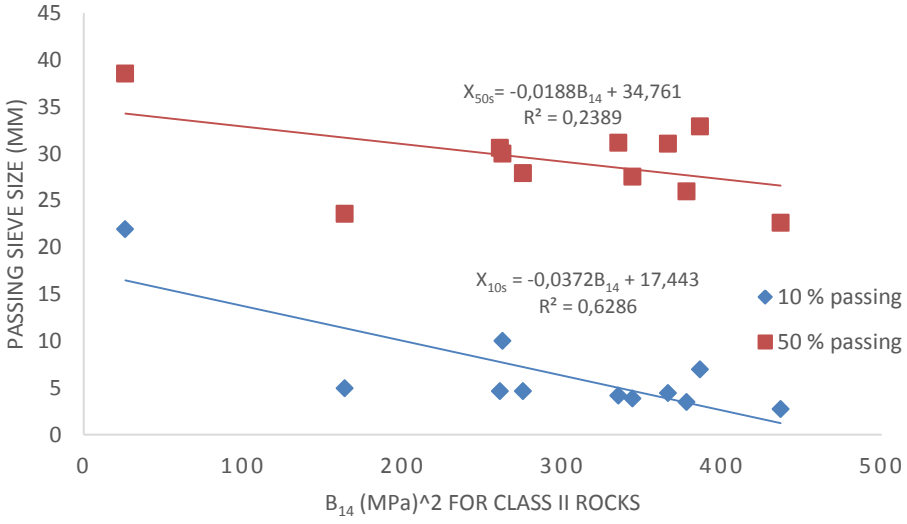

Figure 5.20 B_{14} (MPa)^2 against X_{50} and X_{10} for Class II rocks

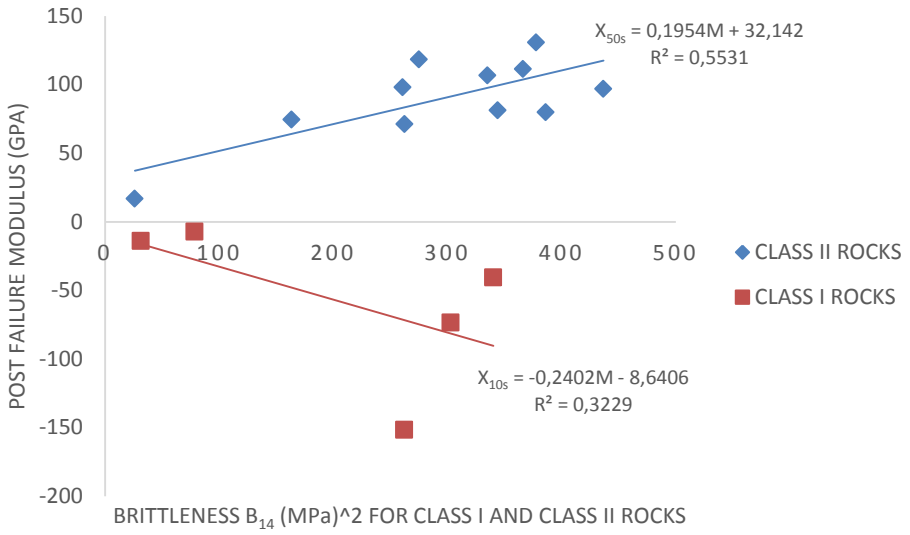

Figure 5.21 B_{13} (MPa)^2 against post-failure modulus for Class I and Class II rocks

5.8.2 Fragmentation and Brittleness Based on Moduli

The statistical analysis shows that fragmentation by compressive failure depends on brittleness k and on the post-failure modulus of the rocks. In addition, B_{16} was shown to correlate with fragmentation from compression. It was also indicated previously, that rocks with positive post-failure modulus or the Class II rocks, have a self-fracturing behaviour thereby enhancing fragmentation during compressive failure. This section will evaluate the relationships between the combined characteristic of the pre- and post-failure moduli with fragmentation. The significance of the analysis is to show the effect of rock brittleness indices based on rock moduli ratios on fragmentation.

As shown in Chapter 2 in Section 2.6.1, brittleness B_{16} is defined as:

$$B_{16} = EM \tag{5.5}$$

With Equation 5.5, B_{16} will always be negative for Class I rocks and positive for Class II rocks. Brittleness B_{16} is weakly correlated with fragmentation of the combined sample but shows correlation with the Class I rocks for the compression tests at both X_{50s} and $X_{10s.}$ It also correlated with the Class II rocks but shows stronger correlation at X_{10s} (Figure 5.22 and 5.23). Therefore it may be said that B_{16} correlated with both rock classes at both X_{50s} and $X_{10s.}$ The relationship shows that the higher the value of brittleness B_{16}, the more finely fragmented the Class II rocks. The same cannot be said for the Class I rocks.

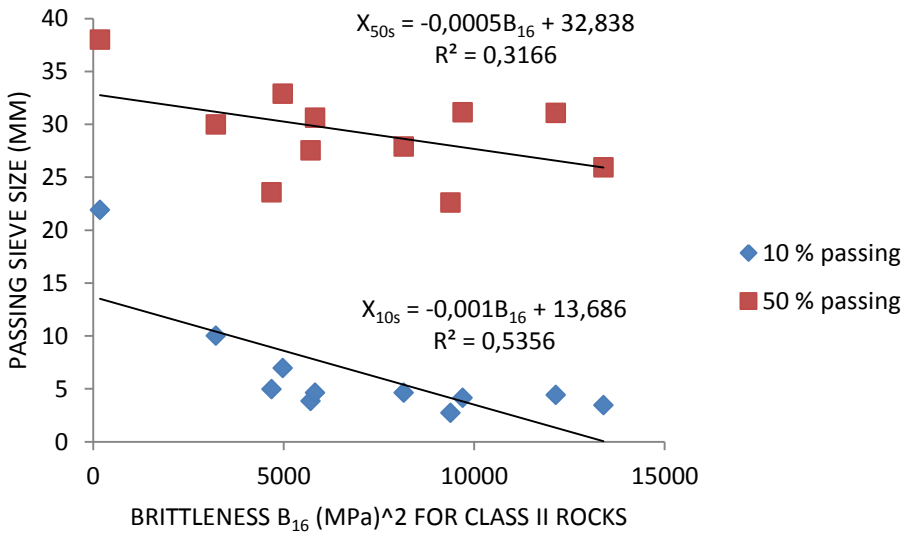

Figure 5.22 B_{16} (GPa)^2 against passing sieve size for Class II rocks

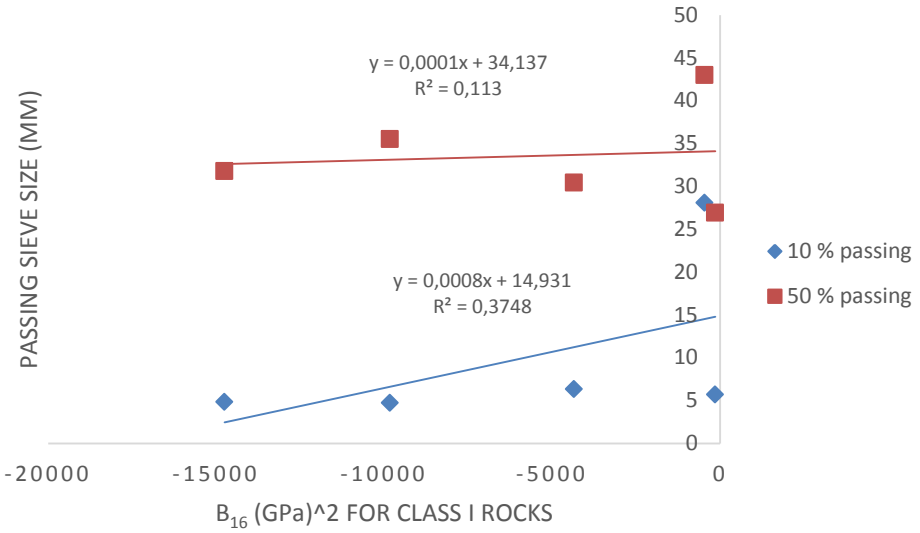

Figure 5.23 B_{16} (GPa)^2 against passing sieve size for Class I rocks

As shown in Chapter 2 in Section 2.6.5, brittleness k is defined as:

$$k = \frac{E - M}{M} \tag{5.6}$$

Note that since the magnitude (i.e. absolute magnitude) of M will always be greater than the magnitude of E, k is always < 0 for both Class I and Class II rocks. Brittleness k correlates with fragmentation for the combined sample and the Class I rocks for compression test at both X_{50s} and X_{10s} (Figures 5.24 to 5.25). However, it shows weaker correlation with the Class II rocks. The higher correlation with the combined sample and Class I rocks are due to the outlier nature of Marble data.

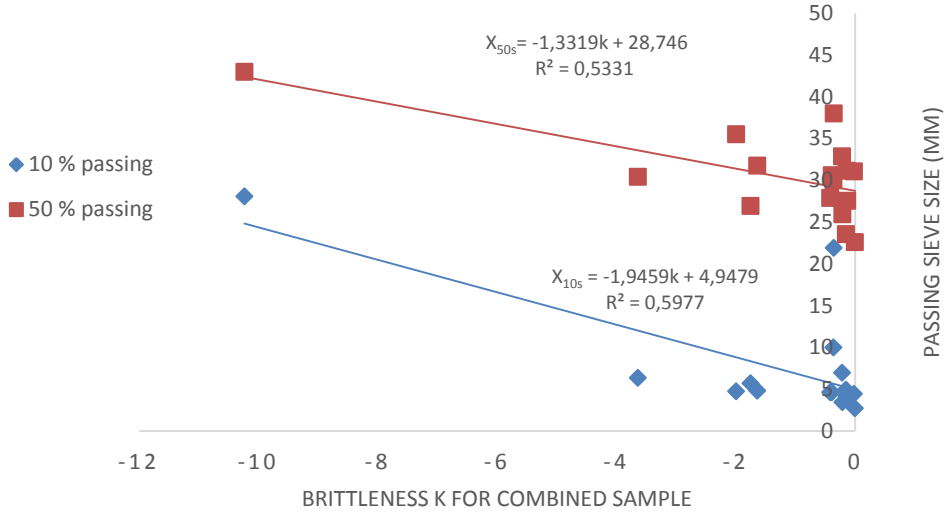

Figure 5.24 Brittleness *k* against passing sieve size for combined sample

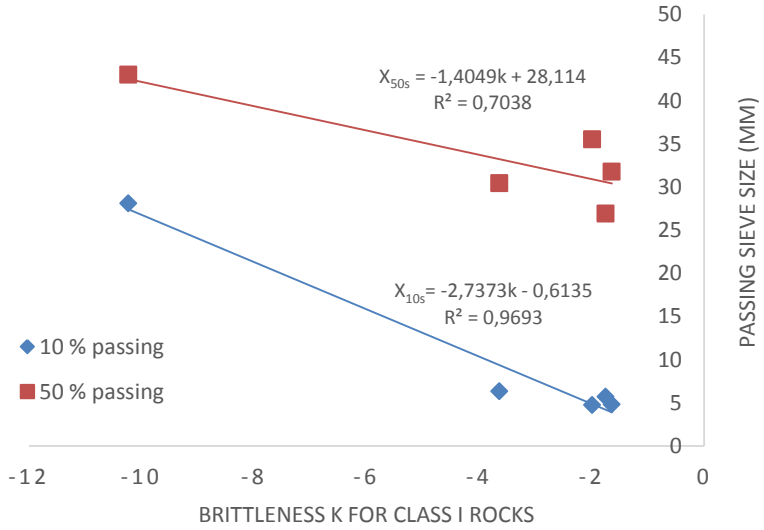

Figure 5.25 Brittleness *k* against passing sieve size for Class I rocks

As shown in Chapter 2 in Section 2.6.5, brittleness k_2 is defined as:

$$k_2 = \frac{E}{M} \tag{5.7}$$

Class I rocks will always have negative k_2 and Class II positive k_2. Brittleness k_2 shows correlation with fragmentation at both X_{50s} and X_{10s}. It correlated with the combined sample and Class I rocks. However, show weaker correlation with the Class II rocks at both X_{50s} and X_{10s}. The correlation coefficients may be misleading because of the outlying nature of Marble data, Figures 5.26 and 5.27. Brittleness k and k_2 show similar relationship with fragmentation from compression and appears to be plotting two points data for both combined sample and the Class I rocks. They may not be reliable concepts to evaluate brittleness of rock for the segregated samples.

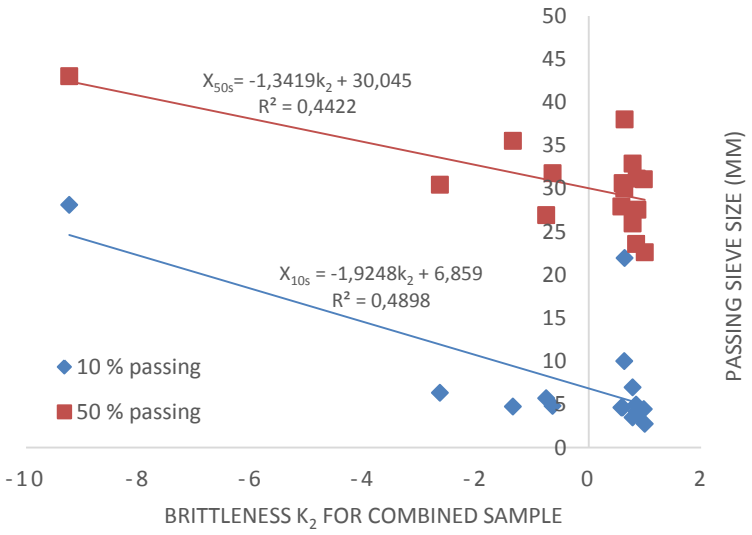

Figure 5.26 Brittleness k_2 against passing sieve size for combined sample

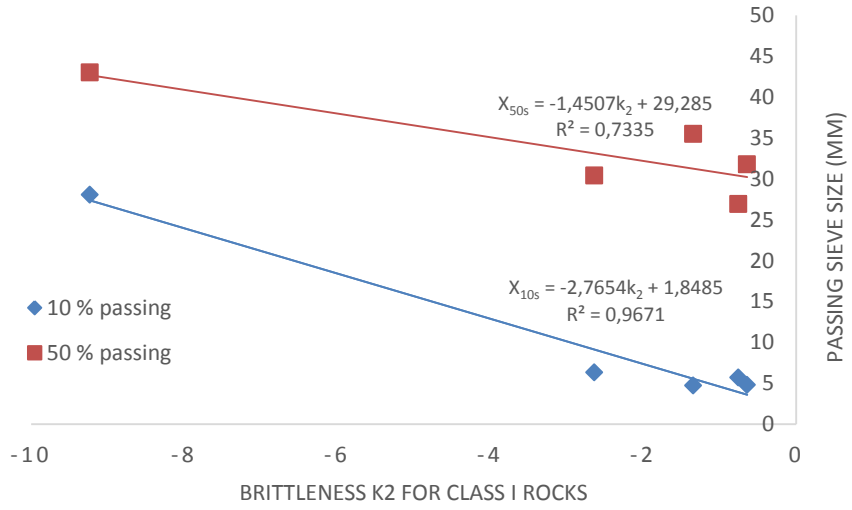

Figure 5.27 Brittleness k_2 against passing sieve size for Class I rocks

Little reliance can be placed on the observed trends in the concepts due to generally low correlation coefficients, despite the fact that some are actually high. However, brittleness k as shown with the statistical analysis could be useful for fragmentation prediction for the combined sample under compressive failure. Brittleness B_{16} could be alternative index for the evaluation of the segregated samples (Class I and Class II), although the correlations are not strong.

5.9 Interim Summary

Probability density distribution models were constructed to show the overall view in the difference between Class II and Class I fragments size. The calculated probability of the distribution at X_{50} and X_{10} (for both blasting and compression) show that the Class II rocks as a group are more fragmented. It can therefore be stated that by breaking rocks under the same steady loading conditions, the Class

II rocks tend to be more fragmented than the Class I. However, the differences are not substantial.

The fragments size produced from failed specimens during uniaxial compression tests were examined by plotting the sieves size against the cumulative percentage passing at both X_{50s} and X_{10s}. In addition, the sieves size passing at X_{50s} and X_{10s} for rocks of similar strength for the Class I and Class II were compared. The analysis show that by breaking rocks under the same loading conditions, the Class II rocks tends to be more fragmented than the Class I rocks of similar strength.

From statistical point of view, the fragmentation of a rock under steady compression depends on brittleness *k* and improve with the post-failure modulus of the rock. Therefore brittleness *k* with post-failure modulus could be a useful index for the prediction of fragmentation for combined sample under compressive failure. The statistical analysis also show that fragmentation is related to rocks properties and brittleness of the rocks.

5.9.1 Comparison of Fragmentation with Static Mechanical Properties

The relationships of static mechanical properties with fragmentation show an inverse relationship, meaning that the higher the property value the finer the fragmentation. The correlation appears stronger for the Class II rocks and also at X_{10s}.

The analysis shows that an increase in rock strength advances fragmentation, and the fragmentation of high strength rock is explosive at failure for the Class II rocks. The stored elastic strain energy increases with rock strength and is made

available at failure stress to shatter the rock. Thus, as the energy increases, the degree of fragmentation also increases. This is in support of Whittles et al. (2006) that increase in the energy needed for breakage increases the degree of fragmentation of the samples. This may qualify the self-fracturing nature of Class II rocks.

5.9.2 Comparison of Fragmentation with Dynamic Properties

From the investigation of the dynamic properties, it shows that fragmentation from compression tests only correlate with the Class II rocks and with an inverse relationship as shown with the rock strengths. It can be suggested that as the dynamic properties of rock increases, the fragments size become finer for the Class II rocks but the same cannot be said for Class I rocks. This may also qualify the self-fracturing nature of Class II rocks.

5.9.3 Correlation of Fragmentation with Brittleness Based on Static Mechanical Properties

The correlations show that there is a link between brittleness and fragmentation. Brittleness B_{13} and B_{14} correlated more with fragmentation for the Class II rocks from compression than other concepts based on static mechanical properties. The correlation becomes stronger at X_{10s}. In addition, fragmentation becomes finer with an increase in brittleness of B_{13} and B_{14} for the Class II rocks. It can be stated that the higher the brittleness, the finer the fragmentation under compressive failure especially for the Class II rocks. Brittleness B_{14} showed relationship with

post-failure modulus of the rocks. Therefore, B_{14} could be a useful index for predicting fragmentation of Class II rocks.

5.9.4 Correlation of Fragmentation with Brittleness Based on Moduli

Little reliance can be placed on the observed trends in the concepts due to low correlation coefficients. Brittleness k and k_2 have similar relationship with fragmentation and appear consistent in correlation with the combined sample and Class I rocks at both X_{50s} and X_{10s}.

On the other hand, B_{16} show fairly good correlation with the segregated samples but more correlated with the Class II rocks. The relationship between B_{16} and fragmentation show that, as the rock brittleness increases fragmentation becomes finer. Therefore B_{16} could be useful index for the prediction of fragmentation for the segregated samples, since it's a direct measure of the post-failure modulus of the rocks.

5.10 Introducing a New Brittleness Concept Based on the Normalised Stress-Axial Strain Curve

Little reliance can be placed on the observed trends in the brittleness concepts based on the static mechanical properties and moduli in their relationship with fragmentation, due to low correlation coefficients, although some are high and appear reasonably good.

However, extraction from the normalised stress-axial strain curves in Section 4.6 Chapter 4 could be useful index of brittleness. As indicated in the section, there

are three types in the deformation process of the rocks. The first type included both Class I and Class II rocks while the second type are entirely Class II rocks. The rock class to which the third type belong could not be determined.

The normalised stress-axial strain curve reveal that the steeper the slope, the more stiff the rocks. Therefore the stiffness might somehow relate with the brittleness of the rock. This is illustrated in Figure 5.28. In the figure, 1 is stiffer than 2 and 2 stiffer than 3. The opposite therefore will be, how soft or brittle the rock is. Thus, the slope of normalised stress-axial strain curve could be useful to evaluate rock brittleness. A brittleness concept based on normalised stress-axial strain curve (NSSC) is proposed for evaluation of brittleness under compressive failure. NSSC is calculated at 70% to 30% of normalised stress. The brittleness based on normalised stress-axial strain curve (designated as NSSC) is expressed in Equation 5.8. This can be defined as the axial strain per unit normalised stress in the direction of application of the stress.

$$\text{NSSC} = axialstrain \big/ normalisedstress = \Delta\varepsilon_a \big/ \Delta n\sigma \tag{5.8}$$

An example of how the NSSC is calculated is shown for Spotted Anorthosite which is Class I using Figure 5.29

$$\text{Spotted Anortosite} = 0.00145 - 0.000581 \big/ 0.700176 - 0.300222 = 0.00217275$$

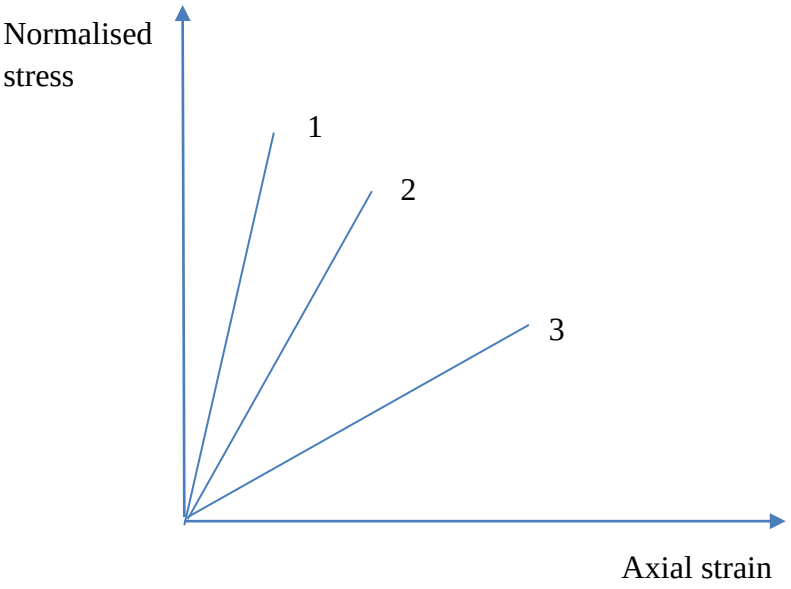

Figure 5.28 Normalised stress-axial strain curve showing rock stiffness

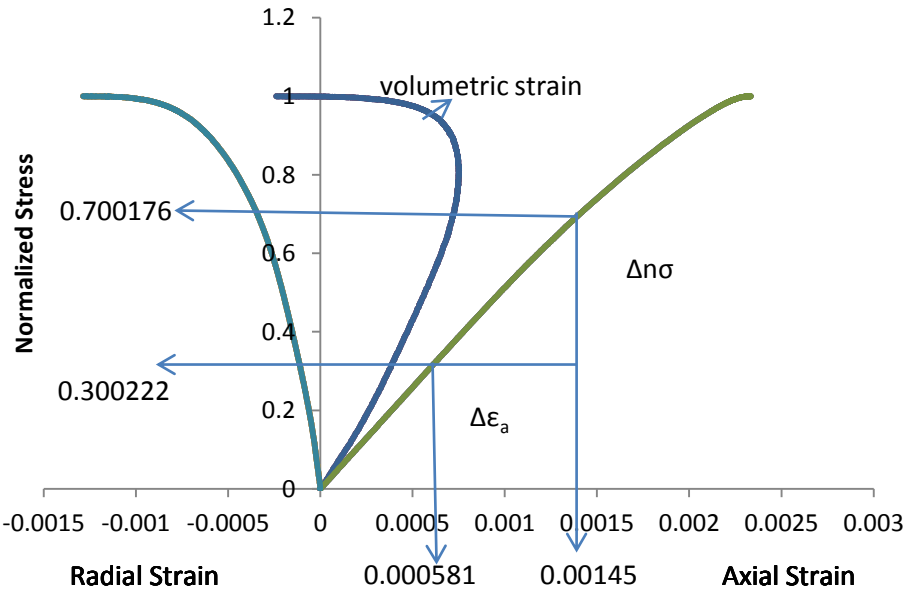

Figure 5.29 NSSC Estimation for Spotted Anorthosite

Brittleness designated as NSSC is compared with the fragmentation from compression for both the combined and the segregated samples. NSSC did not correlate with the fragmentation of the combined sample but shows comparably good correlation with the segregated samples (Appendix 3.4, Figure 5.30 and 5.31). NSSC shows better correlation with the segregated samples (X_{10s} and X_{50s}) than shown for brittleness estimated from both static mechanical properties and moduli. Brittleness NSSC appears treating Class I and Class II rocks as a separate entity that occupies different spaces and arrays. The relationship shows that as the value of NSSC increases, fragmentation become coarser for the Class II rocks, the opposite is shown for Class I rocks. These relationships are opposite to what was shown for B_{16}. Brittleness NSSC could be a good brittleness concept for the prediction of fragmentation under compressive failure for the segregated samples (Class I and Class II) at both X_{10s} and X_{50s}.

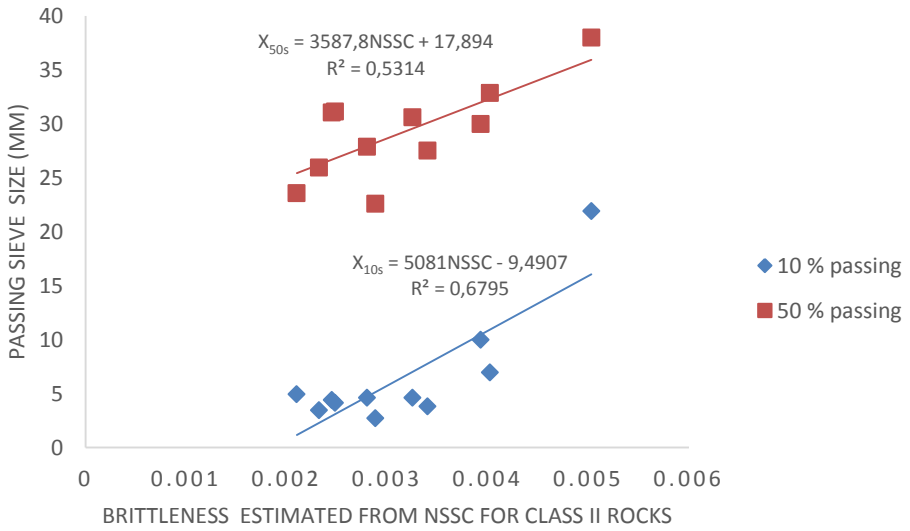

Figure 5.30 NSSC and passing sieve size for Class II rocks

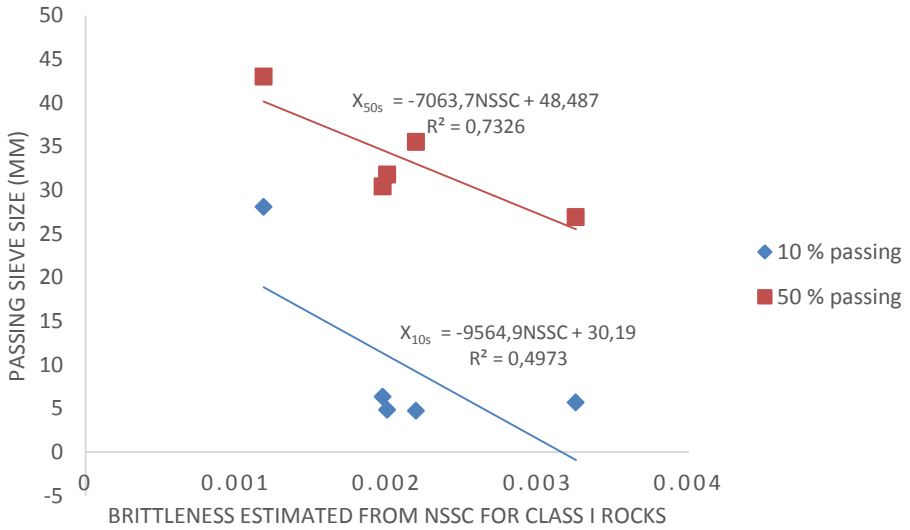

Figure 5.31 NSSC and passing sieve size for Class I rocks

5.11 **Fragmentation from Compression and Brittleness Estimated from Extension Strain Criterion**

Alternative forms of stress-strain behaviour for deformation process of rock after the peak strength are shown in Figure 5.32. The elastic-perfectly plastic may be suitable for week and plastic rock type. An elastic-perfectly plastic constitutive law include the effect of plastic straining, but is hardly appropriate for brittle rock because the obvious material weakening is ignored (Hajiabdolmajid et al., 2002).

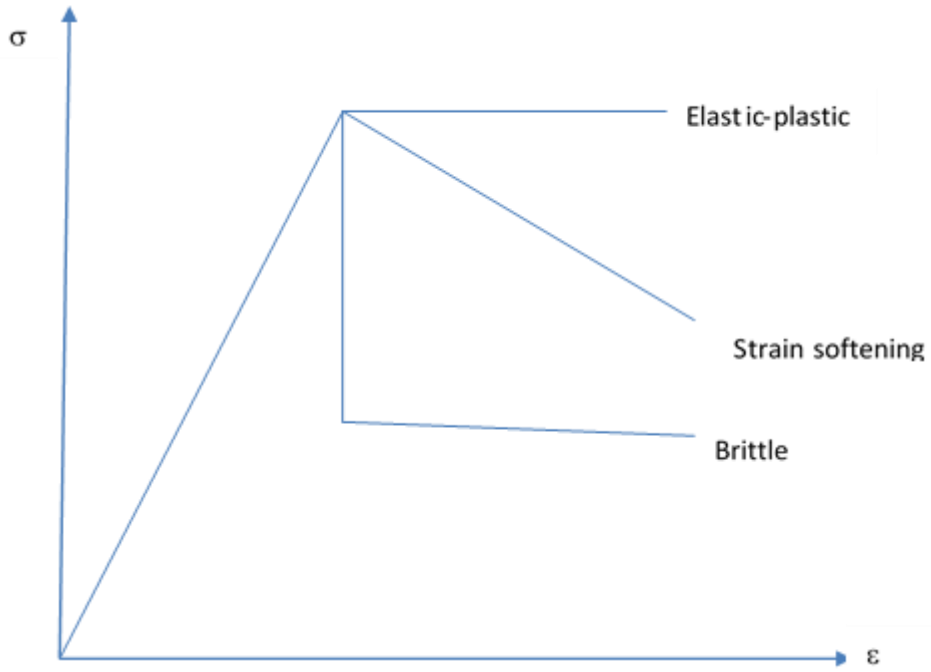

Figure 5.32 Different stress-strain behaviours

For most rocks, stress will drop after the peak load is reached i.e. a strain softening behaviour. For rocks, strength weakening seems more appropriate than strain softening because softening refers to reduction of rock stiffness (Cai et al., 2007). Alternative approach is the cohesion weakening and frictional strengthening. This approach assumed that the rock is initially cohesive and that, as failure start to take place the cohesion breaks down, and the frictional strength build up with increase in plastic strain, (see Figure 2.37 in Section 2.6.1). It may be suitable for evaluating brittleness of rock, however the problem with it, is that it is based on shear stress.

One has to choose an analysis or a constitutive relation that represents the behaviour of the rock under the test condition. An empirical criterion for fracture initiation in brittle rock under laboratory compressive failure can be appropriate

for determining brittle behaviour of rock. “Fracture of brittle rock will initiate when the total extension strain in the rock exceeds a critical value which is characteristic of that rock type” (Stacey, 1981, p471). This empirical criterion is termed extension strain criterion for brittle rock. Fracture initiates when:

$$e \geq e_c \tag{5.9}$$

Where, e_c is the critical value of extension strain.

Damage is induced in rock when it is stressed beyond a certain damage initiation threshold (crack initiation). The critical value of the extension strain is obtained from laboratory test by plotting axial strain against the lateral strain. The point of inflection coincides with the damage/crack initiation threshold (Figure 5. 33). Crack propagation and shattering of the specimen results when a critical stress value is exceeded at the crack tip. The propagation of cracks occurs at the point of reversal or inflection of the axial-lateral strains curve.

The critical extension strain is not affected by the confining pressure (Stacey, 1981; Fujii et al., 1998, p552). This makes it suitable for quantifying the brittle behaviour of rock under unconfined compressive failure since brittleness is subject to the loading condition.

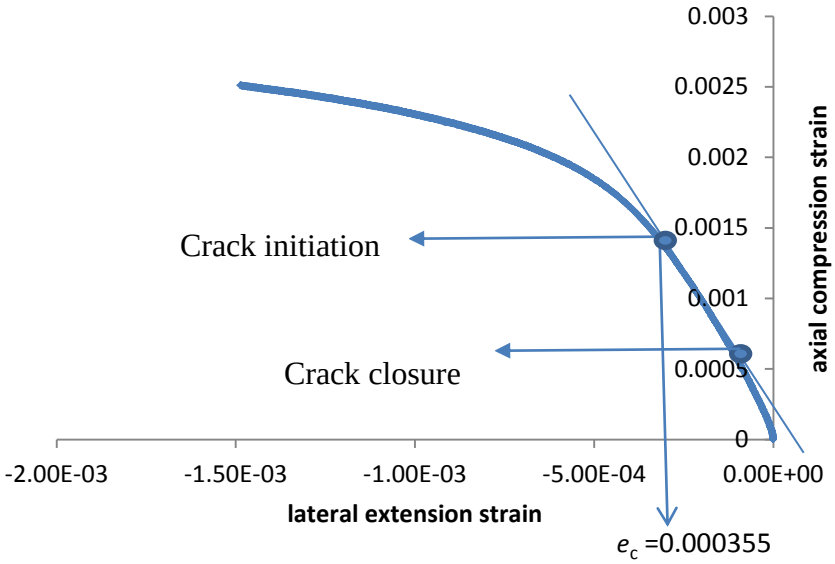

Figure 5.33 Critical extension strain estimation for Norite3

Brittleness estimated from critical extension strain designated as e_c is compared with the fragments size from compression for both the combined sample and the segregated samples. Brittleness e_c did not correlate with the combined sample but show good correlation with the Class II rocks at both X_{50s} and X_{10s} (Figure 5.34). As well, shows no correlation with the Class I rocks, however correlated after the removal of Marble data, see Figure 5.35 (Marble is the least brittle among the rocks tested). It appears therefore, that e_c is applicable to more brittle rocks.

Brittleness estimated as e_c show correlation with brittleness designated as NSSC and stronger correlation with B_{16} for the Class II rocks (Figure 5.37 and 5.36). Similar to NSSC and B_{16}, it also appears that e_c tends to treat Class I and Class II rocks as a separate entity that occupies different spaces. Based on NSSC, B_{16} and e_c, it may be said that the fragmentation of Class I and Class II rocks differs. Critical extension strain, e_c correlated with the post-failure modulus of the rocks

for both segregated samples (Class I and Class II) (Figure 5.38). It may be assumed that the post-failure modulus influences its fragmentation under compressive failure. This was also shown with the statistical analysis. Therefore, e_c could be a good brittleness concept for prediction of fragmentation for compressive failure for the segregated samples especially for the more brittle Class II rocks type. Similar to NSSC, as e_c increases fragmentation becomes coarser for the Class II rocks.

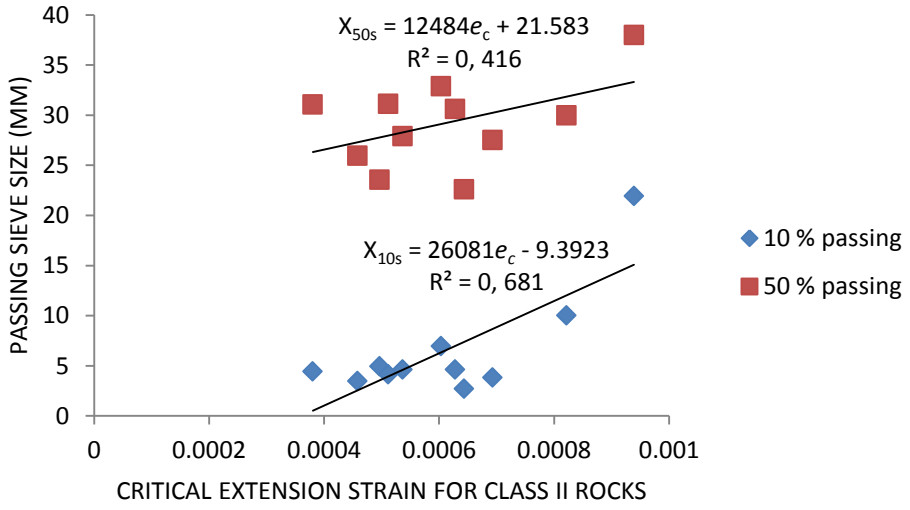

Figure 5.34 Critical extension strain for Class II rocks against passing sieve size (mm)

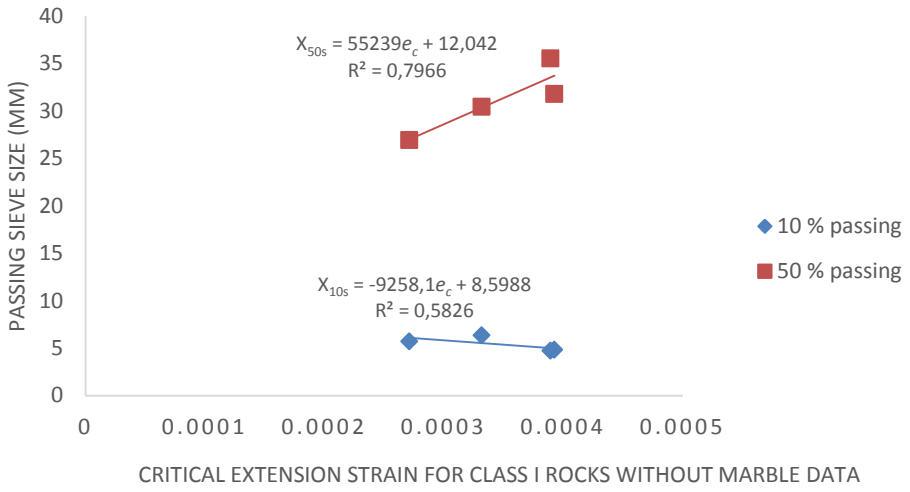

Figure 5.35 Critical extension strain for Class I rocks without Marble data against passing sieve size (mm)

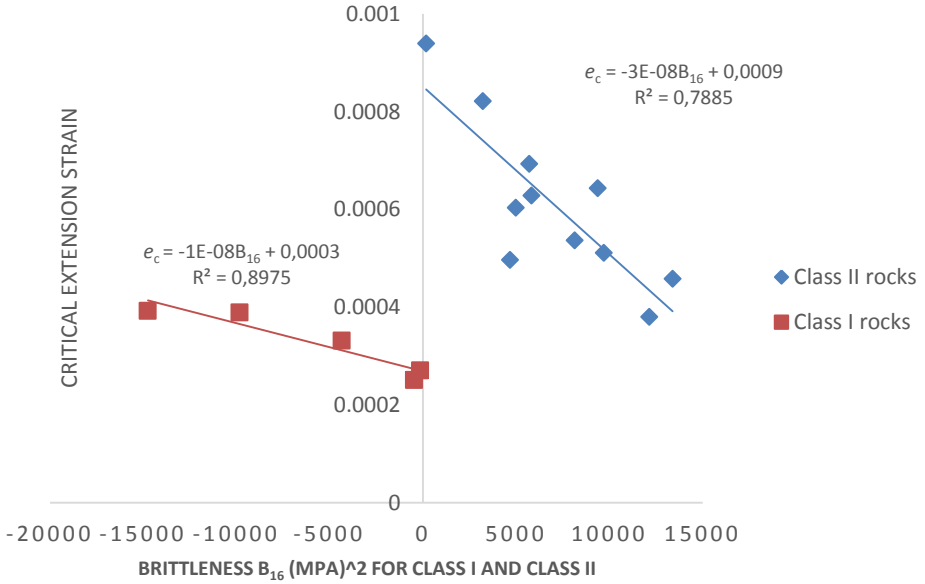

Figure 5.36 Critical extension strain against brittleness B_{16} (GPa)^2

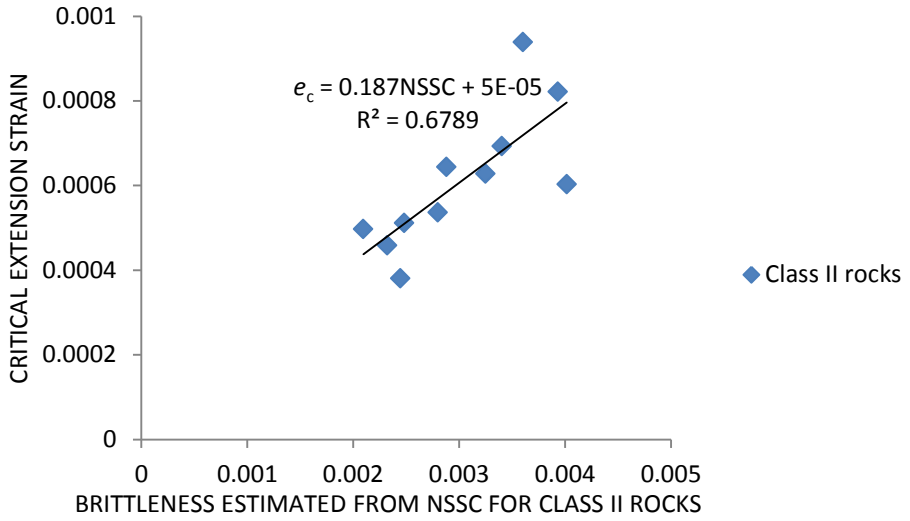

Figure 5.37 Critical extension strain against brittleness NSSC for Class II rocks

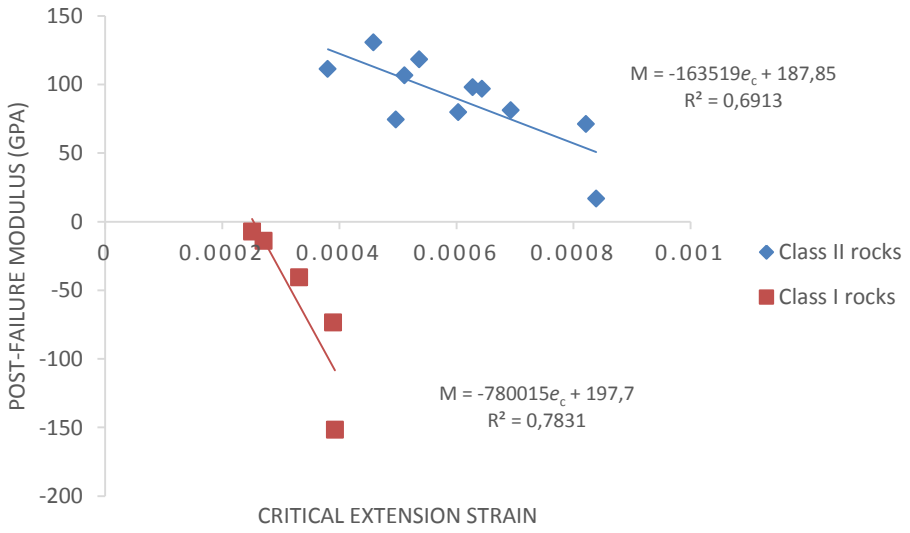

Figure 5.38 Critical extension strain against post-failure modulus (GPa)

5.12 Interim Summary

Much reliance can be placed on the observed trends in the brittleness concepts evaluated from normalised stress-axial strain curve and extension strain criterion. The concepts appear dependable for the estimation of fragments size from compression especially for the more brittle rocks. It appears that both concepts (NSSC and e_c) are much applicable to brittle rocks than less brittle one. Both concepts appear to treat Class I and Class II rocks as a separate entity. The concepts show correlation with B_{16}, as well show correlation with the post-failure modulus of the rocks and as such may be useful to quantify the brittleness of the rock under compressive failure.

5.13 Comparison of Fragments Size from both Compression and Blasting Tests with Various Brittleness Concepts

The fragments size from compression and blasting tests are compared with the various brittleness concepts evaluated above. These include the brittleness concepts estimated from static mechanical properties, moduli, brittleness estimated from normalised stress-axial strain curve and extension strain criterion. These are discussed in the sections that follow.

5.13.1 Comparison of Fragments Size from both Compression and Blasting Tests with Brittleness Based on Static Mechanical Properties

Brittleness B_{11} is compared with fragments size for the compression and blasting tests. The comparison shows that B_{11} did not relate to the combined sample but

shows relationship with the Class II rocks. B_{11} shows correlation with fragments size for blasting at X_{50b} but did not correlate with fragments size for compression at X_{50s} (Figure 5.39) for the Class II rocks. The correlation improves at finer fragments size for both compression and blasting at X_{10s} and X_{10b} (Figure 5.40).

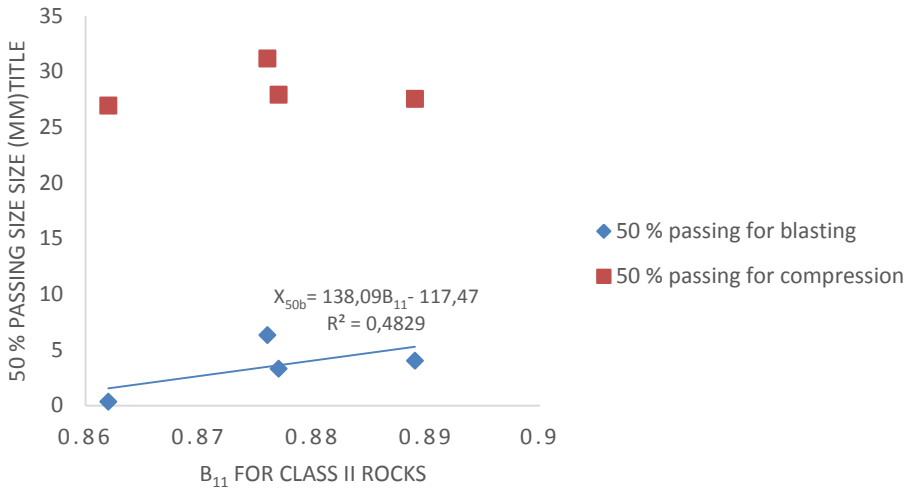

Figure 5.39 B_{11} and 50% passing sieve size for compression and blasting tests

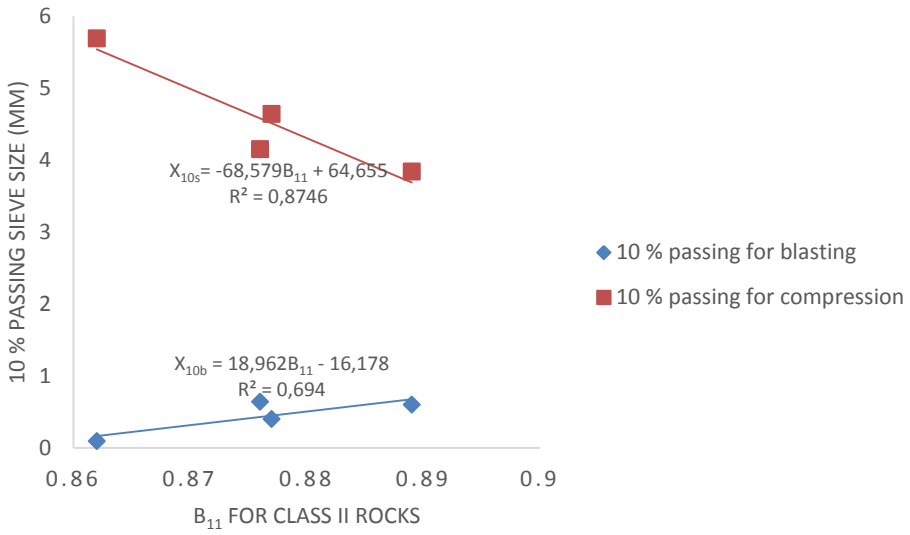

Figure 5.40 B_{11} and 10% passing sieve size for compression and blasting tests

Brittleness B_{13} and B_{14} show similar relationship with fragments size for compression and blasting tests. Both B_{13} and B_{14} did not correlate with the combined sample but show correlation with the Class II rocks (Figure 5.41 to Figure 5.44). The correlation improves with finer fragments size at X_{10s} and X_{10b} for both compression and blasting tests.

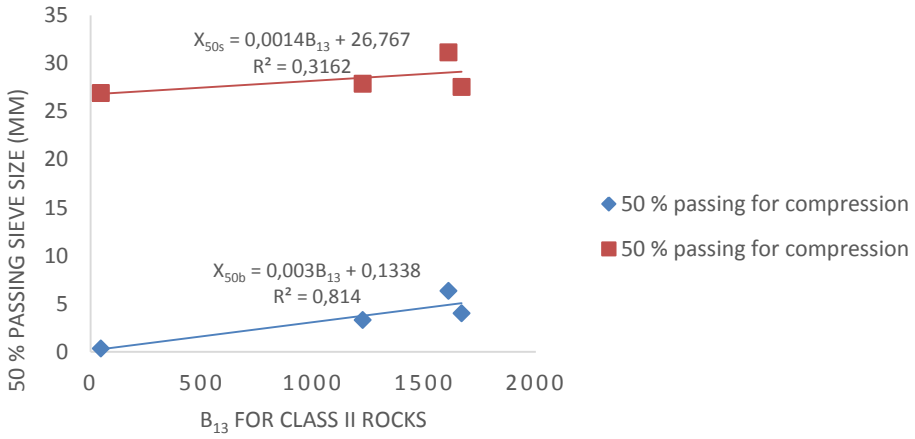

Figure 5.41 B_{13} and 50% passing sieve size for compression and blasting tests

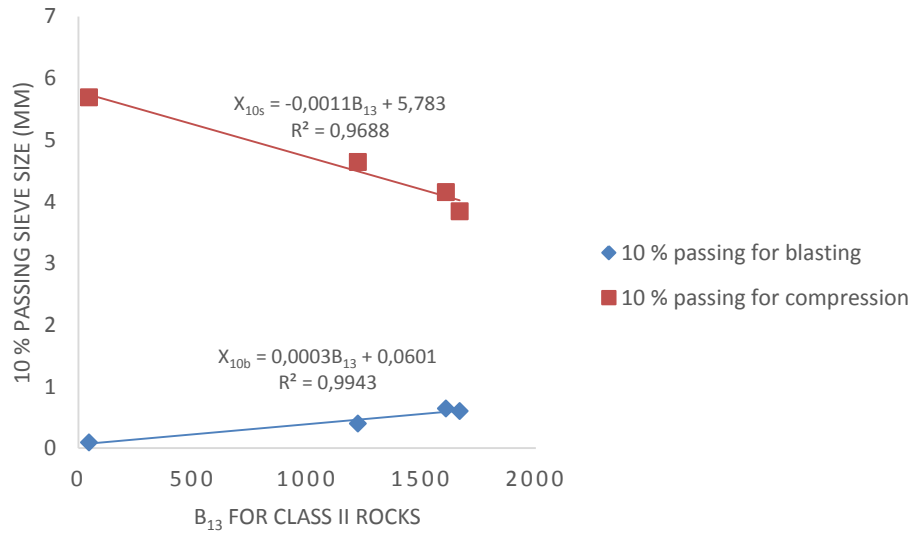

Figure 5.42 B_{13} and 10% passing sieve size for compression and blasting tests

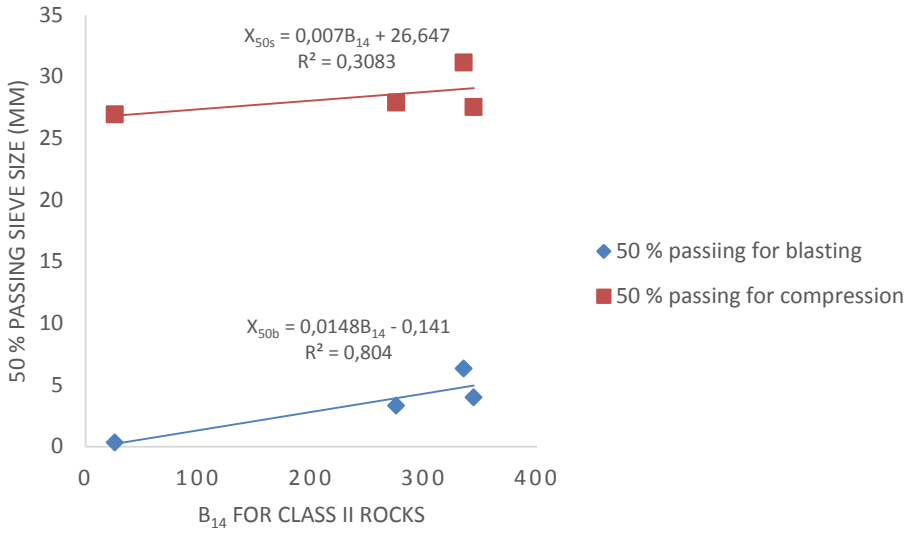

Figure 5.43 B_{14} and 50% passing sieve size for compression and blasting tests

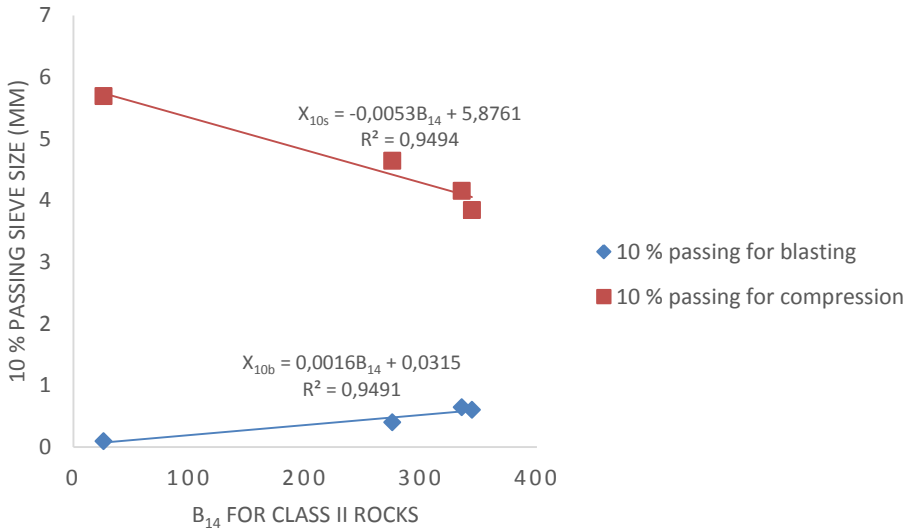

Figure 5.44 B_{14} and 10% passing sieve size for compression and blasting tests

5.13.2 **Comparison of Fragments Size from both Compression and Blasting Tests with Brittleness Based on Moduli**

Brittleness B_{16} and k show similar relationship with fragments size from compression and blasting tests. Both B_{16} and k did not correlate with the combined sample but show correlation with the Class II rocks (Figure 5.45 to Figure 5.48). They are correlated with fragments size for blasting at X_{50b} and $X_{50s.}$ The correlation improve with finer fragments size at X_{10b} and X_{10s} for both compression and blasting tests for brittleness *k.* Brittleness B_{16} shows improved correlation with the Class II rocks at both X_{50b} and X_{10b}.

The brittleness concepts estimated from static mechanical properties and moduli did not correlate with combined sample but shows correlation with the Class II rocks. B_{13} and B_{14} show similar relationship and stronger correlation for the blasting fragments at both X_{50b} and $X_{10b.}$ Brittleness concepts based on static mechanical properties and moduli may not be appropriate concept to evaluate brittleness of rock for combined sample for both tests but could be useful for evaluation of brittleness of Class II rocks, especially the $B_{16.}$

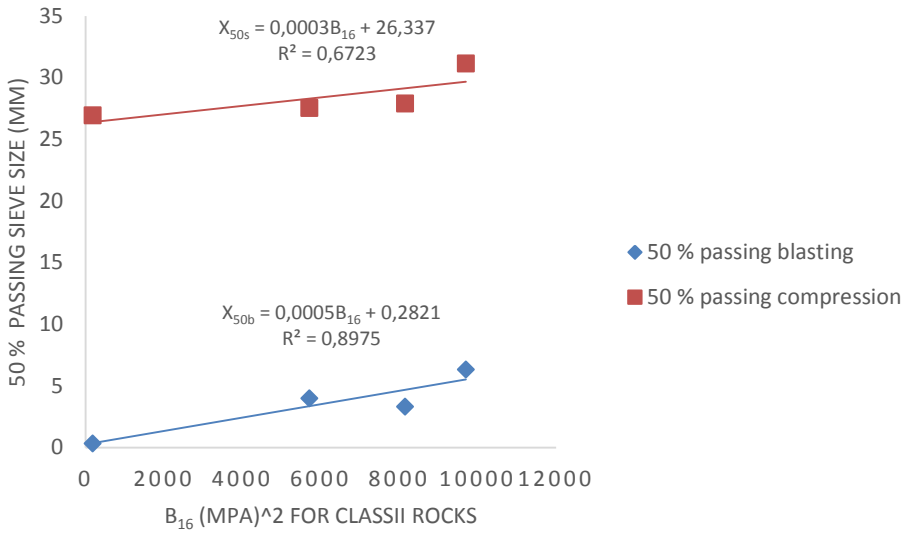

Figure 5.45 B_{16} and 50% passing sieve size for compression and blasting tests for Class II rocks

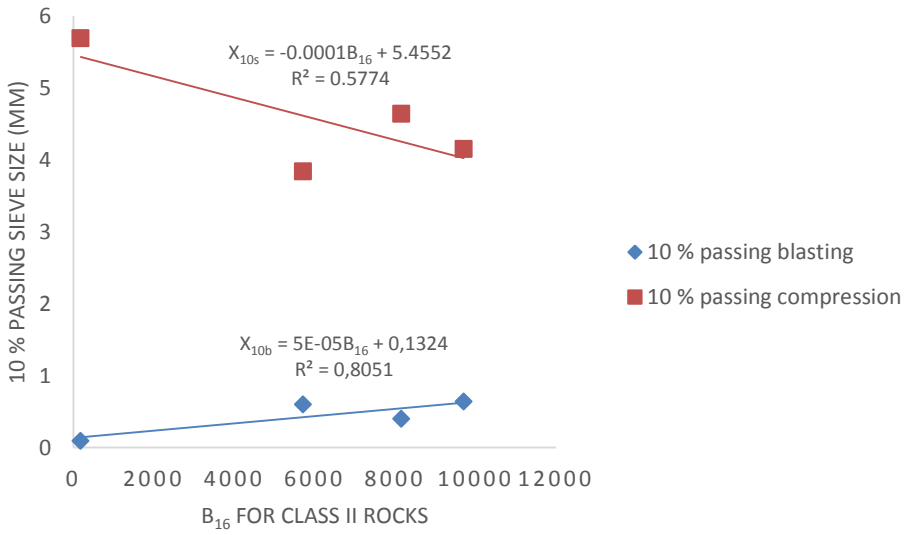

Figure 5.46 B_{16} and 10% passing sieve size for compression and blasting tests

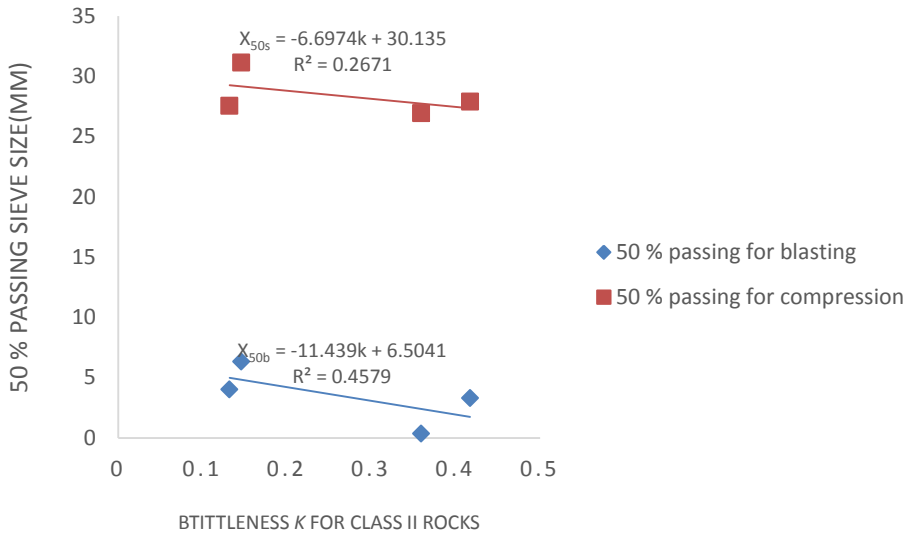

Figure 5.47 Brittleness *k* and 50% passing sieve size for compression and blasting tests

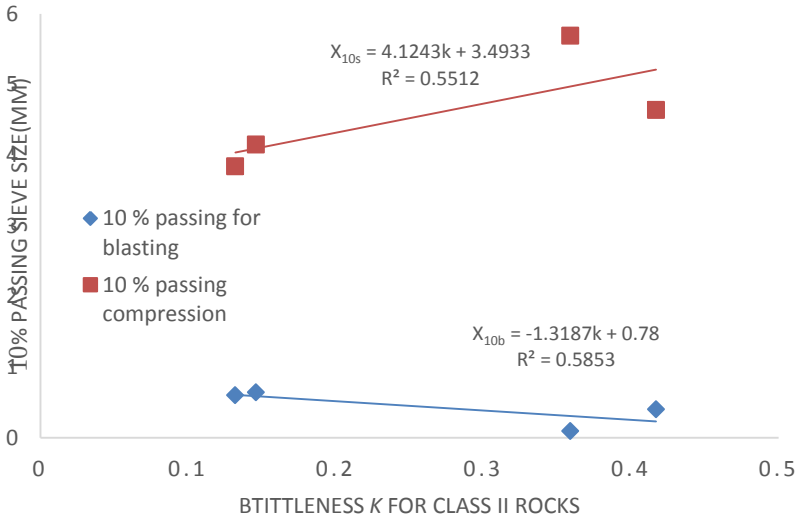

Figure 5.48 Brittleness *k* and 10% passing sieve size for compression and blasting tests

5.13.3 **Comparison of Fragments Size for both Compression and Blasting Tests with Brittleness Estimated from Normalised Stress-Axial Strain Curve, NSSC**

The NSSC brittleness concept, estimated from the normalised stress-axial strain curve is compared with fragments size for compression and blasting tests. The comparison shows that NSSC correlated with the combined samples for both the compression and blasting tests (Figure 5.49 and 5.50), unlike brittleness concepts based on static mechanical properties and moduli. It shows stronger correlation with the blasting fragments at both X_{50b} and X_{10b} than the fragments size from compression. Similarly, NSSC correlated more with X_{50b} and X_{50s} than shown for finer fragments, at X_{10b} and $X_{10s.}$ It can therefore be stated that, the NSSC relates more to fragments size from blasting than compression, in addition correlated better at coarse fragments size (X_{50b} and X_{50s}) for both tests. The relationship shows that as the NSSC value increases, both compression and blasting fragments size at X_{50s} and X_{50b} decrease respectively. Therefore, as brittleness NSSC increases, fragmentation becomes finer.

Brittleness NSSC also correlated with fragments size for the blasting and compression tests for the Class II rocks (Figure 5.51 and 52). Similarly, as shown for the combined sample the correlation becomes weaker for the X_{10b} and X_{10s} for the Class II rocks. The analysis shows that the brittleness NSSC could be a useful index for the prediction of fragments size for compression at X_{50s} and for the blasting tests at both finer and coarse fragments sizes ($X5_{0b}$ and X_{10b}).

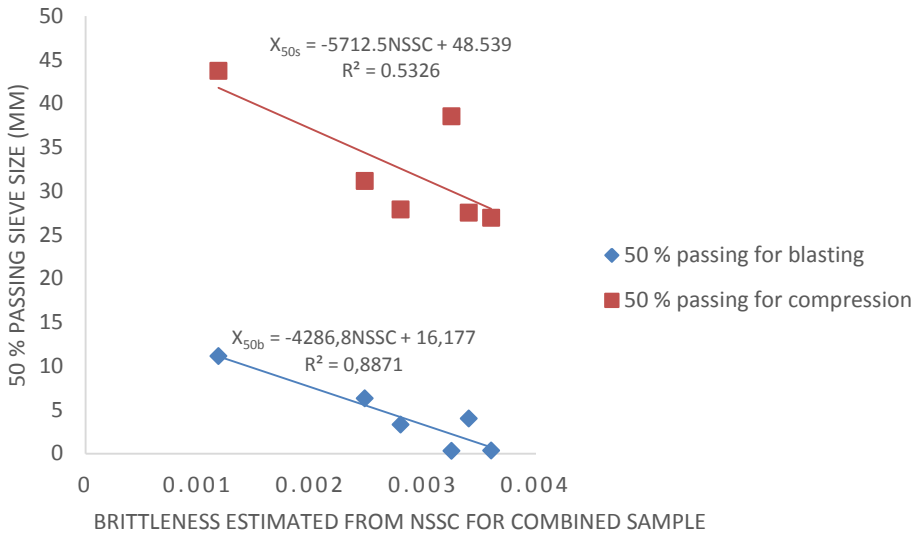

Figure 5.49 Brittleness NSSC and 50% passing sieve size for compression and blasting tests

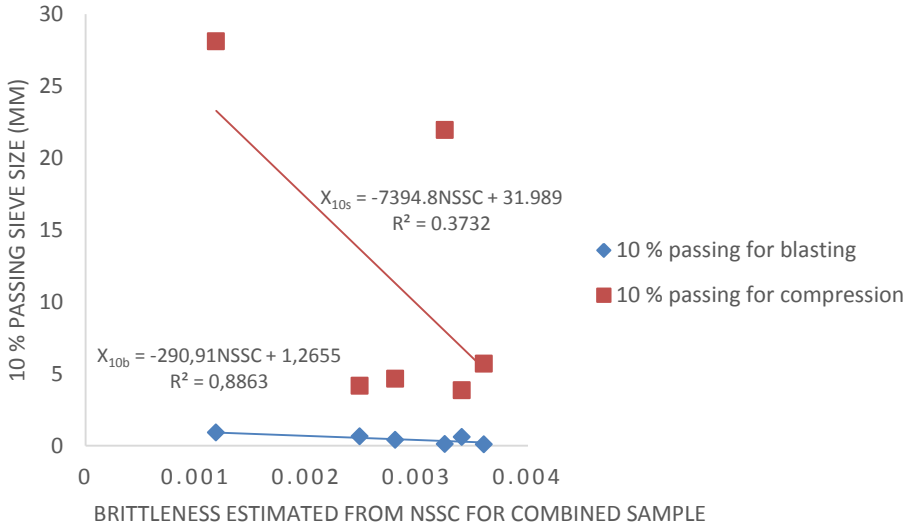

Figure 5.50 Brittleness NSSC and 10% passing sieve size for compression and blasting tests

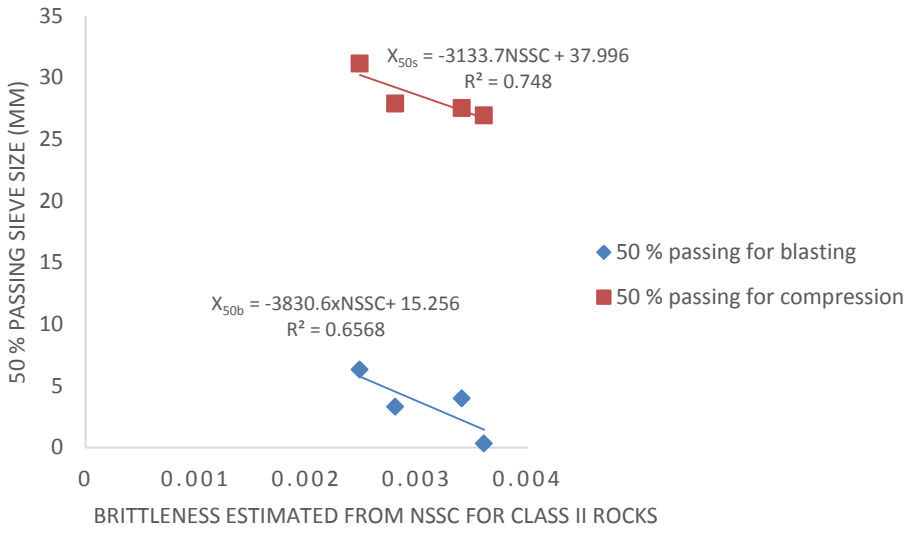

Figure 5.51 Brittleness NSSC and 50% passing sieve size for compression and blasting tests for class II rocks

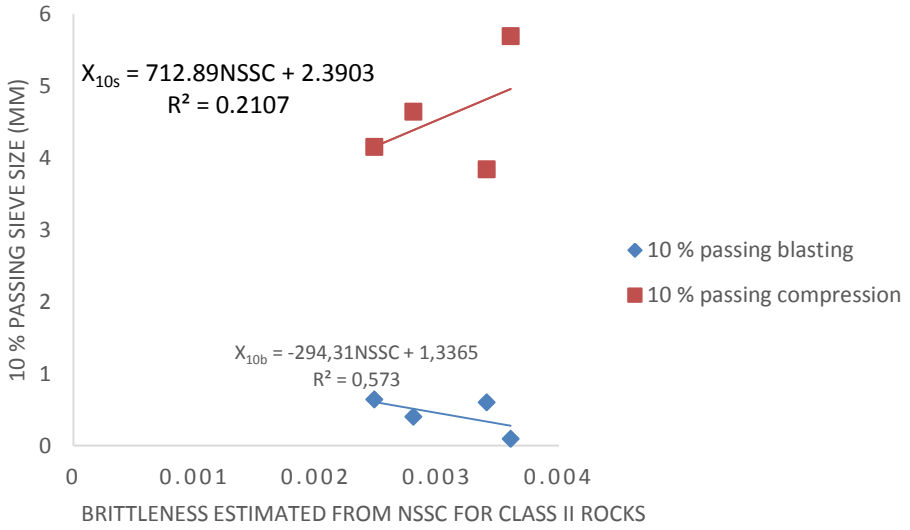

Figure 5.52 Brittleness NSSC and 10% passing sieve size for compression and blasting tests for class II rocks

5.13.4 **Comparison of Fragments Size for Compression and Blasting Tests with Brittleness Estimated from Extension Strain Criterion**

Brittleness estimated from the extension strain criterion is also compared with fragments size from compression and blasting tests. The comparison shows that the brittleness concept correlated with the combined samples for the blasting tests at both X_{50b} and X_{10b} with comparable equal strength (with 0.891 and 0.892 correlation coefficients see Figure 5.53 and 5.54). The relationship shows that as the critical extension strain value increases the fragments size become finer. However, brittleness estimated as critical extension strain poorly correlated with X_{50s} and shows no correlation at $X_{10s.}$ It can therefore be stated that extension strain criterion related more to fragments size from blasting than shows for compression for the combined sample. It was previously shown under compression tests that e_c treated the Class I and Class II rocks differently, that explain the reason for not correlating with the combined compression fragments.

Brittleness estimated as critical extension strain correlated with fragments size for the blasting and compression tests for the Class II rocks (Figure 5.55 and 5.56). The correlation is weaker at X_{50s} and X_{10s} than shown at X_{50b} and X_{10b} for the Class II rocks. The analysis shows that the brittleness estimated as critical extension strain could be a useful index for the prediction of fragmentation of the combined sample particularly for the blasting test at both finer and coarser fragments size ($X5_{0b}$ and X_{10b}).

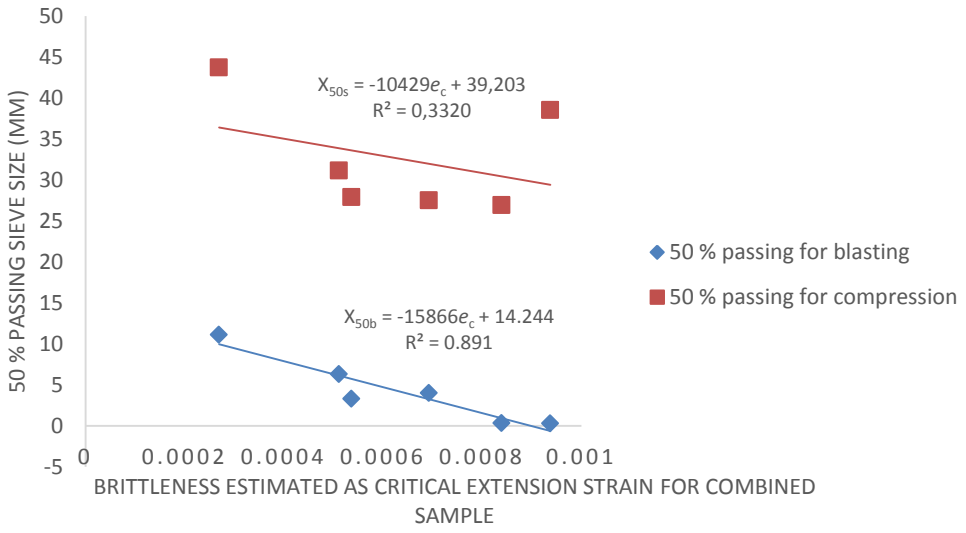

Figure 5.53 Brittleness estimated as Critical Extension Strain and 50% passing sieves size for compression and blasting tests for combined sample

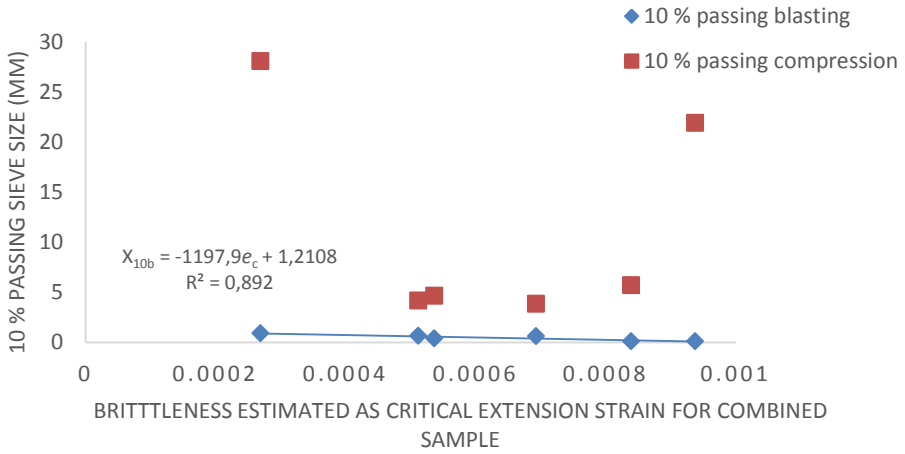

Figure 5.54 Brittleness estimated as Critical Extension Strain and 10% passing sieves size for compression and blasting tests for combined sample

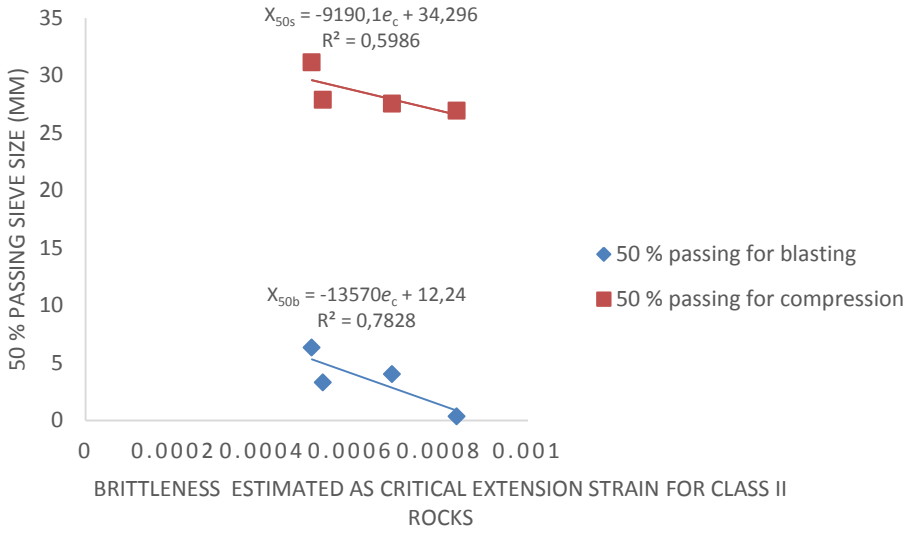

Figure 5.55 Brittleness estimated as Critical Extension Strain and 50% passing sieves size for compression and blasting tests for Class II rocks

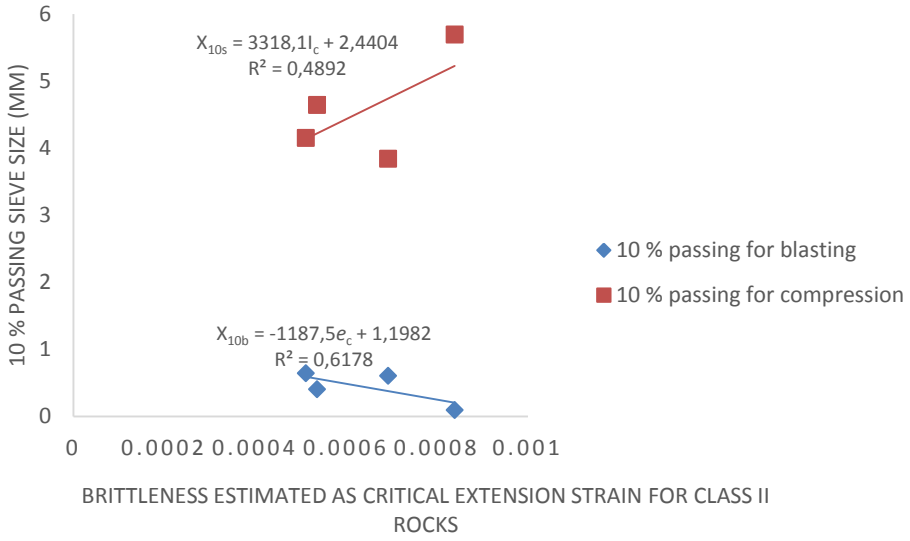

Figure 5.56 Brittleness Critical Extension Strain and 10% passing sieves size for compression and blasting tests for Class II rocks

It was shown in Figure 5.36 to 3.38 that brittleness NSSC, B_{16} (which is a product of post-failure modulus and elastic modulus) and post-failure modulus are related to critical extension strain. It can be argued that critical extension strain is related to post-failure modulus and is able to measure fragmentation in response to post-failure behaviour of the rock. Both NSSC and critical extension strain show that as brittleness of the rocks increases fragmentation becomes finer under blasting test. Hence, it can also be argued that they are quantifying indices for brittleness of rock and do predict fragmentation, especially under the blasting tests.

5.14 Chapter Summary

The calculated probability of the distribution at $X_{50s,}$ X_{50b} and $X_{10s,}$ X_{10b} shows that the Class II rocks as a group are more fragmented. It can therefore be stated that by breaking rocks under the same loading conditions, the Class II rocks tend to be more fragmented than the Class I.

The sieves size passing at $X_{50s,}$ X_{10s} for rocks of similar strength for the Class I and Class II were compared. The analysis shows that by breaking rocks under the same loading conditions, the Class II rocks tend to be more fragmented than the Class I rocks of similar strength.

From the statistical point of view, the fragmentation of rock under steady compression depends on brittleness *k* and improves with the post-failure modulus for the combined sample. Therefore, brittleness *k* could be a useful index for the prediction of fragmentation for combined sample under compressive failure. Also, brittleness index designated as NSSC could be a useful index for quantifying the

brittleness of the segregated samples (Class I and Class II, Table 5.10). Brittleness based on static mechanical properties and moduli only show good correlation with the Class II rocks.

Table 5.10 Correlation coefficient of brittleness based on NSSC and e_c with fragments size from compression

Brittleness Concepts	Correlation coefficient with fragmentation		Fragmentation (% Passing sieve size, mm)
	Class I rocks	Class II rocks	
NSSC	0,7326	0,5314	X_{50s}
	0,4973	0,6795	X_{10s}
e_c	No correlation	0.416	X_{50s}
	No correlation	0.681	k_{10}s

5.14.1 Comparison of Fragments size from Compression with Static Mechanical Properties

The static mechanical properties and fragmentation under compression show an inverse relationship, meaning that the higher the property value the finer the fragmentation. The correlation appears stronger for the Class II rocks and also at X_{10s}.

5.14.2 Comparison of Fragments size from Compression with Dynamic Properties

From the investigation of the dynamic properties, it shows that fragmentation from compression test only relates with the Class II rocks and with an inverse relationship as shown with the strength parameters. It can be suggested that as the dynamic properties of a rock increase, the fragments size becomes finer for the Class II rocks but the same cannot be said for Class I rocks.

5.14.3 Correlation of Fragmentation with Brittleness Based on Static Mechanical Properties

The correlations show that there is a link between brittleness and fragmentation for the Class II rocks. Brittleness B_{13} and B_{14} correlated more with fragmentation under compression for the Class II rocks than other concepts based on static mechanical properties. The correlation becomes stronger at X_{10s}. In addition, fragmentation becomes finer with an increase in brittleness value of B_{13} and B_{14} for the Class II rocks. It can be stated that the higher the brittleness, finer the fragmentation under compressive failure for the Class II rocks. This may qualify the self-fracturing nature of Class II rocks. Brittleness B_{14} also shows relationship with the post-failure modulus of the rocks. Therefore, B_{14} could be a useful index for predicting fragmentation for the Class II rocks.

5.14.4 Correlation of Fragmentation with Brittleness Based on Moduli

Little reliance can be placed on the observed trends in the concepts due to low correlation coefficients. Brittleness k and k_2 show similar relationship with fragmentation and appears consistent in their correlation with the combined sample and Class I rocks at both X_{50s} and X_{10s}. On the other hand, B_{16} shows fairly good correlation with the segregated samples but more correlated with the Class II rocks. The relationship between B_{16} and fragmentation show that, the bigger the brittleness value the finer the fragments size. Therefore B_{16} could be useful index for the prediction of fragmentation for the Class II rocks, since it's a direct measure of the post-failure response of rock.

5.14.5 Correlation of Fragmentation with Brittleness Based on NSSC and e_c

The NSSC brittleness concept correlated with the combined sample for both the compression and blasting tests (Figure 5.49 and 5.50) unlike brittleness concepts based on static mechanical properties and moduli. It shows stronger correlation with the blasting fragments at both X_{50b} and X_{10b} than the fragments size from compression, at X_{50s} and X_{10s}. It can therefore be stated that NSSC relates more to fragments size from blasting than compression. In addition, it shows stronger correlation at coarser fragments size (X_{50b} and X_{50s}) for both tests. The relationship shows that, the bigger NSSC value the finer the fragmentation.

The brittleness concept based on extension strain criterion (estimated as critical extension strain) correlated with the combined samples for the blasting test at both X_{50b} and X_{10b} with comparable equal strength (0.891 and 0.892, Table 5.11 next page) with poor and no correlation at X_{50s} and X_{10s} for the compression test. It can therefore be stated that brittleness estimated as critical extension strain related more to fragments size from blasting and show no correlation with compression for combined samples.

The analysis shows that the brittleness estimated from extension strain criterion could be a useful index for the prediction of fragmentation particularly for the blasting test at both finer and coarser fragments size (X_{50b} and X_{10b}). On the other hand, the brittleness NSSC could be a useful index for the prediction of fragments size at $X_{50b'}$ $X_{50s'}$ for both blasting and compression tests. The bigger the value of both concepts based on extension strain criterion and NSSC, the finer fragmentation.

Table 5.11 Correlation coefficients of the various brittleness concepts with fragmentation (fragments size) for compression and blasting tests.

Brittleness concepts	Correlation coefficient with fragmentation		Fragmentation, % passing sieve size (mm)
	Combined sample	Class II rocks	
NSSC	0,5326	0,7480	X_{50s}
	0,8871	0,6558	X_{50b}
	0,3732	0,2107	X_{10s}
	0,8863	0,5730	X_{10b}
e_c	0,3320	O,5986	X_{50s}
	0,8910	0,7828	X_{50b}
	No correlation	0,4892	X_{10s}
	0,892	0,6178	X_{10b}
B_{16}	No correlation	0,6723	X_{50s}
	No correlation	0,8975	X_{50b}
	No correlation	0,5774	X_{10s}
	No correlation	0,8051	X_{10b}
K	No correlation	0,2671	X_{50s}
	No correlation	0,4579	X_{50b}
	No correlation	0,5512	X_{10s}
	No correlation	0,5853	X_{10b}
B_{11}	No correlation	No correlation	X_{50s}
	No correlation	0,48290	X_{50b}
	No correlation	0.8746	X_{10s}
	No correlation	0,6945	X_{10b}
B_{13}	No correlation	0,3162	X_{50s}
	No correlation	0,8142	X_{50b}
	No correlation	0,9688	X_{10s}
	No correlation	0,9943	X_{10b}
B_{14}	No correlation	0,3083	X_{50s}
	No correlation	0,8045	X_{50b}
	No correlation	0,9494	X_{10s}
	No correlation	0,9491	X_{10b}

CHAPTER SIX

ASSESSMENTS OF FRAGMENTS VOLUMES FROM BOTH COMPRESSION AND BLASTING TESTS

6.1 **Introduction**

As shown in Chapters 5, the brittleness concepts correlated with fragmentation to various degrees. A further assessment is done in this chapter, to evaluate the relationship between fragmentation and brittleness, since there are many ways in which fragmentation can be quantified. In Chapters 5, fragmentation is evaluated as a percentage of fragments passing through selected sieve sizes. However, in this chapter, fragmentation is evaluated in terms of the total number of fragments per volume of rock and the total volume of fines per volume of rock. The estimates are evaluated for both the compression and blasting tests. These are then compared with the various brittleness concepts.

6.2 Total Number of Fragments per Volume of Rock and Brittleness

The number of rock fragments passing each screen size is estimated and summed to give the total number of fragments. If the screen size opening is expressed as an equivalent sphere diameter, the volume of fragments passing through is estimated as the volume of sphere. The volume of the fragments from each screen is

estimated from the ratio of mass retained on the screen, to the rock's density. The total number of fragments, therefore, equals the sum of the ratio of the volume of fragments to the volume of the sphere (i.e. total volume of fragments divided by the volume of an equivalent sphere).

This is expressed as follows:

$$\text{Volume of sphere} = 4/3 \times \pi r^3 \quad (6.1)$$

Where r is the radius of the screen size opening

$$\text{Volume of fragments} = \text{mass retained/density of rock} \quad (6.2)$$

$$\text{Total number of fragments=volume of fragments/volume of sphere} \quad (6.3)$$

Since the volume of the rocks tested cannot be exactly the same for all the tests, the total number of the fragments has to be normalised with respect to the volume of the rock, where the volume of rock is the mass of rock divided by its density. The total number of fragments per volume of rock (mm^{-3}) is compared with the different brittleness concepts as discussed in the following sections. In the sections, the total number of fragments per volume of rock for compression, FV_s, and blasting tests, FV_b, are used to differentiate them.

6.2.1 Total Number of Fragments per Volume of Rock and Brittleness Based on Static Mechanical Properties

The various brittleness concepts based on static mechanical properties are expressed by Equation 6.4 to 6.7.

$$B_{11} = \frac{\sigma_c - \sigma_t}{\sigma_c + \sigma_t} \tag{6.4}$$

$$B_{12} = \sigma_c / \sigma_t \tag{6.5}$$

$$B_{13} = {}^{\sigma_c * \sigma_t}\!/_{2} \ \text{(MPa)}^2 \tag{6.6}$$

$$B_{14} = (\sigma_c \times \sigma_t)^{0.72} \ \text{(MPa)}^2 \tag{6.7}$$

They are compared with the total number of fragments per volume of rock. Brittleness B_{11} and B_{12} correlated with the total number of fragments per volume of rock for both compression and blasting tests (Figures 6.1 to 6.2). The other concepts show correlation but with poor distribution of the data especially for the blasting test (Appendix 4.1). They show better correlation with the compression than the blasting test.

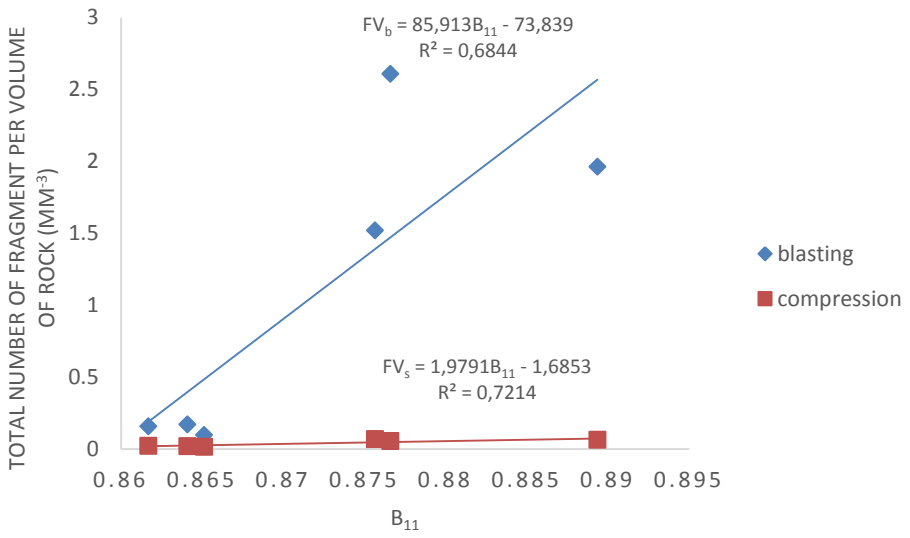

Figure 6.1 Total number of fragments per volume of rock from both tests and brittleness B_{11}.

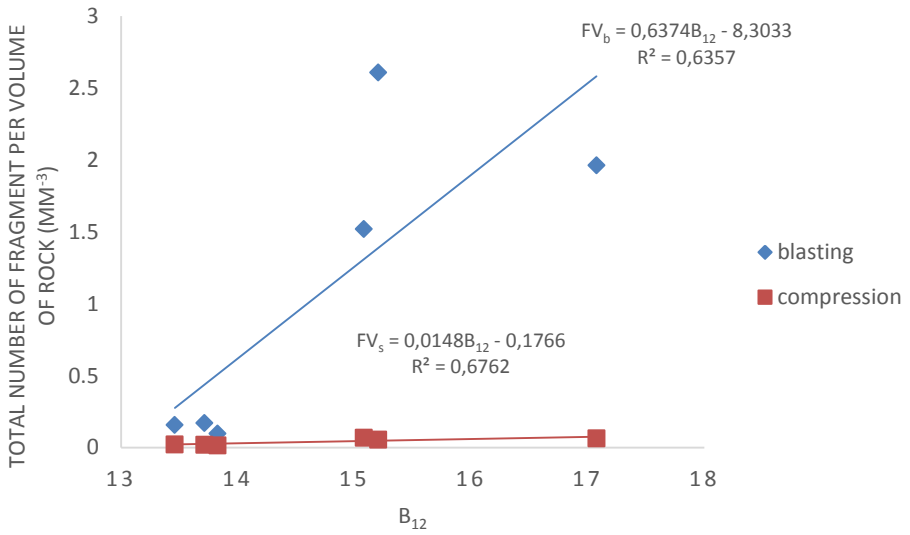

Figure 6.2 Total number of fragments per volume of rock from both tests and brittleness B_{12}.

6.2.2 Total Number of Fragments per Volume of Rock and Brittleness Based on Moduli

The number of fragments per volume of rock shows better correlation with brittleness B_{16} for both tests (Figure 6.3). Brittleness B_{16} is expressed by Equation 6.8.

$$B_{16} = EM \tag{6.8}$$

The other concepts based on moduli did not correlate with the total number of fragments per volume of rock (Appendix 4.2). The relationship shows that as brittleness B_{16} increases, the total number of fragments per volume of rock increases for both the compression and blasting tests.

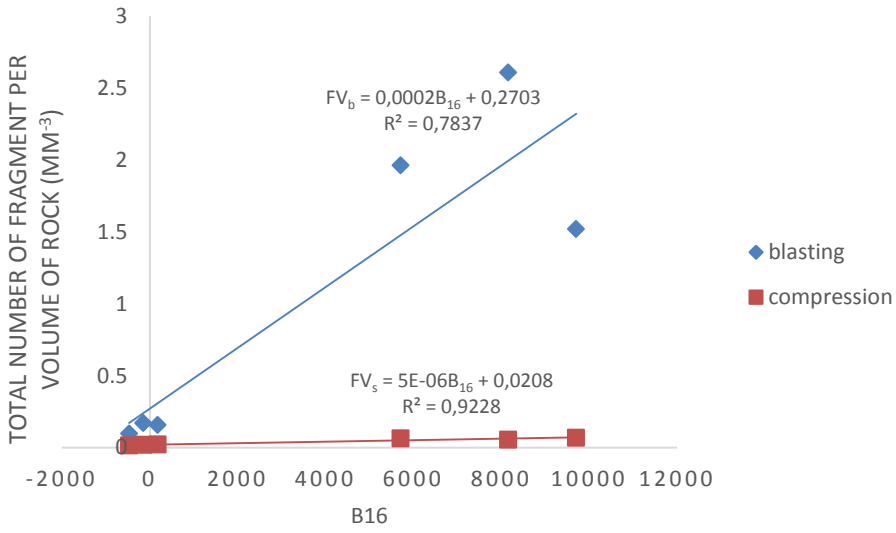

Figure 6.3 Total number of fragments per volume of rock from both tests and brittleness B_{16} (GPa) [2].

6.3 Volume of Fines per Volume of Rock and Brittleness

The mass of fines retained on the pan after sieving was divided by the densities of the rocks to give the volume of fines generated from both compression and blasting tests. The volume of fines was then normalised with the volume of the rock, by dividing the mass of the rock prepared for both blasting and compression tests with the densities of the rocks.

$$\text{Volume of fines} = {}^{mass\ \text{of fines}}\!\!\diagup\!\!_{density\ \text{of rock}} \tag{6.9}$$

$$\text{Volume of fines per volume of rock} = {}^{volume\ of\ fine}\!\!\diagup\!\!_{volume\ of\ rock} \tag{6.10}$$

The volume of fines per volume of rock (VV_b, for blasting and VV_s for compression) is compared with the various brittleness concepts as shown in the following sections.

6.3.1 Volume of Fines per Volume of Rock Produced and Brittleness Based on Static Mechanical Properties

The various brittleness concepts based on the static mechanical properties show correlations with the volume of fines per volume of rock for blasting tests, VV_b but not with the compression tests (Figures 6.4 to 6.7). The concepts show that there is relationship with volume of fines per volume of rock and brittleness based on static mechanical properties for the blasting test.

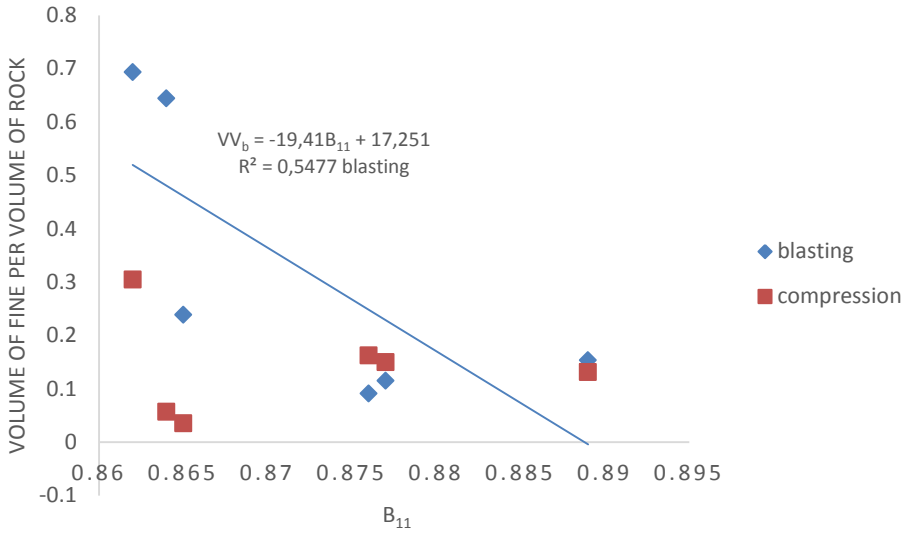

Figure 6.4 Volume of fines per volume of rock produced (mm^3) from both tests and brittleness B_{11}.

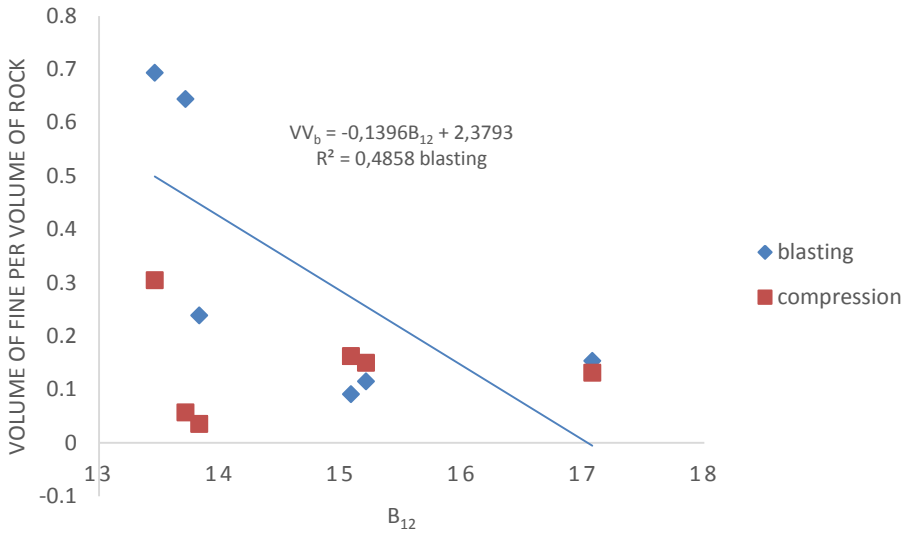

Figure 6.5 Volume of fines per volume of rock produced (mm^3) from both tests and brittleness B_{12}.

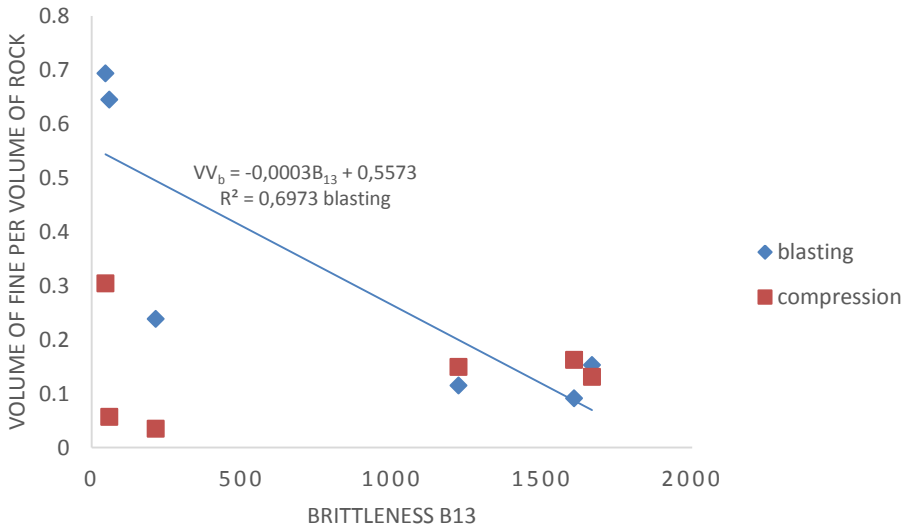

Figure 6.6 Volume of fines per volume of rock produced (mm^3) from both tests and brittleness B_{13}.

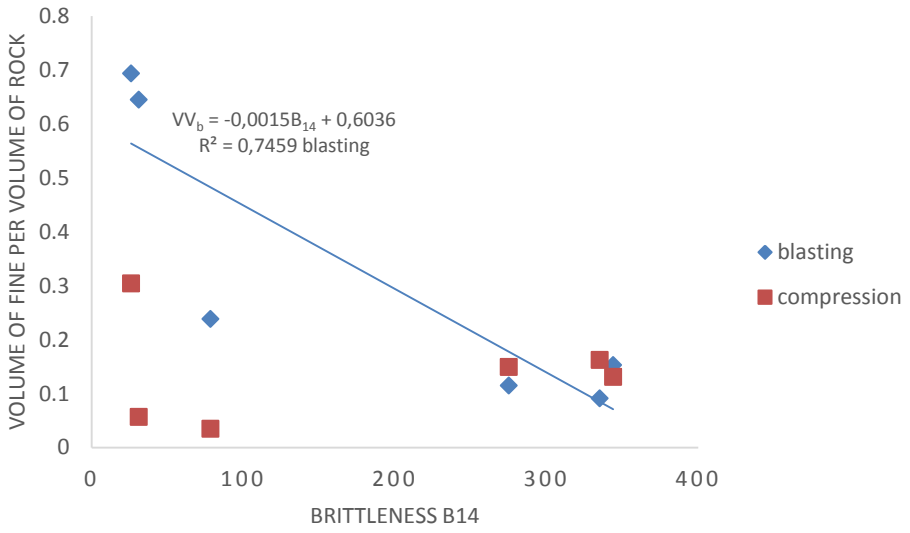

Figure 6.7 Volume of fines per volume of rock produced (mm^3) from both tests and brittleness B_{14} (MPa) [2].

6.3.2 Volume of Fines per Volume of Rock and Brittleness Based on Moduli

The volume of fines per volume of rock shows a better correlation with brittleness B_{16} than the other concepts based on moduli (Figure 6.8, Appendix 4.3). The curve shows similar relationship as indicated by the brittleness concepts based on static mechanical properties with the volume of fines per volume of rock. The other concepts based on moduli show no correlation.

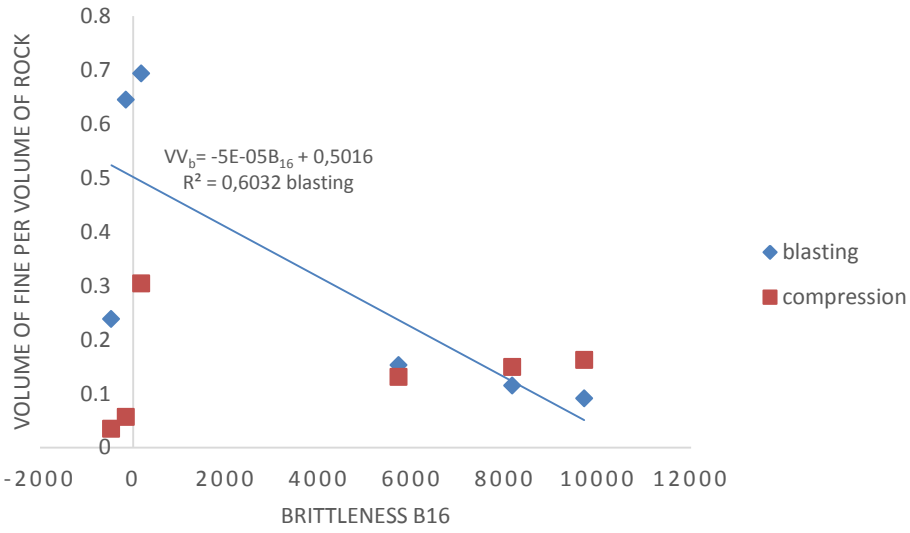

Figure 6.8 Volume of fines produced (mm^3) from both tests and brittleness B_{16} $(GPa)^2$.

6.3.3 Volume of Fines per Volume of Rock Produced and Brittleness Based on Extension Strain Criterion

The volume of fines per volume of rock shows correlation with extension strain criterion for the blasting test but did not correlate with the compression tests (Figure 6.9). The curves show that, as the value of extension strain criterion increases the volume of fines per volume of rock also increase. However, the brittleness based on normalised stress-axial strain curve shows no correlation for both the blasting and compression tests.

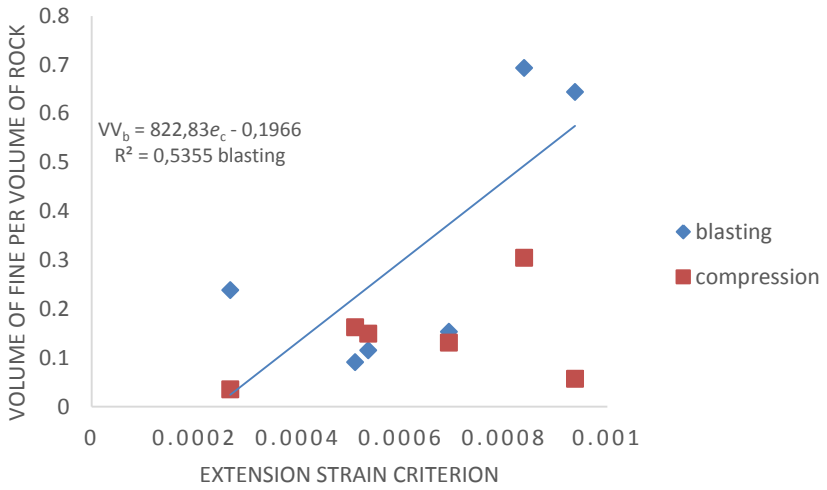

Figure 6.9 Volume of fines per volume of rock produced (mm^3) from both tests and Extension Strain Criterion

6.4 Energy and Fragment Volumes

The estimate of energy in terms of releasable elastic strain energy per unit volume (Equation 6.11) is compared with the fragments volumes.

Releasable elastic strain energy per unit volume= $\sigma^2/2E$ (6.11)

where σ is the UCS and E is the elastic modulus

The total number of fragments per volume of rocks show correlation with the releasable elastic strain energy per unit volume for both blasting and compression tests (Figure 6.10), but stronger for the compression test. The relationship shows that, as the energy utilised in the fragmentation process increases, total number of fragments per volume of rock also increases. However, the releasable elastic strain energy per unit volume shows no correlation with volume of fines per volume of rock.

The total number of fragments per volume of rocks correlated with the post-failure modulus of the rocks (Figure 6.11). The energy estimated as releasable elastic strain energy per unit volume increase as the post-failure modulus assume a postive value.

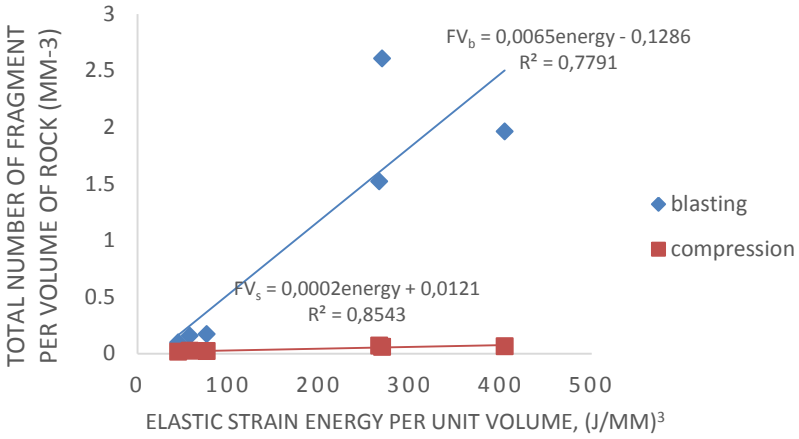

Figure 6.10 Elastic strain energy per unit volume, (J/mm)^3 and total number of fragments per volume of rock (mm^{-3})

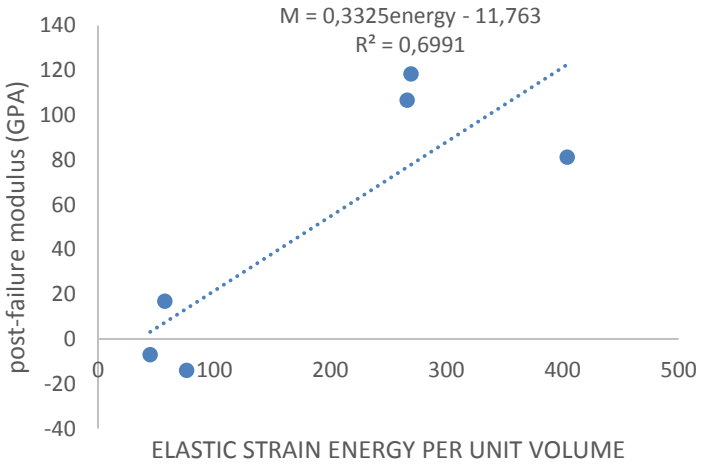

Figure 6.11 Elastic strain energy per unit volume, (J/mm)^3 and post-failure modulus.

6.5 Chapter Summary

The dimensionless brittleness concepts, B_{11} and B_{12} which are based on static mechanical properties are the two brittleness concepts correlating with the total number of fragments per volume of rock for both compression and blasting tests (Table 6.1). The correlations for B_{13} and B_{14} are affected by clusters of data. However, based on the observed trend in other similar concepts from static mechanical properties, it may not be unreasonable to conclude that there are correlations.

It is also observed that brittleness B_{16}, based on moduli correlated with the total number of fragments per volume of rock for both tests. The relationship shows that as the brittleness index increase, the total number of fragments per volume of rock also increase. B_{16} is a better concept to describe the total number of fragments per volume of rock for both tests (Table 6.1).

Little reliance can be placed on fragments volumes as a measure of fragmentation because of low correlation coefficient and poor distribution of the data plotted. From the analysis in chapter 5 and 6 it is obvious that fragmentation is best described as a distribution (at X_{50} and X_{10}) than single entity as fragments volumes.

In the next chapter, the summaries of the finding in Chapters 5-6 are given in form of tables and equations describing the relationship between the different measures of fragmentation and the various brittleness concepts.

Table 6.1 Various Brittleness and Fragments volumes from both compression and blasting tests

Brittleness concepts	**Correlation coefficient with fragmentation**	
	Blasting	**Compression**
Total number of fragments per volume of rock		
Brittleness Based on static mechanical properties		
B11	0,6844	0,7214
B12	0,6357	0,6762
Brittleness Based on Moduli		
B_{16}	0,7837	0,9228
Volume of Fines per Volume of Rock		
Brittleness Based on static mechanical properties		
B11	0,5477	No correlation
B12	0,4858	No correlation
B13	0,6973	No correlation
B14	0,7459	No correlation
Brittleness Based on Moduli		
B16	0,6052	No correlation
Brittleness Based on Extension Strain Criterion	0,5355	No correlation

CHAPTER SEVEN

RELATIONSHIP BETWEEN FRAGMENTATION AND BRITTLENESS

7.1 Introduction

In the previous chapters (Chapters 5 and 6), fragmentation was expressed in different ways. Fragmentation was evaluated at certain selected percentages (X_{50} and X_{10}) passing sieve size and as fragments volumes. The different measures of fragmentation for compression and blasting tests do not show the same relationship with brittleness. Since fragmentation is evaluated for different purposes, the method used will depend on the aim of fragmentation. For this reason, the different methods used to estimate fragmentation based on the brittleness of the rocks are summarised in order to show the ability of each of the concepts in evaluating fragmentation.

7.2 **Fragmentation Based on the Percentage Passing Sieve Size**

The correlation coefficients and the percentage of fragments passing the various sieves size for the compression and blasting tests are summarised in tables, as shown in the following sections.

7.2.1 Percentage Passing Sieves Size for the Compression Test

The coefficients of correlations of the various brittleness concepts with fragmentation at X_{50s} and X_{10s} are summarised in Table 7.1.

Table 7.1 Relationship between brittleness and fragmentation from the compression test based on X_{50s} and X_{10s} passing sieves size.

Brittleness concepts based on	**Fragmentation %Passing sieve size(mm)**	**Correlation coefficient with fragmentation**		
		Combined sample	**Class I**	**Class II**
Static mechanical properties		Correlation coefficient (R^2)		
B_{13}	X_{50s}	0.61	No correlation	0.2046
	X_{10s}	0.6	No correlation	0.5385
B_{14}	X_{50s}	0.63	No correlation	0.2389
	X_{10s}	0.6	No correlation	0.6286
Moduli				
B_{16}	X_{50s}	No correlation	0.3699	0.3166
	X_{10s}	No correlation	0.40505	0.5356
k	X_{50s}	0.5331	0.7038	No correlation
	X_{10s}	0.5977	0.9693	No correlation
k_2	X_{50s}	0.4422	0.7335	0.447
	X_{10s}	0.4898	0.9671	0.560
Estimated as NSSC	X_{50s}	No correlation	0.7326	0.5314
	X_{10s}	No correlation	0.4973	0.6795
Estimated as Critical extension strain	X_{50s}	No correlation	No correlation	0.416
	X_{10s}	No correlation	No correlation	0.681

From the Table 7.1, all the brittleness concepts based on static mechanical properties show no correlation with fragmentation at X_{50s} and X_{10s} for the Class I rocks while B_{13} and B_{14} show correlation with the combined sample and Class II rocks.

Similarly, fragmentation, evaluated as percentage passing sieves size, does not correlation with the brittleness based on the rock moduli for the combined sample at X_{50s} and X_{10s} except for brittleness $k.$ and $k_{2.}$ However the outlier nature of Marble data may influence the relationship. Brittleness B_{16} shows correlation with the segregated sample with good spread in the data plotted. Therefore, B_{16} could be a good index for quantifying the brittleness of Class I and Class II rocks. However the correlation is not strong.

Brittleness estimated from the normalised stress-axial strain curve designated as NSSC did not correlate with the combined sample and appears to treat fragmentation of Class I and Class II rock as separate entity. It shows correlation with the segregated samples with better spread in the distribution of the data plotted. It has stronger correlation than B_{16}. Therefore, NSSC could be a better concept for quantifying the brittleness of rock under compressive failure for the segregated samples.

Brittleness estimated from the extension strain criterion (Critical extension strain) did not correlate with the combined sample and Class I rocks but shows correlation with the Class II rocks. However, correlated with the Class I rocks

after removal of Marble (the least brittle of the rocks tested) data. It appears that brittleness estimated as critical extension strain is applicable to much brittle rocks. Critical extension strain correlated with $B_{16,}$ NSSC and post-failure modulus of the rocks. Therefore could be a good concept for quantifying the brittleness of rock under compressive failure for brittle rocks.

7.2.2 Percentage Passing Sieve Size for the Blasting Tests

The various brittleness concepts and their correlation coefficients with fragmentation determined as the percentage passing sieve size (X_{50b} and X_{10b}) for the blasting test are summarised in Table 8.2. The brittleness concepts based on static mechanical properties except B_{12} show good correlation at X_{50b} and X_{10b} for the Class II rocks, but not for the combined sample. In particular, B_{13} and B_{14} show a stronger correlation with the Class II rocks. Brittleness B_{14} also correlated with the post-failure modulus. Hence could be a useful index for the Class II rock in the present of post-failure modulus.

From the brittleness concepts based on moduli, only B_{16} and k correlated with the Class II rocks but the same cannot be said for the combined sample. Brittleness B_{16} (a product of post-failure modulus and elastic modulus) show stronger correlation with the Class II rocks (Table 8.2) and could be a useful index for the Class II rocks.

Brittleness estimated as critical extension strain and NSSC are the two indices that correlated with the combined sample for the blasting test. The two concepts show better correlation with blasting fragments than other brittleness concepts with

good spread of the data plotted. The critical extension strain shows stronger correlation at X_{50b} and X_{10b} than the NSSC. The critical extension strain also correlated with the post-failure modulus of the rocks. Therefore critical extension strain is a better index for quantifying brittleness of rock under blasting test for both the combined and Class II rocks. The relationship is the same as shown for NSSC, as the critical extension strain increases, fragmentation becomes finer.

Table 7.2 Relationship between brittleness and fragmentation from blasting tests based on % passing sieve size.

Brittleness concepts based on	**Fragmentation, % Passing sieve size(mm)**	**Correlation coefficient with Fragmentation**	
		Combined sample	**Class II rocks**
Static mechanical properties		Correlation coefficient (R^2)	
***B*$_{11}$**	X_{50b}	No correlation	0.4829
	X_{10b}	No correlation	0.6945
***B*$_{13}$**	X_{50b}	No correlation	0,8142
	X_{10b}	No correlation	0.9943
***B*$_{14}$**	X_{50b}	No correlation	0.8045
	X_{10b}	No correlation	0.9491
Moduli			
***B*$_{16}$**	X_{50b}	No correlation	0.8975
	X_{10b}	No correlation	0.8051
k	X_{50b}	No correlation	0.4579
	X_{10b}	No correlation	0.5853
Estimated as NSSC	X_{50b}	0.8871	0.6568
	X_{10b}	0.8863	0.573
Estimated as Critical extension strain	X_{50b}	0.8910	0.7828
	X_{10b}	0.8920	0.6178

7.3 Fragmentation Based on Fragments Volumes

Fragmentation determined as the total number of fragments per volume of rock correlated with the brittleness concepts described as B_{11} and B_{12} (based on static mechanical properties) for both compression and blasting tests. Also, brittleness B_{16} based on moduli correlated with the total number of fragments per volume of rock for both compression and blasting tests (see Table 8.3). Brittleness, B_{16} shows stronger correlation than B_{11} and B_{12}. Since B_{16} is a direct measure of the post-failure response of rock, as such can be used as a measure of brittleness for the estimation of the total number of fragments per volume of rock.

All the brittleness concepts did not correlate with fragmentation as determined by the volume of fines per volume of rock for the compression test. It appears that none of the concepts could predict volume of fines per volume of rock for the compression test. It may be stated that the volume of fines per volume of rock is not a good measure of fragmentation for compression test.

The brittleness concepts based on static mechanical properties of rock show correlation with the volume of fines per volume of rock for the blasting tests. Similarly, brittleness B_{16} based on moduli and critical extension strain show better correlation with the volume of fines per volume of rock as a measure of fragmentation for the blasting test as summarised in Table 8.3. Brittleness B_{13},, B_{14}, and B_{16} have the highest correlation coefficients. Although B_{14} shows correlation with post-failure modulus, B_{16} as a direct measure of the post-failure response of

rock, is preferred as measure of brittleness in the prediction of volume of fines per volume of rock for the blasting test.

Table 7.3 Various brittleness and fragments volumes from both compression and blasting tests

Brittleness Concepts	**Fragmentation Correlation Coefficient**	
	Blasting	**Compression**
Total number of fragments per volume of rock		
Brittleness Based on static mechanical properties		
B11	0,6844	0,7214
B12	0,6357	0,6762
Brittleness Based on Moduli		
B_{16}	0,7837	0,9228
Volume of Fines per Volume of Rock		
Brittleness Based on static mechanical properties		
B11	0,5477	No correlation
B12	0,4858	No correlation
B13	0,6973	No correlation
B14	0,7459	No correlation
Brittleness Based on Moduli		
B16	0,6052	No correlation
Brittleness Based on Extension Strain Criterion	0,5355	No correlation

By way of comparison, based on the relationship (i.e. the correlation coefficients and the distribution of data points) of the different measures of fragmentation with the brittleness concepts discussed in the previous sections, fragments size at X_{50} and X_{10} for the blasting and compression tests are better measure of fragmentation than the "fragments volumes".

7.4 Selection of the Brittleness Concept for Different Measures of Fragmentation

The percentage of fragments passing selected sieve size as a measure of fragmentation is more effective than fragments volumes especially for brittleness estimated as critical extension strain and NSSC.

7.4.1 Brittleness Concepts and Fragments Size as a Measure of fragmentation from Compression Test.

The relationships of the various brittleness concepts with the different measures of fragmentation show poor correlation with the combined sample, based on the correlation coefficients and the distribution of the data plotted. The critical extension strain and NSSC did not correlate with the combined sample. They appear to treat the fragmentation of Class I and Class II rocks as separate entity. However, the statistical analyses suggested that brittleness k is a better concept for the evaluation of fragmentation determined as the 'percentage of fragments passing selected sieve size' (X_{50s}, X_{10s}), for the combined sample under the compression test.

The expression in Equation 7.1 and 7.2 is the result of statistical analysis for fragments size at X_{50s}, X_{10s} and brittleness k for the combined sample.

$$X_{10_S} = -1.798k + 0.435 \quad (7.1)$$

$$X_{50_S} = -1.391k + 28.744 \quad (7.2)$$

For the segregated samples, definition given by NSSC in equation 7.3 and 7.4 are best for the Class II rocks

$$X_{50s} = 3587.8NSSC + 17.894 \quad (7.3)$$

$$X_{10s} = 5081NSSC - 9.4907 \quad (7.4)$$

For the Class I, Equation 7.5 and 7.6 are most appropriate

$$X_{50s} = -7063.7NSSC + 48.487 \quad (7.5)$$

$$X_{10s} = -9564.9NSSC + 30.19 \quad (7.6)$$

7.4.2 Brittleness Concepts and Fragment Size as a Measure of Fragmentation for Blasting Tests

The critical extension strain, e_c and NSSC show better correlation with the combined sample for the blasting tests (Table 8.2). The critical extension strain has stronger correlation at both X_{50b} and X_{10b} than the NSSC. Therefore, critical extension strain is a better index for quantifying brittleness of rock under blasting test for both the combined and Class II rocks. The relationship for the combined sample are given in the Equation 7.7 and 7.8

$$X_{50b} = -15866e_c + 14.244 \quad (7.7)$$

$$X_{10b} = -1197.9e_c + 1.\ 2108 \quad (7.8)$$

7.4.3 Brittleness Concepts and Fragment Volumes as a Measure of fragmentation from Blasting Tests

Brittleness, B_{16} based on moduli is a better concept for the prediction of the total number of fragments per volume of rock for both compression and blasting tests (Table 8.3) and is expressed in Equation 7.9 and 7.10.

$$FV_S = 5E\text{-}06B_{16} + 0.0208 \quad (7.9)$$

$$FV_b = 0.0002B_{16} + 0.2703 \quad (7.10)$$

Also, B_{16} is the better concept for the prediction of volume of fines per volume of rock for blasting test as given in Equation 7.11. On the other hand, none of the concepts correlated with volume of fines per volume of rock for the compression test. It may be said that volume of fines per volume of rocks is not a good measure of fragmentation from compression test. Generally, the 'fragments volumes' show low correlation coefficients with the various brittleness concepts as result of poor distribution of the data plotted. A better relationship is shown with fragments size with brittleness concepts estimated as critical extension strain and NSSC.

$$VV_b = -5E\text{-}05B_{16} + 0{,}5016 \quad (7.11)$$

In summary, it has been shown that:

- Brittleness correlates with fragmentation.
- In the relationship between brittleness and fragmentation, the correlation of Class II rocks are stronger than Class I rocks under compressive failure

- Different definitions of brittleness are more effective in predicting fragmentation as these have different purposes.

7.5 Modification to the Kuz-Ram Model

This research work reveals that fragmentation depends on the rock brittleness. The relationship shows that as the effect of brittleness increases, the fragments size becomes finer and the total number of fragments per volume of rock increases for both the steady compression and blasting tests. Thus, understanding the relationship between fragmentation and brittleness can bring about a strategy for control of fragmentation prediction.

The Kuz-Ram model is possibly the most widely used fragmentation prediction model for practical blasting. The model inherently assumes that the brittleness behaviour of rocks is the same and that explosive energy is related directly with fragmentation. However, the progressive difference in the brittle behaviour of rocks may override the expected relationship of fragmentation and explosive usage assumed in the empirical model. To date, there has apparently been no research towards understanding the effects of increasing rock brittleness on fragmentation.

The analysis of the available experimental data obtained in this research shows that increasing brittleness of rocks resulted in increasing fragmentation, for both steady compression test and dynamic fragmentation of rock by explosive on a laboratory scale. It was also shown that critical extension strain show better relationship with fragments size for blasting test than other concepts evaluated in

this research. In addition, the critical extension strain has almost equal correlation coefficients at both X_{50b} and X_{10b} of 0891 (Figure 7.1) and 0892 respectively.

If Figure 7.1 is extrapolated, the following relationship holds. When the critical extension strain of the rocks tends to zero, then X_{50b} is maximum at 14.244 mm (intercept on X_{50b}). As critical extension strain tends to maximum value, then X_{50b} tends to zero (intercept on e_c). Therefore the fragmentation and brittleness scale in Table 7.4 is obtained.

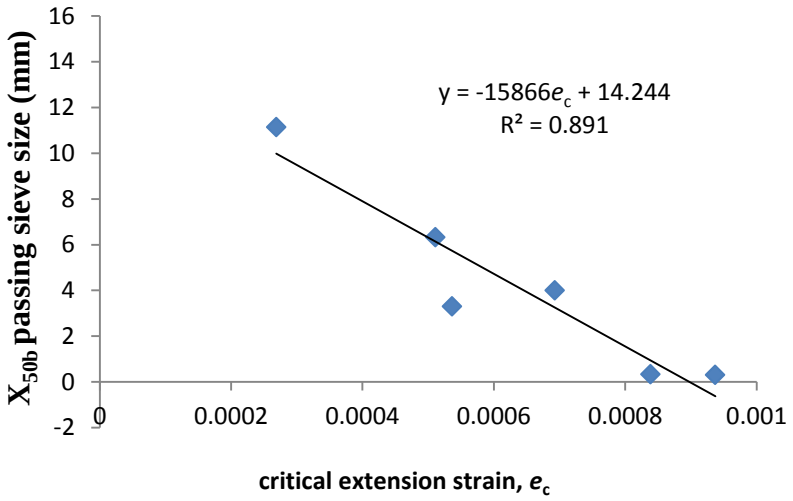

Figure 7.1 critical extension strain, e_c and X_{50b} passing sieve size (mm)

Table 7.4 Fragmentation and brittleness (based on critical extension strain, ε_c) scale

Critical extension strain, e_c	**Fragmentation in terms of Fragment size (mm) at X_{50b}**	**Fragmentation Quotients, *fi* (fragments size divided by average fragments size)**
0.000005	14.16467	1.988861275
0.0001	12.6574	1.777225498
0.0002	11.0708	1.554450997
0.0003	9.4842	1.331676495
0.000448884	**7.122 average fragments size**	1
0.0006	4.7244	0.663352991
0.0007	3.1378	0.440578489
0.0008	1.5512	0.217803988
0.000895	0.04393	0.006168211

Since the maximum fragments size obtainable is 14.244 mm (intercept on X_{50b} axis), therefore the mean fragments size is 14.244 divided by 2. If 7.122 mm is the mean fragments size from the analysis, then fragments above this value becomes coarser while fragments smaller than 7.122 mm becomes finer. The fragmentation quotient can be estimated using Figure 7.2 or $fi = -2227.7e_c + 2$ based on critical extension strain.

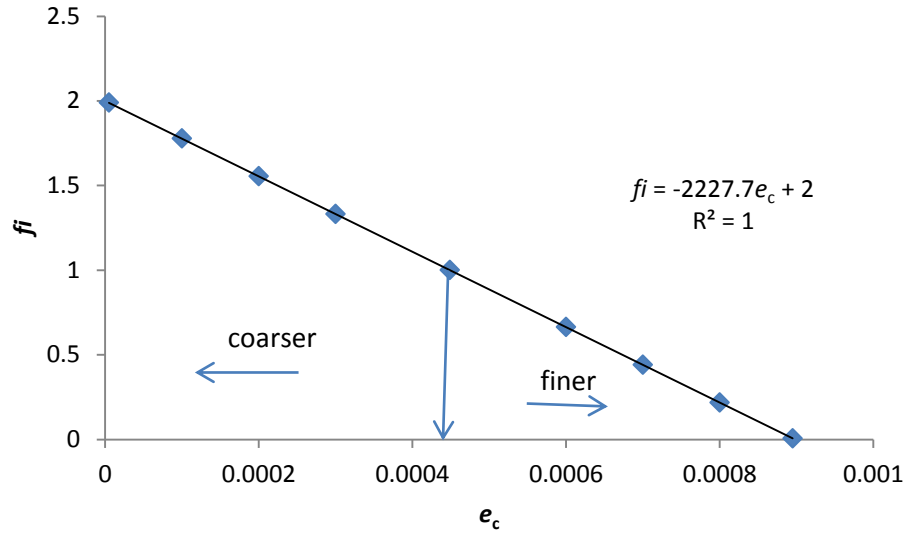

Figure 7.2 critical extension strain, e_c and fragmentation quotient, *fi*

Since the energy delivered by the explosive in the fragmentation process are the same for the blasted rocks, the fragmentation quotient (the fragments size divided by average fragments size) gives idea of utilisation of explosive energy in the fragmentation process of the rocks. The value of critical extension strain therefore gives insight into the effectiveness in the utilization of delivered explosive energy. This is to suggest that rocks with lower critical extension strain will required more explosive usage than rocks of larger critical extension strain value.

Consequently, the adjusted Kuz-Ram model is proposed (with addition factor, *fi*) as:

$$X_{50} = \left(\frac{(\log_e 2)^{1/n}}{\Gamma(1+1/n)}\right) * A * \left(\frac{1}{K^{0.8}}\right) * (fi * Q^{1/6}) * \left(\frac{115}{S_{anfo}}\right)^{19/30} \qquad (7.12)$$

where X_{50} is the mean fragments size (cm), fi is the fragmentation quotient ranging from 0.006 to 1.988 depending on the brittleness of the rock, and can be estimated

using $fi = -2227.7e_c + 2$ where e_c is the critical extension strain, Q is the mass of explosive being used (kg) and S_{anfo} is the relative weight strength of the explosive to ANFO, K is the powder factor (kg/m^3).

It is a fact that there are problems associated with scaling up from a laboratory to full scale blasting, however, this will give an indication of the expected outcome and provide a guide. This research introduces a modification (*fi*) to the empirical Kuz-Ram model to take into account the effect of increasing rock brittleness on fragmentation. It is also recommended that further research on full scale blasting test be initiated in order to appraise the effect of brittleness on fragmentation and the validity of the proposed modification to the Kuz-Ram model.

CHAPTER EIGHT

CONCLUSIONS AND RECOMMENDATIONS

8.1 Conclusions

8.1.1 Fragments Size from Compression Tests

An overall view of the probability density distribution models at X_{50s} and X_{10s} for the compression test, indicates that the X_{50} and X_{10} points are reached at smaller apertures for the Class II rocks than for Class I rocks, therefore, the Class II rocks are more finely fragmented. The comparison of rocks of similar strength using their UCS and BTS values, show that more fragments are passed at X_{50s} and X_{10s} for Class II rocks than the Class I rocks of similar strength. It can be stated that by breaking rocks under the same steady loading condition, the Class II rocks tend to be more fragmented than the Class I rocks.

8.1.1.1 *Comparison of Fragments Size from Compression with Static Mechanical Properties*

The comparison of static mechanical properties with the fragments size as a measure of fragmentation shows an inverse relationship, meaning that the higher the property value the more the fragmentation for the Class II but the same cannot be said for the Class I rocks.

8.1.1.2 *Comparison of Fragments Size from Compression with Dynamic Properties*

The dynamic properties show that fragments size from compression test only relates with the Class II rocks. It may be suggested that as the dynamic properties of rocks increases, the fragments size becomes finer for Class II rocks but the same cannot be said for Class I rocks.

8.1.1.3 *Comparison of Fragments Size from Compression Test with Brittleness Based on Static Mechanical Properties*

The correlations show that there is a link between brittleness and fragments size as a measure of fragmentation. Brittleness B_{13} and B_{14} correlated with fragmentation for the Class II rocks but the same cannot be said of Class I rocks. The correlation becomes stronger with the Class II rocks at lower percentage passing (X_{10s}). In addition, fragmentation becomes finer with increase in brittleness B_{13} and B_{14} at both X_{50s} and X_{10s} for the Class II rocks.

8.1.1.4 *Comparison of Fragments Size from Compression Tests with Brittleness Based on Moduli*

Brittleness B_{16} show correlation with the segregated samples but more correlated with the Class II rocks. The relationship between B_{16} and fragmentation shows that, at higher brittleness values the fragmentation becomes finer. Therefore, B_{16} could be useful index for the prediction of fragmentation for the segregated samples.

8.1.1.5 *Comparison of Fragments Size from Compression Test with Brittleness Based on Normalised Stress-Axial Strain Curve and Extension Strain Criterion*

Brittleness concepts estimated from the normalised stress-axial strain curve designated as NSSC and brittleness estimated from the extension strain criterion (i.e. critical extension strain), both did not correlate with the combined sample and they appear to treat the fragmentation of Class I and Class II rocks as separate entity. They show correlation with segregated samples with better spread in the distribution of the data plotted than other concepts. However, critical extension strain, appears to be applicable to much brittle rocks, as it only correlate with the Class I rocks after the removal of least brittle Marble data. Therefore NSSC could be a better concept for quantifying the brittleness of rock under compressive failure for the segregated samples (Class II and Class I).

8.1.2 Fragments Size from Blasting Tests

Similarly, an overview of fragments size using probability density distribution models at X_{50b} and X_{10b} for blasting test indicates that the X_{50} and X_{10} points are reached at smaller apertures for Class II rocks than Class I rocks, therefore, Class II rocks are more finely fragmented. The cumulative percentage against sieves size show that much are passed for Class II than the Class I rocks, therefore the Class II rocks are more finely fragmented.

8.1.2.1 *Fragments Size from Blasting Test and Brittleness Concepts Based on Static Mechanical Properties*

The brittleness concepts based on static mechanical properties relate with fragments size from the blasting test at X_{50b} and X_{10b} for the Class II rock but the same cannot be said of the combined sample. In comparison, the brittleness indices based on static mechanical properties have much stronger correlations with fragments size from blasting test than with the compression test. In particular, B_{14} appear to have stronger correlation with fragments size than other concepts based on static mechanical properties. Brittleness B_{14} show correlation with post-failure modulus and therefore is a useful tool for quantifying fragments size from blasting for the Class II rocks.

8.1.2.2 *Fragments Size from Blasting Tests and the Brittleness Concepts Based on Rock Moduli*

The brittleness indices based on the rock moduli relate with fragments size of the Class II rocks for blasting test. The relationships are stronger for both the combined sample and Class II rocks than was observed with the compression test. Brittleness B_{16} show better correlation for the Class II rocks and are more consistent in their relationships with the fragments size. It could be a useful index to relate brittleness with the fragments size from blasting test for Class II rocks, since the concept is a direct measure of the post-failure response of rock.

8.1.2.3 *Comparison of Fragments Size from Blasting Test with Brittleness Based on Normalised Stress-Axial Strain Curve and Extension Strain Criterion*

The brittleness concept estimated from normalised stress-axial strain curve, designated as NSSC and brittleness concept from extension strain criterion (i.e. critical extension strain, e_c), show better relationship and good spread in the data ploted for the combined sample of the blasting test than shown for both the brittleness concepts based on static mechanical properties and moduli. The relationships show that the higher the value of the brittleness concepts (i.e. NSSC and critical extension strain, e_c), the finer the fragmentation. The critical extension strain show stronger correlation at both X_{50b} and X_{10b} than the NSSC. Therefore, critical extension strain is a better index for quantifying brittleness of rock under blasting test for both the combined and Class II rocks.

8.1.3 Fragment Volumes and Brittleness

The brittleness concepts B_{16} based on moduli shows better correlation with fragments volumes (as total number of fragments per volume of rock) for both the blasting and compression tests. Similarly, brittleness B_{16} based on moduli and critical extension strain show better relationship with the volume of fines per volume of rock as a measure of fragmentation for the blasting test. Brittleness B_{16} as a direct measure of the post-failure response of rock is preferred as a measure of brittleness in the prediction of fragments volumes for the blasting tests.

8.1.4 Selection of Brittleness Concept Based on Different Measures of Fragmentation

The ability of the various brittleness concepts in their relationship with the different measures of fragmentation determined as the percentage of fragments passing selected sieves size, total number of fragments per volume of rock and volume of fines per volume of rock were assessed. From the assessment, critical extension strain is proposed as a measure of brittleness in the process of rock fragmentation by blasting test while NSSC estimated from normalised stress-axial strain curve is proposed as a measure of brittleness in the process of rock fragmentation under uniaxial compression test for segregated samples. The correlations of the different measures of fragmentation with brittleness increase with increasing effect of brittleness and stronger as rock behaviour is more pronounced as Class II in both the compression and the blasting tests.

8.1.5 Brittleness Concept for Different Measures of Fragmentation

It has been shown that brittleness is linked to fragmentation. There are a number of definitions of brittleness and several ways to measure fragmentation. The link means that it is possible to predict fragmentation by using brittleness. Depending on the measures of fragmentation the user is interested in:

(a) If the user is interested in prediction of fragmentation evaluated as a certain size of fragments at X_{50s} and X_{10s} from compression test, use the definition of brittleness "k" in the Equation 8.1 and 8.2 for combined sample.

Equation 8.1 and 8.2 is the statistical analysis result of fragments at X_{50s}, X_{10s} and brittleness k for the combined sample.

$$X_{10_S} = -1.798k + 0.435 \quad (8.1)$$

$$X_{50_S} = -1.391k + 28.744 \quad (8.2)$$

For the segregated sample, the definition given by NSSC show better relationship and good spread in data plotted. Equation 8.3 and 8.4 are best for the Class II:

$$X_{50s} = 3587.8\text{NSSC} + 17.894 \quad (8.3)$$

$$X_{10s} = 5081\text{NSSC} - 9.4907 \quad (8.4)$$

For the Class I, Equation 8.5 and 8.6 are most appropriate.

$$X_{50s} = -7063.7\text{NSSC} + 48.487 \quad (8.5)$$

$$X_{10s} = -9564.9\text{NSSC} + 30.19 \quad (8.6)$$

(b) If the user is interested in prediction of fragmentation evaluated as a certain size of fragments at X_{50b} and X_{10b} for the blasting test, use the definition of brittleness defined as critical extension strain "e_c" in the Equation 8.7 and 8.8.

$$X_{50b} = -15866e_c + 14.244 \quad (8.7)$$

$$X_{10b} = -1197.9e_c + 1.2108 \quad (8.8)$$

(c) If the user is interested in prediction of fragmentation evaluated as the total number of fragments per volume of rock use the definition of brittleness "B_{16}" in Equation 8.9 for the compression test and Equation 8.10 for blasting test.

$$FV_S = 5\text{E-}06B_{16} + 0.0208 \quad (8.9)$$

$$FV_b = 0.0002B_{16} + 0.2703 \quad (8.10)$$

(d) If the user is interested in prediction of fragmentation evaluated as volume of fines per volume of rock, use the definition of brittleness "B_{16}" in Equation 8.11 for the blasting test.

$$VV_b = -5E\text{-}05B_{16} + 0.5016 \quad (8.11)$$

In summary:

- Brittleness relates with fragmentation.
- The relationship between brittleness and fragmentation is stronger for the Class II rocks than the Class I rocks included in the study.
- Different definitions of brittleness are more effective in predicting fragmentation for different purposes.

8.2 Further Research and Recommendations

8.2.1 Further Research

Detailed research can be initiated to study the relationship between brittleness and fragmentation based on the mineralogy of the rock and energy utilised in the fragmentation process.

More research into laboratory scale and large or field scale blasting should be initiated to compared the results for fragmentation of Class II and Class I rocks. This research should involve many different rock types in order to increase the sample size for the research.

The research could be extended to observe fines generated and fragments size from size reduction equipment such as in a crusher and a mill. The observations should allow comparison for the Class II and Class I rocks.

8.2.2 Recommendations

Although not part of the focus of this research, the knowledge about the post-peak behaviour of rocks will assist in the evaluation of the potential failure of an excavation and the rockburst potential near underground openings (possibly that, Class I failure gradual, Class II failure explosive).

Adjustment to the Kuz-Ram model (Equation 8.12) is proposed to take into account the brittleness behaviour of rock with additional factor, *fi*.

$$X_{50} = \left(\frac{(\log_e 2)^{1/n}}{\Gamma(1+1/n)} \right) * A * \left(\frac{1}{K^{0.8}} \right) * (fi * Q^{1/6}) * \left(\frac{115}{S_{anfo}} \right)^{19/30} \qquad (8.12)$$

where X_{50} is the mean fragments size (cm), fi is the fragmentation quotient ranging from 0.006 to 1.988 depending on the brittleness of the rock, estimated as critical extension strain, Q is the mass of explosive being used (kg) and S_{anfo} is the relative weight strength of the explosive to ANFO, K *i*s the powder factor (kg/m^3).

It is a fact that there are problems associated with scaling up from a laboratory to full scale blasting, however, this will give an indication of the expected outcome and provide a guide. This research introduces a modification to the empirical Kuz-Ram model (*fi*) to take into account the effect of increasing rock brittleness on fragmentation. It is also recommended that further research on full scale blasting

tests be initiated in order to appraise the effect of brittleness on fragmentation and the validity of the proposed modification to the Kuz-Ram model.

REFERENCES

AASHTO T 27/T (2009). *Sieve analysis of fine and coarse aggregates Fop for AASHTO* t 27 (09). Retrieved from http://itd.idaho.gov/manuals/online_manuals/current_manuals/qa%20manual/FOPs/T27%2011_short_wpr.pdf. [Accessed 12 March 2012].

Ahrens, T. J. (Ed.). (1995). *Rock physics & phase relations: A handbook of physical constants* (3rd Ed.). Washington DC: American Geophysical Union.

Al-Chalabi, M., & Huang, C.L. (1974). Stress distribution within circular cylinders in compression. *International Journal of Rock Mechanics and Mining Sciences & Geomechanics Abstracts*, *11*, 45- 56.

Alekseev, A. D., Zhuravlev, V. I., Yarovaya, L. I., & Molchanenko, V. S. (1970). Effect of the geometry and fracturing of rock specimens on their strength. *Journal of Mining Science, 6*(3), 281-285.

Altindag, R. (2002). The evaluation of rock brittleness concept on rotary blast hole drills. *Journal of the South African Institute of Mining and Metallurgy, 102*(1), 61-66.

Altindag, R. (2003). Correlation of specific energy with rock brittleness concepts on rock cutting. *Journal of the South African Institute of Mining and Metallurgy, 103*(3), 163-171.

Altindag, R. (2010a). Assessment of some brittleness indices in rock-drilling efficiency. *Rock Mechanics and Rock Engineering*, *43*(3), 361-370.

Altindag, R. (2010b). Reply to the discussion by Yagiz on "Assessment of some brittleness indices in rock-drilling efficiency". *Rock Mechanics and Rock Engineering*, *43*(3), 375-376. DOI: 10.1007/s00603-009-0057-x.

Altindag, R., & Guney, A. (2010). Predicting the relationships between brittleness and mechanical properties (UCS, TS and SH) of rocks. *Scientific Research and Essays*, *5*(16), 2107-2118.

Andreev, G. E. (1995). *Brittle failure of rock materials: Test results and constitutive models*. Rotterdam, Netherlands: A. A. Balkema.

ASTM. (2002). *Standard method of test for elastic moduli of rock core specimens in uniaxial compression.* American Society for Testing and Material, ASTM (Designation D3148-72). Retrieved from

http://www.nosazimadares.ir/fanni/khak/DocLib4/D%203148%20%E2%80%93%2096%20%20;RDMXNDGTUKVE.pdf [Accessed 19 March 2012].

Baron, L. I., Loguntsov, B. M., & Pozin, E. Z. (1962). Determination of properties of rocks. *(*in Russian).Gozgotekhizdat, Moscow.

Batougina, I. M., Petoukhov, I. M., Vinokur, B. S., Smirnov, V. A., & Rabota, E. N. (1983). *Methodological instructions for rockburst prophylaxis accounting the deposit geodynamics.* Leningrad: VNIMI.

Bergman, S.G.A., & Stille, H. (1983, April). *Rockburst problems in a 2.6 million m^3 underground crude oil storage in Granite*. Proceedings of the 5th Congress of ISRM, Melbourne.

Bieniawski, Z. T. (1966). *Mechanism of rock fracture in compression* (Report No. MEG 459). Pretoria, South Africa: Rock Mechanics Division, National Mechanical Engineering Research Institute, Council for Scientific and Industrial Research.

Bieniawski, Z. T. (1967a). Stability concept of brittle fracture propagation in rock. *Engineering Geology*, *2*(3), 149-162.

Bieniawski, Z. T. (1967b). Mechanism of brittle fracture of rock: Part II--experimental studies. *International Journal of Rock Mechanics and Mining Sciences & Geomechanics Abstracts*, *4*(4), 407-423. Retrieved from

ftp://tiliva.ethz.ch/Neil_Mancktelow/Faults/Wing%20cracks%20stepover%20and%20compressional%20bridges/Bieniawski_1967.pdf [Accessed 23 April 2012]

Bieniawski, Z. T. (1967c). Mechanism of brittle fracture of rock: Part I--theory of the fracture process. *International Journal of Rock Mechanics and Mining Sciences & Geomechanics Abstracts*, *4*(4), 395-404. DOI:10.1016/0148-9062(67)90030-7.

Bieniawski, Z. T. (1967d). Mechanism of brittle fracture of rock: Part III--fracture in tension and under long-term loading. *International Journal of Rock Mechanics and Mining Sciences & Geomechanics Abstracts*, *4*(4), 425-430.

Blake, G. R. (1980, July). *Proposed standards and specifications for quality of sand for sand-soil-peat mixes*. Proceedings of the 3rd International Turf grass Research Conference, Munich, German Federal Republic.

Blanton, T. L. (1981). Effect of strain rates from 10-2 to 10 sec-1 in triaxial compression tests on three rocks. *International Journal of Rock Mechanics and Mining Sciences & Geomechanics Abstracts 18*(1), 47-62.

Blindheim, O. T., & Bruland, A. (1998). Boreability testing Norwegian TBM tunnelling 30 years of experience with TBMs in Norwegian tunnelling. *Norwegian Soil and Rock Engineering Association, 11*, 29-34.

Bohloli, B., Hoven, E. (2007). A laboratory and full-scale study on the fragmentation behaviour of rock. *Journal of Engineering Geology, 89*(1), 1-8.

Bordia, S. K. (1971). The effect of size and stress concentration on the dilatancy and fracture of rock. *International Journal of Rock Mechanics and Mining Sciences & Geomechanics Abstracts, 8*(6), 629-640.

Brace, W. F. (1961). *Dependence of fracture strength of rocks on grain size*. In H. L. Hartman (Ed.), Proceedings of the 4th Symposium on Rock Mechanics. Bulletin of the Mineral Industries Experiment Station (99-103). USA: The Pennsylvania State University.

Brace, W. F., & Byerlee, J. D. (1966). *Recent experimental studies of brittle fracture of rocks*. In C. Fairhurst (Ed.), Proceedings of the 8th US Symposium on Rock

Mechanics (USRMS). Failure and Breakage of Rocks (58-81). Minneapolis, MN, USA: American Institute of Mining, Metallurgical, and Petroleum Engineers Inc.

Brace, W.F., Paulding, B.W., & Scholz, C. (1966). Dilatancy in the fracture of crystalline rocks. *J. Geophysics. Res., 71*, 3939–3953.

Brady, B. T. (1971). An exact solution to the radially end-constrained circular cylinder under triaxial loading. *International Journal of Rock Mechanics and Mining Sciences & Geomechanics Abstracts, 8*(2), 165-178.

Brady, B. T. (1971a). Effects of inserts on the elastic behaviour of cylindrical materials loaded between rough end-plates. *International Journal of Rock Mechanics and Mining Sciences & Geomechanics Abstracts 8*(4), 357-369.

Brady, B. T. (1971b). Initiation of failure in a radially end-constrained circular cylinder of brittle rock. *International Journal of Rock Mechanics and Mining Sciences & Geomechanics Abstracts, 8*(4), 371-387.

Brady, B. T. (1971c). The effect of confining pressure on the elastic stress distribution in a radially end-constrained circular cylinder. *International Journal of Rock Mechanics and Mining Sciences & Geomechanics Abstracts, 8*(2), 153-164.

Brijes, M., Dachao, N. (2013). Experimental investigation of the effect of change in control modes on the post-failure behaviour of coal and coal measures rock. *International Journal of Rock Mechanics & Mining Sciences 60,* 363–369

Broek, D. (Ed.). (1986). *Elementary engineering fracture mechanics* (4th Ed.). Netherlands: Martinus Nijhoff Publishers. (Dordrecht and Boston and Hingham, Mass., U.S.A.) (ISBN 9024725801) 501 p.

Burshtein, L. S. (1967). Tension and compression diagrams for Sandstone. *Journal of Mining Science, 3*(1), 16-20.

Burshtein, L. S. (1969). Effect of moisture on the strength and deformability of Sandstone. *Journal of Mining Science, 5*(5), 573-576.

Cai, M., Kaiser, P. K., Uno, H., Tasaka, Y., Minami, M. (2004). Estimation of rock mass deformation modulus and strength of jointed hard rock masses using GSI system. *Int. J. Rock Mech. Min. Sci. 41,* 3-19.

Coates, D. F., & Parsons, R. C. (1966). Experimental criteria for classification of rock substances. *International Journal of Rock Mechanics and Mining Science & Geomechanics Abstracts, 3*(3), 181-189.

Craggs, J. W. (1960). On the propagation of a crack in an elastic-brittle material. *Journal of the Mechanics and Physics of Solids, 8*(1), 66-75.

Cunningham, C. (1983). *The Kuz-Ram model for prediction of fragmentation from blasting*. In R. Holmberg, & A. Rustan, (Eds.). Proceedings of the First Int. Symp. of Rock Fragmentation by Blasting (439-453). Lulea, Sweden: Lulea Univ. of Tech.

Dahl, F. (2003). The suggested DRI, BWI, CLI Standards. NTNU, Angleggsdrift, Trondheim. Retrieved from

http://www.drillability.com/13A-98eng.pdf [Accessed April 2012]

Dey, T. N., & Wang, C. Y. (1981). Some mechanisms of microcrack growth and interaction in compressive rock failure. *International Journal of Rock Mechanics and Mining Science & Geomechanics Abstracts, 18*(3), 199-209.

Dhir, R. K., & Sangha, C. M. (1973). Relationships between size, deformation and strength for cylindrical specimens loaded in uniaxial compression. *International Journal of Rock Mechanics and Mining Sciences & Geomechanics Abstracts, 10*(6), 699-712.

Djordjevic, N. (1999). *Two-component model of blast fragmentation*. In C.V.B. Cunningham (Ed.), Proceedings of Sixth International Symposium on Rock Fragmentation by Blasting (Symposium Series S21, 213–219). Johannesburg, South Africa: SAIMM.

Du, Y., & Aydin, A. (1991). Interaction of multiple cracks and formation of echelon crack arrays. *International Journal for Numerical and Analytical Methods in Geomechanics, 15*(3), 205-218.

Dulaney, E. N., & Brace, W. F. (1960). Velocity behaviour of a growing crack. *Journal of Applied Physics, 31*(12), 2233-2236.

Eberhardt, E., Stead, D., & Szczepanik, Z. (1998). *Crack initiation and propagation in Granite and granodiorite from the 130 m and 420 m levels of the URL*. (Report No. AECL 122567). Manitoba, Canada : Atomic Energy of Canada Limited.

Eberhardt, E., Stead, D., Stimpson, B., & Lajtai, E. Z. (1998). The effect of neighbouring cracks on elliptical crack initiation and propagation in uniaxial and triaxial stress fields. *Engineering Fracture Mechanics, 59*(2), 103-115.

Eberhardt, E., Stead, D., Stimpson, B., & Read, R. S. (1998). Identifying crack initiation and propagation thresholds in brittle rock. *Canadian Geotechnical Journal, 35*(2), 222-233.

Evans, B., Fredrich, J. T., & Wong, T. F. (1990). The brittle-ductile transition in rocks: Recent experimental and theoretical progress. In A. G. Duba, W. B. Durham, J. W. Handin, & H. F. Wang (Eds.), *The Brittle-Ductile Transition in Rocks: The Heard Volume* (1-20). Corvallis, America: American Geophysical Union

Fredrich, J. T., Evans, B., & Wong, T. F. (1990). Effect of grain size on brittle and semi brittle strength: Implications for micromechanical modelling of failure in compression. *Journal of Geophysical Research, 95*(B7), 10,907-10,920.

Fujii, Y., Kiyama, T., Ishijima1 Y., & Kodama, J. (1998). Examination of a Rock Failure Criterion Based on Circumferential Tensile Strain. *Pure appl. geophys. 152*, 551–577.

Germanovich, L. N., Salganik, R. L., Dyskin, A. V., & Lee, K. K. (1994). Mechanisms of brittle fracture of rock with pre-existing cracks in compression. *Pure and Applied Geophysics*, *143*(1), 117-149.

Gheibie S., Aghababaei H., Hoseinie S.H., & Pourrahimian Y. (2009). Modified Kuz—Ram fragmentation model and its use at the Sungun Copper Mine. *International Journal of Rock Mechanics & Mining Sciences, 46*, 967–973

Goktan, R., & Yilmaz, N. G. (2005). A new methodology for the analysis of the relationship between rock brittleness index and drag pick cutting efficiency. *Journal of the South African Institute of Mining and Metallurgy*, *105*(10), 727.

Grady, D. E., & Kipp, M. E. (1987). *Dynamic rock fragmentation*. London, UK: Academic Press.

Gramberg J., 1989. *A Non-Conventional View on Rock Mechanics and Fracture Mechanics*. Rotterdam, Netherlands: A. A. Balkema

Green, S. J., & Perkins, R. D. (1972). *Uniaxial compression tests at varying strain rates on three geological materials*. In K. E. Grey (Ed.), Proceedings of the 10th Symposium on Rock Mechanics. Basic and Applied Rock Mechanics (35-54). New York: AIME.

Griffith, A. A. (1924). *Theory of rupture*. In C. B. Biezeno & J. M. Burges (Eds.), Proceedings of the First International Congress of Applied Mechanics (55-63). Delft, Netherlands: Tech. Boekhandel en Drukkerij J. Waltwan Jr.

Grosvenor, N. E. (1963). Specimen proportion key to better compressive strength tests. *Mining Engineering, 14*(1), 54.

Gupta, R.N., Ghose, A.K., Mozumdar, B.K., Nabibullah, M.D., Pal Roy, P., & Singh, B., (1990, November). *Design of blasting patterns using presplitting with air deck technique for dragline and heavy shovel benches near populated areas*. Proceedings of International Symposium on Explosive and Blasting Technique (128–135), New Delhi

Haimson, B. (2007). *Experimental rock mechanics*. London, UK: Taylor & Francis.

Hajiabdolmajid, V., & Kaiser, P. (2003). Brittleness of rock and stability assessment in hard rock tunnelling. *Tunnelling and Underground Space Technology, 18*(1), 35-48.

Hakala, M.K., & Heikkilä, E. 1997, S*ummary report, development of laboratory tests and the stress strain behaviour of olkiluoto mica gneiss* (Report No. Posiva 97-04). Helsinki, Finland: Posiva Oy.

Hawkes, I., & Mellor, M. (1970). Uniaxial testing in rock mechanics laboratories. *Engineering Geology, 4*(3), 179-285.

Hawkins, A. B. (1998). Aspects of rock strength. *Bulletin of Engineering Geology and the Environment, 57*(1), 17-30.

He, C., Okubo, S., & Nishimatsu, Y. (1990). A study of the Class II behaviour of rock. *Rock Mechanics and Rock Engineering, 23*(4), 261-273.

Hodgson, K., & Cook, N. G. (1970). The effects of size and stress gradient on the strength of rock. *International Journal of Rock Mechanics and Mining Science & Geomechanics Abstracts, 1*(1-19), 31-34.

Hoek, E. (1977). Rock mechanics laboratory testing in the context of a consulting engineering organization. *International Journal of Rock Mechanics and Mining Sciences & Geomechanics Abstracts 14*(2), 93-101.

Hoek, E., & Brown, E.T. (1980). Underground excavations in rock. London, UK: The Institute of Mining and Metallurgy

Honda, H., & Sanada, Y. (1956). Hardness of coal. *Fuel, 35,* 451.

Horii, H., & Nemat-Nasser, S. (1985). Compression-induced microcrack growth in brittle solids: Axial splitting and shear failure. *Journal of Geophysical Research, 90*(B4), 3105-3125.

Hoskins, J. R., & Horino, F. G. (1969). *Influence of spherical head size and specimen diameters on the uniaxial compressive strength of rocks* (Report No. 7234). Washington, D.C, US: Bureau of Mines, United States Department of the Interior.

Hossaini, M. F., Ghafoori, R., Yarahmadi, A., & Pourghasemi, M. (2013, February). *Effect of dynamic elastic properties of rock on fragmentation in Choghart Iron ore Mi*ne, *Central Iran*. Proceedings of the 13th Coal Operators' Conference (413-418), University of Wollongong, Australia. Retrieved from

http://ro.uow.edu.au/cgi/viewcontent.cgi?article=2142&context=coal [Accessed July 2013]

Hucka, V., & Das, B. (1974). Brittleness determination of rocks by different methods. *International Journal of Rock Mechanics and Mining Sciences & Geomechanics Abstracts*, *11*(10), 389-392.

Hudson, J. A., Brown, E. T., & Fairhurst, C. (1971). Optimizing the control of rock failure in servo-controlled laboratory tests. *Rock Mechanics and Rock Engineering*, *3*(4), 217-224.

Hudson, J. A., Brown, E. T., & Rummel, F. (1972). The controlled failure of rock discs and rings loaded in diametric compression. *International Journal of Rock Mechanics and Mining Sciences & Geomechanics Abstracts*, *9*(2), 241-244.

Hudson, J. A., Crouch, S. L., & Fairhurst, C. (1972). Soft, stiff and servo-controlled testing machines: A review with reference to rock failure. *Engineering Geology*, *6*(3), 155-189.

Hudson, J.A. (1989). *Rock mechanics principles in engineering practice*. London: Butterworth.

Hudson, J.A., Brown, E.T., & Fairhurst, C. (1971). *Shape of the complete stress–strain curve for rock*. In E. Cording (Ed.), Proceedings of the 13th US Symposium on Rock Mechanics (773-795). New York: Am. Soc. Civ. Eng.

Hugman, R. H. H., & Friedman, M. (1979). Effects of texture and composition on mechanical behaviour of experimentally deformed carbonate rocks. *The American Association of Petroleum Geologists Bulletin, 63*(9), 1478-1489.

International Society for Rock Mechanics Commission on Testing Methods. (2007). ISRM suggested methods for rock characterization, testing and monitoring. In R. Ulusay & J. A. Hudson (Eds.), *Draft ISRM suggested method for the complete stress-strain curve for intact rock in uniaxial compression*. Ankara, Turkey: Pergamon Press Ltd published for Commission on Testing Methods, International Society for Rock Mechanics,

International Society for Rock Mechanics. (1981). Rock characterization, testing and monitoring, ISRM suggested methods. In E.T. Brown (Ed.), *Suggested method for determining deformability of rock materials in uniaxial compression* (138-140). New York: Oxford Pergamon Press Published for the Commission on Testing Methods, International Society for Rock Mechanics.

Itasca Consulting Group, Inc. (2003). *Particle flow code in 3 dimensions*. Minneapolis, USA: Itasca

Jackson, K., Kingman, S. W., Whittles, D. N., Lowndes, I. S., & Reddish, D. J. (2008). The effect of strain rate on the breakage behaviour of rock. *Archives of Mining Sciences, 53*(1), 3.

Jaeger, J. C. (1960). Rock failure at low confining pressures. *Engineering, 189*, 283-284.

Jaeger, J.C. (1967). *Brittle fracture of rocks*. In C. Fairhurst (Ed.) Failure and breakage of rock. Proceedings of the 8th Symposium on Rock Mech. (3-58). New York: AIME

Jira´sek, M., Rolshoven, S., & Grassl, P. (2004). Size effect on fracture energy induced by nonlocality. *Int. J. Numer. Anal. Meth. Geomech.*, *28*, 653–70.5

Jirasek, M., Rolshoven, S., & Grassl, P. (2004). Size effect on fracture energy induced by non-locality. *International Journal for Numerical and Analytical Methods in Geomechanics, 28*(7-8), 653-670.

John, M. (1972). *The influence of length to diameter ratio on rock properties in uniaxial compression: A contribution to standardization in rock mechanics testing, South Africa* (No. Rep S Afr CSIR No ME1083/5).

Johnson, R. B., & DeGraff, J. V. (1988). *Principles of engineering geology*. New York: John Wiley and Sons.

Kahraman, S. (2002). Correlation of TBM and drilling machine performances with rock brittleness. *Engineering Geology, 65*(4), 269-283.

Kaiser, P. K., & Morgenstern, N. R. (1981). Phenomenological model for rock with time-dependent strength. *International Journal of Rock Mechanics and Mining Sciences & Geomechanics Abstracts, 18*(2), 153-165.

Kemeny, J., & Cook, N.G.W. (1986). Effective moduli, non-linear deformation and strength of a cracked elastic solid. *International Journal of Rock Mechanics and Mining Sciences & Geomechanics Abstracts*, *23*, 107-118.

Kobayashi, R. (1970). On mechanical behaviour of rocks under various loading-rates. *Japanese Rock Mechanics*, *1*, 56-58.

Kovari, K., & Tisa, A. (1975). Multiple failure state and strain controlled triaxial tests. *Rock Mechanics and Rock Engineering, 7*(1), 17-33.

Kumar, A. (1968). The effect of stress rate and temperature on the strength of basalt and Granite. *Geophysics, 33*(3), 501-510.

Kuznetsov V. M. (1973). The mean diameter of fragments formed by blasting rock. *Soviet Mining Science*, *9*, 144–8.

Lajtai, E. Z., & Lajtai, V. N. (1974). The evolution of brittle fracture in rocks. *Journal of the Geological Society, 130*(1), 1-18.

Lajtai, E. Z., Duncan, E. J. S., & Carter, B. J. (1991). The effect of strain rate on rock strength. *Rock Mechanics and Rock Engineering, 24*(2), 99-109.

Lawn, B. R., & Marshall, D. B. (1979). Hardness, toughness, and brittleness- an indentation analysis. *J. Am .Ceram. Soc., 62*(7), 347-350.

Li, X., Hong, L., Zhou, Z., Yin, T., Liao, G., & Ye, Z. (2009). Energy consumption in rock fragmentation at intermediate strain rate. *J. Cent. South Univ. Technol*. *16*, 0677−0682

Li, X., Lai, H., & Gu D. (1992). Energy absorption of rock fragmentation under impulsive loads with different wave forms. *Journal of Transactions of Nonferrous Metals Society of China*, *2*(4), 10-14 (in Chinese)

Lindholm, U. S., Yeakley, L. M., & Nagy, A. (1974). The dynamic strength and fracture properties of dresser basalt. *International Journal of Rock Mechanics and Mining Science & Geomechanics Abstracts*, *11*(5), 181-191.

Liu, H. Y., Roquete, M., Kou, S. Q., & Lindqvist, P. A. (2004). Characterization of rock heterogeneity and numerical verification. *Engineering Geology*, *72*(1-2), 89-119.

Liu, H., Kou, S., & Arne, P. (2004). *Microscope rock texture characterization and simulation of rock aggregate properties* (SGU project 60-1362). Lulea, Sweden: Geological Survey of Sweden. Retrieved from

http://www.sgu.se/dokument/fou_extern/Hongyuan-et-al_del1.pdf [Accessed October 2011]

Lockner, D. A. (1995). Rock failure. In Ahrens, T. J. (Ed.), *Rock physics and phase Relations—A handbook of physical constants* (127-147). Washington DC: American Geophysical Union.

Lockner, D. A., Moore, D. E., & Reches, Z. (1992, June). *Microcrack interaction leading to shear fracture*. Proceedings of the 33rd US Rock Mechanics Symposium (807-816), Santa Fe, NM, USA.

Lockner, D.A., Byerlee, J.D., Kuksenko, V., Ponomarev, A., & Sidorin A. (1992). Fault mechanics and transport properties of rock. In B. Evans, & T. F. Wong (Eds.), *Observations of quasistatic fault growth from acoustic* emissions (1-20). New York: Academic Press, Harcourt Brace Jovanovich.

Logan, J.M., & Handin, J.M. (1971). Triaxial compression testing at intermediate strain rates. In G. B. Clark, (Ed.), *Dynamic Rock Mechanics. Proceedings of the 12th US Symposium on Rock Mechanics* (167-194). New York: AIME

Manjikov, B.T., Mansourov, VA., Pougacheva, T.N., & Tileguenov, K.T. (1983). Laboratory estimation of rockbursting danger. *SSDRRMODMA*, Frounze, IIim, 94-102 (in Russian)

Martin, C.D. (1993). *The strength of massive lac du bonnet Granite around underground openings*. (Doctoral Dissertation). University of Manitoba, Winnipeg. Retrieved from

http://hdl.handle.net/1993/9785 [Accessed March 2012]

Martin, C.D., & Chandler, N. A. (1994). The progressive fracture of lac du bonnet Granite. *International Journal of Rock Mechanics and Mining Sciences & Geomechanics Abstracts, 31*(6), 643-659.

McSaveney, M.J., & Davies, T.R. (2009). Surface energy is not one of the energy losses in rock comminution. *Engineering Geology*, *109*, 109-113.

Mellegard, K.D., Pfeifle, T.W., Fossum, A.F. & Senseny, P.E. (1993) Pressure and flexible membrane effects on direct-contact extensometer measurements in axisymmetric compression tests. *Journal of Testing and Evaluation, 21* (6), 530-538.

Mellor, M. (1973, July). *Mechanical properties of rocks at low temperatures*. The North American Contribution to the Second International Conference on Permafrost (334-344), Siberia.

Mogi, K. (1966). Some precise measurements of fracture strength of rocks under uniform compressive stress. *Rock Mech. Eng. Geol, 4*(1), 41-55.

Mogi, K. (2007). *Experimental rock mechanics*. London: Taylor & Francis.

Mogi, K. (1962). The influence of the dimensions of specimens on the fracture strength of rocks. *Bulletin of Earthquake Research Institute, 40,* 175-185.

Moser, Cheimanoff, Ortiz & Hochholdinger, (2000). Explosive and blasting technique. In R. Holmberg (Ed.), *Breakage characteristics in rock blasting*. Rotterdam: Balkema, A. A.

Moser, P., Olsson, M., Ouchterlony, F. & Grasedieck, A. (2003). *Comparison of the blast fragmentation from lab-scale and full-scale tests at Bårarp*. In R. Holmberg (Ed.), Proceedings of EFEE Second World Conference on Explosives and Blasting Technique (449–458). Rotterdam: Balkema, A. A.

MTS Systems Corporation (1996). *TestStar A to Z An encyclopaedia of testing*. Eden Prairie, MN: MTS. Retrieved from

http://amet-me.mnsu.edu/userfilesshared/DATA_ACQUISITION/mts/backup/New060904/ts2/docs/tsii_a2z.pdf [Accessed November 2010]

MTS Systems Corporation (2004). R*ock and concrete mechanics testing systems: technical description*. Eden Prairie Minnesota: MTS.

Nishimatsu, Y., Okubo, S., Yamaguchi, T., & Koizumi, S. (1981). The effect of strain rate on the failure process of rocks in compression. *J. Min. Me-Tall. Inst. Japan, 97*, 1163-1168.

Obert, L., & Duvall, W. I. (1967). *Rock mechanics and the design of structures in rock*. New York: John Wiley and Sons.

Obert, L.K., Windes, S.L. & Duvall, W.I. (1946). *Standardised tests for determining the physical properties of mine rocks* (Report No. 3891). Washington, D.C, US: Bureau of Mines, United States Department of the Interior.

Ouchterlony, F (2005a). What does the fragments size distribution of blasted rock look like? *Brighton Conference Proceedings, R. Holmberg et al (Ed.), European Federation of Explosives Engineers, ISBN 0-9550290-0-7.*

Ouchterlony, F. (2005b). The Swebrec© function: linking fragmentation by blasting and crushing. Trans. *Inst. Min. Mater. Metall*. A. Vol.114.

Ojo, O., & Brook, N. (1990). The effect of moisture on some mechanical properties of rock. *Mining Science and Technology, 10*(2), 145-156.

Okubo, S., & Fukui, K. (1996). Pre- and post-failure stress strain curves for various rock types in uniaxial tension. *International Journal of Rock Mechanics and Mining Sciences & Geomechanics Abstracts, 33*(6), 549-556.

Okubo, S., & Nishimatsu, Y. (1985). Uniaxial compression testing using a linear combination of stress and strain as the control variable. *International Journal of Rock Mechanics and Mining Sciences & Geomechanics Abstracts, 22*(5), 323-330.

Okubo, S., Nishimatsu, Y., & He, C. (1990). Technical note: Loading rate dependence of Class II rock behaviour in uniaxial and triaxial compression tests: An application of a proposed new control method *International Journal of Rock Mechanics and Mining Sciences & Geomechanics Abstracts, 27*, 559-562.

Olsson, W. A. (1974). Grain size dependence of yield stress in Marble. *Journal of Geophysical Research, 79*(32), 4859-4862.

Onodera, T. F., & Kumara, H. M. (1980). Relationship between texture and mechanical properties of rocks. *Bulletin of International Association of Engineering Geology, 22*, 173-177.

Ozkahraman, H. T. (2008). Breakage mechanisms and an encouraging correlation between the bond parameters and the friability value. *The Journal of the Southern African Institute of Mining and Metallurgy, 110,* 153-159.

Pan, P. Z., Feng, X. T., & Hudson, J. A. (2006). Numerical simulations of Class I and Class II uniaxial compression curves using an elasto-plastic cellular automaton and a linear combination of stress and strain as the control method. *International Journal of Rock Mechanics and Mining Sciences, 43*(7), 1109-1117.

Pan, P. Z., Feng, X. T., & Hudson, J. A. (2009). Study of failure and scale effects in rocks under uniaxial compression using 3D cellular automata. *International Journal of Rock Mechanics and Mining Sciences, 46*(4), 674-685.

Paterson, M. S. (1978). *Experimental rock deformation- the brittle field*. New York: Springer-Verlag.

Peng, S. D. (1971). Stresses within elastic circular cylinders loaded uniaxially and triaxially. *International Journal of Rock Mechanics and Mining Sciences & Geomechanics Abstracts, 8*(5), 399-432.

Peng, S. S. (1973). Time-dependent aspects of rock behaviour as measured by a servo-controlled hydraulic testing machine. *International Journal of Rock Mechanics and Mining Sciences & Geomechanics Abstracts, 10*(3), 235-236.

Peng, S., & Johnson, A. M. (1972). Crack growth and faulting in cylindrical specimens of Chelmsford Granite. *International Journal of Rock Mechanics Mining Science and Geomechanics Abstract, 9*, 37-386.

Perkins, R. D., Green, S. J., & Friedman, M. (1970). Uniaxial stress behaviour of porphyritic Tonalite at strain rates to 10^{-3}/second. *International Journal of Rock Mechanics and Mining Sciences & Geomechanics Abstracts 7*(5), 527-528.

Pratt, H. R., Black, A. D., Brown, W. S., & Brace, W. R. (1972). The effect of specimen size on the mechanical properties of unjointed diorite. *International Journal Rock Mechanics Mining Science, 9*, 513-529.

Prikryl, R. (2001). Some microstructural aspects of strength variation in rocks. *International Journal of Rock Mechanics and Mining Sciences, 38*(5), 671-682.

Protodyakonov, M. M. (1963). Mechanical properties and drillability of rocks. In Fairhurst C. (Ed.), *Proceedings of the 5th Symposium on Rock Mechanics,* University of Minnesota (103-118). Minnesota, USA: Oxford, Pergamon Press

Qi, C., Wang, M., & Qian, Q. (2009). Strain-rate effects on the strength and fragmentation size of rocks. *International Journal of Impact Engineering, 36*(12), 1355-1364.

Quinn, J. B., & Quinn, G. D. (1997). Indentation brittleness of ceramics: A fresh approach. *Journal of Materials Science, 32*(16), 4331-4346.

Ramsay, J. G. (1967). *Folding and fracturing of rocks*. London, UK: McGraw-Hill.

Reches, Z., & Lockner, D. (1990). Self-organized cracking-a mechanism for brittle faulting. *EOS, Amer. Geophysics Union Trans., 71*, 1586.

Rini, A.A., & Mohd, F. M. A. (2008). Verification of post failure behaviour of rock using closed-circuit servo-controlled testing machine. *Bulletin of the Geological Society of Malaysia 54 (2008) 17 – 20, doi: 10.7186/bgsm2008003*

Roberts, D. K., & Wells, A. A. (1954). The velocity of brittle fracture. *Engineering, 178*, 820-821.

Romanov, K. I. (2001). The Drucker stability of a material. *Journal of Applied Mathematics and Mechanics*, *65*(1), 155-162.

Rosin P., & Rammler E. (1933). The laws governing the fineness of powdered coal. *Journal of the Institute of Fuel*, *7*, 29–36.

Rummel, F., & Fairhurst, C. (1970). Determination of the post-failure behaviour of brittle rock using a servo-controlled testing machine. *Rock Mechanics and Rock Engineering*, *2*(4), 189-204.

Saito, T., Hasuka, Y., & Nishii, O. (1983*). Post-failure behaviour in triaxial compression test controlled by radial deformation*. Proceedings of the 15th Symposium on Rock Mechanics (36-40), Tokyo.

Sammis, C., & Biegel, R. (2004). Mechanics of strengthening in crystalline rock at low temperatures: A preliminary assessment. *Proceedings of the 26th Seismic Research Review: Trends in Nuclear Explosion Monitoring* (475-484). Retrieved from

http://l2a.ucsd.edu/local/Meetings/2004_SRR/PAPERS/04-11.pdf [Accessed July 2012]

Sano, O., Terada, M., & Ehara, S. (1982). A study on the time-dependent microfracturing and strength of Oshima Granite. *Tectonophysics, 84*(2-4), 343-362.

Santarelli, F.J., & Brown, E.T. (1989). Failure of three sedimentary rocks in triaxial and hollow cylinder compression tests. International Journal of Rock Mechanics and Mining Sciences, *26*(5), 401-403.

Sellers, E., Furtney, J., & Onederra, I. (2012a, February). *Field-scale modelling of blasting in kimberlite using the Hybrid Stress Blasting Model*. Proceedings of the 38th Annual Conference on Explosive and Blasting Technique (627-638). Nashville, TN, USA.

Sellers, E., Furtney, J., Onederra, I., & Chitombo, G. (2012b). Improved understanding of explosive-rock interactions using the hybrid stress blasting model. *The Journal of the Southern African Institute of Mining and Metallurgy, 112* (8), 721-728

Senseny, P.E. (1987, November). *Deformation measurements in rock mechanics using direct-contact extensometers*. Proceedings of the 4th Annual Hostile Environments and High Temperature Measurements Conference, SEM, Windsor Locks, CT. Retrieved from http://www.respec.com/file/109-deformation-measurements-in-rock-mechanics-using-direct-contact-extensometers?start=100 [Accessed August 2011]

Sergey, V. Z. (2003). Fragm: *A Blasting Fragmentation Model of Rocks*. (Master of Science Thesis). West Virginia University, Morgantown. Retrieved from

Shimizu, H., Koyama, T., Ishida, T., Chijimatsu, M., Fujita, T., & Nakama, S. (2010). Distinct element analysis for Class II behaviour of rocks under uniaxial compression. *International Journal of Rock Mechanics and Mining Sciences, 47*(2), 323-333.

Simon, R., Aubertin, M., & Deng, D. (2003, September). *Estimation of post-peak behaviour of brittle rocks using a constitutive model for rock joints*. Proceedings of the 56th Canadian Geotechnical Conference, 4th joint IAH-CNC/CGS Conference (2003 NAGS conference) (9), Winnipeg, Canada. Retrieved from http://www.enviro-geremi.polymtl.ca/pdf/articles/Simon_CGS112.pdf [Accessed May 2010]

Simpson, D. R., & Fergus, J. H. (1968). The effect of water on the compressive strength of diabase. *Journal of Geophysical Research, 73*(20), 6591-6594.

Spathis, A. T. (2005). A correction relating to analysis of the original Kuz-Ram model. Int. Journal of Fragmentation and Blasting (*Fragblast*) *8*, 201-205.

Stacey, T. R. (1981). A Simple Extension Strain Criterion for Fracture of Brittle Rock. *International Journal of Rock Mechanics and Mining Sciences & Geomechanics Abstracts. 18,* 469-474.

Stavrogin, A. N., & Protossenia, A. G. (1985). *Rock strength and excavation stability in great depth*. Moscow: Nedra press.

Stowe, R. L., & Ainsworth, D. L. (1968, May). *Effect of rate of loading on strength and young's modulus of elasticity of rock*. Proceedings of the 10th US Symposium on Rock Mechanics (USRMS) (3), Austin TX, USA.

Tang, C. A., Liu, H., Lee, P. K. K., Tsui, Y., & Tham, L. G. (2000). Numerical studies of the influence of microstructure on rock failure in uniaxial compression--part I: Effect of heterogeneity. *International Journal of Rock Mechanics and Mining Sciences, 37*(4), 555-569.

Tang, C. A., Tham, L. G., Lee, P. K. K., Tsui, Y., & Liu, H. (2000). Numerical studies of the influence of microstructure on rock failure in uniaxial compression--part II: Constraint, slenderness and size effect. *International Journal of Rock Mechanics and Mining Sciences, 37*(4), 571-583.

Tarasov, B. & Potvin, Y. (2013). Universal criteria for rock brittleness estimation under triaxial compression. *International Journal of Rock Mechanics & Mining Sciences, 59*, 57–69.

Tarasov, B. G. (2010, October). *Superbrittleness of rocks at high confining pressure*. Proceeding of the 5th International Seminar on Deep and High Stress Mining (119-133), Santiago, Chile.

Tarasov, B. G. (2012). New criteria for rock brittleness estimation at triaxial compression. Proceedings of XL International Summer School–Conference APM (Advanced Problems in Mechanics). Available online at

http://www.ipme.ru/ipme/conf/APM2012/2012-PDF/2012-367.pdf (accessed 3rd August 2014)

Tarasov, B. G., & Randolph, M. F. (2008). Frictionless shear at great depth and other paradoxes of hard rocks. *International Journal of Rock Mechanics and Mining Sciences, 45*(3), 316-328.

Terada, M., Yanagitani, T., & Ehara, S. (1984). *AE rate controlled compression test of rocks*. In H. R. Hardy (Ed.), Proceedings of the 3rd Conference on Acoustic Emission Microseismic Activity in Geologic Structures and Materials (159-171). Pennsylvania, USA: Trans Tech Publications.

Tiryaki, B., & Dikmen, A. C. (2006). Effects of rock properties on specific cutting energy in linear cutting of Sandstones by picks. *Rock Mechanics and Rock Engineering, 39*(2), 89-120.

Tugrul, A., & Zarif, I. H. (1999). Correlation of mineralogical and textural characteristics with engineering properties of selected granitic rocks from turkey. *Engineering Geology, 51*(4), 303-317.

Tuncay, E., & Hasancebi, N. (2009). The effect of length to diameter ratio of test specimens on the uniaxial compressive strength of rock. *Bulletin of Engineering Geology and the Environment, 68*(4), 491-497.

Van der Merwe, J. N. (2003). A laboratory investigation into the effect of specimen size on the strength of coal samples from different areas. *Journal of South African Institute of Mining and Metallurgy, 103*(5), 273-280.

Vutukuri, V. S., Lama, R. D., & Saluja, S. S. (1974). *Handbook on mechanical properties of rocks: testing techniques and results*. Clausthal and Bay Village: Trans Tech Publications.

Wang, J. A., & Park, H. D. (2001). Comprehensive prediction of rockburst based on analysis of strain energy in rocks. *Tunnelling and Underground Space Technology, 16*(1), 49-57.

Wawersik, W. R., & Brace, W. F. (1971). Post-failure behaviour of a Granite and diabase. *Rock Mechanics and Rock Engineering, 3*(2), 61-85.

Wawersik, W. R., & Fairhurst, C. (1970). A study of brittle rock fracture in laboratory compression experiments. *International Journal of Rock Mechanics and Mining Sciences & Geomechanics Abstracts, 7*(5), 561-564.

Whittles, D. N., Kingman, S., Lowndes, I., & Jackson, K. (2006). Laboratory and numerical investigation into the characteristics of rock fragmentation. *Minerals Engineering, 19*(14), 1418-1429.

Wiebols, G. A., Cook, N. G. W., & Jaeger, J. C. (1968, May). *Rock property tests in a stiff testing machine*. Proceedings of the 10th US Symposium on Rock Mechanics (USRMS) (297-329), Austin TX, USA.

Wong, T. F. (1982). Micromechanics of faulting in westerly Granite. *International Journal Rock Mechanics Mining Science and Geomechanics Abstract, 19*, 49-63.

Yagiz, S. (2009). Assessment of brittleness using rock strength and density with punch penetration test. *Tunnelling and Underground Space Technology*, *24*(1), 66-74.

Yang, S. Q., Dai, Y. H., Han, L. J., & Jin, Z. Q. (2009). Experimental study on mechanical behaviour of brittle Marble samples containing different flaws under uniaxial compression. *Engineering Fracture Mechanics*, *76*(12), 1833-1845.

Yang, S. Q., Su, C. D., & Xu, W. Y. (2005). Experimental and theoretical study of size effect of rock material. *Eng. Mech. (Gongcheng Lixue)*, *22*(4), 112-118.

Yarali, O., & Soyer, E. (2011). The effect of mechanical rock properties and brittleness on drillability. *Scientific Research and Essays*, *6*(5), 1077-1088.

Yashima, S., Kanda, Y., Saito, F., Sasaki, T., Iijima, M., & Hashimoto, H. (1983). *Mechanical properties of brittle materials and their single fracture under dynamic loading.* Research Institutes of Mineral Dressing and Metallurgy, Departmental Bulletin Paper (254-269), Tohoku University (electronic library service). Retrieved from http://ci.nii.ac.jp/els/110004639900.pdf?id=ART0007355689&type=pdf&lang=en&host=cinii&order_no=&ppv_type=0&lang_sw=&no=1387198792&cp= [Accessed August 2010]

Yathavan, K., & Stacey, T. R. (2004). Laboratory observations relevant to fracture initiation at low stress levels. South African National Institute of Rock Engineering, SANIRE–The Miner's Guide through the Earth's Crust. Retrieved from

http://www.sanire.co.za/component/docman/cat_view/64-proceedings/67-symposium-2004?Itemid=228 [Accessed July 2011]

Yilmaz, N. G., Karaca, Z., Goktan, R. M., & Akal, C. (2009). Relative brittleness characterization of some selected granitic building stones: Influence of mineral grain size. *Construction and Building Materials*, *23*(1), 370-375.

Zaruba, Q. (1965). Geology of the Orlik dam site. *Water Power*, *17*, 273-279.

Zhang, C. Chu, W. Liu, N. Zhu, Y., & Hou, J. (2011). Laboratory tests and numerical simulations of brittle Marble and squeezing schist at Jinping II hydropower station, *China Journal of Rock Mechanics and Geotechnical Engineering*, *3*(1), 30–38

Zhang, L., Jin, X., & He, H. (1999). Prediction of fragments number and size distribution in dynamic fracture. *Journal of Physics D: Applied Physics*, *32*, 612.

Zhang, Z. X., Kou, S. Q., Yu, J., Yu, Y., Jiang, L. G., & Lindqvist, P. A. (1999). Effects of loading rate on rock fracture. *International Journal of Rock Mechanics and Mining Sciences*, *36*(5), 597-611.

Zhao, J., Liu, Q., Lee, K. W., Choa, V., The, C. I. (1999). Underground cavern development in the Jurong sedimentary rock formation. *Tunnelling and Underground Space Technology*, *14*, 449-459.

Zhou, X. P. (2006). Triaxial compressive behaviour of rock with mesoscopic heterogeneous behaviour: Strain energy density factor approach. *Theoretical and Applied Fracture Mechanics*, *45*(1), 46-63.

APPENDICES

APPENDIX 1.1 Rock Specimen Preparations, Water and Density Determination

1.1 Rock Specimen Preparation

The International Society for Rock Mechanics Commission on Testing Methods, ISRM (2007) described the requirements of rock specimen for rock mechanics tests. This method entails following the process to determine the diameter, height and perpendicularity or smoothness of the specimen meeting the required specification. The specimen preparation procedures are the same for all the tests performed. The rock specimen preparation was carefully and meticulously done to meet the ISRM standard specification for all the rock types. The following apparatus was used to achieve this:

- Diamond drill machine used to obtain cores of selected size from sample blocks
- Diamond saw cutting machine used to cut drilled cores into selected height
- Lapping or polishing machine used to obtain required parallelism for specimen ends

1.1.1 Sample Coring and Equipment Description

The machine used was a Matheys drilling machine (Optiver II). It has a moveable table with a dimension of 40 cm by 40 cm for mounting the rock sample. The

table can travel vertically upward or downward by 31.12 cm. A 42 mm diameter drill is attached to the drilling machine in order to drill 42 mm diameter specimen. This machine is able to achieve a constant speed (Appendix 1.1.1).

1.1.1.1 *Procedure for Sample Coring*

To perform sample coring, a drill table was lowered and a rock block is placed on a flat wooden base. A 42 mm diameter drill rod or core barrel was connected to the drill press by screwing it in as far as possible. An 'X' mark was drawn on the location to be drilled on the sample block and aligned to the centre of the drill bit (Appendix 1.1.1). After coring the specimen, its sides were checked for smoothness or irregularities.

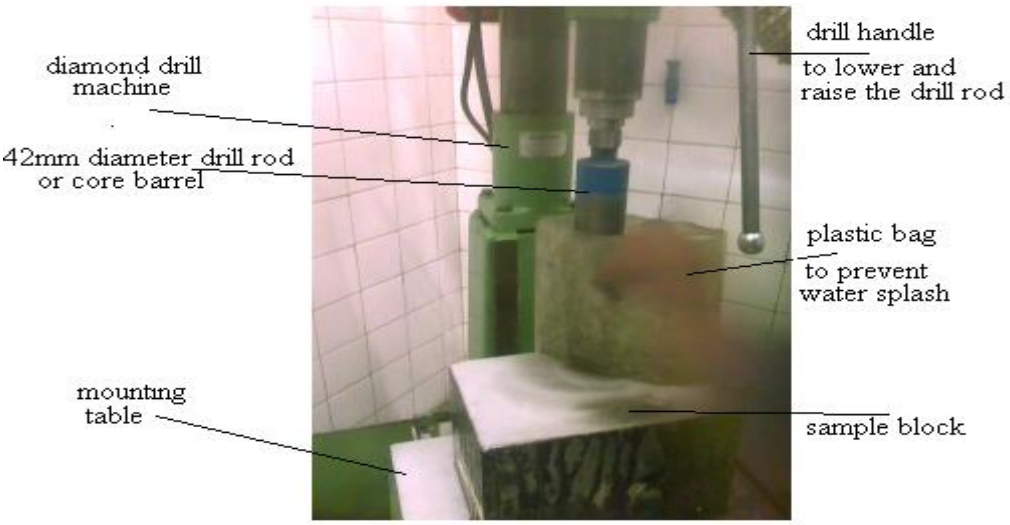

Appendix 1.1.1 A diamond drill machine with a sample mounting table during coring.

1.1.2 Rock Specimen Cutting and Equipment Description

A diamond cutting machine was used for cutting the rock specimen into the required length. The diamond cutting machine is fitted with a diamond abrasive wheel blade, specimen mounting table, clamp and water hose. The speed of the wheel is regulated by two fixed speeds (high and low speed). The mounting table is a moveable type. It can move horizontally against the wheel blade. A Vanier calliper was used to measure the length of the rock specimen (Appendix 1.1.2a). With this machine it is possible to accurately cut the required length without deflection.

1.1.2.1 *Procedure for Cutting of Rock Specimen*

For UCS tests, pre-failure and post-failure stress-strain curves in uniaxial compression and sonic velocity determination, a ratio of height to diameter of 2.5 was used to meet the ISRM (2007) suggested standard. For Brazilian tensile tests, a ratio of thickness to diameter of 0.5 was used (according to ISRM standard). In order to cut the specimen into the required length, the diamond saw and water supply was turned on. The specimen with the clamp was slowly moved against the saw blade.

1.1.3 Rock Polishing Machine and Equipment Description for Polishing of Rock Specimen Ends Surfaces

A polishing or lapping machine was used to achieve a smooth surface for the ends of the rock specimen. The lapping machine has two circular flat metal disc

surfaces. The upper disc contains slots for the specimen placement. There is a small amount of clearance between the two surfaces and the discs (Appendix 1.1.2b). This machine has the capability to meet ISRM standard for flatness and smoothness of end surfaces.

1.1.3.1 *Procedure for Polishing Rock Specimen End Surfaces*

The specimens are placed into the slots of the lapping machine. The screws are then tightened to secure the specimen in place. As the two surfaces rotate in the opposite direction to each other, an of 220 grit size (66 µm) abrasive material was spread between the surfaces. When the surfaces are effectively smoothened with the abrasive, the core end was reversed and the other end surfaces were ground.

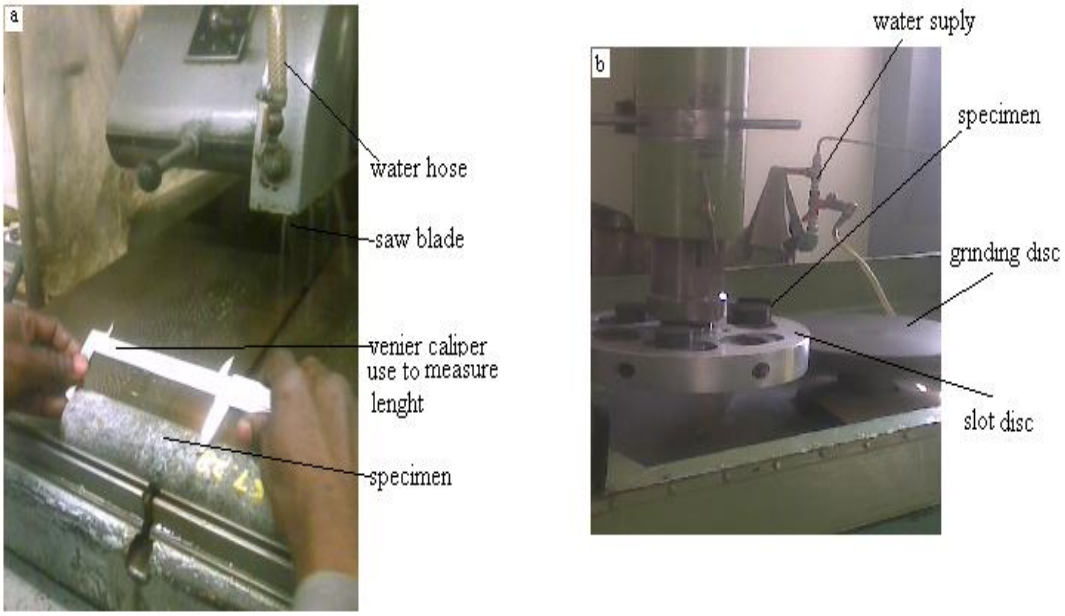

APPENDIX 1.1.2 (a) Cutting machine (b) lapping machine.

1.1.4 Description of Estimation of Specimen Ends and Sides Tolerances and Equipment

The end and side of the rock specimen were checked for smoothness in accordance with the specification of the ISRM (2007) method. The equipment used to estimate the rock specimen end and side tolerances were: a dial gauge: a V-block and a smooth support surface. The dial gauge has a mounting pad and a gauge. The V-block as the name implies has a V-shaped groove at 90^0 from its sides in a rectangular block. This instrument is very sensitive to even the smallest departure from smoothness and parallel end.

1.1.4.1 *Procedure for Estimation Specimen End and Side Tolerance*

The specimens were placed on a flat and smooth support surface. A dial gauge was placed such that its mounting pad was in contact with the top of the specimen. The mounting pad of the dial gauge was moved across the diameter of the specimen end surface. The differences between the maximum and minimum readings on the dial gauge were noted. ISRM (2007) suggested that the end of the specimen shall be flat to ±0.01 mm.

Again, the specimen side's smoothness and perpendicularity were estimated. The specimen was laid on its side on a V-block support surface. The dial gauge mounting pad made contact with the side of the specimen. As the specimen was moved along the V-block the dial readings were noted. The difference between maximum and minimum readings observed on the dial gauge was estimated. ISRM (2007) suggested that the side of the specimen shall be smooth and free of

abrupt irregularities and straight to within 0.3 mm over the length of the specimen and shall not depart from perpendicularity to the axis of the specimen by more than 0.05 over 50 mm (Appendix 1.1.3). Specimens that meet the specification for end and side of the specimen conditions were kept aside as test specimens.

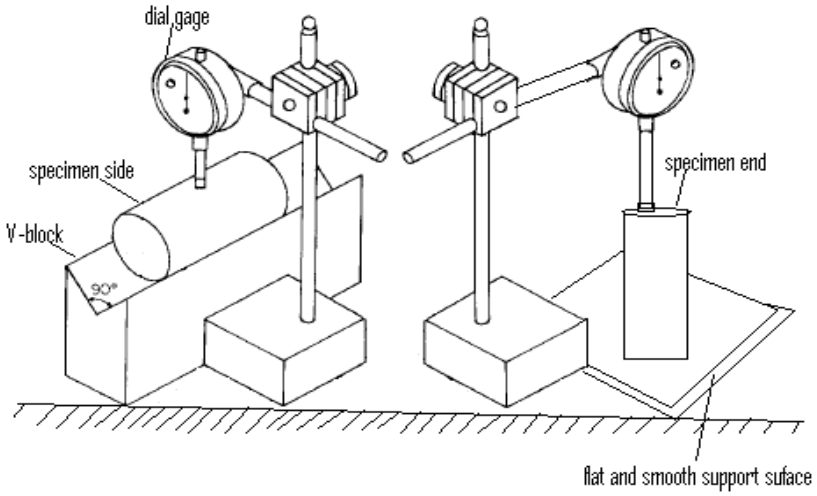

Appendix 1.1.3 Apparatus assembly for determining the perpendicularity of specimen side and flatness of specimen end surfaces.

1.1.5 Determination of Density of Rock Specimens and Equipment Description

Density is a basic property of rocks. It was used to estimate dynamic parameters. Since fragmentation of rock is a dynamic process, it may be necessary to correlate it with a dynamic property such as dynamic modulus. The equipment used to determine the density of a rock specimen includes a desiccator, electronic balance and calliper. This method is simple but reliable.

1.1.5.1 Procedure for Determination of Density of Rock specimen

The density of a rock specimen was determined from the ratio of its grain mass to bulk volume. The specimen was dried to a constant mass at a temperature of 105^0C in a desiccator. The bulk volume was estimated by calliper measurement.

1.1.6 Determination of Water Content of Rock Sample and Equipment Description

This test was performed to estimate the mass of water in a given mass of the rock sample as a percentage of the oven-dry sample mass as the percentage of water in a rock specimen affects it strength value. As a consequence, ISRM suggests that the water content of a sample be reported alongside the rock strength. The equipment items used for determination of water content includes an electric oven, sample container and electronic balance. This method is simple and straightforward.

1.1.6.1 Procedure for Determination of Water Content of Rock Sample

The procedure for the determination of water content of the rock sample follows this sequence. The mass of empty, clean, and dry sample containers of non-corrodible material with an airtight lid was determined (a). The mass of sample plus container was determined (b). The sample was placed in the electric oven that was set at a constant temperature of 105°C. The mass of the container with the sample and lid was determined (c). The water content (wc) of the sample was determined using Equation 1.1.1

$$wc = \frac{b-c}{c-a} \times 100 \tag{1.1.1}$$

APPENDIX 1.2 MTS (815) Testing System

1.2 The Testing Machine

The testing machine used was The Rock Mechanics System model MTS 815 (Appendix 1.2.1). The load unit assembly, test processor or load unit assembly control, test controller, accessories and a microcomputer together form the digital closed loop control system arrangement or configuration to determine the pre-failure and post-failure stress-strain curves under uniaxial compression. Each of these components is described in the following sections.

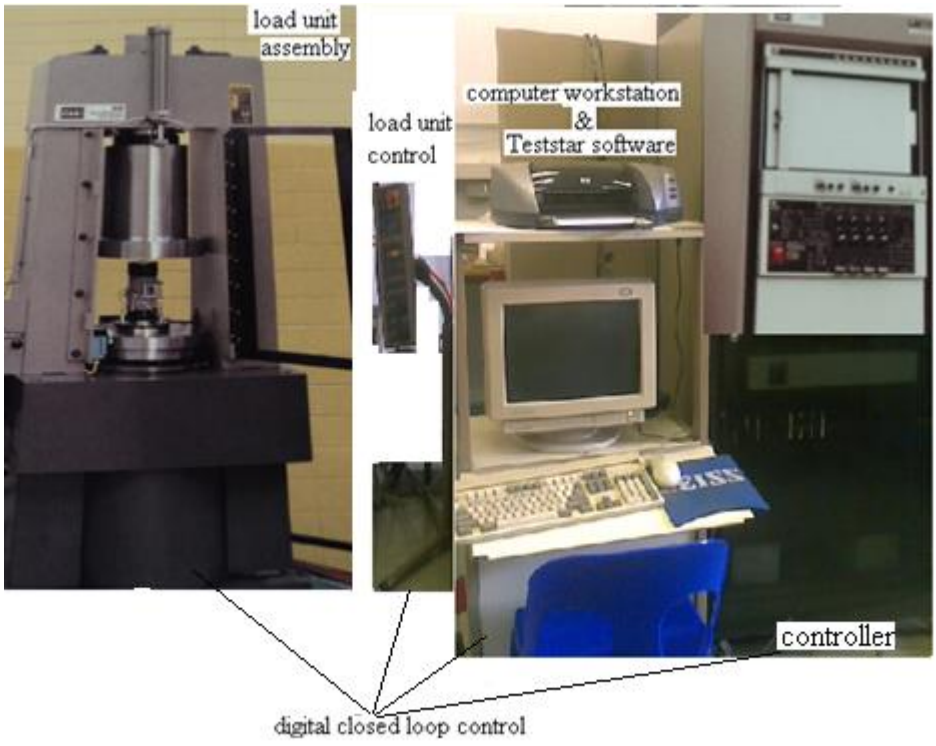

Appendix 1.2.1 Rock mechanics testing system model MTS 815.

1.2.1 The Load Unit Assembly

The testing machine applied load to the test specimens in response to commands from the controller. The assembly consists of a load unit with two solid steel columns and moveable crosshead to provide a stiff, low deflection force. The assembly contains hydraulic lifts to position the crosshead and hydraulic locks for clamping the crosshead in position. The hydraulic actuator is mounted on the crosshead. The moveable crosshead ensures precision alignment of the longitudinal axis of the top loading platen to the actuator centre line. The load cell is mounted on the hydraulic actuator rod end. The actuator was used to raise and lower the pressure vessel. The base or bottom of the pressure vessel chamber is made larger than its body and is called the baseplate. The top bearing of the actuator is mounted within the lower part of the baseplate. This arrangement ensures precision alignment as the reaction load in the bearing is kept close to the specimen loading location (Appendix 1.2.2).

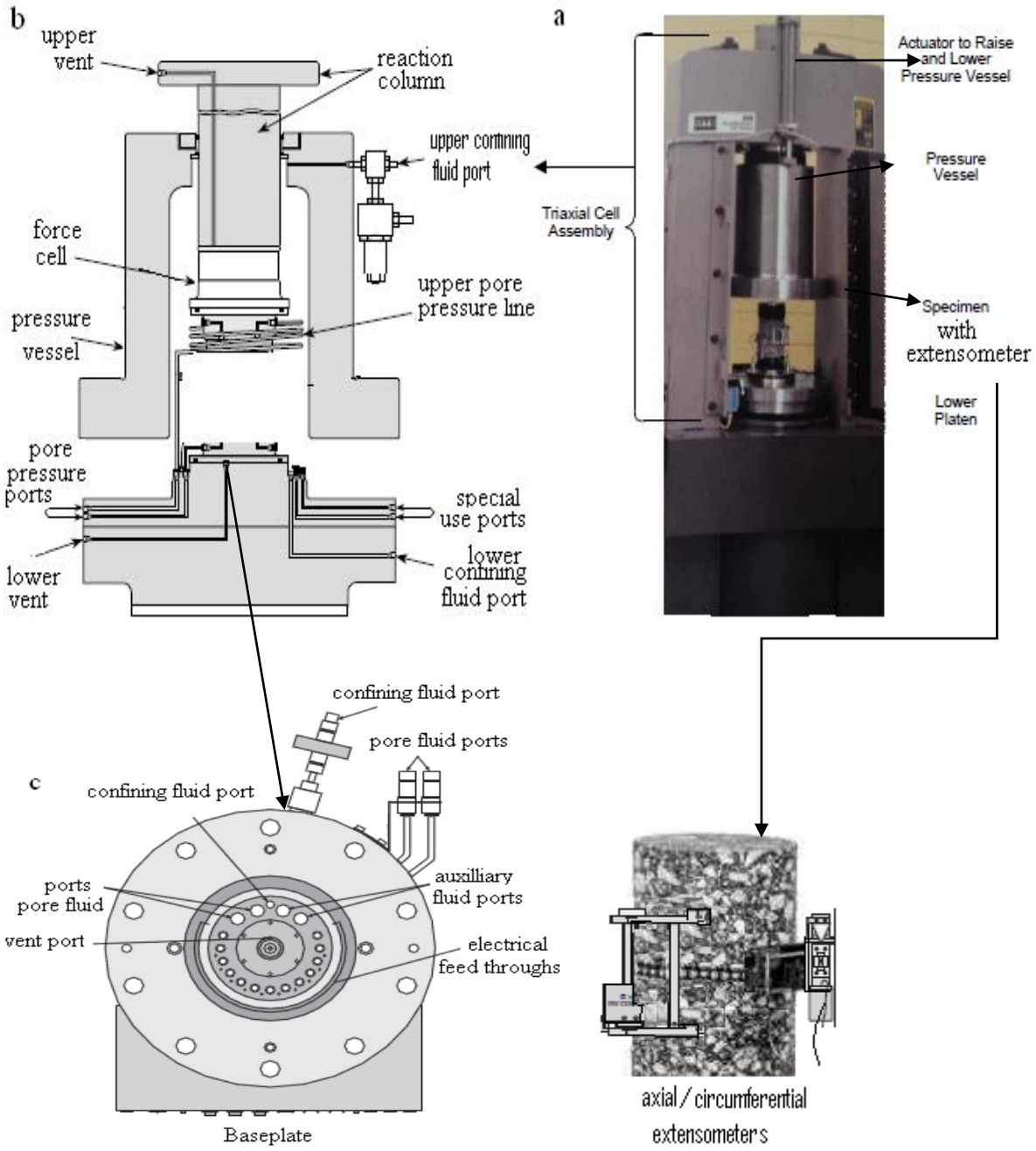

Appendix 1.2.2 (a) load unit assembly (b) triaxial cell assembly (c) baseplate (d) specimen with extensometer (modified from MTS, 2004).

1.2.2 The Load Unit Control and the Test Controller

The load unit control is a stand-alone module close to the load unit assembly. The panel of the control contains a main module and 4 control channel modules. It

provides an interface for an operator to control the load unit assembly. It was used to control the hydraulic, placement and loading of specimen. Another unit is the test controller. The test controller is a complete stand-alone unit with keypad modules for setting up control parameters and to run the program. It provides the interface between the computer workstation and the system. It is an interface to transfer information between the operator and the control system. The code required to control the system is provided by the computer workstation.

1.2.3 The Compression Platens

Apart from the mechanical system described in the previous paragraphs, additional fixtures are used to provide the needed sensitivity and accuracy. These mechanical fixtures or accessories are the compression platens (Appendix 1.2.3). The platens are made of case-hardened alloy steel which is chrome plated and has a surface flatness is greater than 0.0005 mm.

The lower portion of the platen is stiff while the upper portion is spherically seated. The lower portion is made stiff to minimise deflection during compression. The spherically seated upper platen is for alignment of the platen with the specimen surface. In addition, there are three sets of placers which are 21 mm in diameter and 79 mm thick. Each set of the placers is drilled and tapped for the threaded stud of the spherically-seated platen.

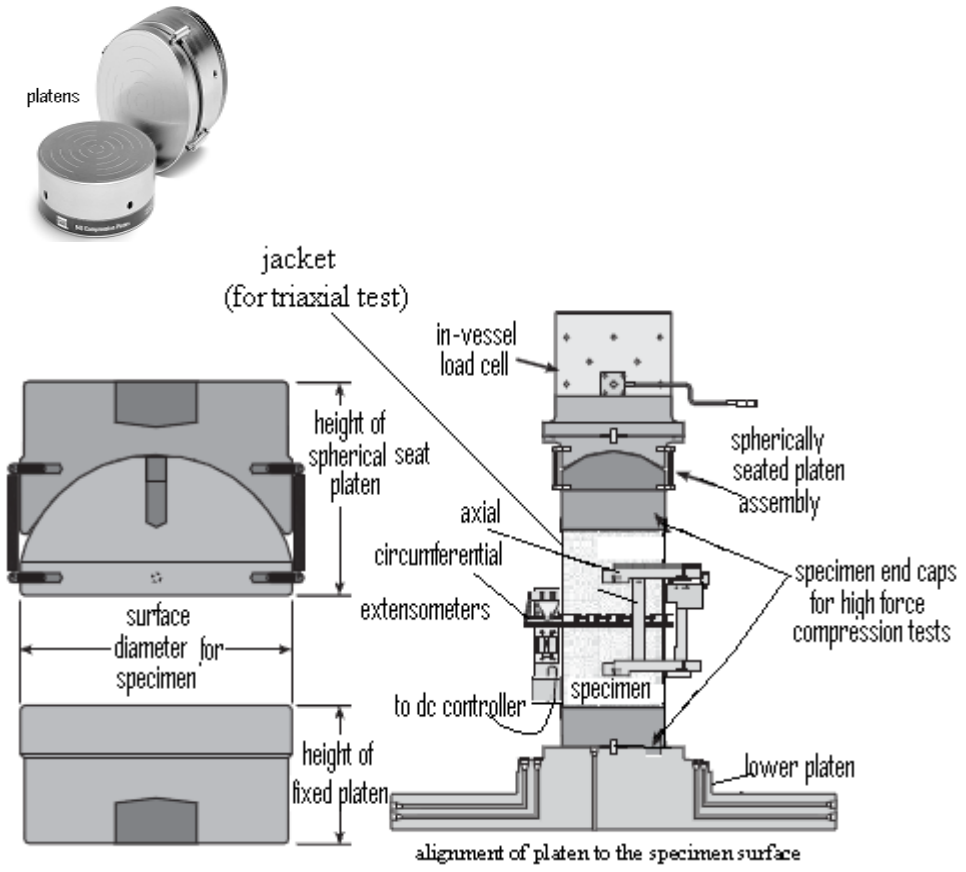

Appendix 1.2.3 Compression platen alignments with specimen (modified from MTS, 2004).

1.2.4 The Extensometers

Another important part of the instrumentation is the extensometers. These are attached to the specimen under the influence of the compressive load to measure its dimensional changes. There are two types used. These are axial and circumferential direct contact extensometers with sensitivity of 3.4 mv/v at full scale (Appendix 1.2.4). The axial extensometer is a MTS 632.9xx series model. It has three arms, each arm contacts the specimen through pins set at 25% and 75%

of specimen full length at 120^0 on its sides. It has a gauge length of 50.8 mm and was set within 0.0125 mm with its arms pins.

In order to measure circumferential deformation, a circumferential extensometer was used. This extensometer consists of a roller-link chain, a transducer and springs. The transducer was attached to the ends of the chain. The roller-link chain was made to contact the specimen around its mid-height. Once the extensometers are attached to the specimen, a cord from the extensometer was extended to a DC controller (from where the extensometer receives commands).

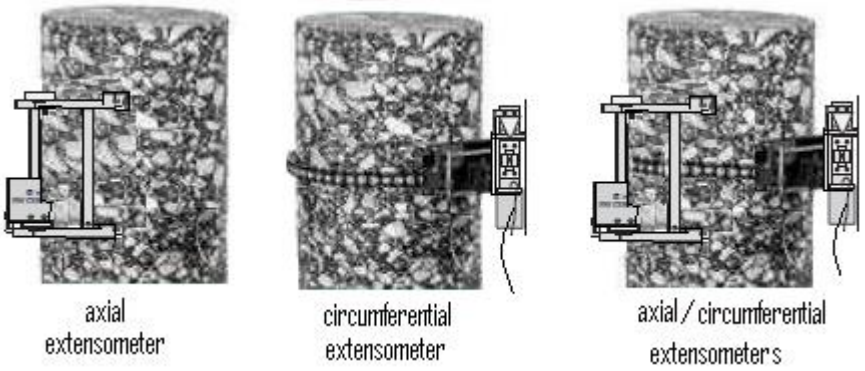

Appendix 1.2.4 Axial, circumferential and axial-circumferential extensometers arrangement.

However, a correction was applied to the measurement made with the circumferential extensometer because the extensometer measures the change in chord length between the two ends of the chain instead of the change in specimen circumference. Equation 1.2.1 was used to correct the change in chord length relative to actual change in diameter (Appendix 1.2.5).

$$\Delta C = \frac{\pi\left(l_f - l_i\right)}{\sin\left(\frac{\theta_i}{2}\right) + \left(\pi - \frac{\theta_i}{2}\right)\cos\left(\frac{\theta_i}{2}\right)} \tag{1.2.1}$$

Where:

ΔC is the change in specimen diameter

l_f -l_i is the change in chord length (extensometer output)

θ_i is the angle subtended by the initial chord length, l_i in radians

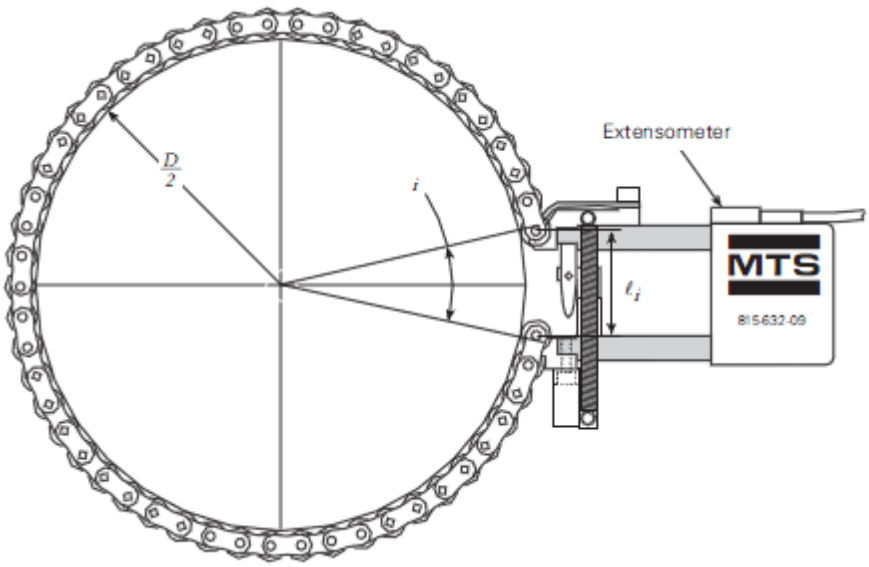

Appendix 1.2.5 circumferential extensometer geometry used in Equation 1.2.1 to determine the change in diameter in relationship with the change in chord length (MTS, 2004).

Besides the use of extensometer for measuring deformation, ISRM (2007) suggested other alternative methods. These include linear variable differential transformers (LVDT) and electrical resistance strain gauges. LVDT measure the displacement of actuator and specimen-machine interface during testing. Axial

deformation is measured with displacement transducers mounted on the loading piston. Lateral displacement is measured with the use of a dilatometer. The axial deformation is a measure of the piston displacement relative to the pressure vessel while lateral displacement is a measure of axial deformation and constant pressure that results from the flow of fluid from the pressure vessel.

However, they do not measure directly the actual deformation of the specimen. It measures specimen deformation as a result of frame deformation and contact surface displacement. Dilatometer sensitivity is low when compared with the measurement of oil volume which withdraws from the pressure vessel to the loading piston movement, as well as the very small change in volume of the specimen (Senseny, 1987). Besides, ISRM (2007) emphasises that to control specimen that exhibits Class II behaviour using LVDT may pose difficulty at the post failure stage. This is a result of time delay of LVDT to respond to alternating current conditioning electronics which can affect the control loop closure rate.

Moreover since deformation of test specimen is small, any measurement adopted should be sensitive to detect small deformational changes in contact with the test specimen. Direct contact extensometer and strain gauge satisfied this condition. However deformation measurement with the use of strain gauges is not provided with the MTS 815 testing system, nonetheless there exits some stand-alone system to accomplish it. The use of direct-contact axial extensometer eliminates the influence of measuring frame deformation, the displacement of actuator and specimen-machine interface.

1.2.5 Computer Workstation

Multi-purpose Test Ware application software was installed on a standalone PC computer to perform real-time control. The feedback control was monitored from the PC. Appendix 1.2.6 shows the closed loop control of Multi-purpose Test Ware application software. From the software interface, the stages of deformation of the specimen was viewed and monitored.

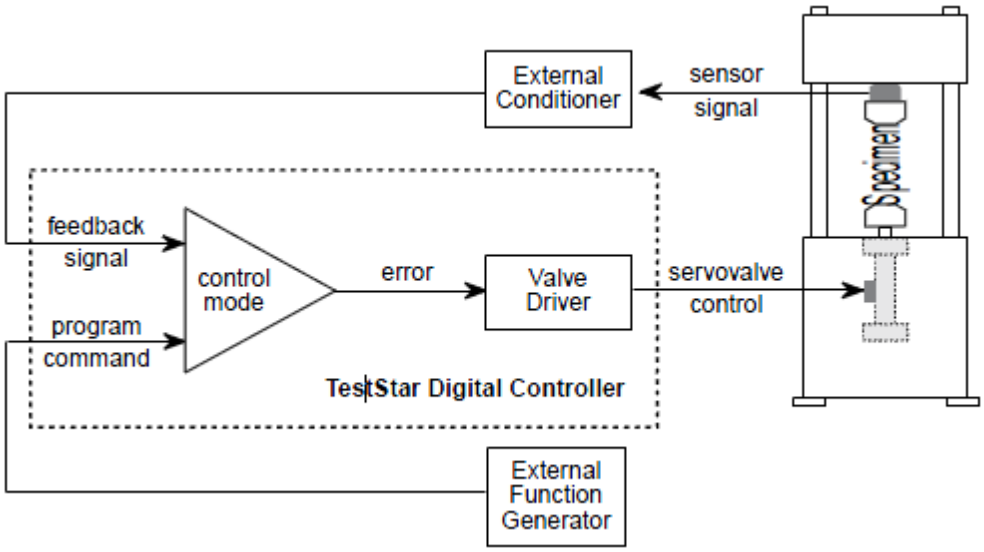

Appendix 1.2.6 Multipurpose Test Ware application software with closed loop control (MTS, 2004).

APPENDIX 1.3 MPT PROCEDURE TESTING TEMPLATE AND PARAMETERS

MPT PROCEDURE PARAMETERS - <Procedure Folder>\Uni42mms.000 9/24/2012 9:58:30 AM
Items proceeded by an asterisk (*) have been modified.

Application Information
- Name : Multipurpose TestWare (MPT)
- Version : 5.35A 3447

Station Information
- Path : C:\MTS 793\Controllers\MTS FlexTest 60\Config
- Configuration : Uniaxial.cfg
- Parameter Set : 500 kN (rock2)

Procedure: Uni42mms.000
- Sequencing
  - Procedure is done when : Specimen failure (force lower limit).Done
    : Failure (radial minimum limit).Done
    : Force down to 5 kN. Done

- Procedure / Table to contact: Segment Command
  - Sequencing
    - Start : <Procedure>.Start
    - Interrupt : Force limits 0.5 kN. Done
  - General
    - Process Enabled : True
    - Execute Process : 1
    - Counter Type : None
  - Command
    - Segment Shape : Ramp
    - *Rate : 0.20000 mm/min
    - Adaptive Compensators : None
    - Do Not Update Counters : False
    - Relative End Level : False
  - Channels
    - Axial
      - Control Mode : Displacement
      - Absolute End Level : 5.0000 (mm)

- Procedure / Force limit 0.5 kN: Data Limit Detector
  - Sequencing

Start : <Procedure>.Start
Interrupt : None
General
Process Enabled : True
Execute Process : 1
Counter Type : None
Limits
Force
Upper Limit : 0.50 kN
Lower Limit : Disabled
Settings
Limit Mode : Absolute
Process completes when : Any selected signal exceeds its limit
Log Message As : Information
Action : None

Procedure / Data 1: Timed Acquisition
Sequencing
Start : <Procedure>.Start
Interrupt : Table to contact. Done
General
Process Enabled : True
Execute Process : 1
Counter Type : None
Acquisition
Time Between Points : 1.0000 (s)
Continuous Sampling : Enabled
Signals
: Running Time
: Displacement
: Force
: Circumferential
: Strain 1
Destination
Buffer Size : 1024
Data Header : Table to contact
Destination : Specimen data file
Buffer Type : Linear
Write First Data Header Only : False
Output Units
UAS : SISETSM - SI (Systeme International d'Unites) - small special

Procedure / Force to 90 kN (or radial limit): Segment Command
Sequencing

Start : Force limit 0.5 kN. Done
Interrupt : Radial displacement limit. Done
General
Process Enabled : True
Execute Process : 1
Counter Type : None
Command
Segment Shape : Ramp
* Rate : 0.001/mm/mm/s
Adaptive Compensators : None
Do Not Update Counters : False
Relative End Level : False
Channels
Axial
Control Mode : Force
* Absolute End Level : 90.000 kN
Control Mode : Displacement
Absolute End Level : 0.00000 (mm)

Procedure / Radial displacement limit: Data Limit Detector
Sequencing
Start : Force limit 0.5 kN. Done
Interrupt : None
General
Process Enabled : True
Execute Process : 1
Counter Type : None
Limits
Circumferential
*Upper Limit : 0.0120 (mm)
Lower Limit : Disabled
Settings
Limit Mode : Absolute
Process completes when : Any selected signal exceeds its limit
Log Message As : Information
Action : None

Procedure / Data 2: Timed Acquisition
Sequencing
Start : Force limit 0.5 kN. Done
* Interrupt : Force to 90 kN (or radial limit).Done
General
Process Enabled : True
Execute Process : 1

Counter Type : None
Acquisition
Time Between Points : 1.0000 (s)
Continuous Sampling : Enabled
Signals
: Running Time
: Displacement
: Force
: Circumferential
: Strain 1
Destination
Buffer Size : 1024
Data Header : Force to 90 kN
Destination : Specimen data file
Buffer Type : Linear
Write First Data Header Only : False
Output Units
UAS : SISETSM - SI (Systeme International d'Unites) - small special

Procedure / Circumferential displacement: Segment Command
Sequencing
* Start : Force to 90 kN (or radial limit).Done
Interrupt : Axial strain upper limit. Done
: Force lower limit 2 kN. Done
: Radial minimum lower limit. Done
: Manual override. Done
General
Process Enabled : True
Execute Process : 1
Counter Type : None
Command
Segment Shape : Ramp
* Rate : 0.0001 mm/mm/s
Adaptive Compensators : None
Do Not Update Counters : False
Relative End Level : False
Channels
Axial
Control Mode : Circumferential
Absolute End Level : 3.0000 (mm)
Control Mode : Displacement
Absolute End Level : 0.00000 (mm)

Procedure / Axial strain upper limit: Data Limit Detector

Sequencing
Start : Force to 90 kN (or radial limit).Done
Interrupt : None
General
Process Enabled : True
Execute Process : 1
Counter Type : None
Limits
Strain 1
* Upper Limit : 0.08000 (mm/mm)
Lower Limit : Disabled
Settings
Limit Mode : Absolute
Process completes when : Any selected signal exceeds its limit
Log Message As : Information
Action : None

Procedure / Force lower limit 2 kN: Data Limit Detector
Sequencing
Start : Force to 90 kN (or radial limit).Done
Interrupt : None
General
Process Enabled : True
Execute Process : 1
Counter Type : None
Limits
Force
Upper Limit : Disabled
Lower Limit : 2.00 kN
Settings
Limit Mode : Absolute
Process completes when : Any selected signal exceeds its limit
Log Message As : Information
Action : None

Procedure / Radial minimum lower limit: Data Limit Detector
Sequencing
Start : Force to 90 kN (or radial limit).Done
Interrupt : None
General
Process Enabled : True
Execute Process : 1
Counter Type : None
Limits

Circumferential
Upper Limit : Disabled
Lower Limit : 0.0000 (mm)
Settings
Limit Mode : Absolute
Process completes when : Any selected signal exceeds its limit
Log Message As : Information
Action : None

Procedure / Manual override: Operator Event
Sequencing
Start : Force to 90 kN (or radial limit).Done
Interrupt : None
General
Process Enabled : True
Execute Process : 1
Counter Type : None
Settings
Button ID : Button 1
Button Label : Force down
Description : Go to the next step
Options
Trigger Mode : Trigger Once
Log Message As : Information

Procedure / Specimen failure (force lower limit): Program Control
Sequencing
Start : Force lower limit 2 kN. Done
Interrupt : None
General
Process Enabled : True
Execute Process : 1
Counter Type : None
Action
Action : Station Power Off
Log Message As : Information
Message : Specimen failure (force lower limit)
Include Counters : False

Procedure / Failure (radial minimum limit): Program Control
Sequencing
Start : Radial minimum lower limit. Done
Interrupt : None
General

Process Enabled : True
Execute Process : 1
Counter Type : None
Action
Action : Station Power Off
Log Message As : Information
Message : Specimen failure (radial minimum limit)
Include Counters : False

Procedure / Data 3: Timed Acquisition
Sequencing
*Start : Force to 90 kN (or radial limit).Done
Interrupt : Circumferential displacement. Done
General
Process Enabled : True
Execute Process : 1
Counter Type : None
Acquisition
Time Between Points : 1.0000 (s)
Continuous Sampling : Enabled
Signals
: Running Time
: Displacement
: Force
: Circumferential
: Strain 1
: Force 2
Destination
Buffer Size : 1024
Data Header : Circ. disp. to 3 mm
Destination : Specimen data file
Buffer Type : Linear
Write First Data Header Only : False
Output Units
UAS : SISETSM - SI (Systeme International d'Unites) - small special

Procedure / Force down to 5 kN: Segment Command
Sequencing
Start : Circumferential displacement. Done
Interrupt : Force lower limit 2 kN. Done
General
Process Enabled : True
Execute Process : 1
Counter Type : None

Command
Segment Shape : Ramp
Rate : 5.0000 kN/s
Adaptive Compensators : None
Do Not Update Counters : False
Relative End Level : False
Channels
Axial
Control Mode : Force
Absolute End Level : 5.0000 kN
Control Mode : Displacement
Absolute End Level : 0.00000 (mm)

Procedure / Table to 0 mm: Segment Command
Sequencing
Start : Force down to 5 kN. Done
Interrupt : None
General
Process Enabled : True
Execute Process : 1
Counter Type : None
Command
Segment Shape : Ramp
Rate : 0.20000 mm/min
Adaptive Compensators : None
Do Not Update Counters : False
Relative End Level : False
Channels
Axial
Control Mode : Displacement
Absolute End Level : 0.00000 (mm)

Execution Options
Hold State Support : Enable Hold
Resume Test After Stop : Enable Resume
Required Power : High
Command Hold Behaviour : Stay at Level
Command Stop Behaviour : Stay at Level
Set point : Disable and Reset
Span : Disable and Reset
Confirm actions that may affect resuming the test : True
Specimen Options
Data File Mode : Append
Data File Format : Excel

Specimen Log Mode : Append
Data File Time Stamp : Time
Clear Counters on Reset : True
Recovery Options
Enable saving recovery status: : True
Upon program state change : True
At least every: : 60.000 (s)
Message Options
Message Capture
Minimum Severity : Information
Source : All Applications
Archive Auto Deletion
Delete Older Than : Disabled
Control Panel Display Options
Test Progress
Run Time : Display As HH:MM:SS
Counters
Channel Counters : Display As Cycles
Sequence Counters : Display As Cycles
Specimen
Procedure Name : True
Procedure State : True
Station Status
Power : True
Procedure Properties
Description :
Author :
Unit Selection
Current UAS : Use Station Unit Assignment Set
MPT Variables
Category 27

APPENDIX 2.1 BRAZILIAN TENSILE TEST, LOAD AND COMPRESSION CURVES

Appendix 2.1.1 Brazilian tensile test specimen after failure

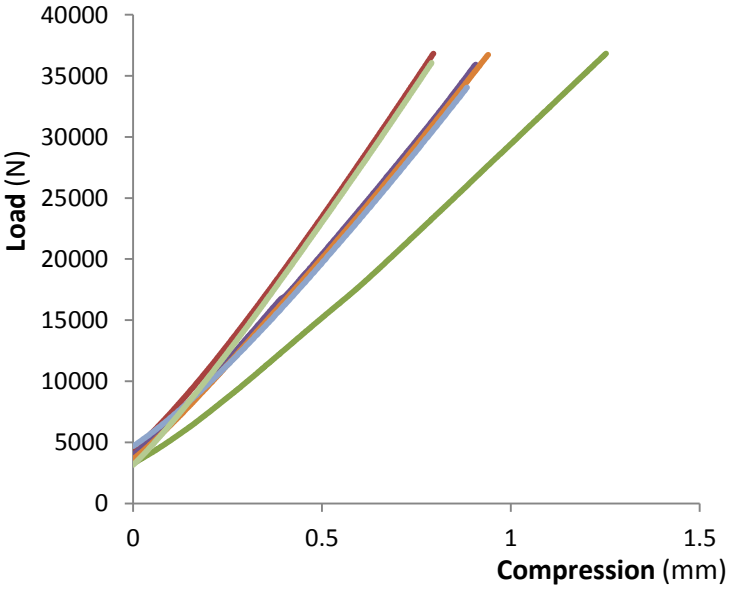

Appendix 2.1.2 Load compression curves for Gabbro under Brazilian tensile test.

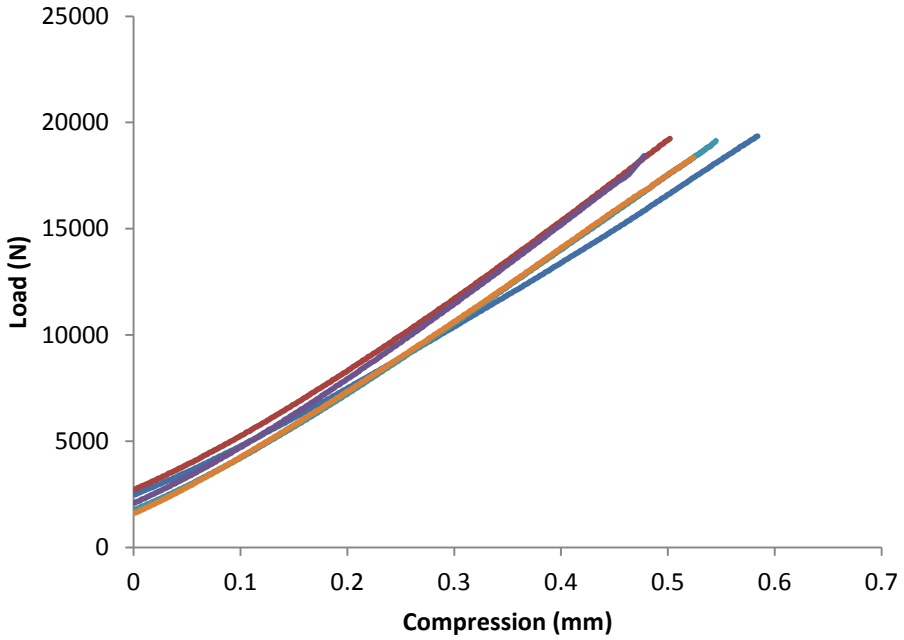

Appendix 2.1.3 Load compression curves for Granite1 under Brazilian tensile test.

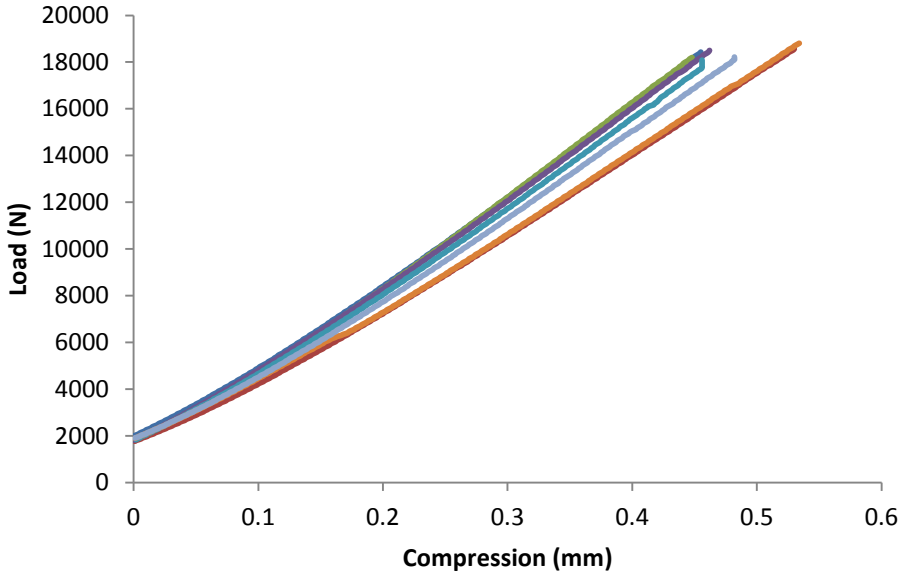

Appendix 2.1.4 Load compression curves for Granite2 under Brazilian tensile test.

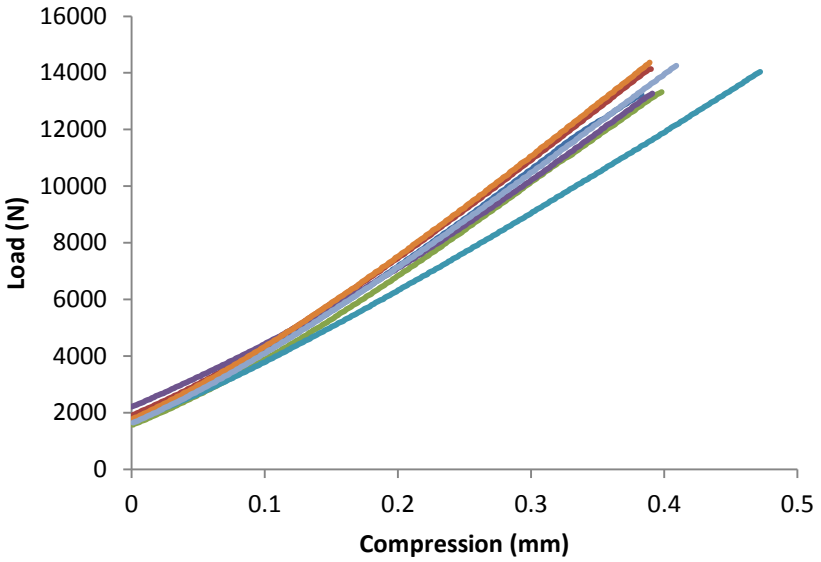

Appendix 2.1.5 Load compression curves for Granite3 under Brazilian tensile test.

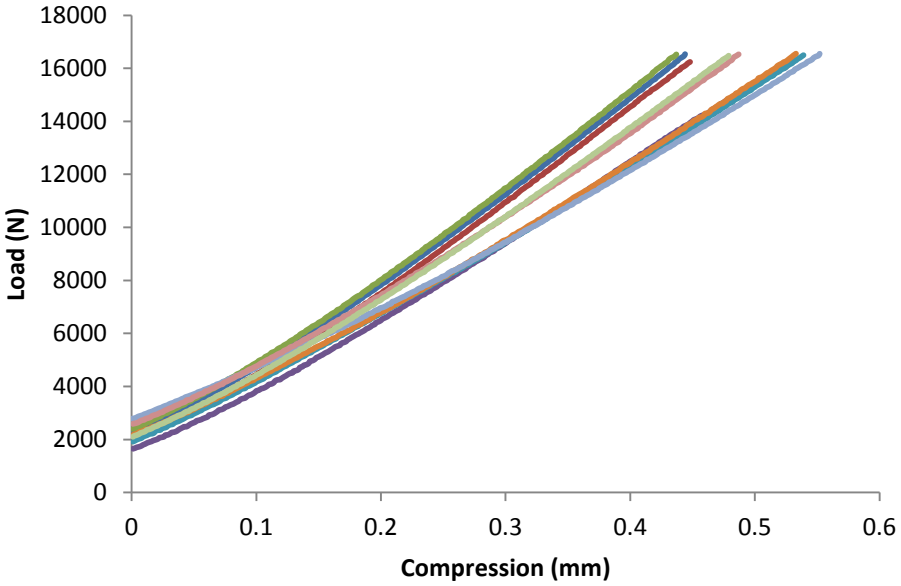

Appendix 2.1.6 Load extension curves for Granite4 under Brazilian tensile test.

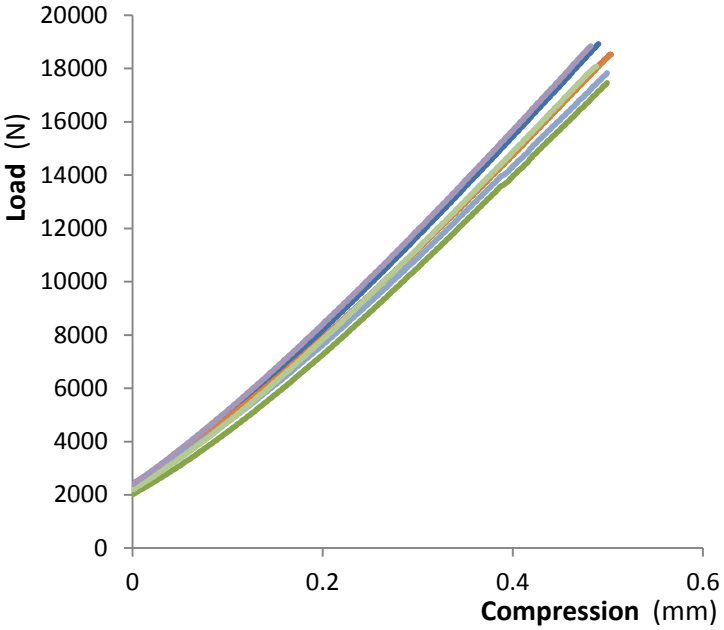

Appendix 2.1.7 Load compression curves for Granite5 under Brazilian tensile test.

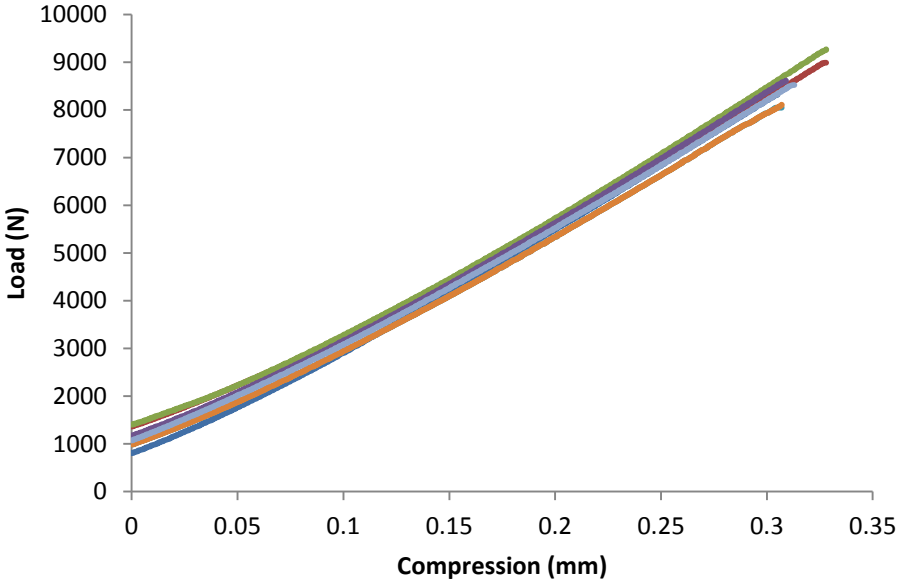

Appendix 2.1.8 Load compression curves for Marble under Brazilian tensile test.

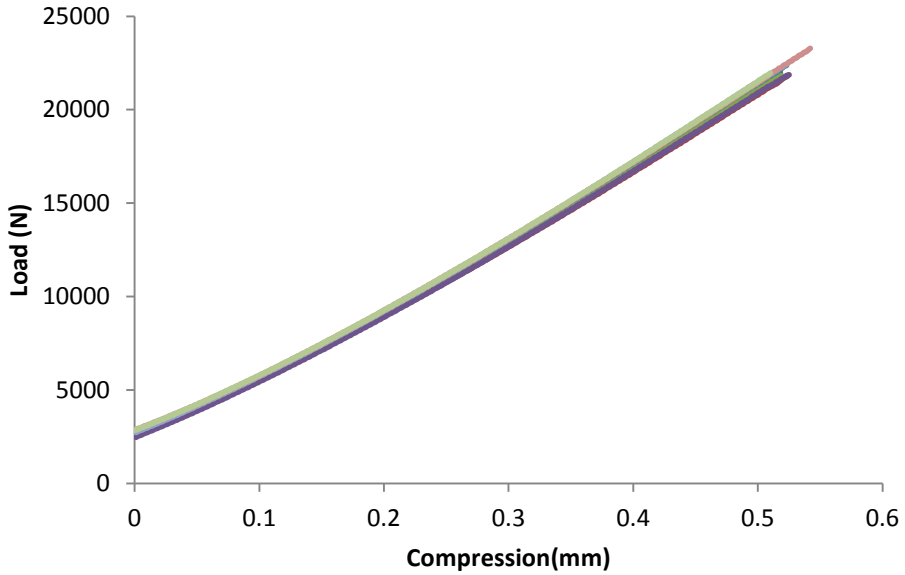

Appendix 2.1.9 Load compression curves for Mottled Anorthosite under Brazilian tensile test.

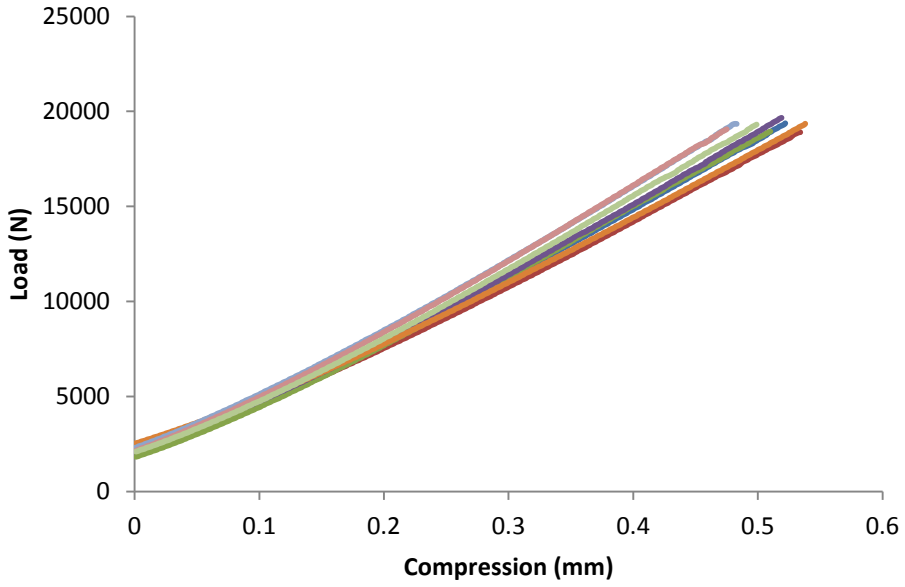

Appendix 2.1.10 Load compression curves for Norite1 under Brazilian tensile test.

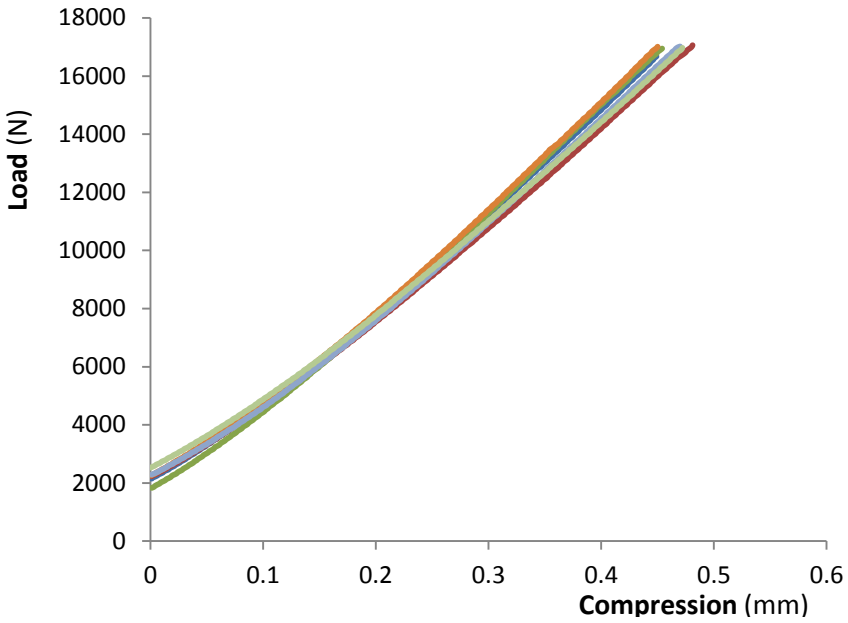

Appendix 2.1.11 Load compression curves for Norite2 under Brazilian tensile test.

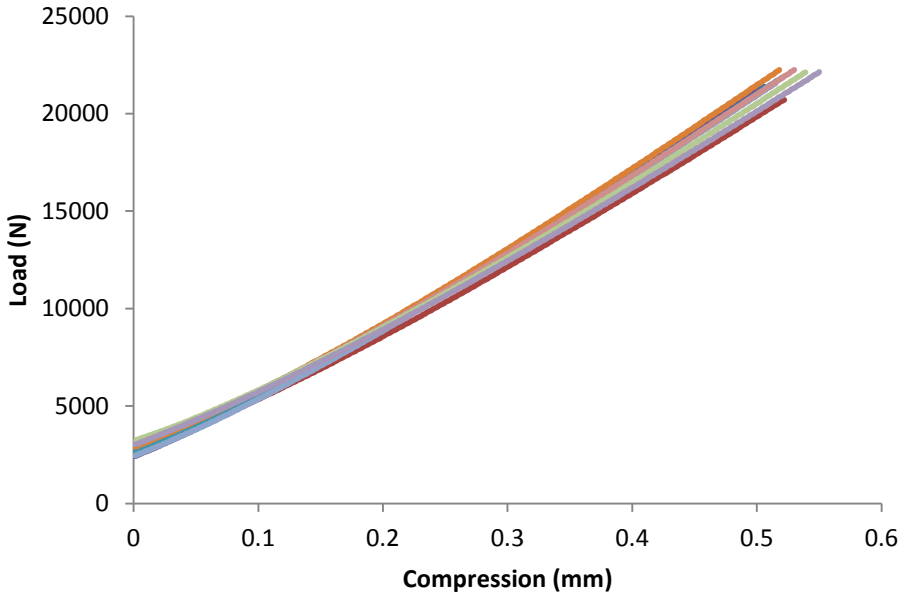

Appendix 2.1.12 Load compression curves for Norite3 under Brazilian tensile test.

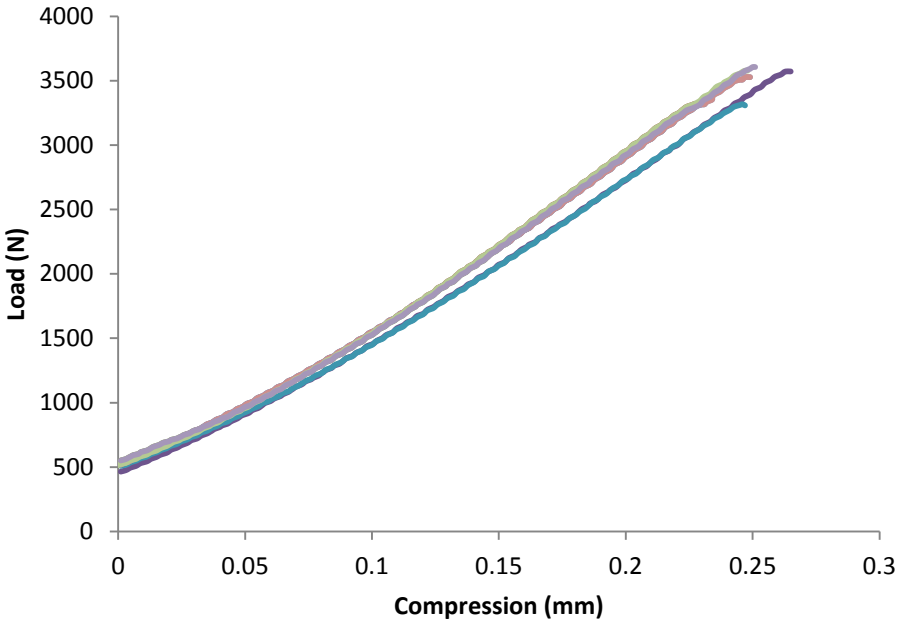

Appendix 2.1.13 Load compression curves for Quartz Arenite under Brazilian tensile test.

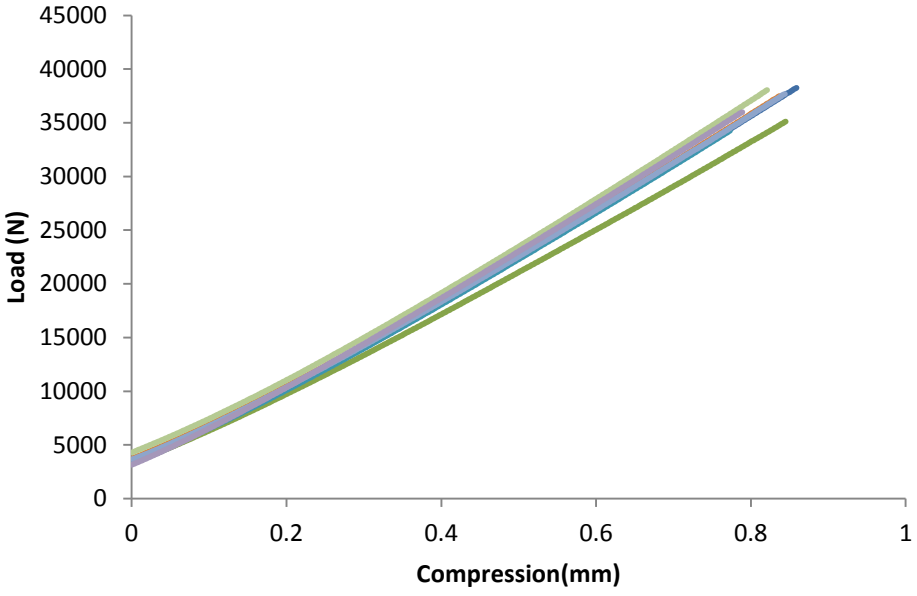

Appendix 2.1.14 Load compression curves for Quartzite2 under Brazilian tensile test.

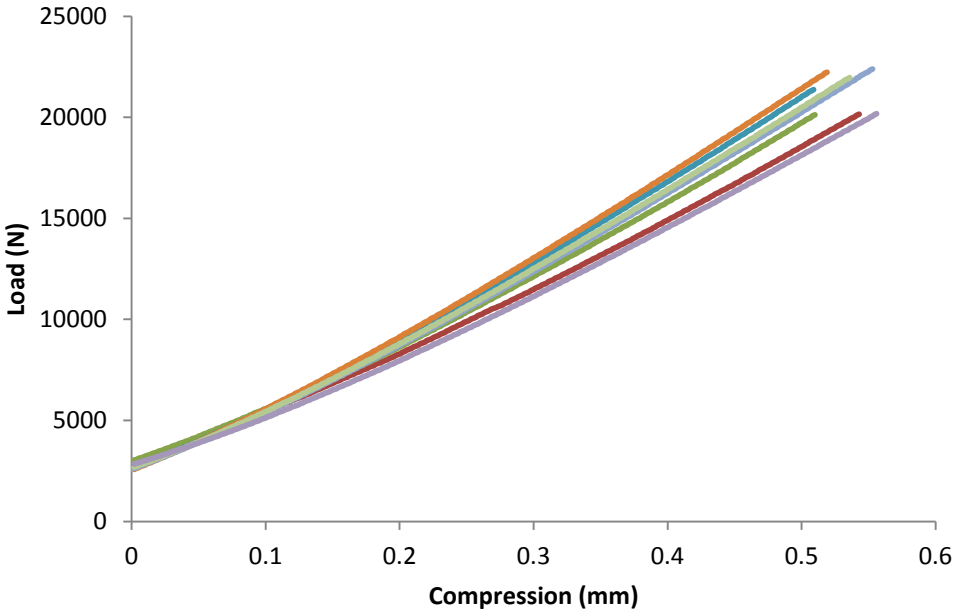

Appendix 2.1.15 Load compression curves for Quartzite1 under Brazilian tensile test.

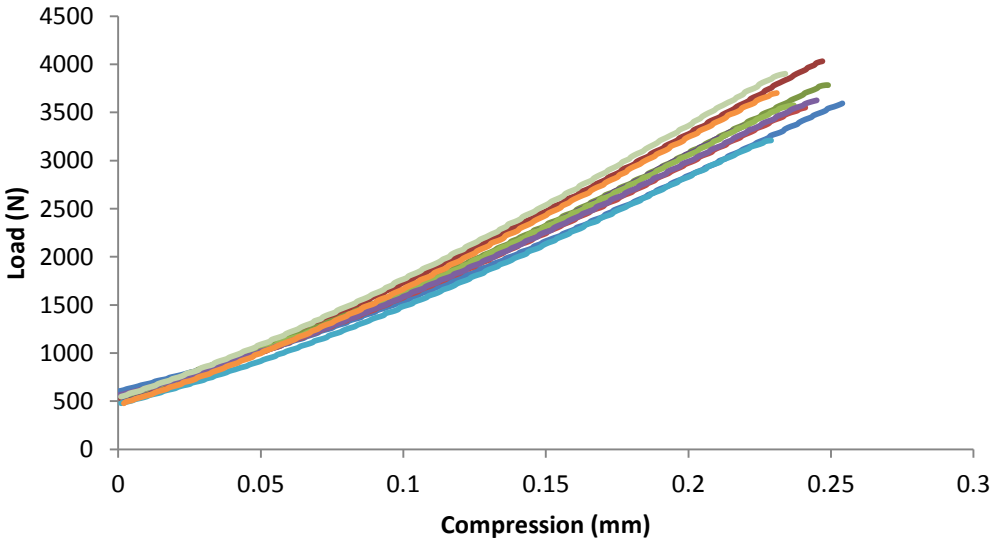

Appendix 2.1.16 Load compression curves for Sandstone under Brazilian tensile test.

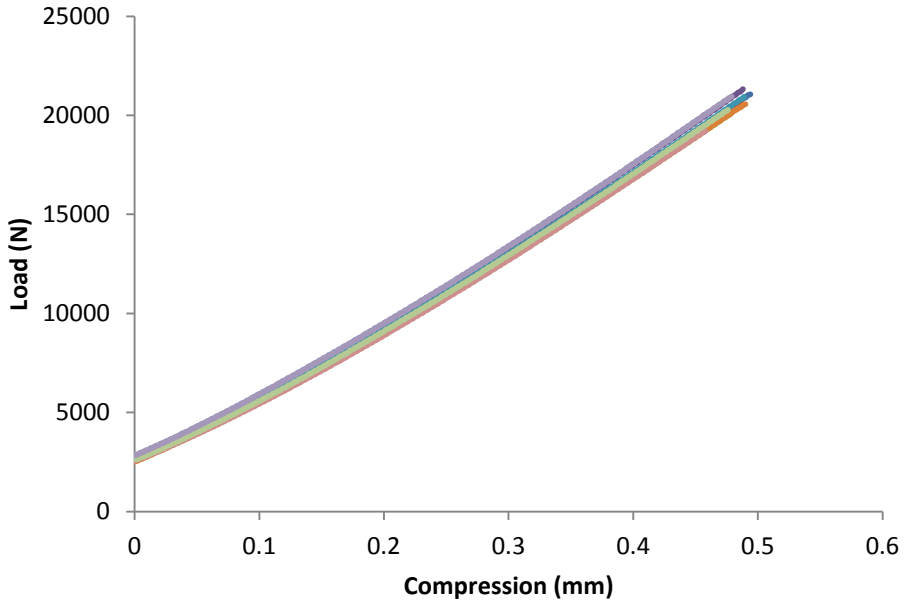

Appendix 2.1.17 Load compression curves for Spotted Anorthosite under Brazilian tensile test.

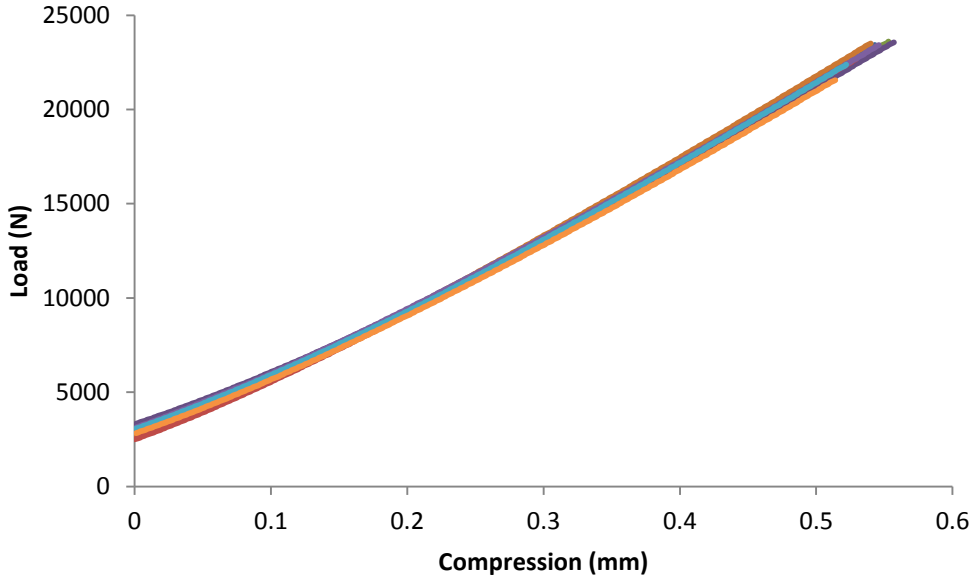

Appendix 2.1.18 Load compression curves for Troctolite1 under Brazilian tensile test.

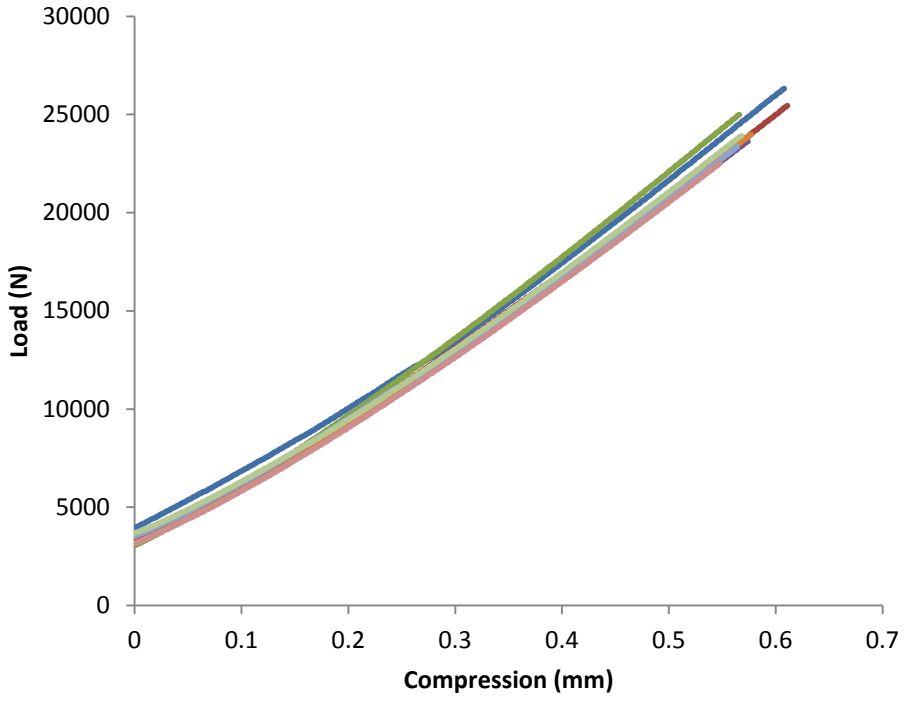

Appendix 2.1.19 Load compression curves for Troctolite2 under Brazilian tensile test.

APPENDIX 2.2 CHARACTERISTIC PRE- AND POST-FAILURE CURVES

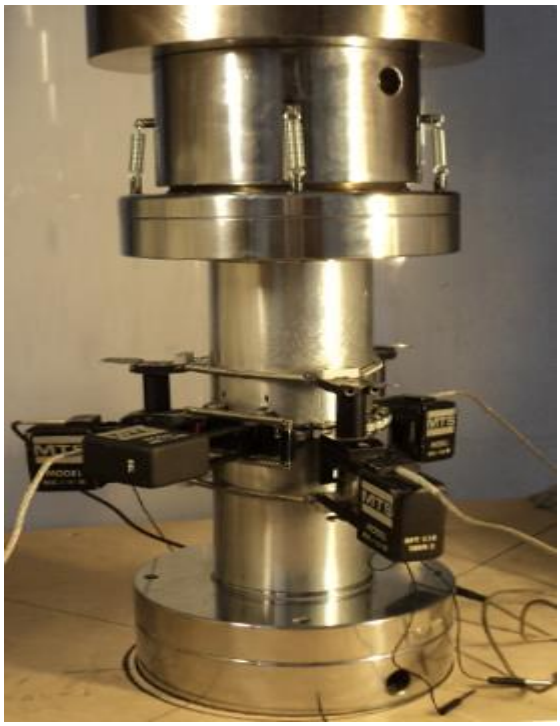

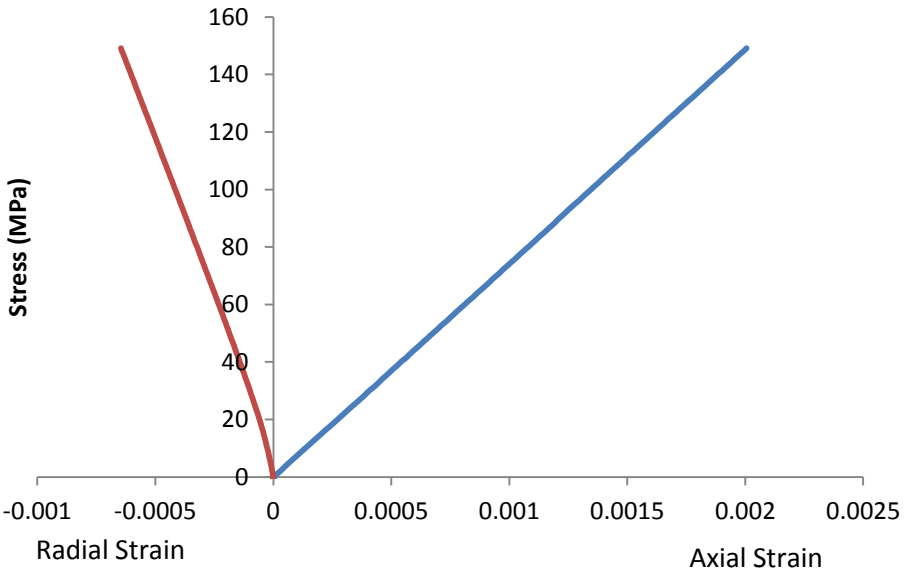

Appendix 2.2.1 The characteristic curves for aluminium specimen for calibration.

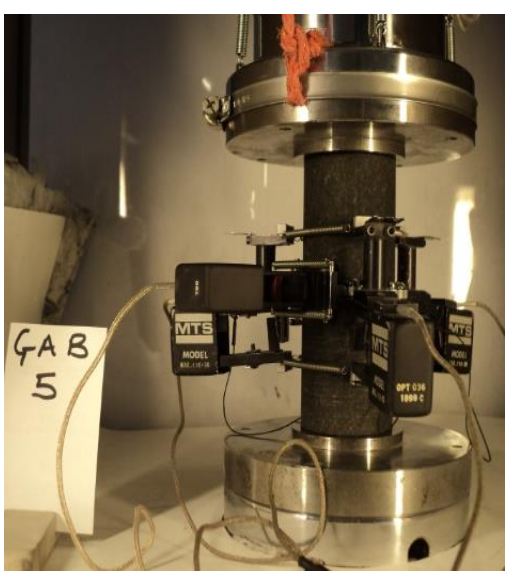

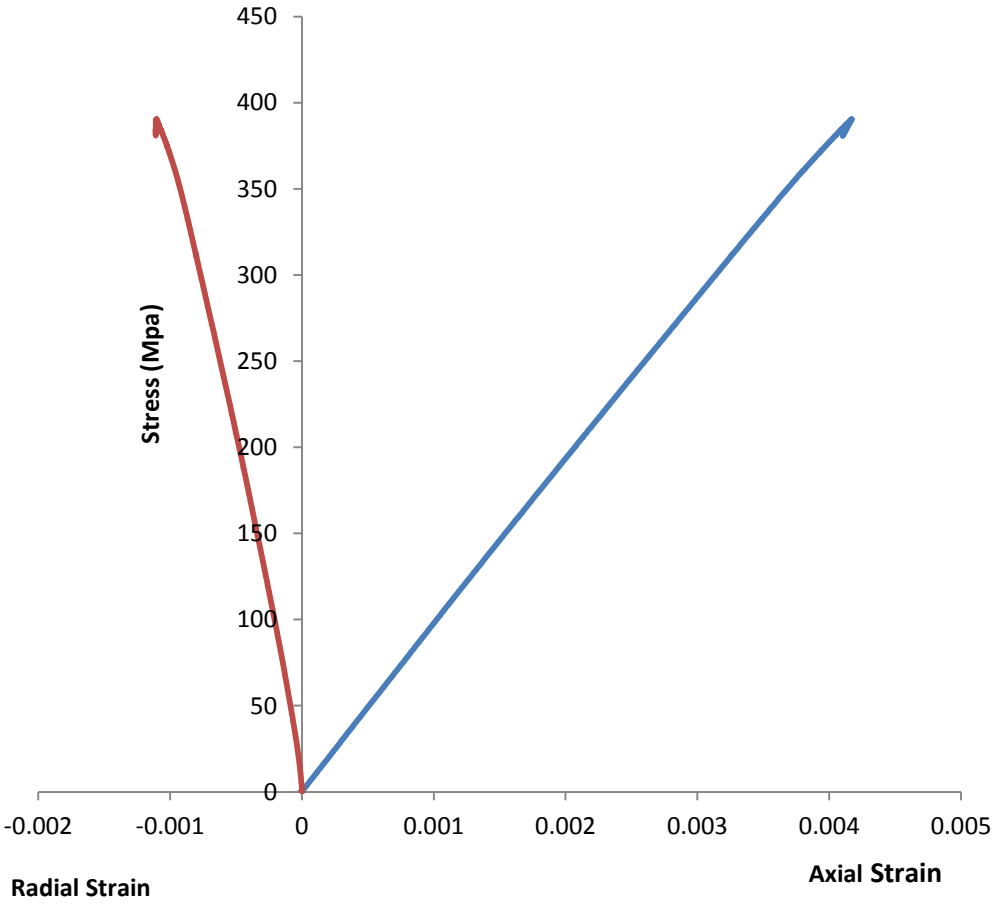

Appendix 2.2.2 On top show specimen before failure left, specimen after failure right and below is characteristic pre-failure curves for Gabbro.

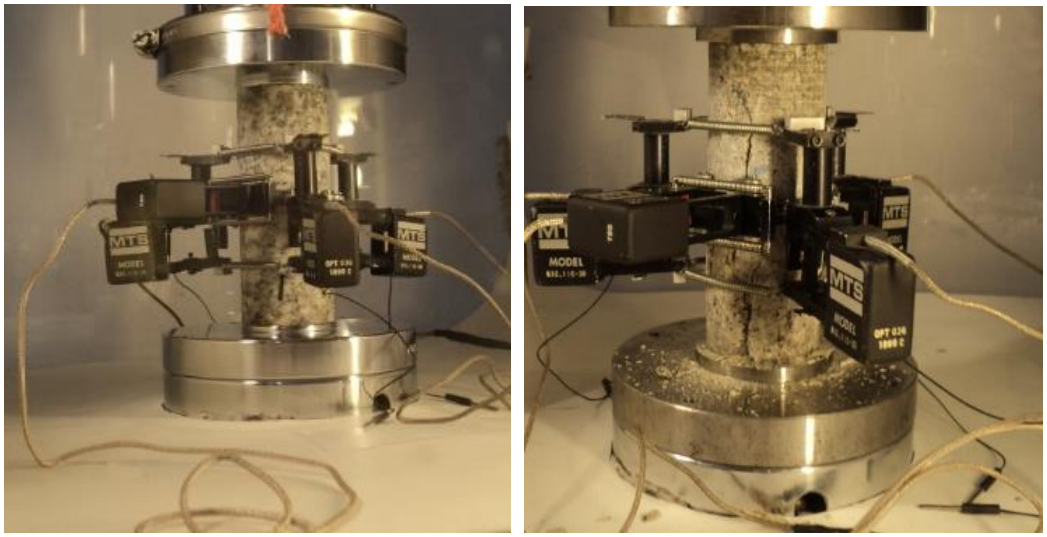

Before failure After failure

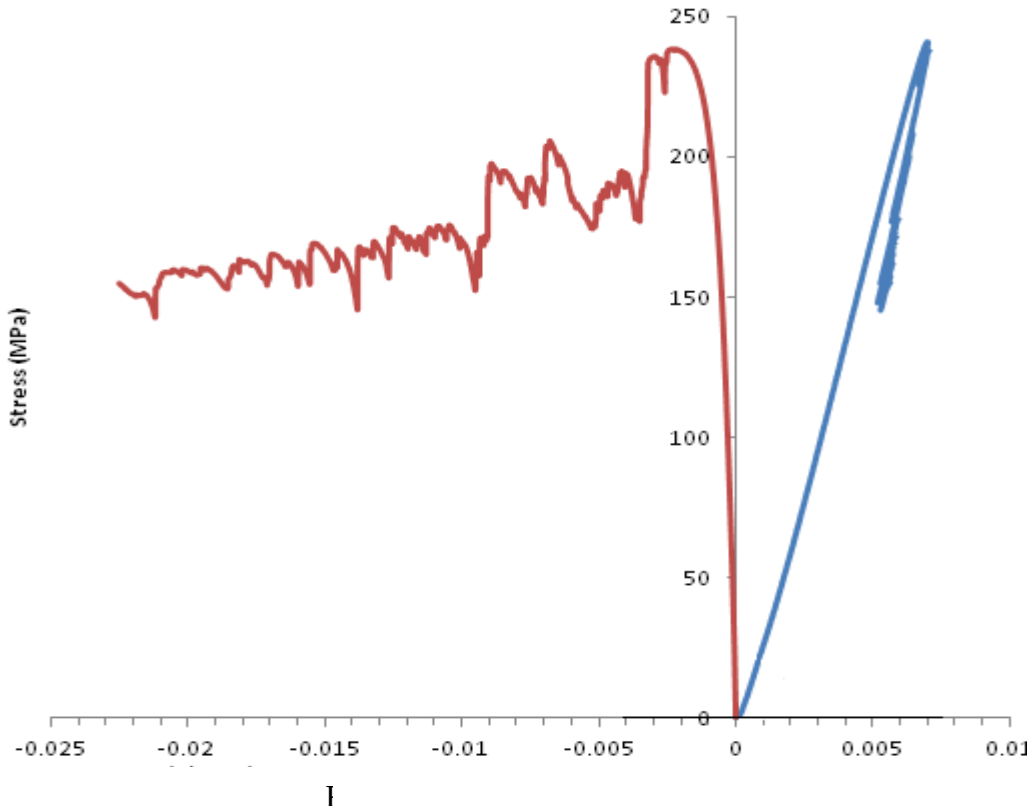

Appendix 2.2.3 On top show specimen before failure left, specimen after failure right and below is characteristic pre- and post-failure curves for Tonalite.

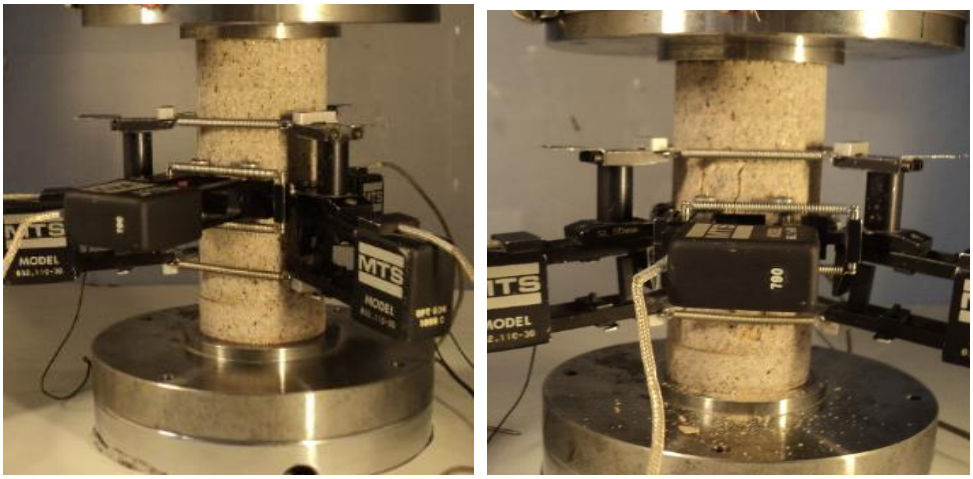

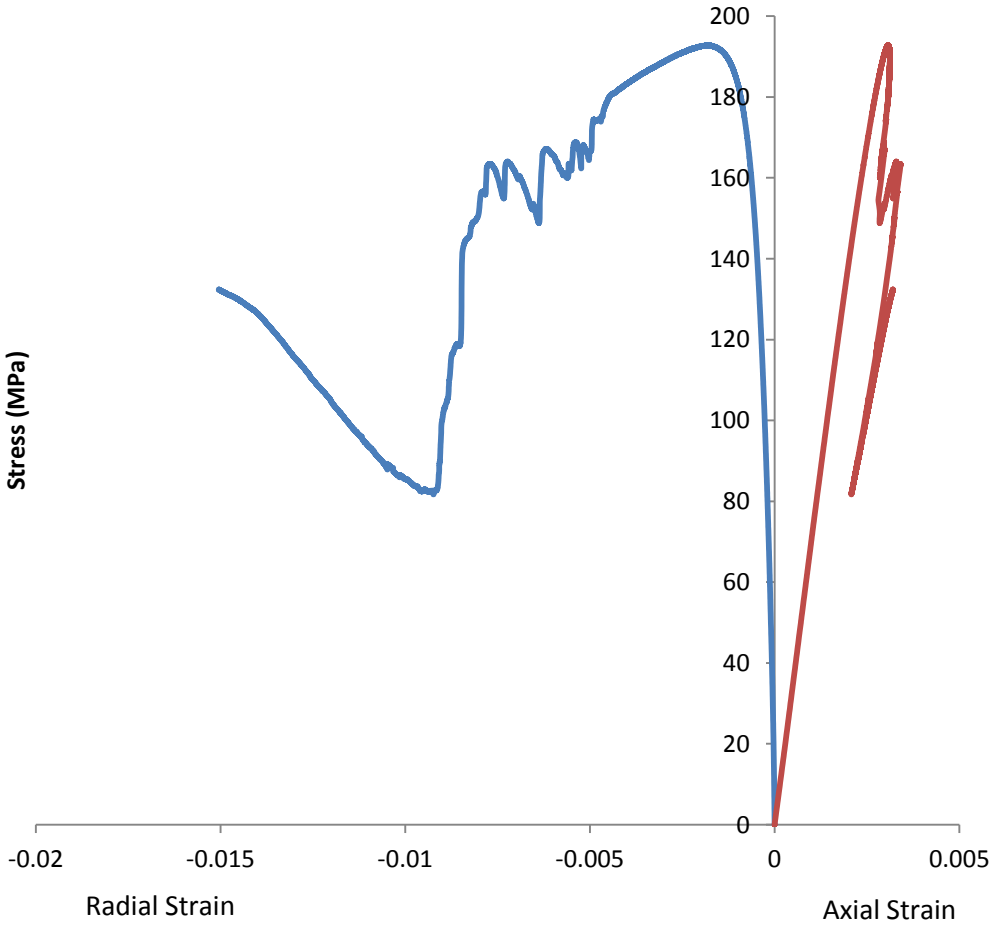

Appendix 2.2.4 On top show specimen before failure left, specimen after failure right and below is characteristic pre-failure and post-failure curves for medium-grained Granite2.

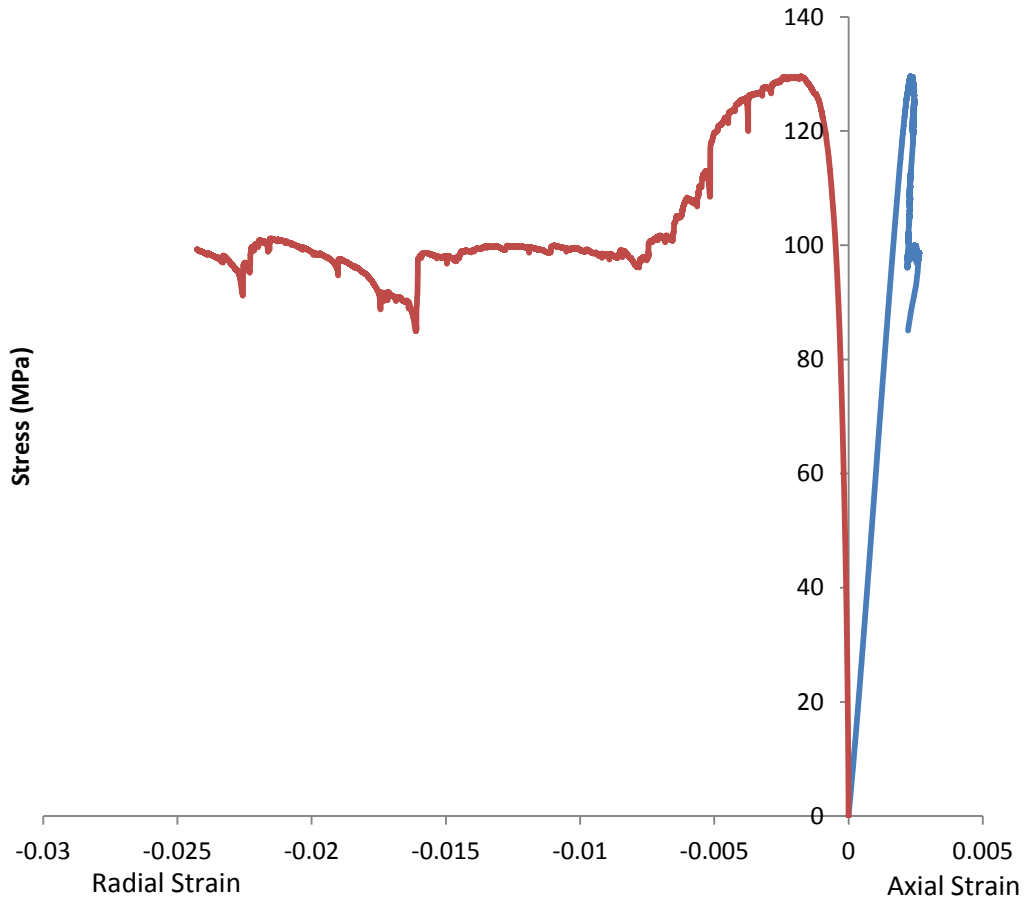

Appendix 2.2.5 On top show specimen before failure left, specimen after failure right and below is characteristic pre- and post-failure curves for coarse-grained Granite3.

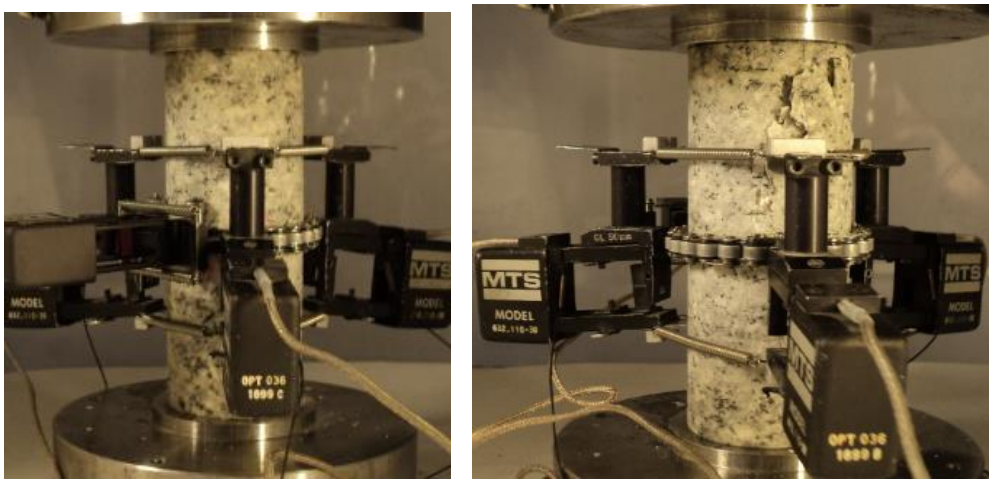

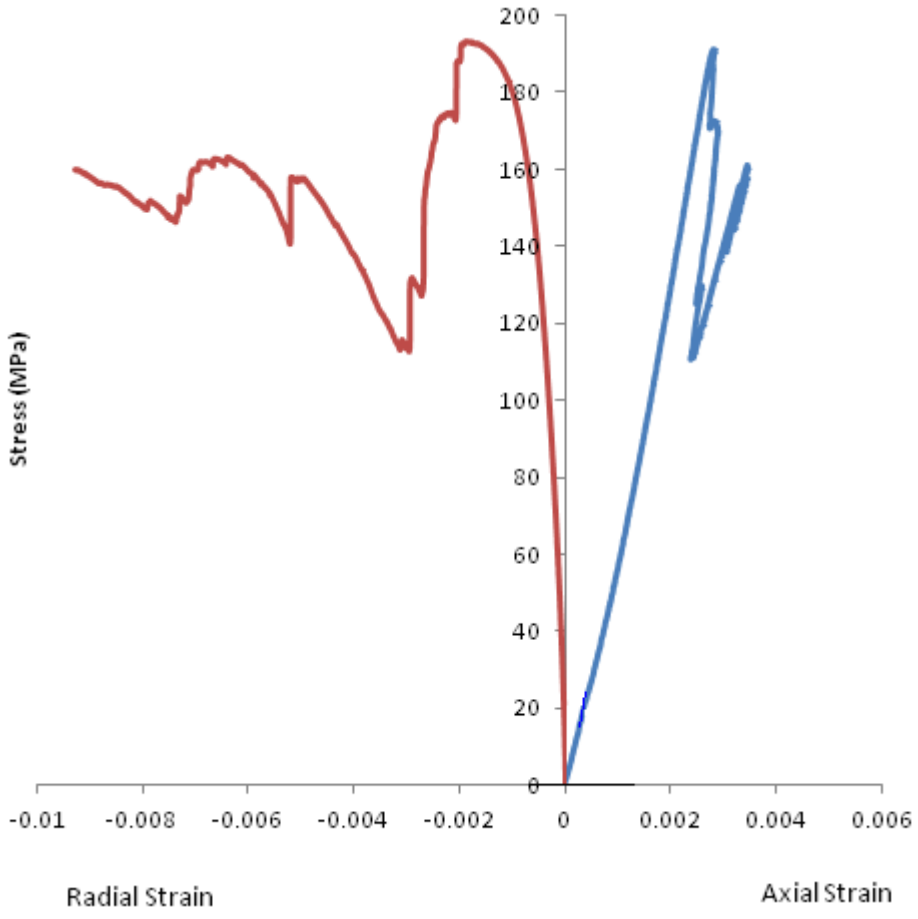

Appendix 2.2.6 On top show specimen before failure left, specimen after failure right and below is characteristic pre- and post-failure curves for Granite4.

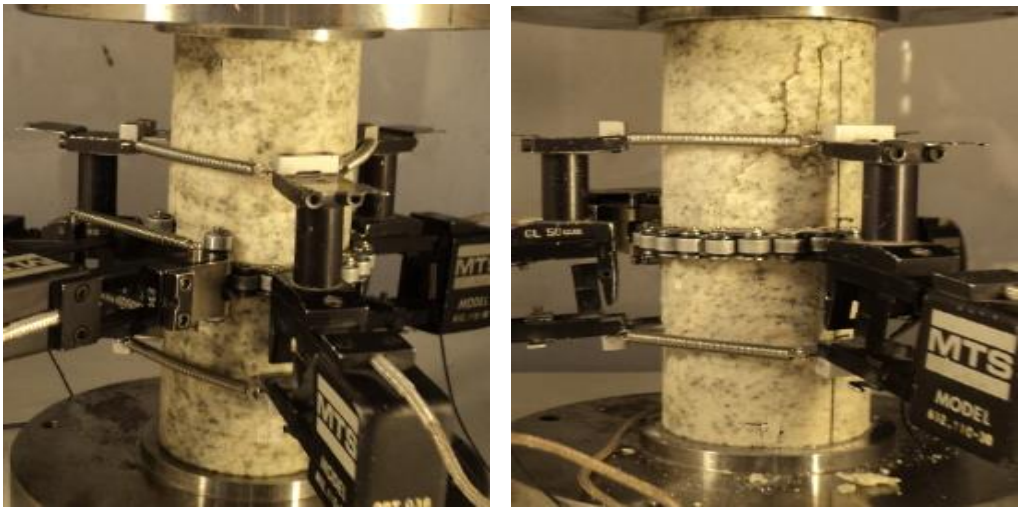

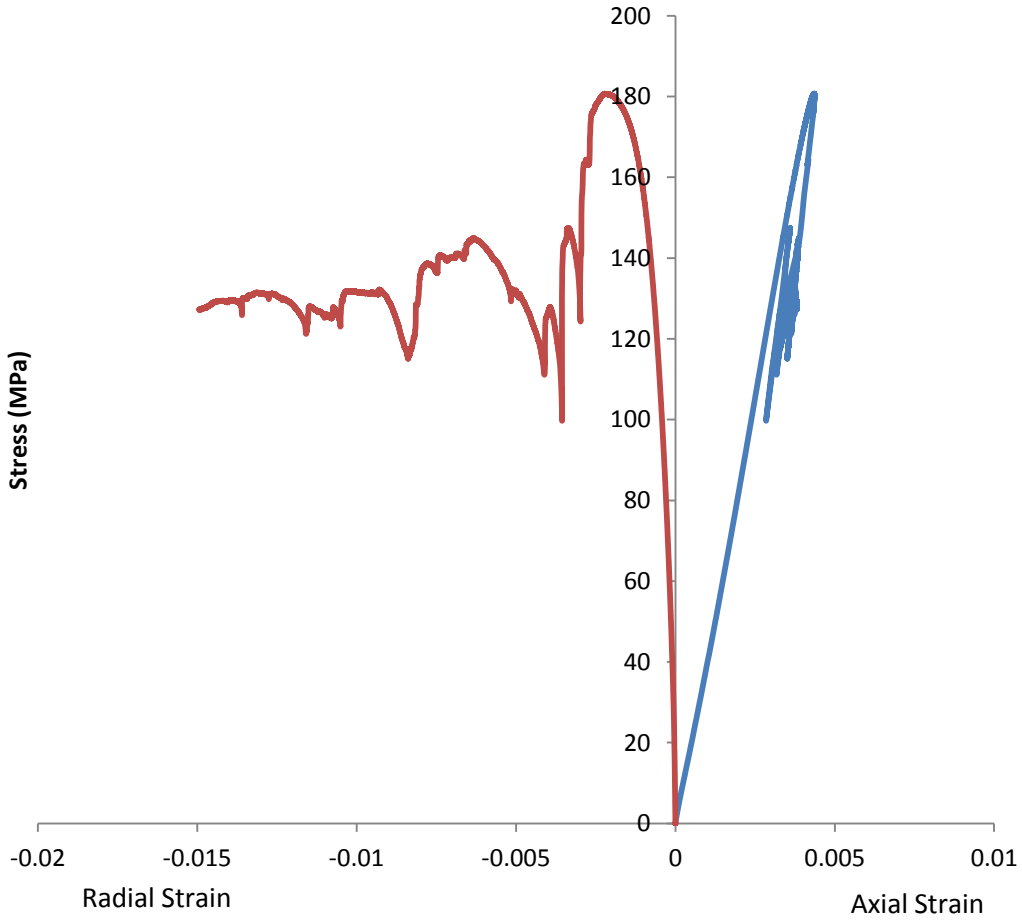

Appendix 2.2.7 On top show specimen before failure left, specimen after failure right and below is characteristic pre- and post-failure curves for fine-to-medium-grained Granite5.

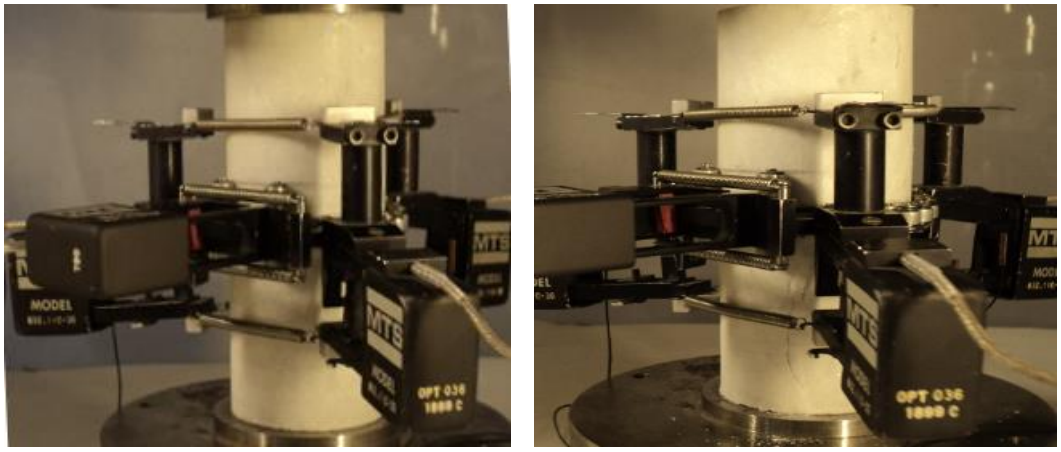

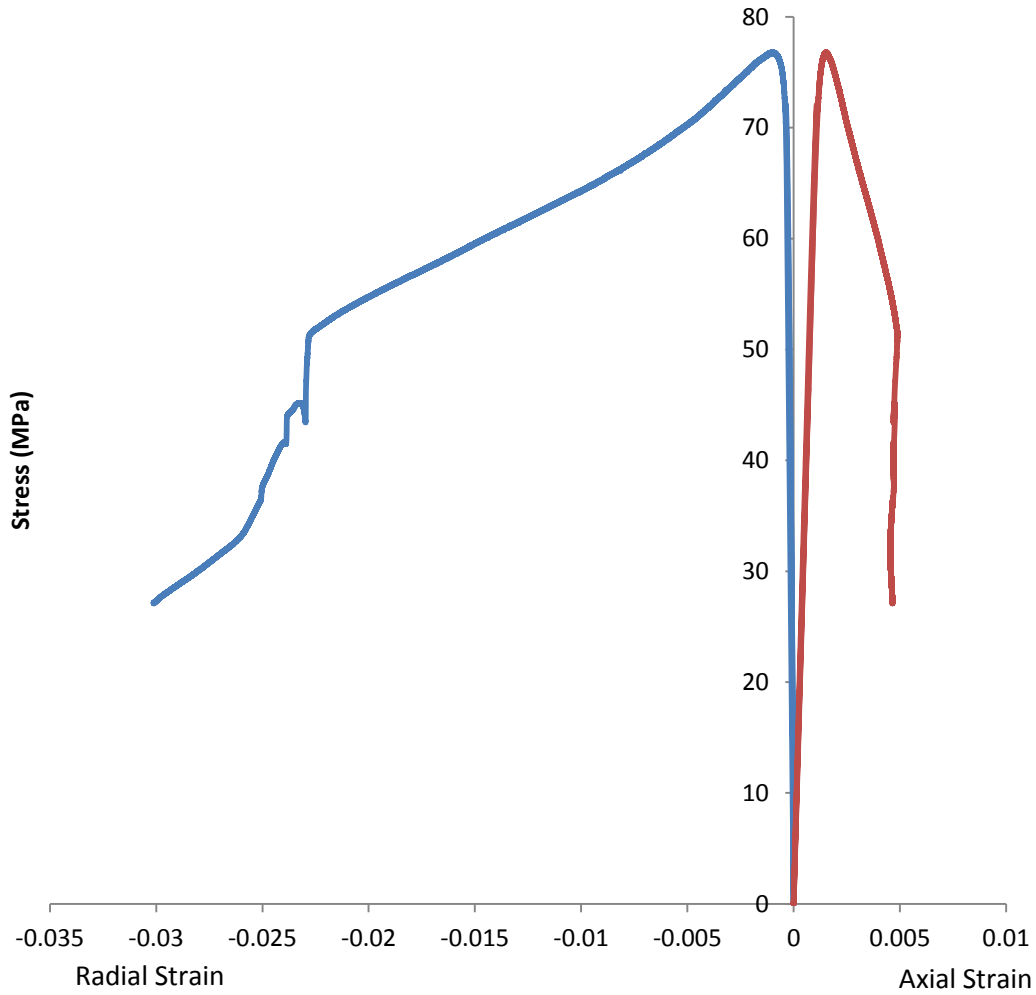

Appendix 2.2.8 On top show specimen before failure left, specimen after failure right and below is characteristic pre- and post-failure curves for Marble.

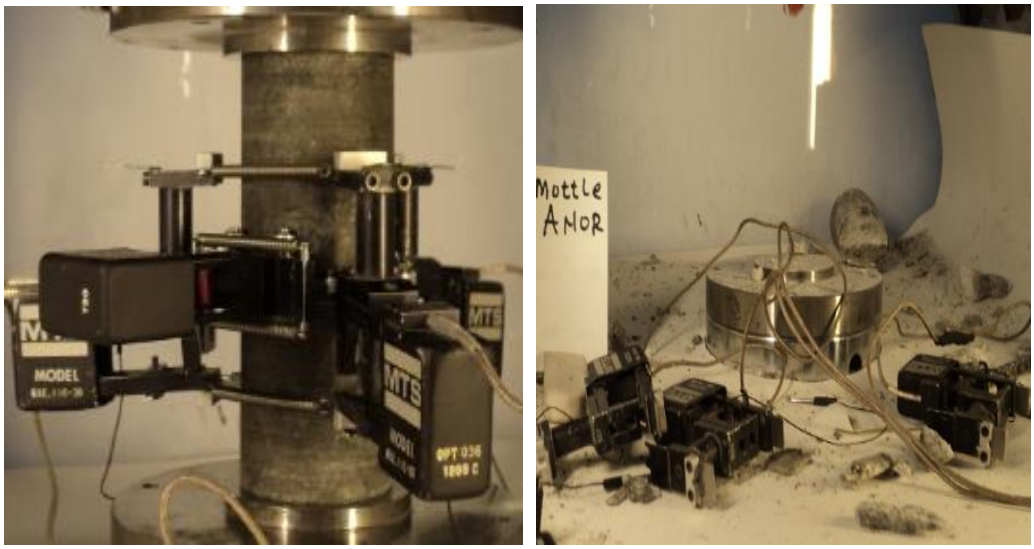

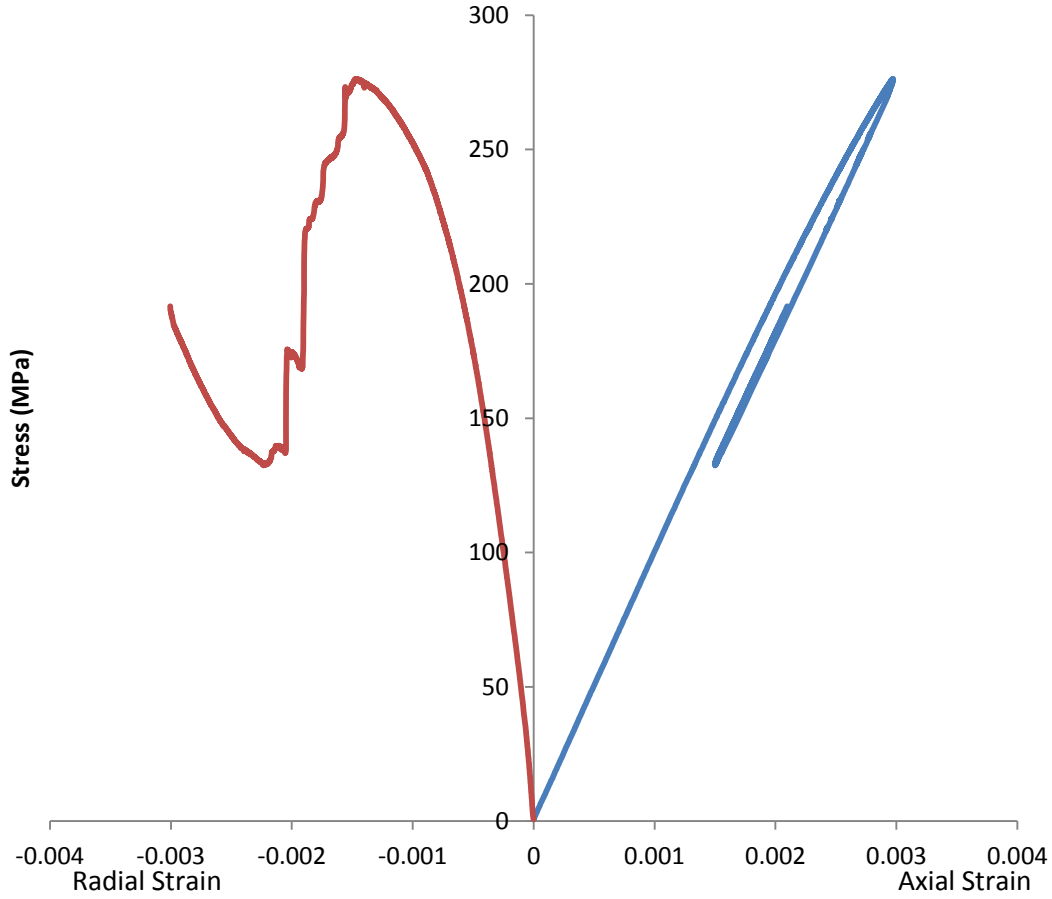

Appendix 2.2.9 On top show specimen before failure left, specimen after failure right and below is characteristic pre- and post-failure curves for Mottled Anorthosite.

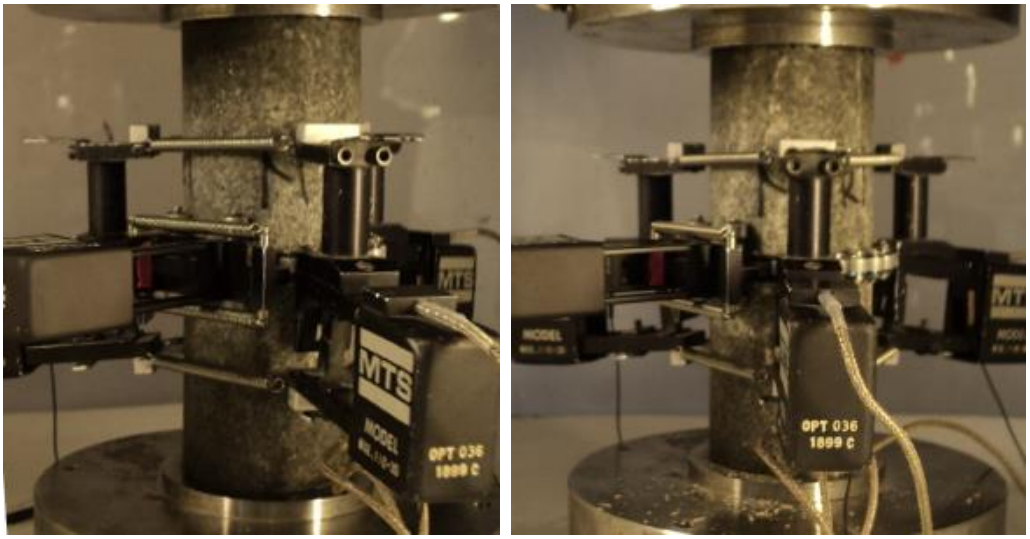

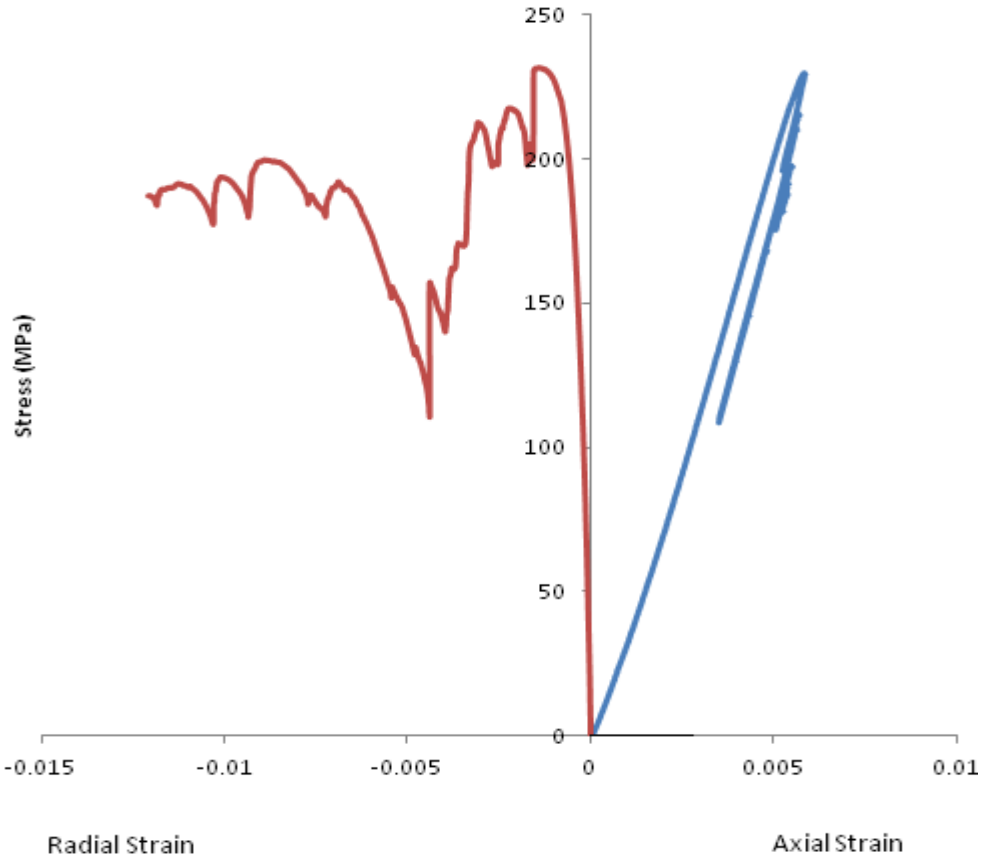

Appendix 2.2.10 On top show specimen before failure left, specimen after failure right and below is characteristic pre- and post-failure curves for Norite1.

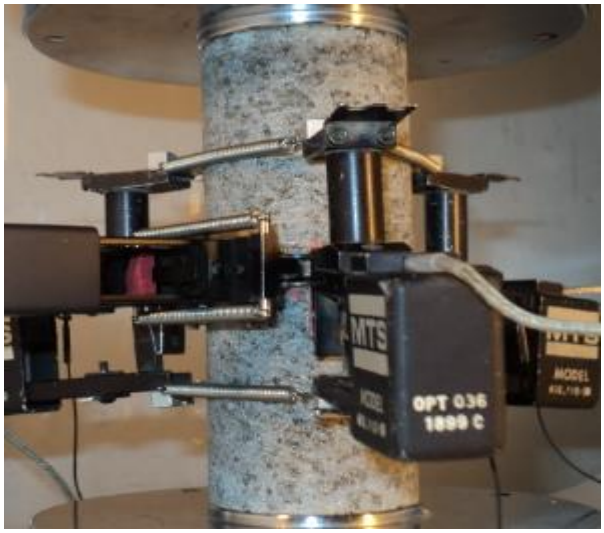

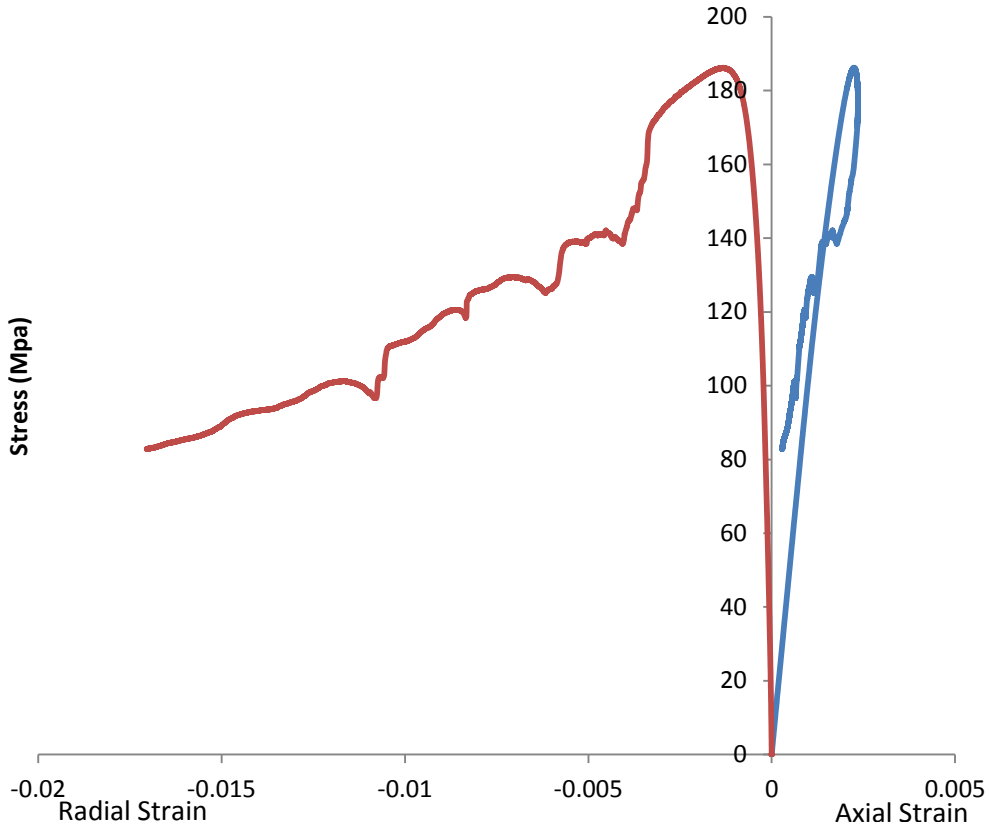

Appendix 2.2.11 On top show specimen before failure left, specimen after failure right and below is characteristic pre- and post-failure curves for Norite2.

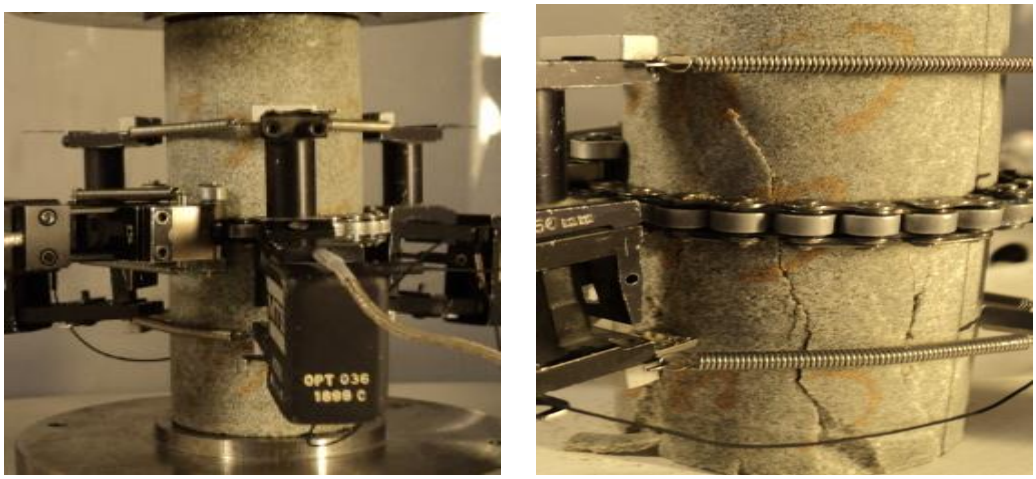

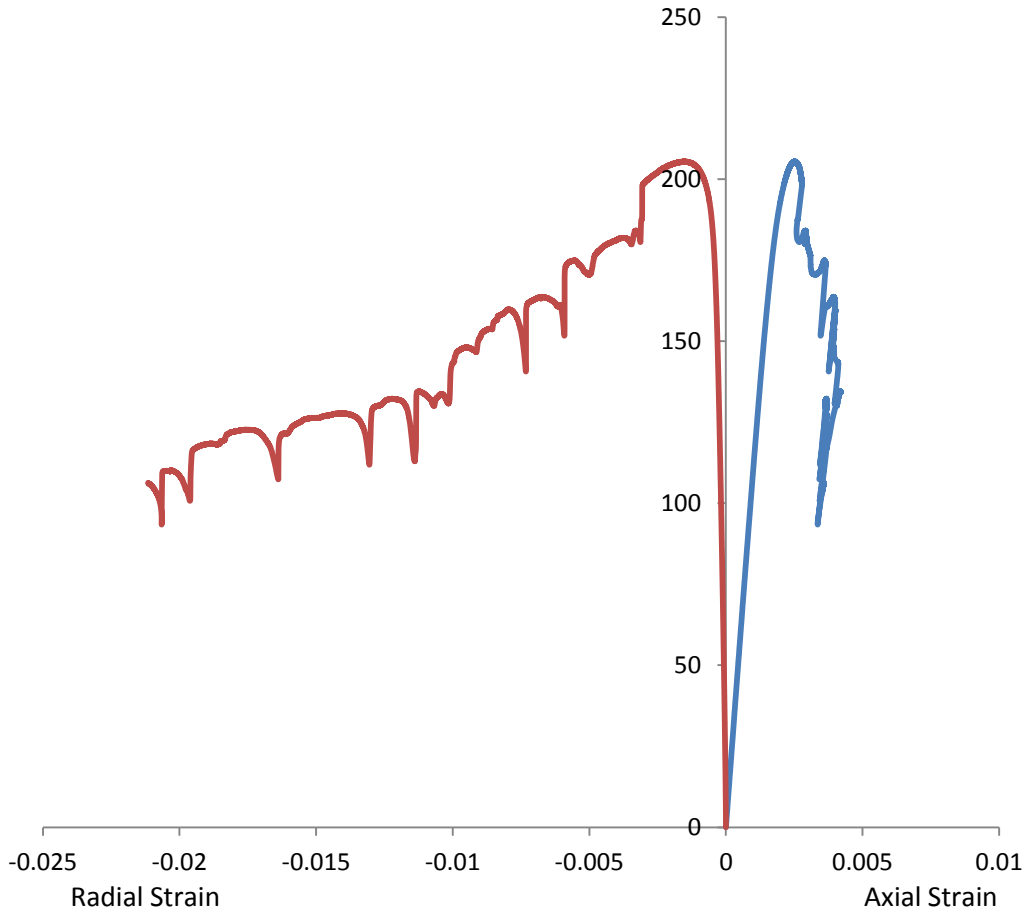

Appendix 2.2.12 On top show specimen before failure left, specimen after failure right and below is characteristic pre- and post-failure curves for Norite3.

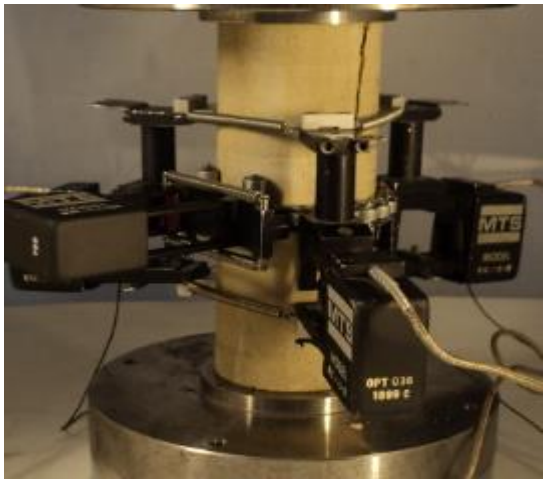

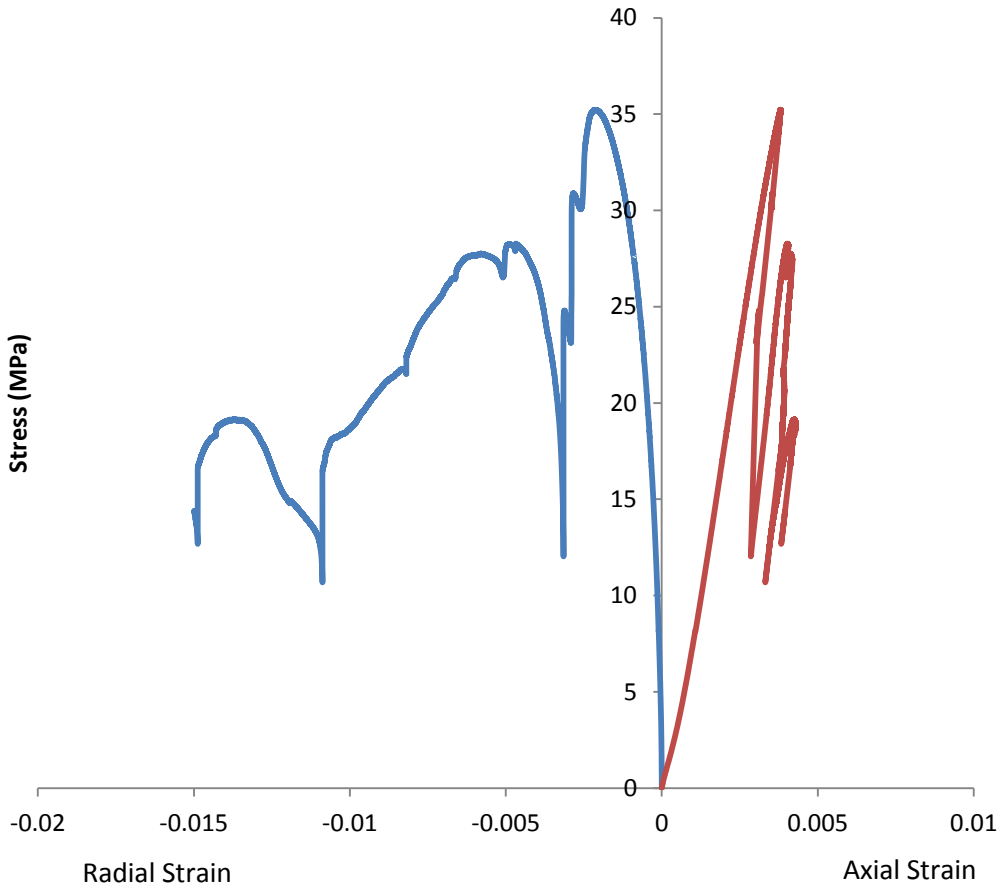

Appendix 2.2.13 On top show specimen before failure left, specimen after failure right and below is characteristic pre- and post-failure curves for Quartz Arenite.

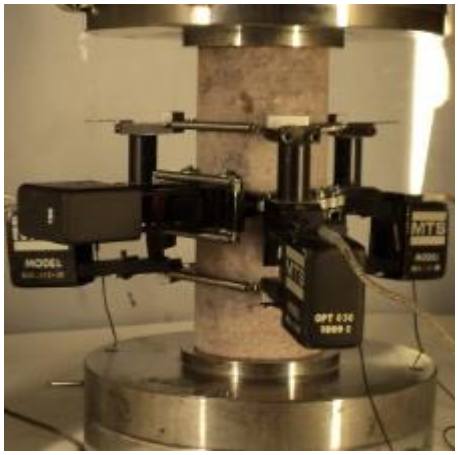

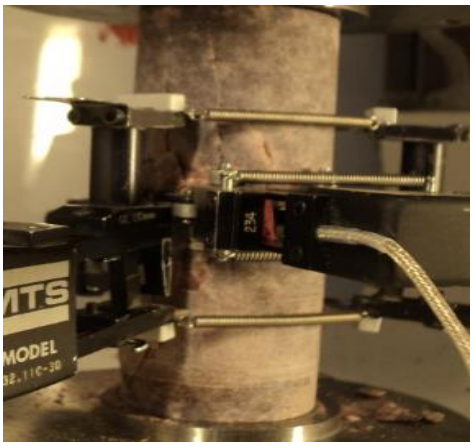

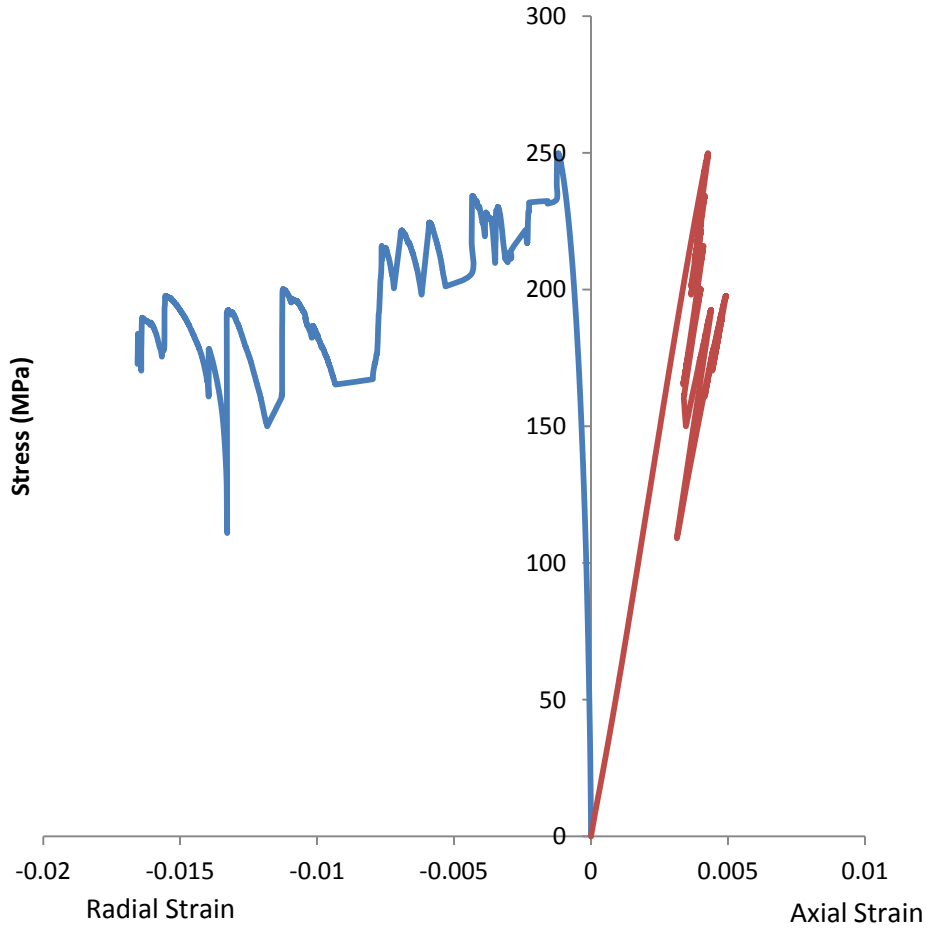

Appendix 2.2.14 On top show specimen before failure left, specimen after failure right and below is characteristic pre- and post-failure curves for Quartzite1.

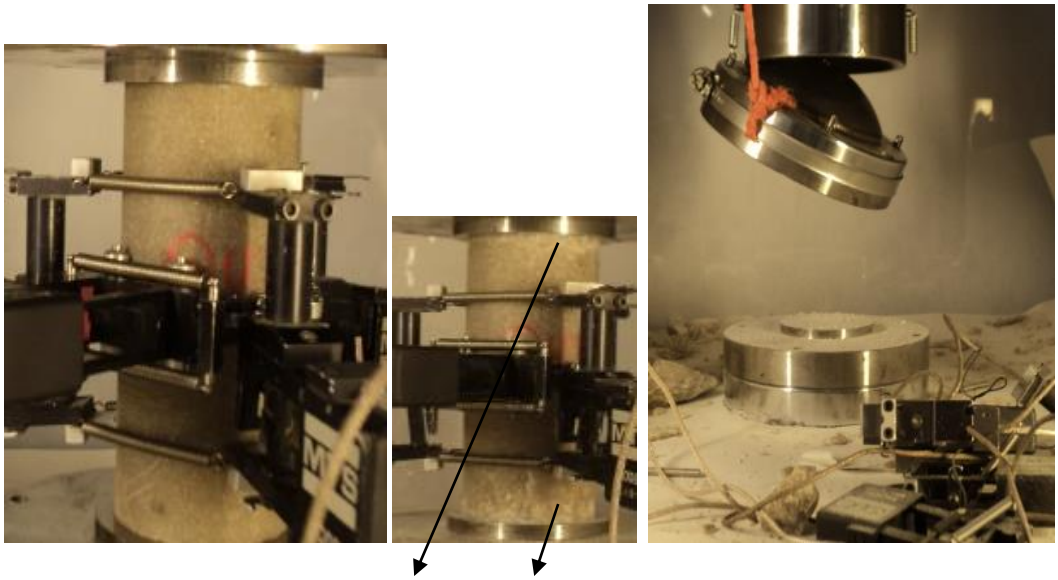

Spalling at the ends thereby reducing in

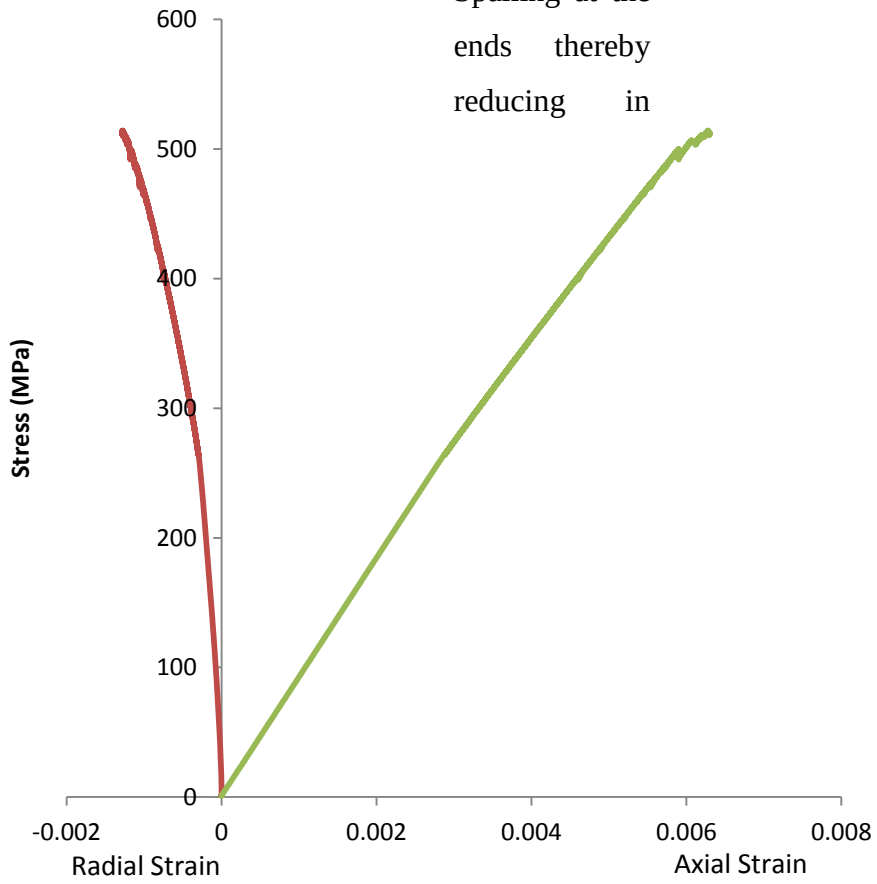

Appendix 2.2.15 On top show specimen before failure left, specimen after failure right and below is characteristic pre-failure curves for Quartzite2.

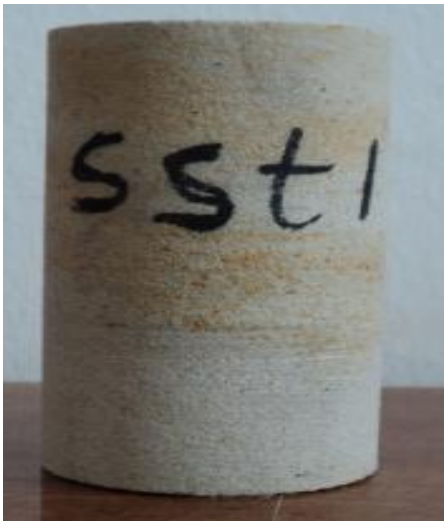

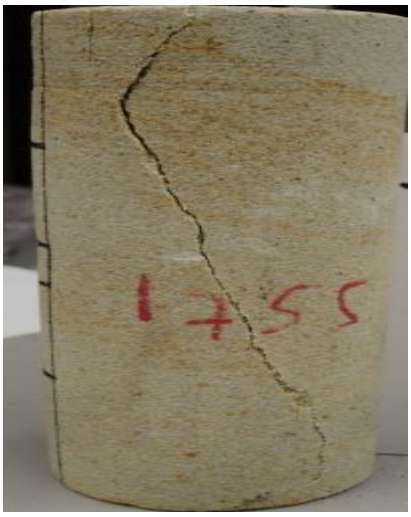

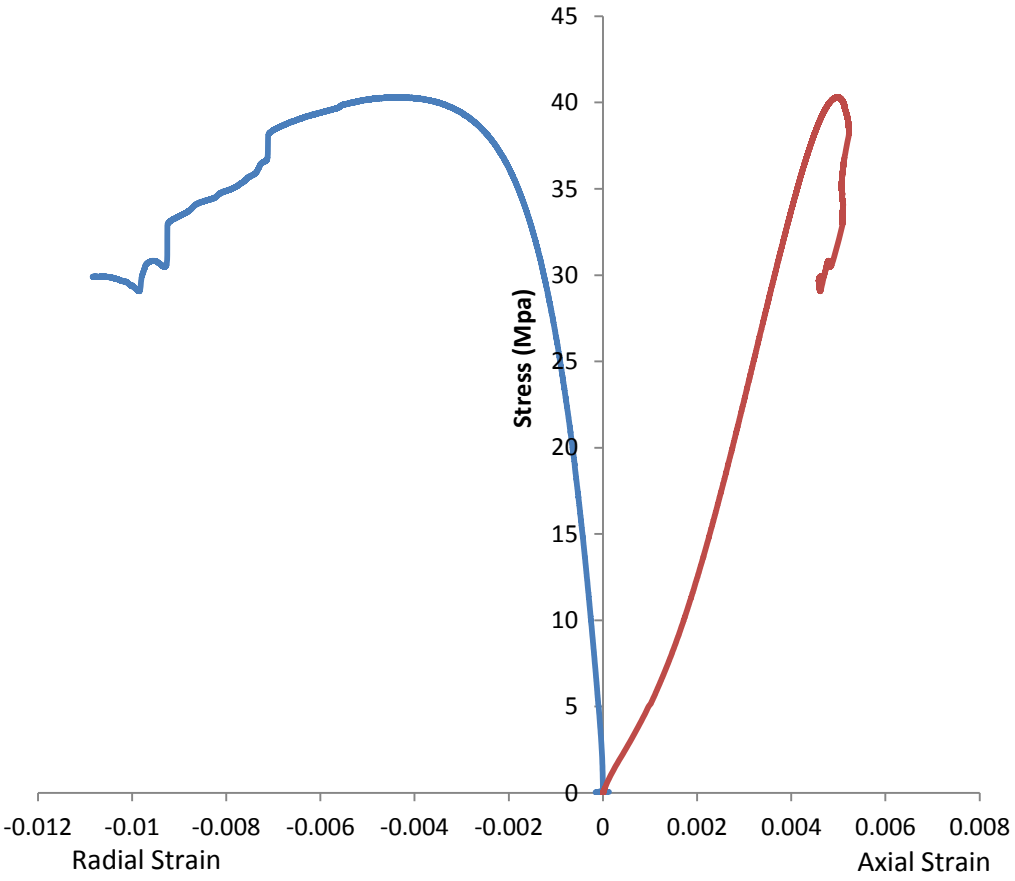

Appendix 2.2.16 On top show specimen before failure left, specimen after failure right and below is characteristic pre- and post-failure curves for Sandstone.

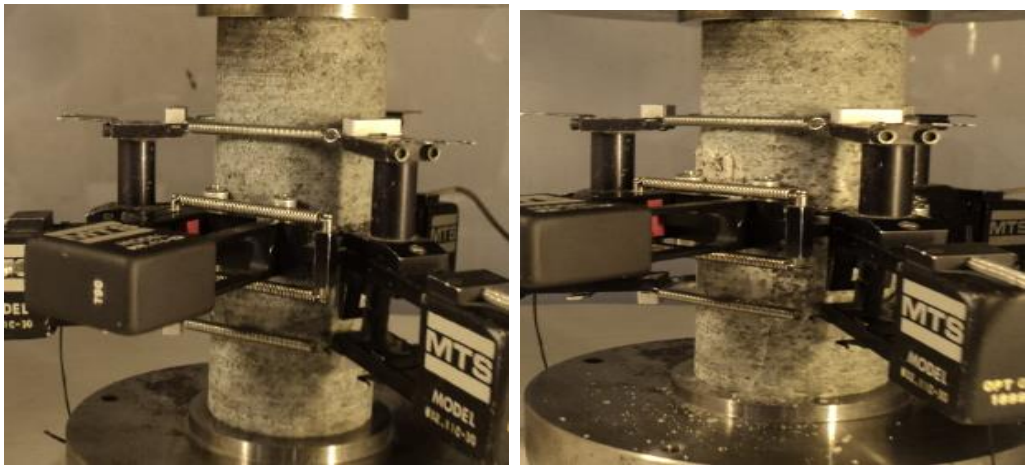

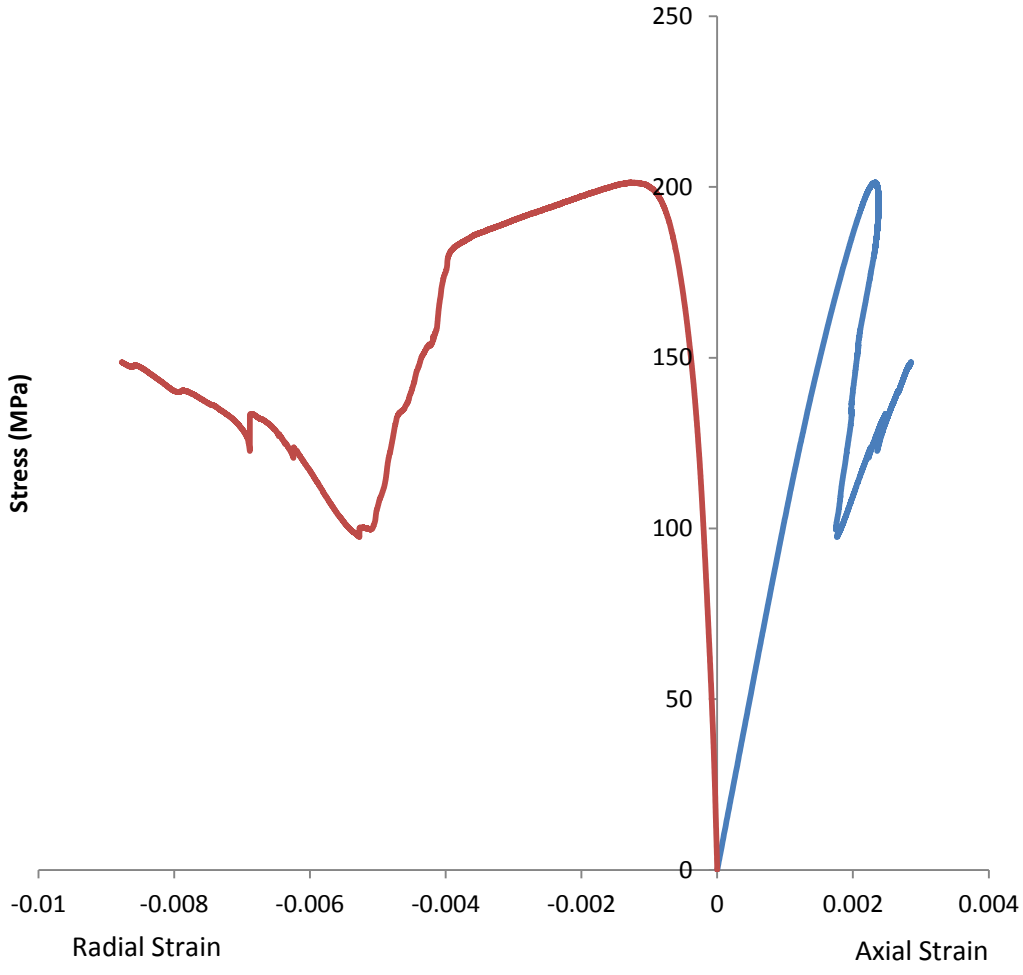

Appendix 2.2.17 On top show specimen before failure left, specimen after failure right and below is characteristic pre- and post-failure curves for Spotted Anorthosite.

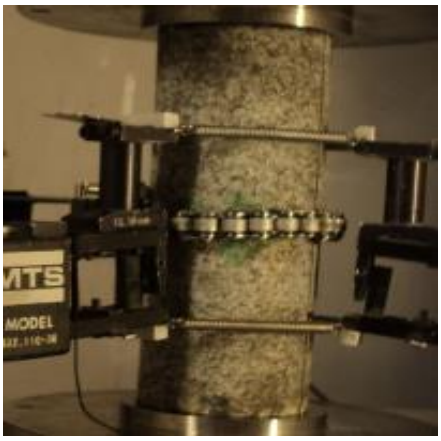

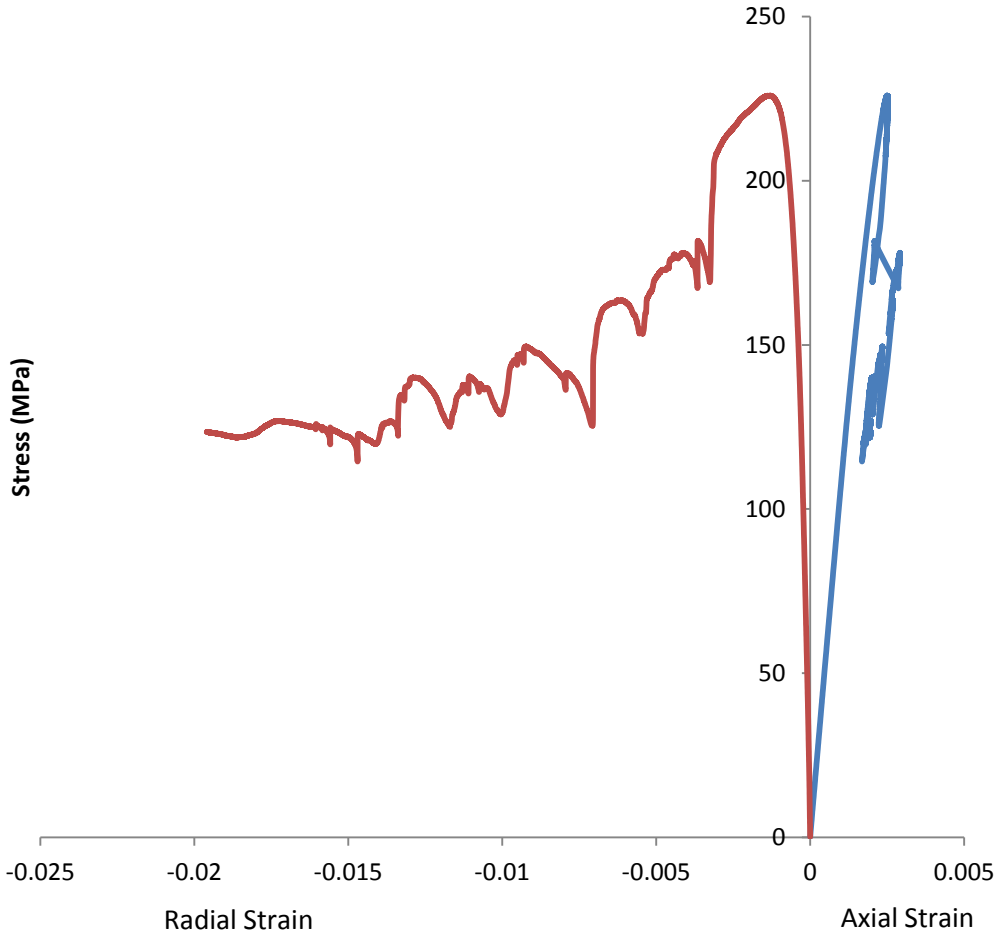

Appendix 2.2.18 On top show specimen before failure left, specimen after failure right and below is characteristic pre- and post-failure curves for Troctolite1.

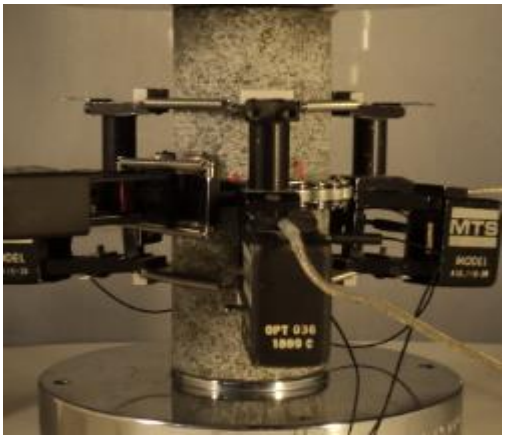

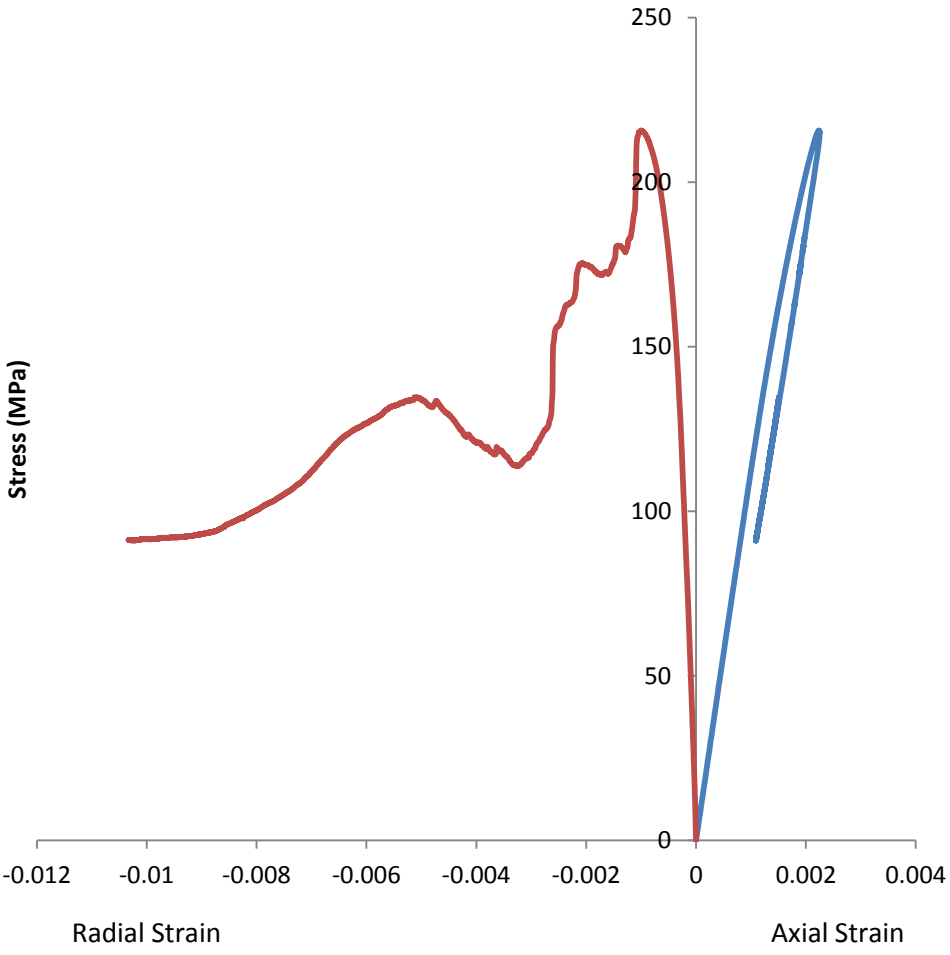

Appendix 2.2.19 On top show specimen before failure left, specimen after failure right and below is characteristic pre- and post-failure curves for Troctolite2.

APPENDIX 3.1 COMPARISON OF FRAGMENTATION FROM COMPRESSION AND STATIC MECHANICAL PROPERTIES

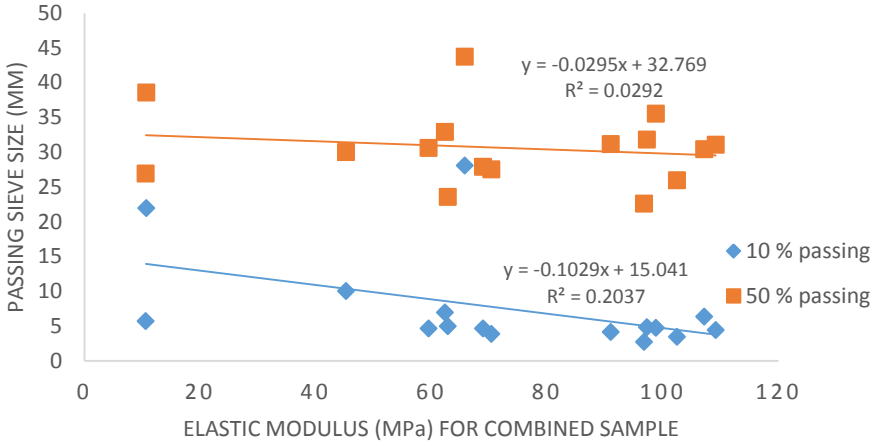

Appendix 3.1.1 Elastic modulus and passing sieve size at X_{50s} and X_{10s} for combined sample

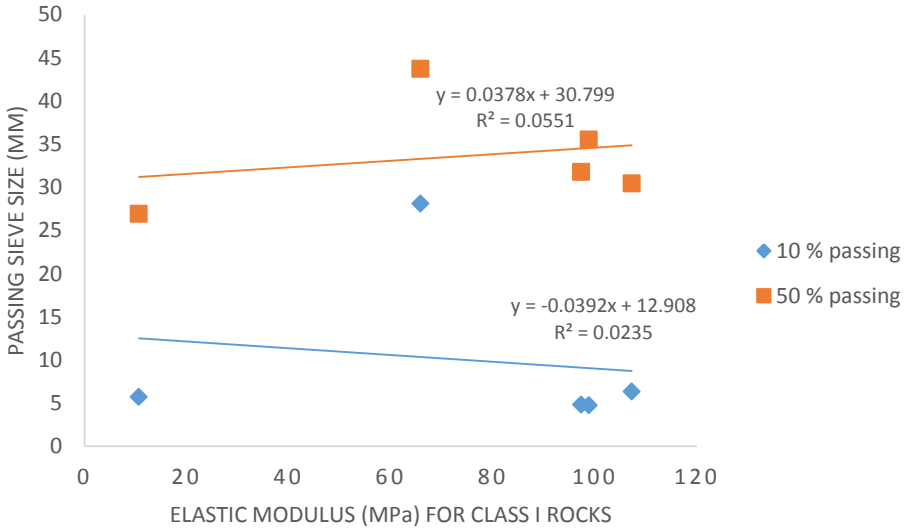

Appendix 3.1.2 Elastic modulus and passing sieve size at X_{50s} and X_{10s} for Class I rocks

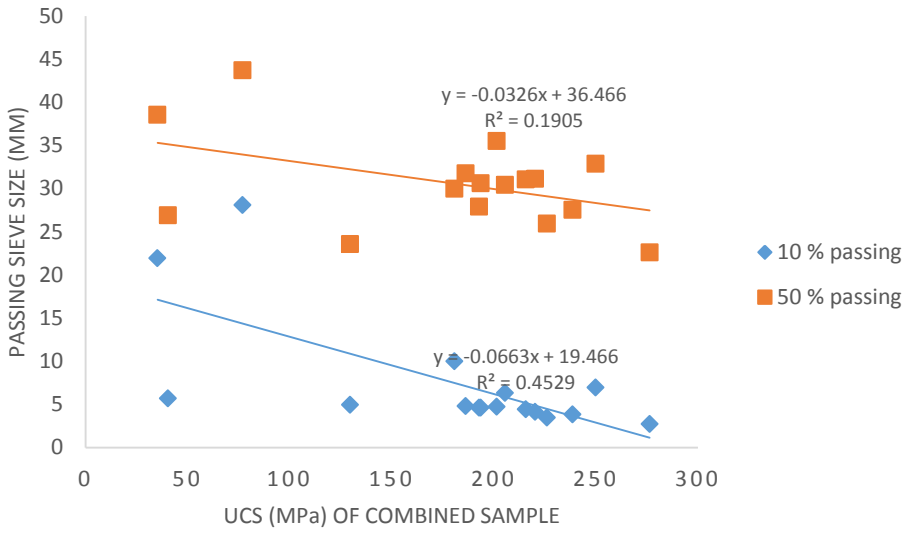

Appendix 3.1.3 UCS and passing sieve size at X_{50s} and X_{10s} for combined sample

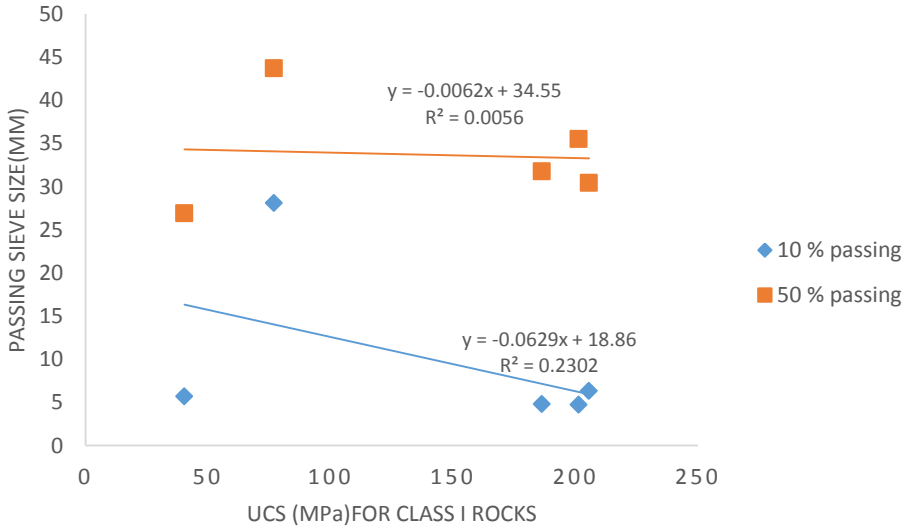

Appendix 3.1.4 UCS and passing sieve size at X_{50s} and X_{10s} for Class I rocks

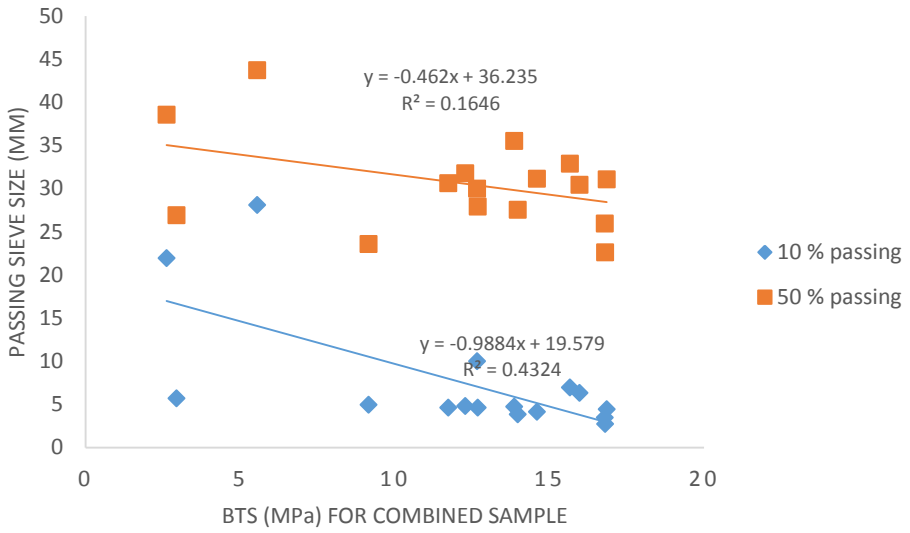

Appendix 3.1.5 BTS and passing sieve size at X_{50s} and X_{10s} for combined sample

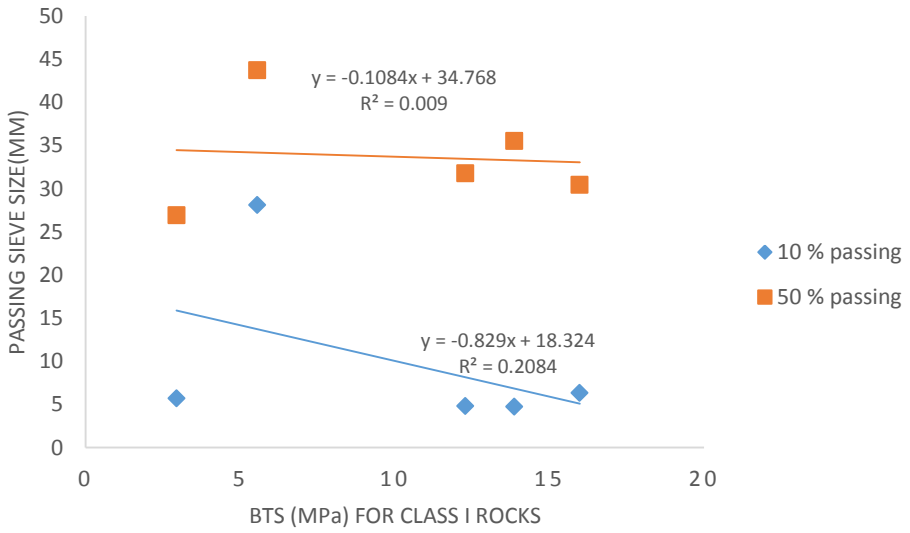

Appendix 3.1.6 BTS and passing sieve size at X_{50s} and X_{10s} for class I rocks

APPENDIX 3.2 COMPARISON OF FRAGMENTATION FROM COMPRESSION AND BRITTLENESS BASED ON STATIC MECHANICAL PROPERTIES

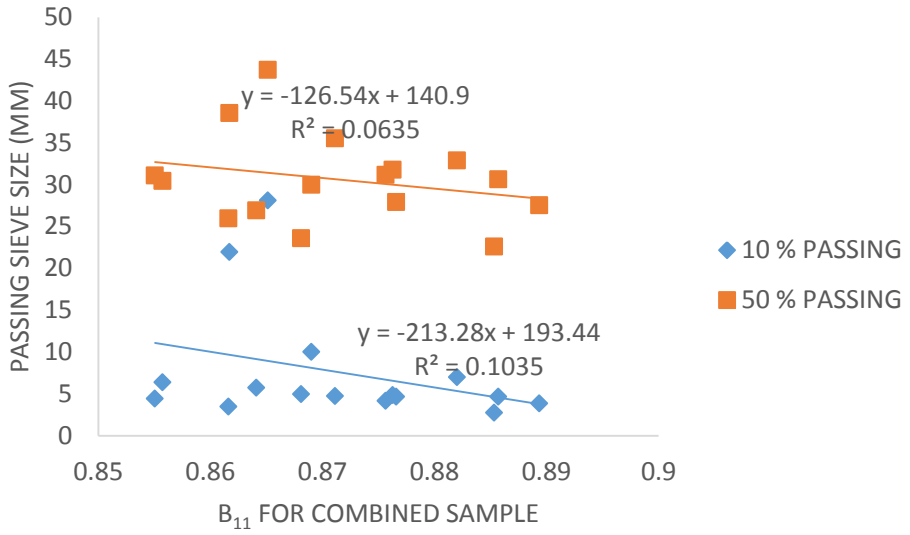

Appendix 3.2.1 B_{11} and passing sieve size at X_{50s} and X_{10s} for combined sample

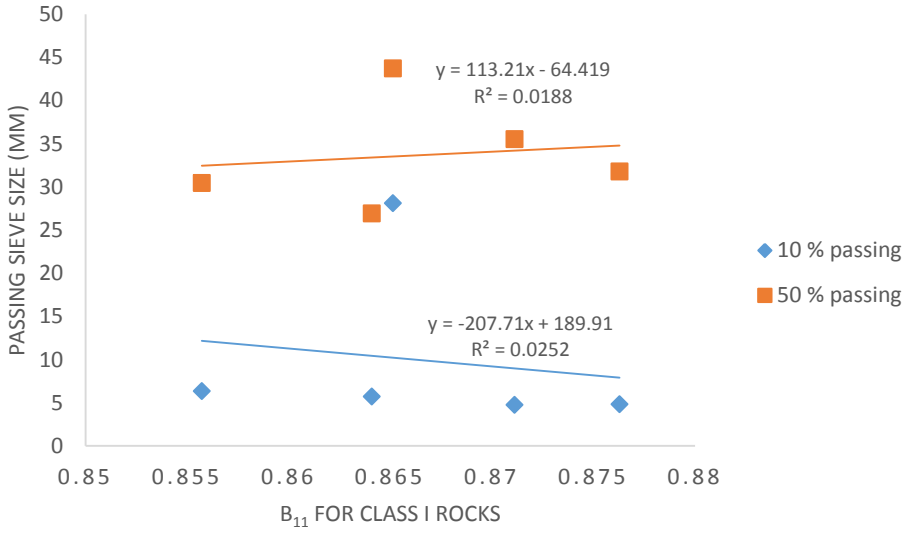

Appendix 3.2.2 B_{11} and passing sieve size at X_{50s} and X_{10s} for Class II Rocks

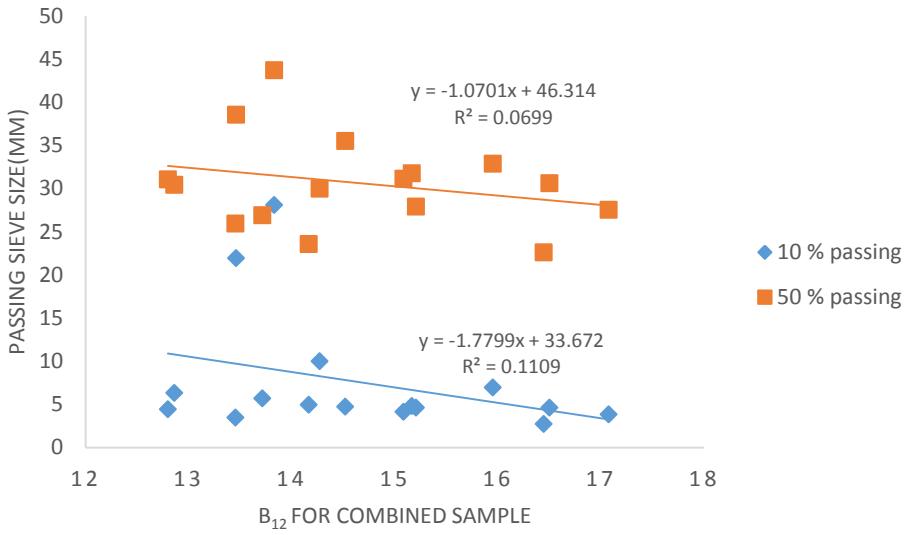

Appendix 3.2.3 B_{12} and passing sieve size at X_{50s} and X_{10s} for combined sample

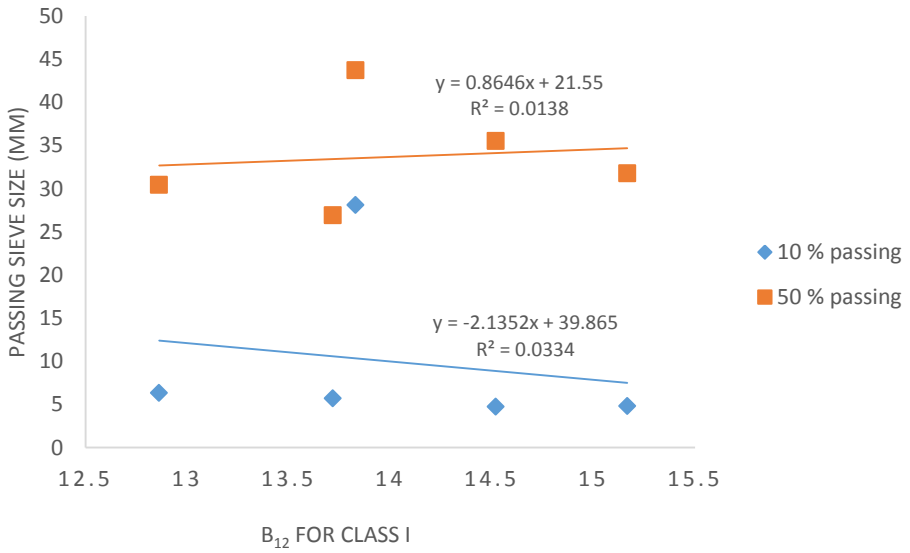

Appendix 3.2.4 B_{12} and passing sieve size at X_{50s} and X_{10s} for Class I Rocks

APPENDIX 3.3 COMPARISON OF FRAGMENTATION FROM COMPRESSION AND BRITTLENESS BASED ON MODULI

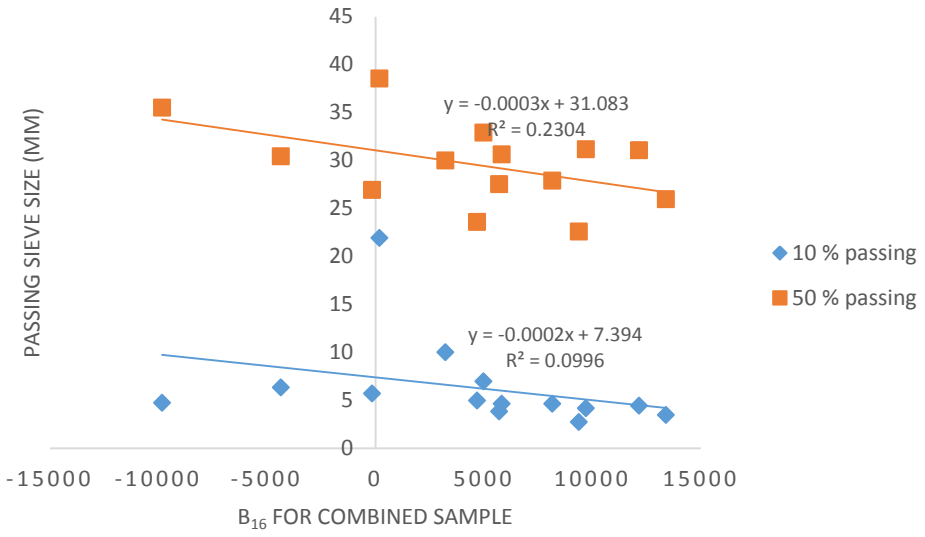

Appendix 3.3.1 B_{16} and passing sieve size at X_{50s} and X_{10s} for combined sample

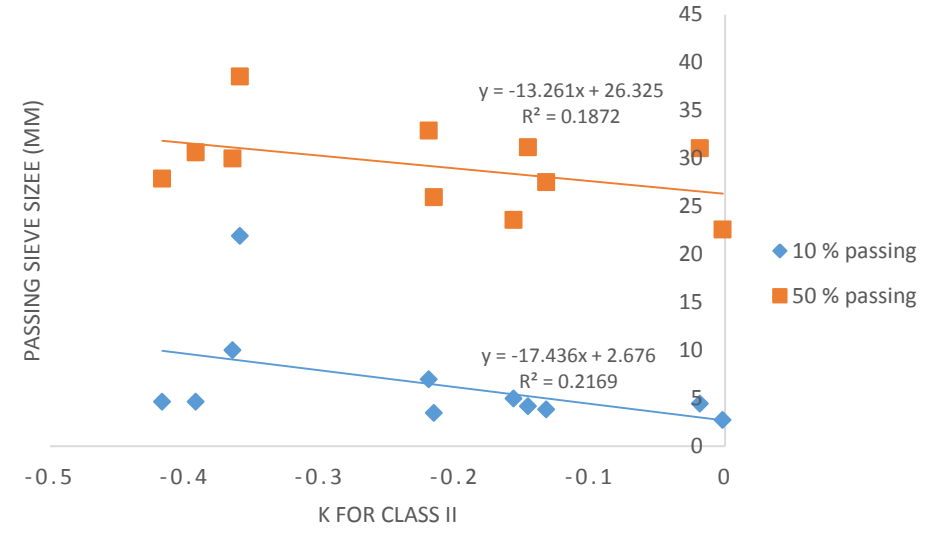

Appendix 3.3.2 k and passing sieve size at X_{50s} and X_{10s} for Class II Rocks

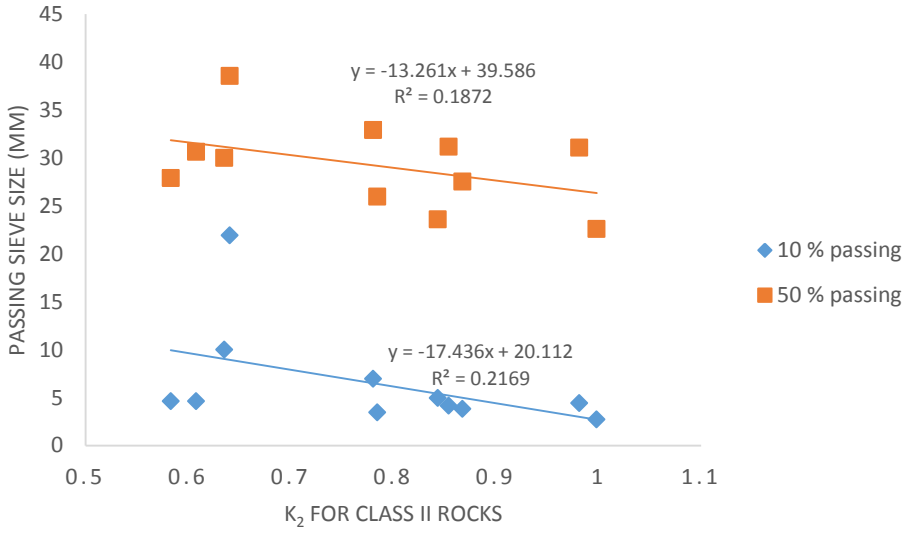

Appendix 3.3.3 k_2 and passing sieve size at X_{50s} and X_{10s} for Class II Rocks

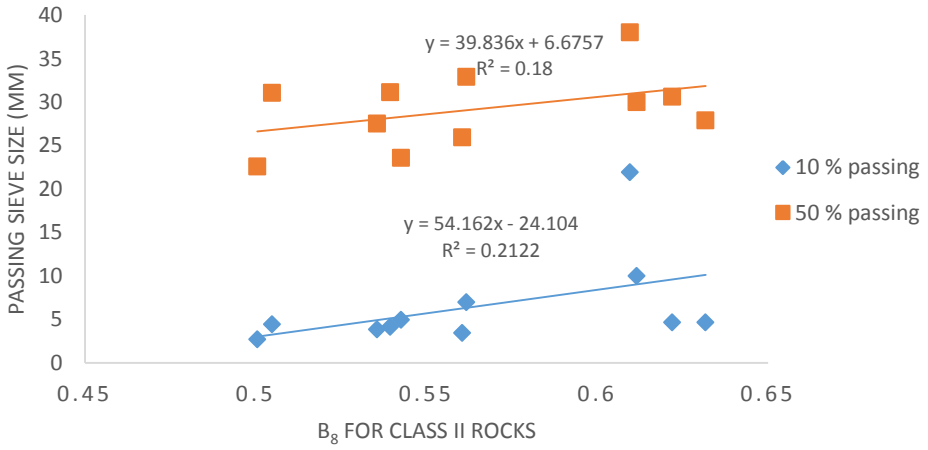

Appendix 3.3.4 B_8 and passing sieve size at X_{50s} and X_{10s} for Class II Rocks

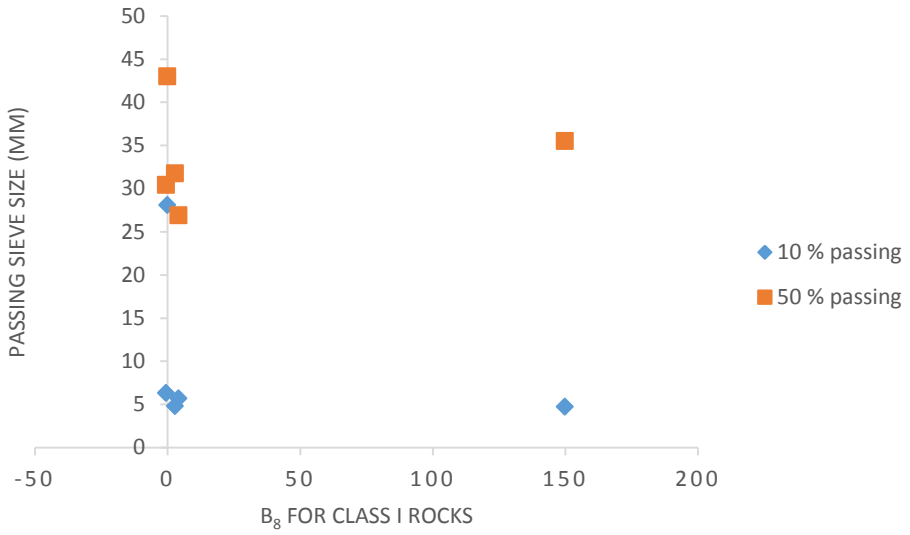

Appendix 3.3.5 B_8 and passing sieve size at X_{50s} and X_{10s} for Class I Rocks

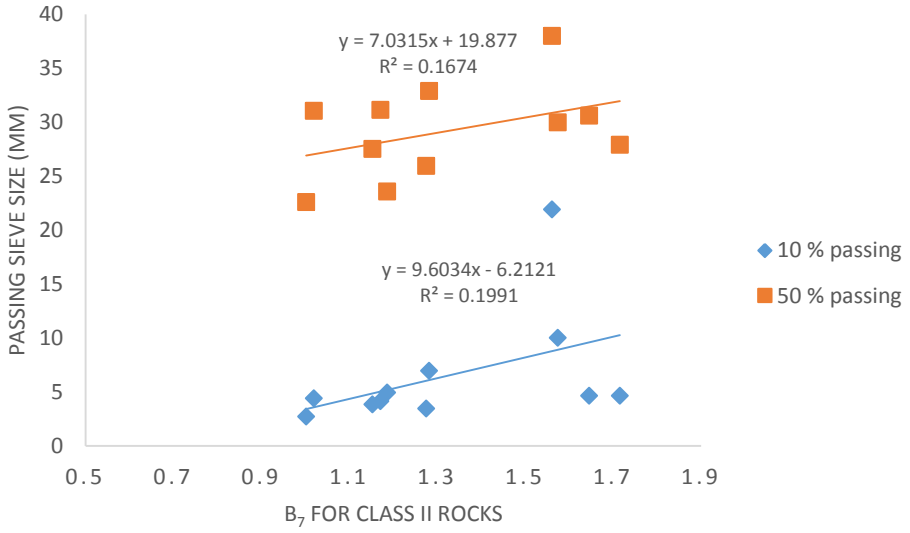

Appendix 3.3.6 B_7 and passing sieve size at X_{50s} and X_{10s} for Class II Rocks

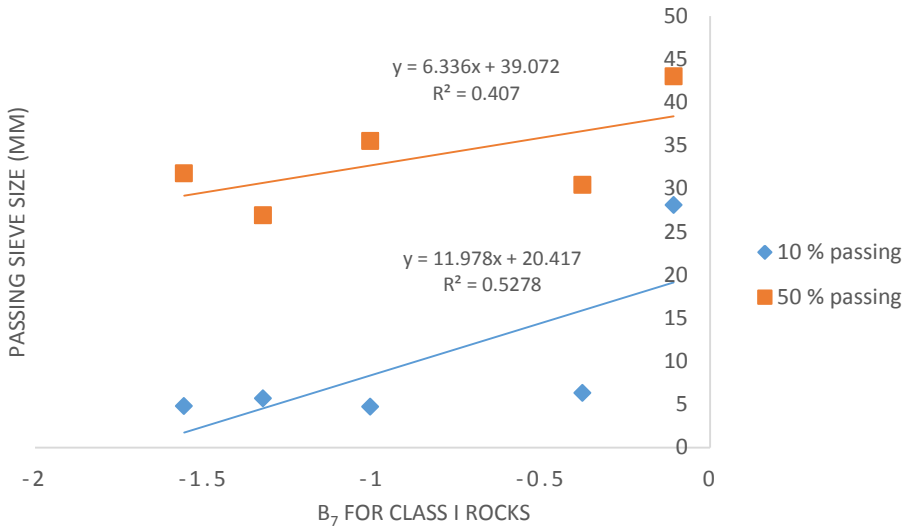

Appendix 3.3.7 B_7 and passing sieve size at X_{50s} and X_{10s} for Class I Rocks

APPENDIX 3.4 COMPARISON OF FRAGMENTATION FROM COMPRESSION WITH BRITTLENESS BASED ON NSSC AND CRITICAL EXTENSION STRAIN

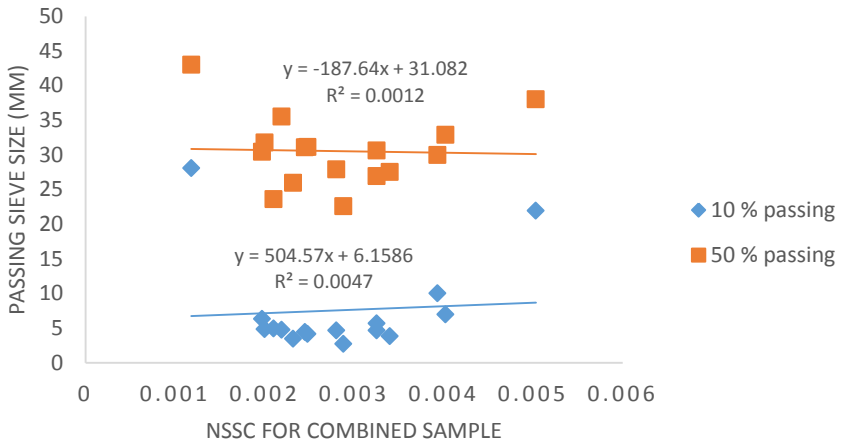

Appendix 3.4.1 NSSC and passing sieve size at X_{50s} and X_{10s} for combined sample

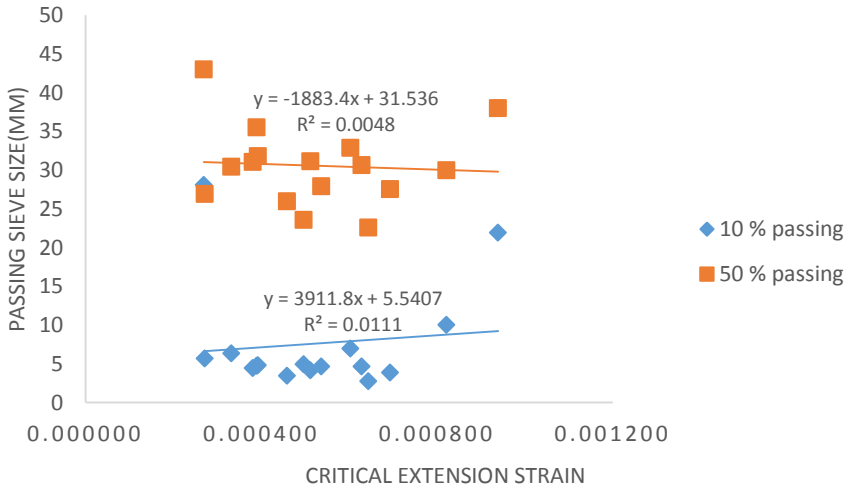

Appendix 3.4.2 Critical extension strain and passing sieve size at X_{50s} and X_{10s} for combined sample

APPENDIX 4.1 TOTAL NUMBER OF FRAGMENTS PER VOLUME OF ROCK AND BRITTLENESS BASED ON STATIC MECHANICAL PROPERTIES

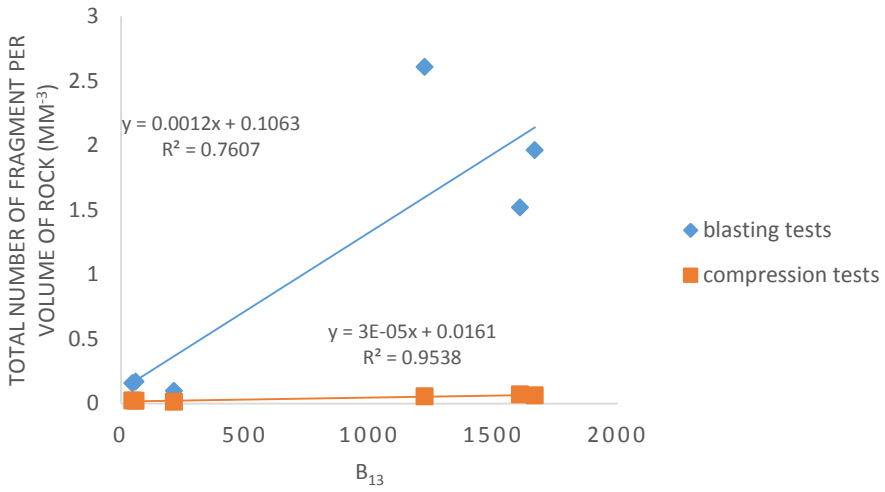

Appendix 4.1.2 Total number of fragments per volume of rock from both tests and brittleness B_{13}

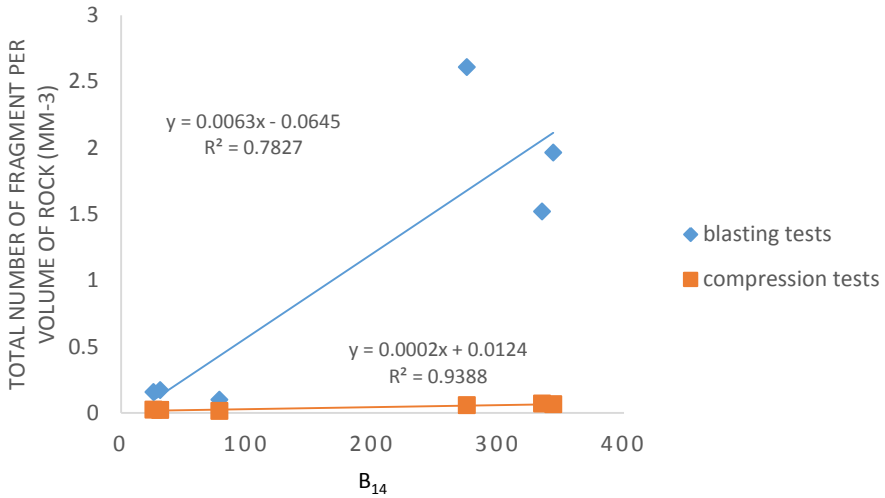

Appendix 4.1.2 Total number of fragments per volume of rock from both tests and brittleness B_{14}

APPENDIX 4.2 TOTAL NUMBER OF FRAGMENTS PER VOLUME OF ROCK AND BRITTLENESS BASED ON MODULI

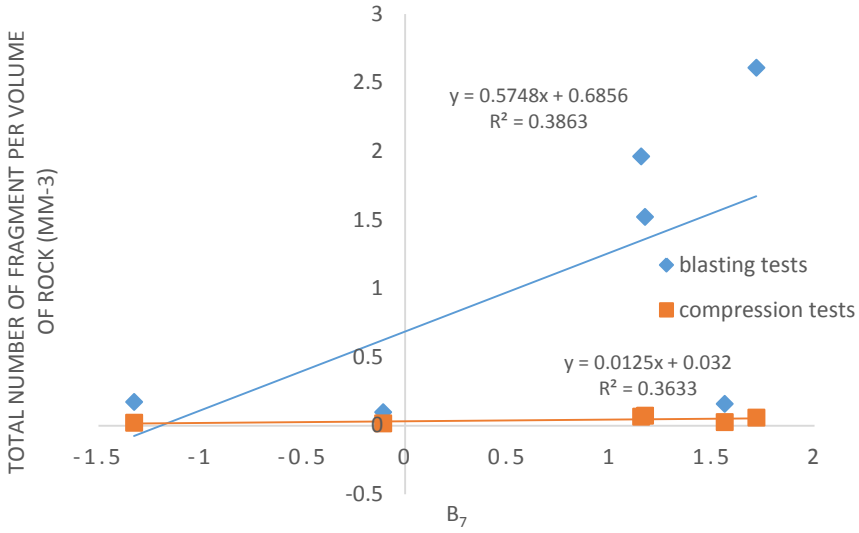

Appendix 4.2.1 Total number of fragments per volume of rock from both tests and brittleness B_7

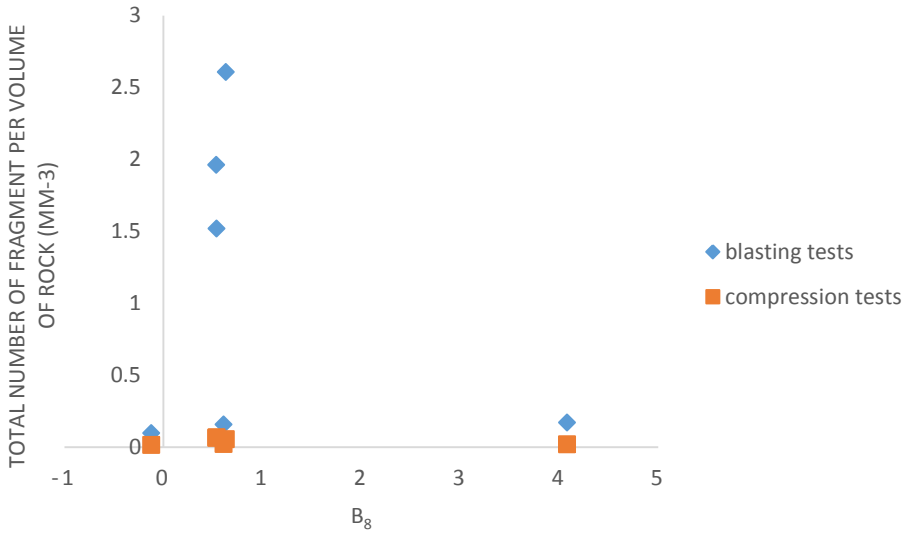

Appendix 4.2.2 Total number of fragments per volume of rock from both tests and brittleness B_8

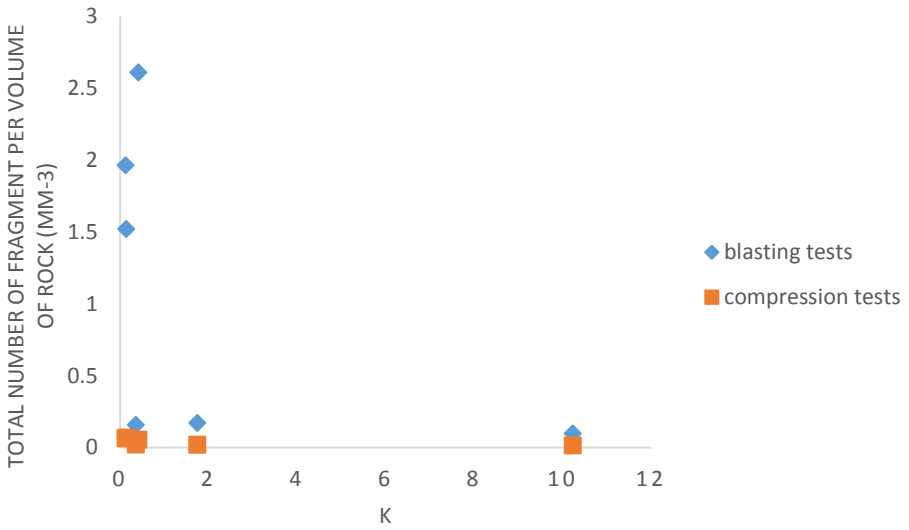

Appendix 4.2.3 Total number of fragments per volume of rock from both tests and brittleness *k*

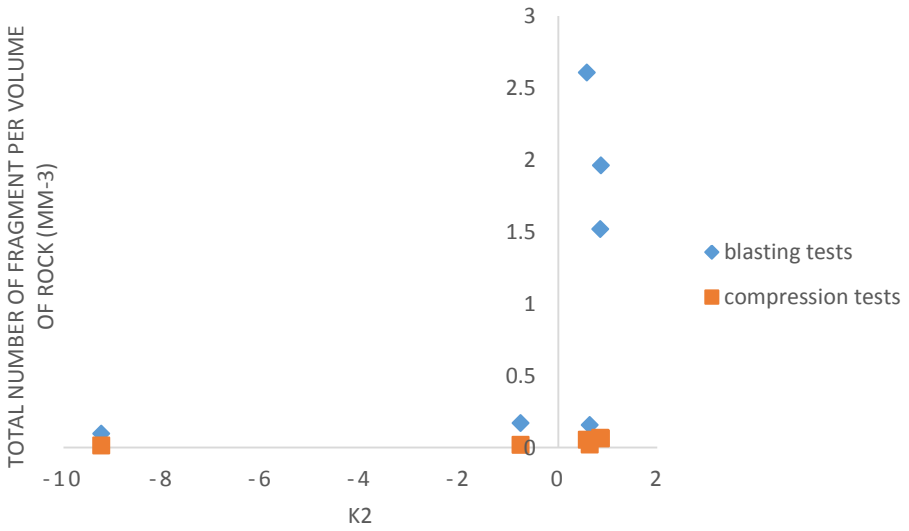

Appendix 4.2.4 Total number of fragments per volume of rock from both tests and brittleness k_2

APPENDIX 4.3 VOLUMES OF FINES PER VOLUME OF ROCK PRODUCED AND BRITTLENESS BASED ON MODULI

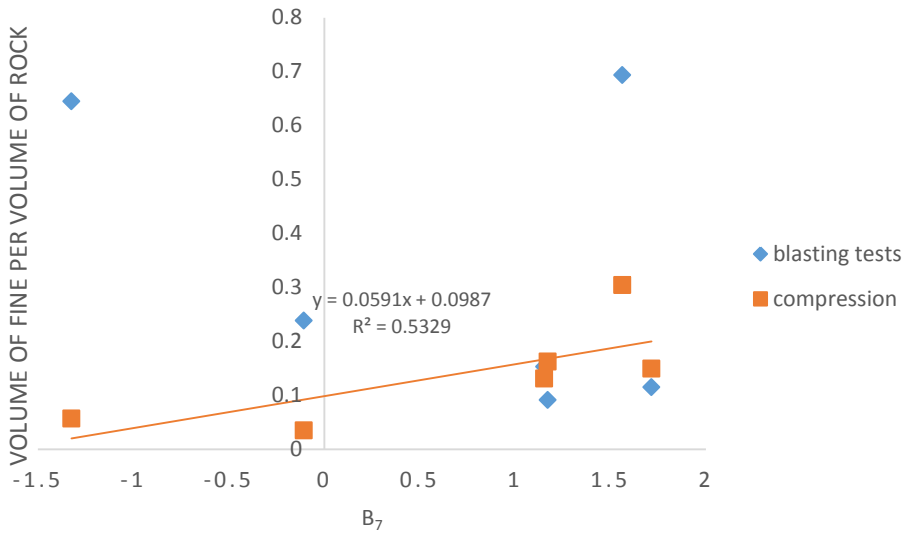

Appendix 4.3.1 Volume of fines per volume of rock from both tests and brittleness B_7

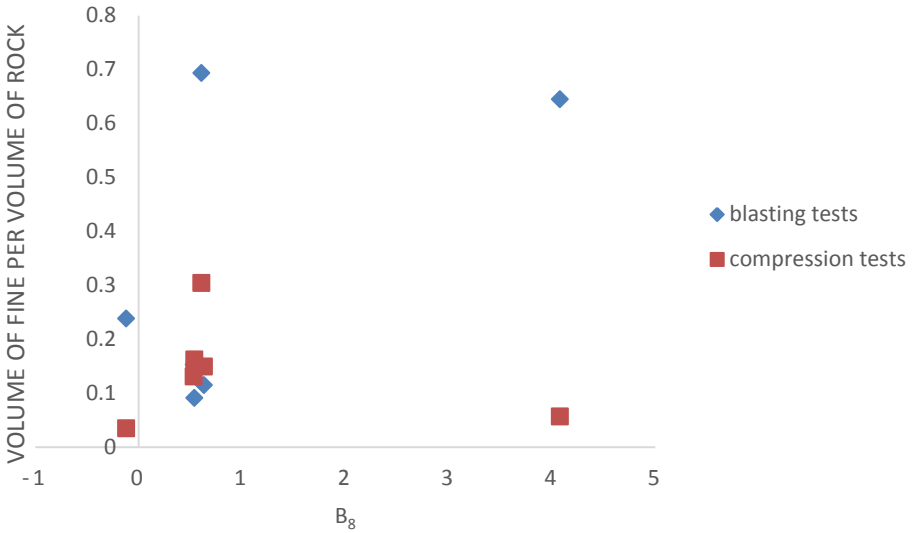

Appendix 4.3.2 Volume of fines per volume of rock from both tests and brittleness B_8

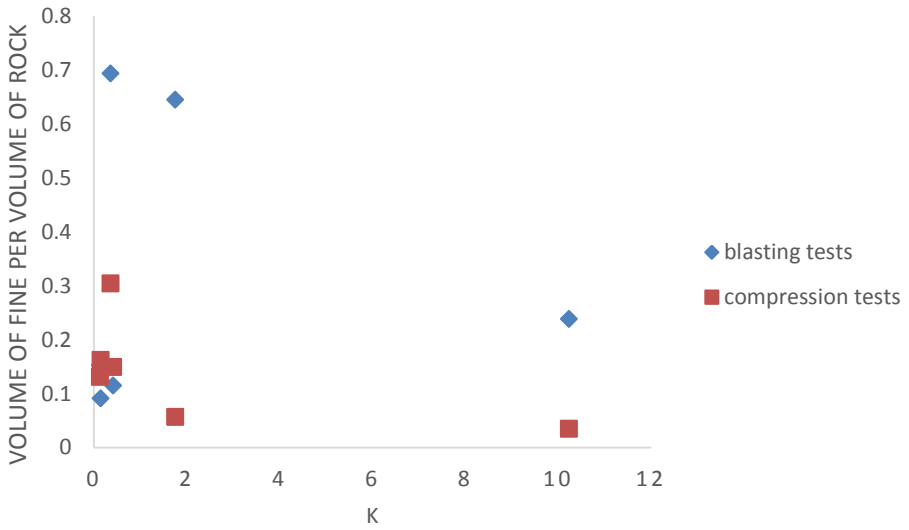

Appendix 4.3.2 Volume of fines per volume of rock from both tests and brittleness *k*

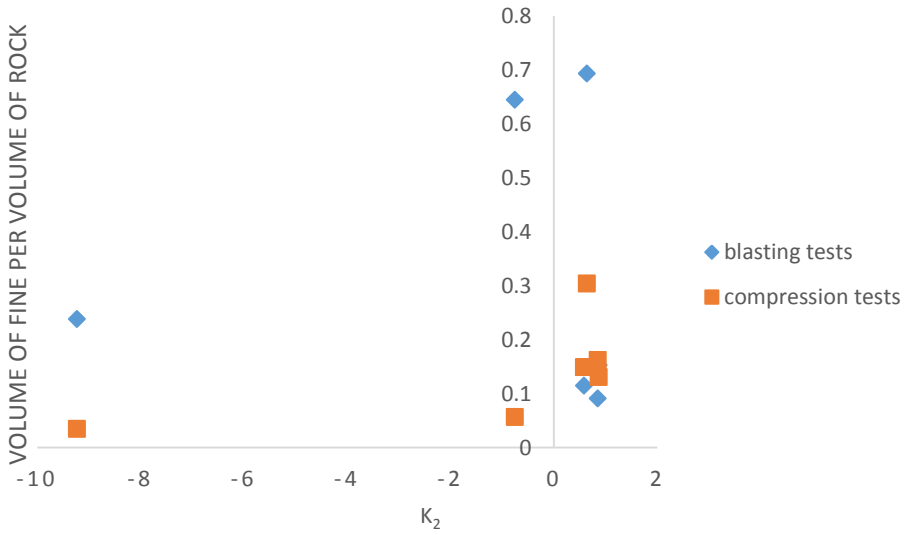

Appendix 4.3.2 Volume of fines per volume of rock from both tests and brittleness k_2

APPENDIX 4.4 VOLUMES OF FINES PER VOLUME OF ROCK PRODUCED AND BRITTLENESS BASED ON NSSC

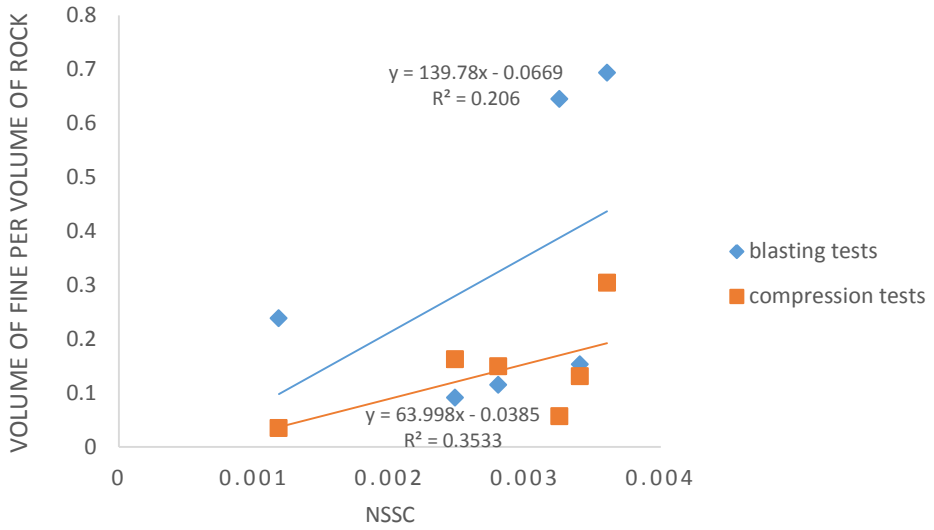

Appendix 4.4 Volume of fines per volume of rock from both tests and brittleness NSSC